

Integrated Modelling and Analysis of Buildings and Community Energy Systems



Sambu Kanteh Sakiliba

School of Engineering
Cardiff University

A thesis submitted for the degree of

Master of Philosophy

Cardiff, 2019

ACKNOWLEDGEMENT

In the Name of Allah, the Most Gracious, the Most Merciful

I would like to acknowledge the PhD scholarship I received from the Engineering and Physical Sciences Research Council, and the Toshiba Research Europe Limited which also enabled me to spend collaborative research time at the Telecommunications Research Laboratory (TRL), Bristol, United Kingdom. I pay my gratitude to my industrial supervisor Prof. Mahesh Sooriyabandara, for providing necessary infrastructure and resources to accomplish my research work. Under his guidance I successfully overcame many difficulties and learned a lot. I would never forget his support. Likewise, many thanks to Dr. Silviu Nistor and Dr. Tim Farnham for their help during my research time in TRL.

I would like to take this moment to express my sincere and absolute gratitude to my main supervisor Prof. Jianzhong Wu for his cooperation, professionalism, advice, encouragement and support. Furthermore, for his trust, and opportunity given to me on this exciting field of research. Also, my sincere gratitude to my second supervisor Prof. Nick Jenkins for his advice and feedback which improved the quality of the research work.

I am also thankful to Cardiff University, and the useful meetings with all colleagues from the Centre for Integrated Renewable Energy Generation and Supply (CIREGS).

I would like to say thanks, for the collaborative research support, to Mr. Joe Dickinson and M. Nick Bolton from Electric Corby Enterprise, Mr. Anthony Morgan from the Carbon Free Group, and Mr. David Hogg from Bright Green Hydrogen.

I would like to dedicate this research work to my beloved children Sulayman and Fatima. Also, I thank my spouse Mrs Faye Saho for her patience, support and positive spirit to overcome the various challenges which have confronted me. At this juncture I think of my parents Mr Sulayman Kanteh and Mrs Nyima Sakiliba, whose sacrificial life and their great efforts with pain and tears and unceasing prayers has enabled me to reach the present position in my life. I should not forget my brothers Idrissa and Musa for their continuous love, support, understanding, and good wishes whenever I needed.

I would like to acknowledge Dr. Abubakar Sani Hassan, Dr. Seyed Hamid Reza Hosseini, Mr. Khalil Alhusiny, and Mr. Foday Danso, for their continued encouragement and support during my study. Finally, I thank all those who have helped me directly or indirectly in the successful completion of my thesis. Anyone missed in this acknowledgement are also thanked.

LIST OF PUBLICATIONS

Journal Articles

- **Sambu Kanteh Sakiliba**, Jianzhong Wu, Nick Bolton, Mahesh Sooriyabandara, The Energy Performance and Techno-Economic Analysis of Zero Energy Bill Homes, Energy and Buildings, Volume 228, 2020. <https://doi.org/10.1016/j.enbuild.2020.110426>.

Technical Reports

- X. Nan, Abeysekera. M, **Sambu Kanteh Sakiliba**, J. Wu and N. Jenkins “Recommendations for improved energy monitoring at Corby Business Academy (CBA)” District of Future Work Package 3, Cardiff University, 2015.
- Abeysekera. M, X. Nan, and **Sambu Kanteh Sakiliba** “Corby’s Participation in the FP7 District of the Future Project” Final Report 1st November 2013 – 31st October 2016, Electric Corby CIC and Cardiff University, 2016.

Other Publication

- **S. K. Sakiliba**, A. S. Hassan, E. Saja and J. Wu “Assessment of Stand-Alone Residential Solar Photovoltaic Application in Sub-Saharan Africa: A Case Study of Gambia,” Hindawi, 2015. <http://dx.doi.org/10.1155/2015/640327>.

ABSTRACT

The Business, Energy, and Industrial Strategy (BEIS), the United Kingdom (UK) government has concluded that greenhouse gas emissions should be brought to net zero by 2050[1]. To ensure completion of this goal, the government has started to use low carbon technologies (LCT) such heat pumps (ASHPs) and rooftop solar photovoltaic systems in domestic dwellings. However, this has a potential impact on low voltage electricity networks (e.g. voltage drops), and communities that also consider renewable energy technologies [2]. In this context, the presented work in this thesis evaluates the external effects of Zero Energy Bill Homes (ZEBHs) in a low voltage (LV) distribution grid and a community which produces hydrogen (H_2) through an electrolyser that works with wind and solar power. The H_2 produced dispenses for fuel cell electrical vehicles (FCEVs). The framework at both, network and community level are achieved through the development of two modelling environments as part of the Building Control Virtual Test Bed interface. The first modelling environment, MATLAB/Simulink platform, allowed LV grid and hydrogen energy simulation which integrated all aspects of the community between buildings. The second one, EnergyPlus software, provided the building energy modelling and simulation, including occupant behaviour as a boundary condition for variables such as appliance and lighting usage, and domestic hot water tap flows. There is a significant interest from academics, industry and policy makers in different parts of the world to identify and realise the opportunities of integrating buildings and community energy systems while avoiding any undesirable impacts. Hence, the aim of this research is to develop a model for the integrated modelling and analysis of buildings and community energy systems. As part of this thesis, three key components of the model were developed:

- i) **The energy modelling, calibration for validation purposes, simulation, and techno-economic analysis of a set of ZEBHs for evaluating their energy performance and zero-energy bill status.** The selected dwellings were involved in the District of Future (DoF) European Union project [3] that had strongly objectives in achieving zero energy bills. Therefore, the comparison outputs between the ZEBHs pointed out the significance of occupancy elements as a factor that can influence thermal and electrical demand. The economic assessment exerted that the zero-energy bill concept would be impractical if the UK government subsidies are withdrawn.
- ii) **The development of an integrated building and electricity platform** that allowed the link of ZEBHs and LV networks to exploit ASHP load shifting when there were voltage drops below the UK statutory limits. The results quantified the ZEBHs energy demand flexibility that can be provided to the LV network
- iii) **Development of an optimisation method to manage the energy demand flexibility of ZEBHs for a UK-based community's Hydrogen Energy System (HES)** in which the ZEBHs ASHP load (connected to a Low Voltage Distribution Network) are shifted to maximize the production of H_2 for FCEVs. It was found that when the heat pump loads were shifted it maximised the hydrogen production by 1.73% on a winter week.

LIST OF CONTENTS

| | |
|--|-----------|
| ACKNOWLEDGEMENT..... | 2 |
| LIST OF PUBLICATIONS..... | 3 |
| ABSTRACT | 4 |
| LIST OF CONTENTS | 5 |
| LIST OF FIGURES | 11 |
| LIST OF TABLES | 16 |
| NOMENCLATURE..... | 17 |
| LIST OF ABBREVIATIONS | 23 |
| 1 CHAPTER 1 – INTRODUCTION | 25 |
| 1.1 Zero Carbon Homes..... | 27 |
| 1.2 Zero Energy Bill Homes | 28 |
| 1.3 Distribution Networks Role in the UK’s Carbon Emission Reduction | 31 |
| 1.3.1 Electrical Distribution Networks..... | 31 |
| 1.3.2 Distributed Energy Resources in Low-Voltage Networks | 32 |
| 1.3.3 Residential-Scale Low-Carbon Technologies..... | 33 |
| 1.4 Integrated Community Energy Systems | 35 |
| 1.4.1 ICES Definition | 35 |
| 1.4.2 Technical Integration..... | 36 |
| 1.4.3 Energy Demand Flexibility: Concepts and Definition | 38 |
| 1.4.3.1 Concepts | 38 |
| 1.4.3.2 Definition..... | 38 |
| 1.5 Research Gaps | 39 |
| 1.6 Research Objectives..... | 40 |
| 1.7 Thesis Outline..... | 40 |
| 2 CHAPTER 2 – LITERATURE REVIEW | 44 |
| 2.1 Buildings | 44 |
| 2.1.1 Zero Carbon Homes | 44 |
| 2.1.2 Net Zero Energy Buildings..... | 45 |
| 2.1.2.1 Building Fabric Efficiency | 46 |
| 2.1.2.2 Technology Solutions..... | 47 |
| 2.1.3 Nearly-Zero Energy Buildings | 48 |
| 2.1.3.1 Cost Optimality Method..... | 49 |

| | | |
|---|--|-----------|
| 2.1.3.2 | Drivers and Barriers | 50 |
| 2.1.4 | Zero Energy Bill Homes | 50 |
| 2.1.4.1 | Concept | 51 |
| 2.2 | Distributed Energy Resources Integration in Community Energy Systems | 51 |
| 2.2.1 | Wind Turbines | 52 |
| 2.2.2 | Solar PV | 52 |
| 2.2.3 | Proton Exchange Membrane Electrolysers | 52 |
| 2.2.4 | Fuel Cell Electrical Vehicles | 53 |
| 2.2.5 | Hydrogen Storage | 54 |
| 2.3 | Integrated Community Energy Systems | 54 |
| 2.3.1 | Building-to-Community-Level Perspective | 55 |
| 2.3.2 | Building and Energy Grid Systems | 56 |
| 2.3.3 | Building Energy Demand Flexibility | 57 |
| 2.3.4 | Integrated Energy Systems | 58 |
| 2.3.5 | Energy Networks | 59 |
| 2.3.6 | Modelling Tools | 60 |
| 2.4 | Optimisation Methods | 61 |
| 2.4.1 | Problem Formulation | 61 |
| 2.4.1.1 | Function Optimisation | 61 |
| 2.4.1.2 | Decision Variables | 62 |
| 2.4.1.3 | Constraints | 62 |
| 2.4.1.4 | Objective Function | 62 |
| 2.4.1.5 | Variable Bounds | 63 |
| 2.4.2 | Optimisation Methods | 63 |
| 2.5 | Summary | 65 |
| CHAPTER 3- ENERGY PERFORMANCE AND TECHNO-ECONOMIC ANALYSIS OF ZERO ENERGY BILL HOMES | | 66 |
| 3.1 | INTRODUCTION | 66 |
| 3.2 | BUILDING MODELLING TOOL | 66 |
| 3.3 | ZERO ENERGY BILL HOMES DESCRIPTION | 67 |
| 3.4 | METHODOLOGY | 67 |
| 3.4.1. | Zero Energy Bill Homes Data Collection | 69 |

| | | |
|---|---|------------|
| 3.4.2. | Building Modelling..... | 69 |
| 3.4.3. | Weather and Climate | 69 |
| 3.4.4. | Geometry and Buildings Envelope | 70 |
| 3.4.5. | Occupancy Levels and Activity Profiles | 72 |
| 3.4.6. | Electrical Appliances and Lighting..... | 72 |
| 3.4.7. | Solar Photovoltaic Thermal Assisted Heat Pump..... | 73 |
| 3.4.7.1. | Solar Photovoltaic Thermal Panels | 74 |
| 3.4.7.2. | Air Source Heat Pumps | 75 |
| 3.4.7.3. | Hot Water Tank and Domestic Hot Water Demand..... | 77 |
| 3.4.8. | Space Heating Demand..... | 81 |
| 3.4.9. | Electrical and Net Electrical Demand | 84 |
| 3.4.10. | Data Measurement..... | 85 |
| 3.4.11. | Calibration Method..... | 85 |
| 3.4.12. | Solar PV/T Model Verification Method | 86 |
| 3.4.13. | Techno-Economic Study..... | 86 |
| 3.5. | RESULTS AND DISCUSSION..... | 88 |
| 3.5.1. | Measured Data Analysis..... | 88 |
| 3.5.2. | Measured Data vs Initial and Calibrated Model | 88 |
| 3.5.3. | Statistical Index Evaluations..... | 95 |
| 3.5.4. | Building Energy Performance..... | 97 |
| 3.5.4.1. | Electrical Energy Demand | 97 |
| 3.5.4.2. | Thermal Energy Demand..... | 98 |
| 3.5.5. | Solar PV/T Panels Energy Generated..... | 99 |
| 3.5.6. | Techno-Economic Analysis | 102 |
| 3.5.6.1. | Zero Energy Bill Assessment..... | 102 |
| 3.5.6.2. | NPV Analysis | 104 |
| 3.6. | SUMMARY..... | 104 |
| | | |
| CHAPTER 4- ANALYSIS AND QUANTIFICATION OF ENERGY DEMAND FLEXIBILITY ON LV ELECTRICAL DISTRIBUTION NETWORKS | | 107 |
| 4.1 | INTRODUCTION | 107 |
| 4.2 | OBJECTIVES..... | 108 |
| 4.3 | METHODOLOGY | 109 |

| | | |
|---|--|------------|
| 4.3.1 | Scenarios..... | 109 |
| 4.3.2 | Interface and Coupling Method..... | 110 |
| 4.3.3 | Zero Energy Bill Homes Load Demand | 112 |
| 4.3.4 | Benchmark Test Feeder Model..... | 114 |
| 4.3.4.1 | Transformer and Network Data..... | 114 |
| 4.3.4.2 | IEEE 33-Node Test Feeder Model | 116 |
| 4.3.5 | Energy Demand Flexibility Analysis | 117 |
| 4.3.5.1 | Flexibility..... | 117 |
| 4.3.5.2 | Voltage Below Limits | 118 |
| 4.4 | OPTIMIZATION MODEL..... | 118 |
| 4.4.1 | Objective Function | 119 |
| 4.4.2 | Constraint Conditions | 119 |
| 4.4.2.1 | Voltage Constraint..... | 119 |
| 4.4.2.2 | ZEBHs Water Tank Constraints | 120 |
| 4.4.2.3 | Indoor Temperature Constraints..... | 120 |
| 4.4.2.4 | ASHP ON Mode Constraint..... | 121 |
| 4.4.2.5 | ASHP OFF Mode Constraint..... | 121 |
| 4.5 | RESULTS AND DISCUSSION..... | 121 |
| 4.5.1 | Solar Photovoltaic Thermal Assisted Heat Pump..... | 121 |
| 4.5.2 | Water Tank and Indoor Temperatures | 122 |
| 4.5.3 | Net Electrical Demand..... | 122 |
| 4.5.4 | IEEE 33-Node Test Feeder | 125 |
| 4.5.5 | Energy Demand Flexibility Analysis | 127 |
| 4.6 | SUMMARY..... | 129 |
| CHAPTER 5- INTEGRATED COMMUNITY ENERGY SYSTEM WITH HYDROGEN ENERGY STORAGE | | 130 |
| 5.1 | INTRODUCTION | 130 |
| 5.2 | OBJECTIVES | 131 |
| 5.3 | ICES-H ₂ MODEL DESCRIPTION..... | 132 |
| 5.3.1 | Wind Turbine and Solar PV Panels..... | 134 |
| 5.3.1.1 | Wind Turbine Model..... | 134 |
| 5.3.1.2 | Solar PV Panels Model | 136 |

| | | |
|---------|---|------------|
| 5.3.2 | Inverters and Rectifier..... | 137 |
| 5.3.3 | Buildings Load Demand and Residual Load Calculation..... | 137 |
| 5.3.4 | Modified IEEE 33-Node Test Feeder..... | 138 |
| 5.3.5 | H ₂ Refuelling Station | 138 |
| 5.3.5.1 | Proton Exchange Membrane Electrolyser..... | 140 |
| 5.3.5.2 | Compressor | 143 |
| 5.3.5.3 | Buffer and Hydrogen Storage Tanks | 144 |
| 5.3.6 | Hydrogen Demand for Fuel Cell Electrical Vehicles | 145 |
| 5.3.7 | Operation Strategy | 147 |
| 5.4 | OPTIMIZATION MODEL..... | 149 |
| 5.4.1 | Objective Function | 149 |
| 5.4.2 | Constraint Conditions | 150 |
| 5.4.2.1 | Hydrogen and Buffer Tank Constraints..... | 150 |
| 5.4.2.2 | ZEBHs Water Tank Constraints | 150 |
| 5.4.2.3 | Indoor Temperature Constraints..... | 151 |
| 5.4.2.4 | ASHP ON Mode Constraint..... | 151 |
| 5.4.2.5 | ASHP OFF Mode Constraint..... | 151 |
| 5.5 | INTERFACE AND COUPLING METHOD..... | 152 |
| 5.6 | SCENARIOS | 154 |
| 5.7 | RESULTS AND ANALYSIS..... | 154 |
| 5.7.1 | Green Electricity Generation | 154 |
| 5.7.2 | Scenario 1 | 155 |
| 5.7.3 | Scenario 2..... | 160 |
| 5.7.4 | Comparison of Results Under Different Scenarios | 164 |
| | CHAPTER 6- CONCLUSIONS AND FUTURE WORK..... | 167 |
| 6.1 | CONCLUSIONS..... | 167 |
| 6.1.1 | Integrated Community Energy Systems with Hydrogen Storage | 168 |
| 6.2 | FUTURE WORK | 168 |
| | REFERENCES..... | 170 |
| | APPENDIX A | 183 |
| A1 | Building Fabric Data..... | 183 |
| A2 | Heat Loss Calculations | 184 |

| | |
|---|------------|
| A2.1. Manual Calculation | 185 |
| A2.2 Manual Calculation vs Simulation Results..... | 187 |
| A3 Solar PV/T Panels Modelling and Verification method | 188 |
| A3.1 MATLAB Model..... | 188 |
| A3.2 EnergyPlus Simulation Method | 190 |
| A3.3 Verification of Solar PV/T Model | 191 |
| APPENDIX B | 192 |
| B1 Transformer and Network Parameters | 192 |
| B2 Electrical Network Power Flow- Newton Raphson..... | 192 |
| B2.1. Nodal Formulation and Admittance Matrix..... | 193 |
| B2.2. Solution of Electrical Power Flow by Newton-Raphson Method..... | 197 |
| B3 Voltage Calculation Method for a Radial Network..... | 202 |
| APPENDIX C | 204 |
| C1 Electricity Generation Equipment..... | 204 |
| C2 Solar PV Panel Schematics | 205 |
| C3 Hydrogen Refuelling Station Parameters..... | 207 |

LIST OF FIGURES

| | |
|---|----|
| Figure 1-1: Reductions of fossil fuels CO ₂ by sector since 2009[5] | 25 |
| Figure 1-2: UK greenhouse gas emissions by source sector in 2011 (left) and 2018 (right) [8]..... | 26 |
| Figure 1-3: Structure of the introduction chapter..... | 27 |
| Figure 1-4: Zero carbon homes' requirements [17] | 28 |
| Figure 1-5: ZEBH concept..... | 29 |
| Figure 1-6: Features of ZEBH..... | 30 |
| Figure 1-7: Electrical distribution network | 31 |
| Figure 1-8: ICES scheme on three levels of an energy system | 35 |
| Figure 1-9: Interactions between energy vectors, coupling components, and renewable energy sources [46]..... | 37 |
| Figure 1-10: Integrated community energy system (ICES) model and thesis outline | 43 |
| Figure 2-1: Schematic representation of important concepts in an NZEB, showing the connection between buildings and energy grid [55]. | 46 |
| Figure 2-2: NZEB's technology pathways [63] | 47 |
| Figure 2-3: Minimum cost and distance to Nearly-Zero Energy [80]..... | 49 |
| Figure 2-4: Schematic representation of a PEM electrolyser [96]..... | 53 |
| Figure 2-5: Schematic representation of a PEM fuel cell (left) and Fuel Cell Electrical Vehicle (right) | 54 |
| Figure 2-6: Building-to-Community level perspective concept [103]. | 55 |
| Figure 2-7: Integrated Energy Systems [115]..... | 58 |
| Figure 2-8: Combined Heat And Power With Absorption Chiller [118] | 59 |
| Figure 2-9: Energy Network Interactions [123] | 60 |
| Figure 2-10: Optimal Design Procedure Flowchart [131] | 62 |

| | |
|--|----|
| Figure 3-1: Left- ZEBHs building aspect and Right - site plan highlighting the Electric Homes facing North-East..... | 67 |
| Figure 3-2: Overview of procedure used..... | 68 |
| Figure 3-3: Representation of the building model. a) axonometric view. b) ground floor. c) first floor | 69 |
| Figure 3-4: January winter month profile in EnergyPlus | 70 |
| Figure 3-5: Domestic dwelling floorplan views with defined zones. a) front view; b) cross-section view; c) first floor plan view; and d) and ground floor plan view..... | 71 |
| Figure 3-6: ZEBHs energy supply system..... | 73 |
| Figure 3-7: Cross section view of a PV/T collector [139]..... | 74 |
| Figure 3-8: Illustration of an air source heat pump | 76 |
| Figure 3-9: Modelled Hot Water Storage Tank. Courtesy of Electric Corby and EDP Consulting Limited[149]..... | 80 |
| Figure 3-10: EH-Plot 272 Contour Plot graph to analyse measured data..... | 89 |
| Figure 3-11: EH-Plot 273 Contour Plot graph to analyse measured data..... | 89 |
| Figure 3-12: EH-Plot 274 Contour Plot graph to analyse measured data..... | 90 |
| Figure 3-13: EH-Plot 349 Contour Plot graph to analyse measured data..... | 90 |
| Figure 3-14: EH-Plot 272 Measured vs Initial and Calibrated model..... | 91 |
| Figure 3-15: EH-Plot 273 Measured vs Initial and Calibrated model..... | 92 |
| Figure 3-16: EH-Plot 274 Measured vs Initial and Calibrated model..... | 93 |
| Figure 3-17: EH-Plot 349 Measured vs Initial and calibrated model..... | 94 |
| Figure 3-18:EH-Plot 272 NMBE and CV(RMSE) calibration results..... | 95 |
| Figure 3-19: EH-Plot 273 NMBE and CV(RMSE) calibration results..... | 96 |
| Figure 3-20: EH-Plot 274 NMBE and CV(RMSE) calibration results..... | 96 |
| Figure 3-21: EH-Plot 274 NMBE and CV(RMSE) calibration results..... | 96 |

| | |
|---|-----|
| Figure 3-22: Annual breakdown of electricity use in the Electric Homes..... | 97 |
| Figure 3-23: Annual breakdown of thermal energy use in the Electric Homes | 98 |
| Figure 3-24: Annual PV electrical and thermal energy generated in EH-Plot 272 | 100 |
| Figure 3-25: Annual PV electrical and thermal energy generated in EH-Plot 273 | 100 |
| Figure 3-26: Annual PV electrical and thermal energy generated in EH-Plot 274 | 101 |
| Figure 3-27: Annual PV electrical and thermal energy generated in EH-Plot 349 | 101 |
| Figure 3-28: EH-Plot 272 Economic analysis monthly plot | 102 |
| Figure 3-29: EH-Plot 272 Economic analysis monthly plot | 102 |
| Figure 3-30: EH-Plot 274 Economic analysis monthly plot | 103 |
| Figure 3-31: EH-Plot 274 Economic analysis monthly plot | 103 |
| Figure 3-32: NPV analysis results | 104 |
| Figure 4-1: Illustration of integrated building and electricity network model | 109 |
| Figure 4-2: Integrated Buildings and Electricity Network Framework..... | 110 |
| Figure 4-3: Controller in MATLAB/Simulink | 111 |
| Figure 4-4: System model for coupled simulation in BCVTB | 111 |
| Figure 4-5: XML file script..... | 112 |
| Figure 4-6: Total energy demand of modelled ZEBHs comprised by building type in a winter day (7 th of January)..... | 113 |
| Figure 4-7: Total average demand of modelled ZEBHs comprised by building type in a winter day (7 th of January)..... | 113 |
| Figure 4-8: Peak demand of ZEBHs comprised by building type in a winter day (7 th of January) .. | 113 |
| Figure 4-9: Building clusters diversified demand in a winter day- 7 th of January | 114 |
| Figure 4-10: Configuration of the IEEE-33 node Feeder with100 ZEBHs..... | 115 |

| | |
|--|-----|
| Figure 4-11: Scenario 1-Buildings connected in the test feeder. From top to bottom the water tank dynamic (water tank temperature, ASHP thermal power, PV/T thermal power), indoor and outdoor temperatures, ASHP electrical power and net electrical demand. | 123 |
| Figure 4-12: Scenario 2-Buildings connected in the test feeder. From top to bottom the water tank dynamics (water tank temperature, ASHP thermal power, PV/T thermal power); indoor and outdoor temperatures; ASHP electrical power, and control operation; and net electrical demand..... | 124 |
| Figure 4-13: Feeder voltage profile on scenarios 1 and 2 | 125 |
| Figure 4-14: Branches 2 and 5 active and reactive power flows for scenario 1 (top) and scenario 2 (bottom) | 126 |
| Figure 4-15: Branches 22 and 27 active and reactive power flows for scenario 1 (top) and scenario 2 (bottom) | 126 |
| Figure 4-16: Top- flexibility provided by each type of ZEB home and Bottom- average flexibility provided. | 127 |
| Figure 4-17: Top- VBL during a winter day (7 th of January) and Bottom- VBL time percentage for scenarios 1 and 2..... | 128 |
| Figure 5-1:HES model | 133 |
| Figure 5-2: Aerial image of the LCEP wind turbine. Courtesy of Bright Green Hydrogen..... | 134 |
| Figure 5-3: Power curve of the GWP47 wind turbine [185] | 135 |
| Figure 5-4: LCEP installed solar PV panels. 178 PV panels on roof of FIFE centre (left) and 440 PV panels on stadium ground. Courtesy of Bright Green Hydrogen..... | 136 |
| Figure 5-5: Modified IEEE 33-node test feeder | 139 |
| Figure 5-6: Schematic of H ₂ refuelling station..... | 140 |
| Figure 5-7: Hydrogenic PEM electrolyser installed in the LCEP. Courtesy of Bright Green Hydrogen | 140 |
| Figure 5-8: LCEP H ₂ Tank. Courtesy of Bright Green Hydrogen..... | 144 |
| Figure 5-9: Hyundai ix35 FCEV [196]..... | 145 |
| Figure 5-10: Daily driving distance distribution in the UK [197] | 146 |
| Figure 5-11:ICES-H ₂ Operation Strategy..... | 148 |

| | |
|---|-----|
| Figure 5-12: ICES-H ₂ framework..... | 152 |
| Figure 5-13: ICES-H ₂ system model for coupled simulation in BCVTB interface | 153 |
| Figure 5-14: ICES-H ₂ XML file script..... | 153 |
| Figure 5-15: Wind turbine and solar PV system electricity generated during a winter (top) and a summer week (bottom)..... | 155 |
| Figure 5-16: Scenario 1-Buildings connected in the test feeder. From top to bottom the water tank dynamics (water tank temperature, ASHP thermal power, PV/T thermal power), indoor and outdoor temperatures, ASHP electrical power and net electrical demand. | 157 |
| Figure 5-17: Scenario 1- RE generation output, ZEBHs demand, grid electricity import/export... | 158 |
| Figure 5-18: Scenario 1- PEM electrolyser power, efficiency current and voltage | 158 |
| Figure 5-19: Scenario1- Buffer tanks accumulated hydrogen and pressure, compressor H ₂ flow and H ₂ tank pressure level..... | 159 |
| Figure 5-20: Scenario 1- FCEV's distance drove, consumption and fuelled and non-fuelled cars .. | 159 |
| Figure 5-21: Scenario 2-Buildings connected in the test feeder. From top to bottom the water tank dynamics (water tank temperature, ASHP thermal power, PV/T thermal power), indoor and outdoor temperatures, ASHP electrical power and net electrical demand. | 161 |
| Figure 5-22: Scenario 2- RE generation output, ZEBHs demand, grid electricity import/export... | 162 |
| Figure 5-23: Scenario 2- PEM electrolyser power, efficiency current and voltage | 162 |
| Figure 5-24: Scenario 2- Buffer tanks accumulated hydrogen and pressure, compressor H ₂ flow and H ₂ tank pressure level..... | 163 |
| Figure 5-25: Scenario 2- FCEV's distance drove, consumption and fuelled and non-fuelled cars... | 163 |
| Figure 5-26: H ₂ tank pressure levels from scenarios 1 and 2..... | 164 |
| Figure 5-27: Comparison of IEEE 33-node test feeder voltage variations between scenarios 1 and 2 | 165 |
| Figure 5-28: a) Total H ₂ produced and b) FCEV's performance in scenarios 1 and 2 | 165 |

LIST OF TABLES

| | |
|---|-----|
| Table 1-1: Advantages and disadvantages of LCTs | 34 |
| Table 2-1: nZEB's driver and barriers | 50 |
| Table 2-2: Types of tools reviewed | 61 |
| Table 3-1: Considered building standards for modelled domestic dwellings..... | 70 |
| Table 3-2: Occupancy information | 72 |
| Table 3-3: Distributed lighting system in the residential buildings..... | 72 |
| Table 3-4: Overview of considered household appliances and their required properties for the buildings modelling..... | 73 |
| Table 3-5: PV/T Key parameters [146]..... | 74 |
| Table 3-6: ASHP parameters description..... | 76 |
| Table 3-7: DHW flow rate to calculate hot water demand..... | 81 |
| Table 3-8: Tariffs used for feasibility calculations..... | 86 |
| Table 3-9: Energy supply system cost parameters | 87 |
| Table 3-10: Economic analysis results | 103 |
| Table 3-11: Summary of 25 years NPV analysis results | 104 |

NOMENCLATURE

Roman Symbols

| | |
|----------------------------|--|
| A | electrolyser cell area in m^2 |
| a | voltage in the real component (v) |
| A_{abs} | absorber area (m^2) |
| A_{cells} | areas of the cells (m^2) |
| A_i | connected to the overall heat transfer coefficient surface area (m^2) |
| A_{surf} | area of the PV/T panel in m^2 |
| A_{surf} or A_{panels} | module area (m^2) |
| A_T | exterior surface area of the storage tank (m^2) |
| A_{onyc} | external surface of the storage tank when heat is transferred from environment and load is on in m^2 |
| A_{offyc} | external surface of the storage tank when heat is transferred from environment and load is off |
| $A_{windows}$ | windows area in m^2 |
| B | susceptance (imaginary component) in S |
| b | voltage in the imaginary component (v) |
| $BufferTankPressure_{max}$ | maximum buffer tank pressure in bars |
| $BufferTankPressure_{min}$ | minimum buffer tank pressure in bars |
| C_{H^+} | H_2 ions in PEM membrane (mol/m^3) |
| $Cost_{Elec}$ | imported electricity cost (\pounds/kWh) |
| $C_{p,air}$ | represents the specific heat capacity of the air ($J/(kg/^\circ C)$) |
| $C_{p,fluid}$ | specific heat capacity of the circulating fluid ($J/Kg^\circ C$) |
| $C_{p,water}$ | specific heat capacity of water ($4.187kJ/kg^\circ C$) |
| C_{pf} or C_p | heat capacity of the heat exchange fluid ($J/Kg^\circ C$) |
| C_{pT} | heat capacity of the storage fluid ($J/Kg^\circ C$) |
| d | number of days |
| d | discount rate (%) |
| D_{H^+} | diffusivity of H_2 ions in PEM membrane in m^2/s |
| E_{DHW} | domestic hot water load (kWh/day) |
| $Elec_{dmd}$ | electricity demand from the households (kWh) |
| $Elec_{Exp}$ | electricity exported to the grid (kWh) |
| E_o | cell efficiency (%) |
| E_t | temperature coefficient of cell efficiency ($\%/^\circ C$) |
| F | Faraday's constant (Ah/mol) |
| $f^{(n)}(x_0)$ | n^{th} derivative of f evaluated at the point x_0 |
| $FCEV$ | fuelled and non-fuelled Fuel Cell Electrical Vehicles |
| FiT_{price} | electricity tariff in (\pounds/kWh) |
| F_{LA} | equipment load factor |

| | |
|-----------------------------------|---|
| F_r | fraction of radiation transmitted through the windows (<80%) |
| FR | heat removal factor |
| F_{SL} | light special allowance factor |
| F_{UA} | equipment use factor |
| F_{UL} | light use factor |
| G | conductance (real component) in ohms ⁻¹ |
| G_T | solar irradiance (W/m ²) |
| h_0 | heat transfer coefficient for external conditions |
| H_2 TankPressure _{min} | hydrogen tank minimum pressure in bars |
| H | time horizon |
| h_{out} and h_{in} | enthalpies of the refrigerant at the outlet and inlet of the condenser (kJ/kg) |
| h_r | heat transfer coefficient for internal conditions |
| I | current (A) |
| i | index of the branch section across the feeder |
| $I_{o,an}$ and $I_{o,cat}$ | exchange current density of anode and cathode in A/cm ² |
| I_{dir} and I_{diff} | direct and diffuse solar radiation (W/m ²) |
| I_{mpp} | temperature coefficient of Cell efficiency (%/°C) |
| j | imaginary number ($\sqrt{-1}$) |
| J | Jacobian |
| k | thermal conductivity of the material layer (W/(mK)) and heat exchange coefficient between storage fluid and ambient air (W/m ² °C) |
| $k!$ | factorial of n |
| kW_e | kilowatt electrical |
| kW_{th} | kilowatt thermal |
| m | total mass of water in the tank (kg/s) |
| m_{f1} and m_{f2} | mass flow rates of fluid through the heat exchangers (kg/s) |
| m_{fluid} | mass flow rate of the circulating fluid (kg/s) |
| m_{fr} | mass flow rate of the refrigerant (kg/s) |
| m_{hw} | mass flow rate of hot water (kg/s) |
| m_{sup} | mass flow rate on the supply side of the tank (kg/s) |
| n | total number of window areas, or number of mol of H ₂ |
| N | total number of time steps or nodes |
| n ($I, J,$ and K) | codes $I, J,$ and K or total number of branches on feeder |
| n_{cells} | total number of cells |
| n_F | efficiency of electrolyser in % |
| n_{H2} | hydrogen produced in mols/s |
| NPV | net present value (£) |
| N_{PV} | total number of PV panels |
| n_s | total number of stacks |
| P | active or real power (kW _e) |
| $P.F$ | fraction of absorber plate area covered by solar cells |

| | |
|---|--|
| P_1, buffer | pressure from buffer tank |
| P_2 | optimal intermediate pressure in bars |
| P_a | rated electrical power (W) |
| P_a | Pascals |
| $P_{ASHIP,operation}$ | operation of the ASHP (ON/OFF) |
| $P_{bldg, dmd}$ | sum of the building loads (kW) |
| $P_{Buffer, Tank}$ | buffer tank pressure in bars |
| P_c | compressor rated power in kW _e |
| P_{comp} and P_{pump} | electrical power of compressor and pump (W) |
| P_{cr} | critical pressure (Pa) |
| P_D | demand active power (kW) |
| P_{dmd} | total building electrical demand in kW _e |
| $P_{elec,heat, dmd}$ | electric heating ASHPs, and the water tank immersion heaters load (kW) |
| P_G | real power generator injection (kW _e) |
| $P_{GreenElec}$ | total output electricity from wind turbine and solar panels in kW _e |
| $P_{GreenElec}$ | total power generated from solar PV system and wind turbine (kW _e) |
| P_{H2Tank} | H ₂ tank pressure in bars |
| $P_{inv,load}$ | electrical power converted from DC into AC for the homes load in kW _e |
| P_l | installed light wattage (W) |
| P_{Load} | homes load demand (kW _e) |
| P_{mpp} | nominal Power at maximum power point (W) |
| P_{net} | net electrical demand in kW _e |
| $P_{PV/T,gen}$ | power generated by the PV/T panels (kW) |
| P_R | rated power output of wind turbine generator (kW _e) |
| $P_{rated, electrolyser}$ and P_{stack} | electrolyser and stack electrical powers in W |
| $P_{rect,electrolyser}$ | electrical power converted from AC into DC for electrolyser in kW _e |
| $P_{Res,load}$ | homes residual load in kW _e supplied by the grid |
| P_T | transmitted active power (kW) |
| $PVTElec_{out}$ | electrical output from the photovoltaic thermal panels (kWh) |
| Q | reactive Power (kVA _r) |
| Q_{app} | heat gained from appliances and lighting (W) |
| Q_{cond} | condenser heat capacity (W) |
| q_{net} | net heat transfer rate to the tank water in W |
| q_{heater} | heat added by the heating element in W |
| $q_{oncyclepara}$ | heat added due to on-cycle parasitic loads (zero when off) in W |
| $q_{oncycleloss}$ | heat transfer to/from the ambient environment (zero when on) in W |
| q_{use} | heat transfer to/from the heat use side connections in W |
| q_{source} | heat transfer to/from the source side connections in W |
| Q_D | demand reactive power (kVA _r) |
| Q_{el} | heat gains in a building that are caused by appliances and lighting systems (W) |
| Q_{el} and P_{el} | electricity generated from the collectors (W) |

| | |
|---------------------------------------|---|
| Q_G | reactive power generator injection (KVA _r) |
| Q_{ground} | heat losses through the ground (W) |
| Q_{hd} | space heating demand (W) |
| Q_{hg} | heat gains (W) |
| Q_{hl} | heat losses (W) |
| Q_{hsp} | air source heat pump power consumption (W) |
| Q_{hw} | heat transferred to the heat sink (W) |
| Q_{loss} | thermal loss from the collectors due to convection and radiation (W) |
| Q_p | heat gains in a building that are caused by occupants (W) |
| Q_{sirr} | heat gains in a building that are caused by solar radiation (W) |
| Q_{solar} | net rate solar radiation absorbed by the collector (W) |
| Q_T | heat flux exchange between the storage fluid and the heat exchanger fluid (W) or transmitted reactive power (kVA _r) |
| Q_{therm} | the thermal energy collected in W |
| Q_{trans} | transmission heat losses in W |
| R | ideal gas constant (8.3144J/mol/K) or universal gas constant 8.3144621e ⁻⁵ (mol ³ /molK) |
| $R_{eq, an}$ and $R_{eq, cat}$ | anode and cathode resistances in ohms |
| R_n | cash flow (£) |
| SC_{Elec} | electricity standing charge cost (£/day) |
| sin and cos | sinus and cosinus |
| $SPVTAH_{cost}$ | solar photovoltaic thermal assisted heat pump system total cost (£) |
| T | module Temperature at Normal Operating Cell Temperature (°C), buffer and hydrogen storage tanks, or electrolyser cell temperature in K |
| t | time step or time in s |
| T_T | temperature of the water tank in °C |
| T_{abs} | temperature of the absorber plate (°C) |
| T_{air} | outdoor air temperature (°C) |
| T_{air} | ambient temperature in °C |
| $Tariff_{Elecprice}$ | exported electricity price (£/kWh) |
| t_{base} | baseline temperature (°C) |
| T_{cell} , T_{cat} , and T_{an} | cell, cathode, and anode constant temperatures (353K) |
| T_{cr} | critical temperature (K) |
| $T_{dmd, side}$ and T_{sup} | inlet fluid temperature on the demand side and outlet fluid temperature on the supply side (°C) |
| t_g | the ground temperature in °C |
| T_i | fluid inlet temperature (°C) |
| T_{i1} , T_{i2} | inlet temperatures of the heat exchanger (°C) |
| t_{ind} | indoor temperature in °C |
| t_{ind} | indoor temperature in °C |

| | |
|---------------------------------------|--|
| $T_{ind, min}$ and $T_{ind, max}$ | minimum and maximum indoor temperature in °C |
| t_o | outdoor temperatures (°C) |
| T_o | fluid outlet temperature (°C) |
| T_{o1}, T_{o2} | outlet temperatures of the heat exchanger (°C) |
| T_{source} and T_{use} | source and use water tank temperatures in °C |
| T_{out} and T_{in} | output and input mains supply water temperatures (°C) |
| t_r | indoor temperature (°C) |
| T_{tank} | water tank temperature in °C |
| $t_{tank, ASHP's shifting algorithm}$ | hot water tank temperature when the ASHP shifting algorithm is applied in °C. |
| $T_{tank, min}$, and $T_{tank, max}$ | minimum and maximum hot water tank temperature in °C |
| $t_{tank, base}$ | base temperature of the hot water tank (°C) |
| $T_{w, in}$ and $T_{w, out}$ | inlet and outlet water temperatures in °C |
| U_i | overall heat transfer coefficient (W/(m ² /°C)) |
| U_L | collector thermal loss coefficient (W/m ² °C) |
| V | volume of the house (m ³), daily volume of hot water draw (m ³ /day), voltage magnitude (v), or tank volume in m ³ |
| V_s | Source voltage at secondary side in v |
| v | wind speed (m/s) or voltage |
| V_1 | overvoltage from gas and water pressure (V) |
| V_2 | voltage from plate membrane |
| V_3 | activation overvoltage in V |
| v_{CI} | cut-in speed (m/s) |
| v_{CO} | cut-out speed (m/s) |
| $V_{electrolyser}$ | electrolyser cell terminal voltage (V) |
| V_{mpp} | nominal voltage maximum power point (V) |
| V_o | reversible cell voltage (V) |
| v_R | rated wind speed in m/s |
| V_s | voltage at secondary side of transformer (v) |
| V_T | total volume of the tank (m ³) |
| W | work done by the compressor in Joules |
| X_i | branch reactance in p.u |
| x_o | set of unknown state variables |
| y | admittance (S) |
| z | electrons transferred per ion in H ₂ or impedance in (ohms) |
| z | impedance (ohms) |

Greek Symbols

| | |
|--|---|
| θ | angle of incidence or phase angle (°) |
| θ_A and θ_Z | solar azimuth and zenith angles (°) |
| $\theta_{A, Array}$ | reflects the azimuth angles of the array |
| δ_m | PEM membrane thickness in cm |
| ρ_{air} | density of air at indoor temperature (kg/m ³) |
| η_{el} | electrical efficiency of photovoltaic thermal collector |
| $\eta_{o,e}$ | photovoltaic thermal collector effective optical efficiency |
| $\eta_{eff,system}$ | PV system efficiency (%) |
| $\eta_{eff,inverter}$ | inverter efficiency (%) |
| ρ_T | density of the storage tanks (kg/m ³) |
| θ_T | tilt angle of the array (°) |
| $\eta_{thermal}$ | thermal efficiency of photovoltaic thermal collector (%) |
| ϵ_{use} and ϵ_{source} | heat exchanger effectiveness for the heat use and source sides in W |
| $\eta_{eff,inverter}$ and $\eta_{eff,rectifier}$ | efficiency of inverter and rectifier in % |
| δ | thickness of the material layer (m) or voltage phase angle (°) |
| $\tau\alpha$ | transmittance- absorptance product |
| ph_2 and p_{o2} | anode and cathode partial pressures (bars) |
| τ_1 | starting of heating period (h) |
| τ_2 | end of heating period (h) |
| ϵ_{use} and ϵ_{source} | heat exchanger effectiveness for the heat use and source sides in W |
| ϵ | specified tolerance value (10e ⁻⁴) |
| Δ | variance |
| α_{an} and α_{cat} | anode and cathode transfer coefficients |
| arcsinh | inverse of hyperbolic sine function, |
| $\partial/\partial x$ | derivative- Leibniz's notation |
| Ω | ohms |
| γ | polytropic index, or car arrival rate |
| η_c | mechanical and motor drive efficiency (%) |
| λ | average number of cars |
| α | hydrogen flow through the compressor (moles/s) |

LIST OF ABBREVIATIONS

| | |
|-----------------|--|
| AC | Alternating Current |
| ACH | Air Changes per Hour |
| AI | Artificial Intelligence |
| <i>ASHP</i> | Air Source Heat Pump |
| BCVTB | Building Control Virtual Test Bed |
| BEIS | Business, Energy, and Industrial Strategy |
| BIPE | Buildings Performance Institute Europe |
| BLAST | Building Loads Analysis and System Thermodynamics |
| <i>BRE</i> | Building Research Establishment |
| <i>CA</i> | Concerted Action |
| CAD | Computer Aided Design |
| CCHP | Combined Cooling Heat and Power |
| <i>CHP</i> | Combined Heat and Power |
| CIBSE | Chartered Institution of Building Services Engineers |
| CO ₂ | Carbon Dioxide |
| DC | Direct Current |
| DCLG | Department for Communities and Local Government |
| <i>DER</i> | Distributed Energy Resources |
| <i>DHW</i> | Domestic Hot Water |
| <i>DP</i> | Dynamic Programming |
| <i>DNO</i> | Distributed Network Operator |
| DOE | Department of Energy |
| <i>ECBCS</i> | Energy Conservation in Buildings and Community Systems |
| EH | Electric Homes |
| EHP | Electric Heat Pump |
| EMS | Energy Management System |
| EPBD | Energy Performance Buildings Directive |
| EPW | EnergyPlus Weather |
| ESI | Energy System Integration |
| EU | European Union |
| FC | Fuel Cells |
| FCEV | Fuel Cell Electrical Vehicles |
| <i>FEES</i> | Fabric Energy Efficiency Standards |
| <i>FiT</i> | Feed in Tariff |
| <i>GHG</i> | greenhouse gas emission |
| GUI | Graphical User Interface |
| <i>GW</i> | Gigawatt |
| HAWT | Horizontal-Axis Wind Turbine |
| <i>HES</i> | Hydrogen Energy System |

| | |
|---------------|---|
| <i>ICES</i> | Integrated Community Energy System |
| <i>IDEAS</i> | Integrated District Energy Assessment by Simulation |
| <i>IEA</i> | International Energy Agency |
| <i>IEEE</i> | Institute of Electrical and Electronics Engineers |
| <i>LCT</i> | Low Carbon Technologies |
| <i>LCEP</i> | Levenmouth Community Energy Project |
| <i>LP</i> | Liner Programming |
| <i>LV</i> | Low Voltage |
| <i>MILP</i> | Mixed Integer Linear Programming |
| <i>NLP</i> | Non-Liner Programming |
| <i>nZEB</i> | Nearly Zero Energy Buildings |
| <i>NZEB</i> | Net Zero Energy Building |
| <i>OF</i> | Objective Function |
| <i>PEM</i> | Proton Exchange Membrane Electrolyser |
| <i>PEM</i> | Proton Exchange Membrane |
| <i>PV</i> | Photovoltaic |
| <i>PV/T</i> | Photovoltaic thermal |
| <i>PV/T</i> | Photovoltaic Thermal |
| <i>RE</i> | Renewable Energy |
| <i>RES</i> | Renewable Energy Sources |
| <i>SHC</i> | Solar Heating and Cooling |
| <i>SPVTAH</i> | Solar Photovoltaic Thermal Assisted Heat Pump |
| <i>U.S</i> | United States |
| <i>UK</i> | United Kingdom |
| <i>ZCH</i> | Zero Carbon Homes |
| <i>ZEB</i> | Zero Energy Buildings |
| <i>ZEBH</i> | Zero Energy Bill Homes |

CHAPTER 1 – INTRODUCTION

Since the call released for the Climate Change Act in 2008, the population in the United Kingdom (UK) has witnessed, over the past few years, a reduction in the use of fossil fuels. Fossil fuel usage has reduced with a shift to cleaner sources that entails the use of low-carbon technology (LCT). The reduction in coal consumption in the past years has significantly affected the carbon footprint, whose major driver in the early 1990s was the consumption of gas[3][4] .

Since 2009, as shown in Figure 1-1, each fossil fuel has contributed to the overall decline in total carbon dioxide (CO₂) emissions from fossil fuels [5][6]. The reduction in coal consumption in the past decade has been responsible for the largest reduction in CO₂ emissions in the UK [7].

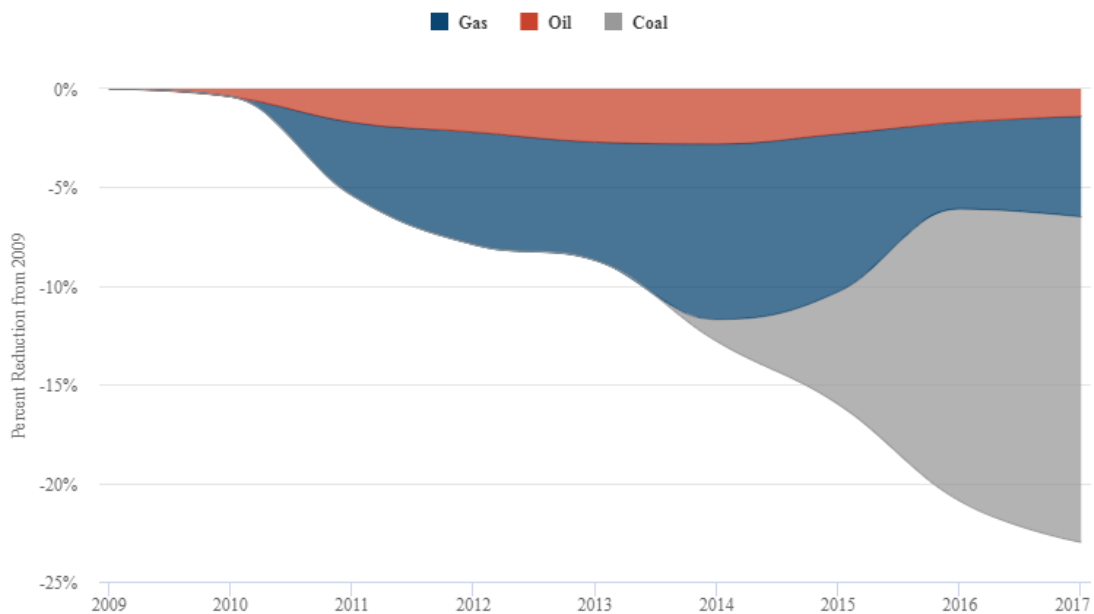


Figure 1-1: Reductions of fossil fuels CO₂ by sector since 2009[5]

Figure 1-2: UK greenhouse gas emissions by source sector in 2011 (left) and 2018 (right) [8].

presents an example of a greenhouse gas emissions in which the energy and transport supply percentage ratios appear to have dominated since 2011 [8][9].

Furthermore, in June 2019, the Business, Energy, and Industrial Strategy (BEIS), announced that the UK government has concluded that greenhouse gas emissions should be brought to net zero by 2050 as compared to the quantity used in 1990 [10][1] .

In many sectors of the UK economy, technologies exist that can bring emissions to zero. For instance, in electricity, this can be done by using renewable energy technologies. Vehicles that runs on hydrogen, well-insulated homes and industrial processes based on electricity can all help to bring sectoral emissions to absolute zero. Therefore, the motivation of this thesis was to present

technological options at community level that can contribute for to reduce greenhouse gas emissions in the UK, hence, becoming ‘net zero’ for the economy as a whole.

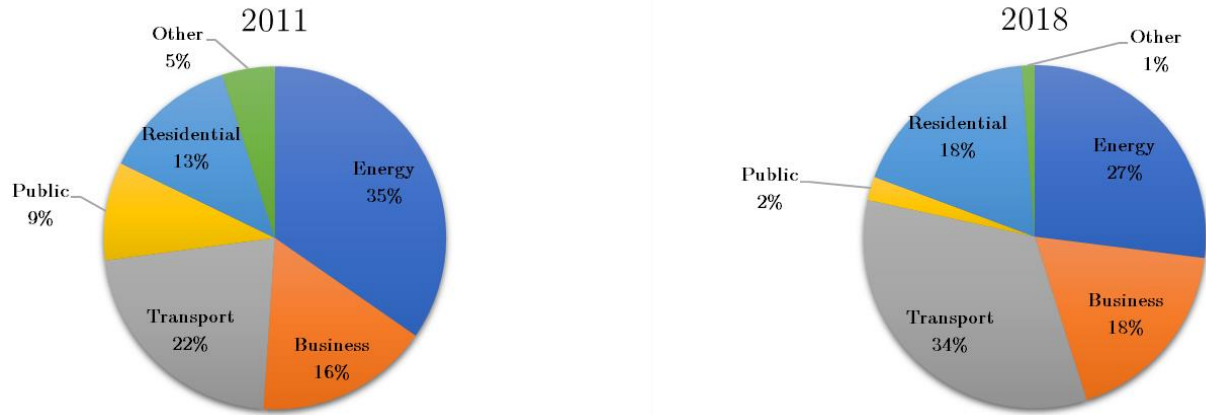


Figure 1-2: UK greenhouse gas emissions by source sector in 2011 (left) and 2018 (right) [8].

To ensure completion of this goal, the government has also started to use LCT in buildings. It has also urged the UK government to increase the envelope insulation level of buildings [2] in order to reduce the space heat demand and implement other LCT such as heat pumps in domestic dwellings.

This thesis presents an Integrated Community Energy System (ICES) as an essential part of the UK’s energy system. ICES can basically comprise several groups of community initiatives, such as power generation and sharing, local generation, and trading. It can also consider grid connectivity, society, and location (e.g.: rural, urban).

However, the concept of ICES in this thesis is focused on the use of the following:

- a) Electrical distribution networks
- b) Renewable energy systems
- c) Residential buildings with on-site microgeneration
- d) Electrical vehicles

Section 1.4 of this chapter details the concepts (definition and technology integration) of ICES that were considered in this thesis. In addition to this, **Chapter 2** presents a literature review that investigates the notion, renewable energy technologies, integrated energy systems and modelling tools of ICES. Figure 1-3 illustrates a flowchart of the topics discussed in this Chapter.

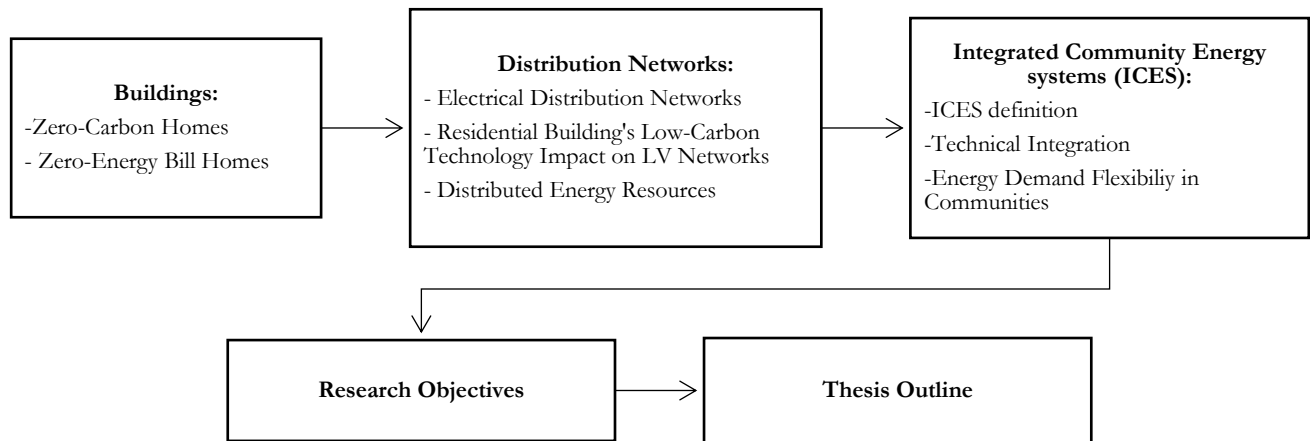


Figure 1-3: Structure of the introduction chapter

1.1 ZERO CARBON HOMES

The UK is called to implement the Energy Performance Buildings Directive (EPBD) with respect to energy performance in buildings [11][12]. This particular directive outlines the initial phase of guidelines of several areas that a nation can adhere to enhance energy efficiency. The first phase of the EPBD – Concerted Action (CA) – was implemented in June 2007 that embedded new actions to supplement the European Union (EU) countries.

After three years of initiation, the second phase was implemented. Upon revision of the EPBD, the second phase in 2010 declared that new buildings, occupied and owned by public authorities, must be Nearly Zero Energy Buildings (nZEB)¹ after 31 December 2018, and all new buildings ought to be nZEB by 31st December 2020 (Directive 2010/31/EU) [13].

The implementation of the EPBD in the UK is the responsibility of the Department for Communities and Local Government (DCLG), Department of the Environment, Food and Rural Affairs (DEFRA), and the BEIS [14]. With the enactment of the Climate Change Act in 2008 to minimise carbon emissions from residential constructions [10], the DCLG proposed a principle that stipulated that all newly constructed homes should be ‘*zero carbon homes*’ from 2016 onwards [15]–[17] to serve not only as guidance but also as compliance standards in understanding the initiative of ‘*zero carbon homes*’.

¹ The term nZEB, as defined by the Buildings Performance Institute Europe (BPIE), is used commercially to define energy-efficient buildings that are able to generate energy (electrical/thermal) to compensate for its energy demand.

The zero carbon homes initiative is closely aligned with the revised EPBD (Directive 2010/31/EU) [17] that demands all new buildings to be nZEB from the year 2020. However, such actions only weigh in CO₂ emissions from regulated energy use. Figure 1-4 portrays a diagram that reflects this approach and suggests improvisation [18].

The first definition of a zero-carbon home in the UK was a home achieving Level 6 of the Code for Sustainable Homes. This included emissions of both regulated energy (space heating, hot water, lighting, and ventilation) and unregulated energy (using appliances and cooking).

The essential requirements for homes to qualify as zero carbon have been listed as follows:

1. High levels of energy efficiency with the lowest limit of Fabric Energy Efficiency Standards (FEES)
2. LCTs to minimise carbon emission
3. Off-site and on-site energy generation solutions where it is not possible to reduce regulated carbon emissions to zero

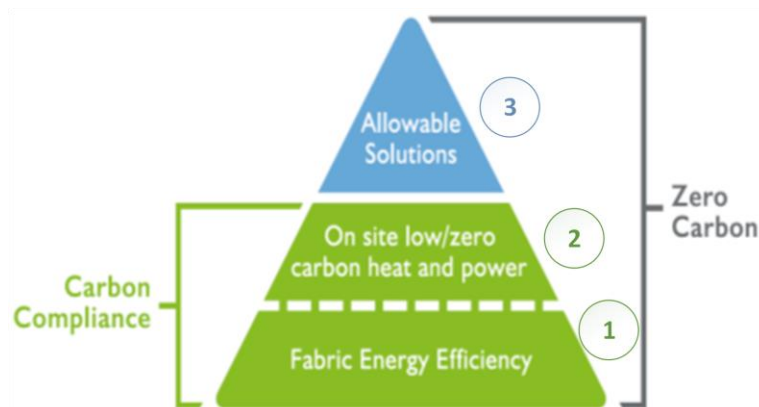


Figure 1-4: Zero carbon homes' requirements [17]

1.2 ZERO ENERGY BILL HOMES

A novel concept recently adopted in the UK town-Corby under an EU project called “the District of Future (DoF)” is the Zero Energy Bill Home (ZEBH) [3]. These homes are domestic dwellings that generate as much energy as possible through solar photovoltaic (PV) systems so that the annual energy bill is zero. These dwellings include building material with low U-values², storage systems (thermal), heat pumps, and solar PV panels on the roof. A zero energy bill can be achieved with the UK’s Feed-in-Tariff Scheme (FiT) and the export of excess electricity to the electricity grid [19]. This thesis develops a framework to introduce the novel concept of ZEBHs.

² U-values (sometimes referred to as heat transfer coefficients or thermal transmittances) are used to measure the effectiveness of the elements of a building’s fabric as insulators. In other words, U-values measure how effective they are at preventing the transmission of heat from the inside of a building to the outside.

To meet the requirements of ZEBH, the total amount of energy generated by a building's solar PV system should be able to cover the occupants' needs and send the excess energy that is generated back to the grid (see Figure 1-5).

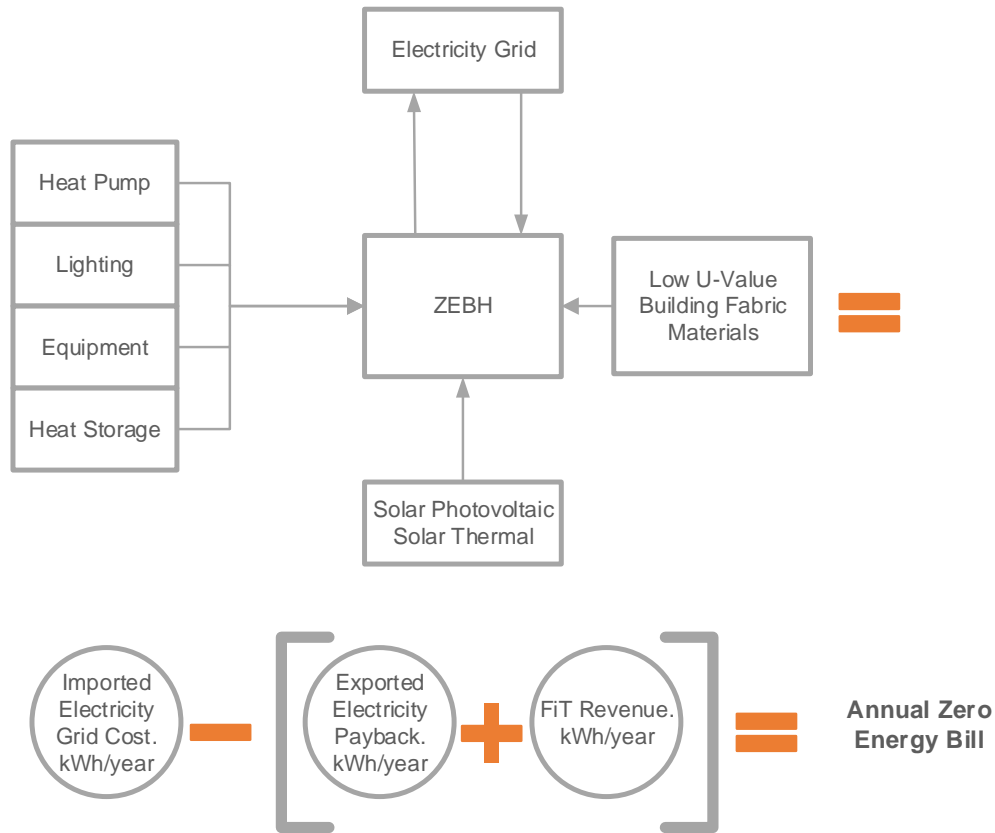


Figure 1-5: ZEBH concept

To ensure the feasibility of ZEBH, an economic assessment should be conducted; thus, the following factors should be considered:

1. The cashback revenue of every electricity unit that is generated
2. The financial reward for every excess unit that is exported to the grid
3. The cost of electricity unit imported to cover the demand when no electricity is generated by the PV panels (e.g., during nights)
4. The period of time in which only solar power is used without importing electricity from the grid
5. The capital expenditure on a solar PV system and maintenance costs against the income generated during its lifetime

Through building-grid interaction, the ZEBH becomes an active part of the renewable energy infrastructure. A ZEBH has unprecedented potential to transform the way buildings use energy. The advantage of ZEBH is the possibility of exclusion of occupants from future energy price increases. In addition, reduced thermal loss in buildings helps in keeping indoor temperatures constant for a longer period due to a reduction in the building envelope's U-values.

In summary, besides the UK FiT and revenues from exporting electricity to the grid, the annual zero energy bill of a ZEBH is achieved through a combination of solar technologies, heat pumps, combined heat and power technology (e.g., solar PV thermal panels), and energy-efficiency measures such as high insulation levels of building fabric to reduce space heating demand. Figure 1-6 depicts the main features of a ZEBH.

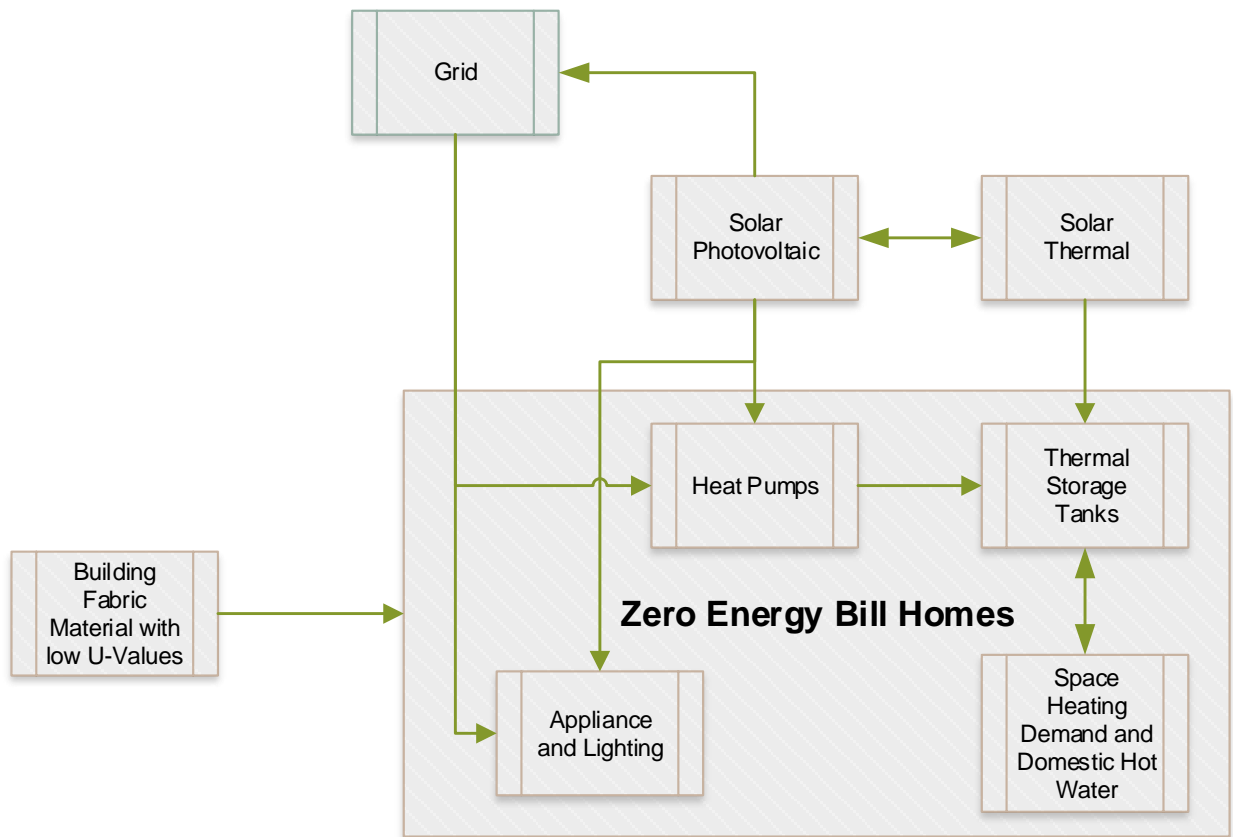


Figure 1-6: Features of ZEBH

1.3 DISTRIBUTION NETWORKS ROLE IN THE UK'S CARBON EMISSION REDUCTION

The Intergovernmental Panel on Climate Change introduced targets to decrease anthropogenic carbon emissions and made them the top priority for many governments, including the UK [20]. Subsequently, the UK has committed to supply approximately 30% of the electrical demand through renewable energies by 2020 [21]. This sense of urgency to reduce emissions is the main driver in the UK for the promotion of Distributed Energy Resources (DER) and LCTs for residential customers, with the corresponding connection of these technologies at the low-voltage (LV) distribution network level.

To gain a greater understanding of DER and LCTs, this section presents the definitions and outlines the main characteristics of these networks.

1.3.1 Electrical Distribution Networks

An electrical distribution network, according to European legislation, refers to electrical systems that are supplied by one or more voltage sources, including all radially operated systems. The Electricity Safety, Quality, and Continuity Regulations in the UK states the following:

“Network means an electrical system supplied by one or more sources of voltage and comprising all the conductors and other equipment used to conduct electricity for the purposes of conveying energy from the source or sources of voltage to one or more consumer’s installations, street electrical fixtures, or other networks...” [22].

Electrical power is distributed based on a hierarchical voltage level method; simultaneously, the voltages that operate from supply to load decrease. As depicted in Figure 1-7, these electrical networks serve as an agent that supplies the generated electricity to end-users. A distribution network is composed of a step-down, on-load, tap-changing transformer of 33kV/11kV at a major supply point and a series of step-down and three-phase transformers of 11kV/430V. Finally, electricity is supplied to the three-phase and four-wire network with 240V single-phase supplies to houses and similar loads [23].

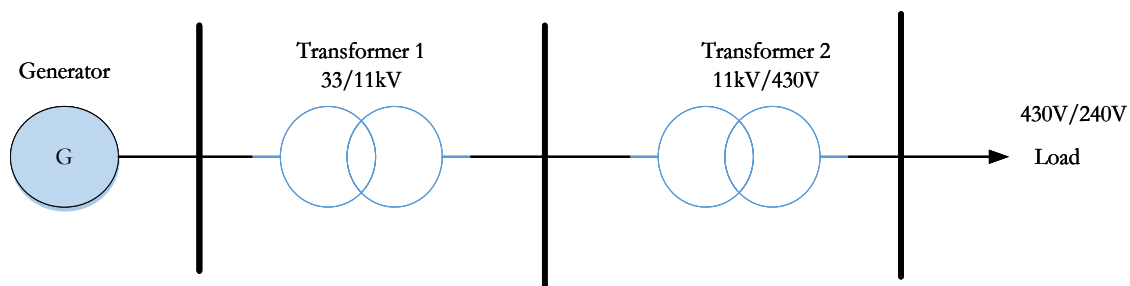


Figure 1-7: Electrical distribution network

1.3.2 Distributed Energy Resources in Low-Voltage Networks

DER is a term that encompasses an array of energy generating, storing, monitoring, and controlling solutions [24]. DER can be tailored to very specific requirements and user applications, including ensuring energy efficiency, security of supply, and carbon reduction.

The issue of global climate change has renewed interest in the deployment of DER. Furthermore, technical and economic benefits, along with changing energy policies and new technologies, have significantly added to the renewed interest in DER deployment globally. For example, in 1999, there was less than 0.7 GW of energy being supplied by installed solar PV systems globally; this number has now risen to 40 GW, with a cumulative PV capacity of 180 GW [25].

From the perspective of Distribution Network Operators (DNO)³, intermittent deployment of DER in networks from solar and wind can be of technical and economic benefit. However, high penetration of DER, along with an unprecedented growth in demand, has created challenges in the distribution network, such as overloading of distribution transformer, loss of power, rise in voltage, and drops in voltage [26]. The LV networks in the UK have witnessed significant changes in the last 20 years as a result of privatisation of the electricity sector, changing climatic conditions, and the increased adoption of DER [27].

It should be noted that the role of fossil fuel-based thermal power plants in future network systems is changing due to climate change policies.

Significant efforts have been put into investigating new pathways for the efficient integration of DER into future electricity network supply systems. However, there is a need to focus on smart energy systems that integrate the electricity, heating, and transport sectors to effectively maximise the use of fluctuating renewable energy sources [28].

Improvements in future LV networks may involve the integration of the following technologies into the traditional system [29]:

- Energy storage: battery, hydrogen, and thermal storage tanks
- Electrical vehicles
- Building microgeneration
- Virtual power plants
- Power generation: wind energy, biomass, hydro power, and combined heat and power technology

³ DNO maintains the distribution networks infrastructure in an asset-based investment manner. The role of DNO is completely regulated, and no commercial operation is possible.

1.3.3 Residential-Scale Low-Carbon Technologies

The UK has taken serious action against carbon emission by considering it as the top agenda of the country after careful observations of all the instructions and compliance highlighted in the zero-carbon homes target. The main target of the government's plan is to develop a flexible and smart energy system for the successful establishment of zero-carbon homes [30]. Ofgem is an energy regulating agency that, along with the government, is committed to ensuring the successful working of energy systems for domestic and business purposes. Smart and flexible energy systems are beneficial for both consumers and the overall economy. Currently, with the development of LCTs (e.g., solar PV panels), customers usually need to be connected with the distribution networks and have experience with the same type of services; therefore, the generation of electricity is no longer limited to power stations because consumers have now also become prosumers, as they can generate electricity on their own [31].

The campaign to reduce the emission of carbon from the environment has increased the need for energy-efficient homes and now, customers are more interested in using electricity to heat their houses and business offices [32]. Currently, natural gas is the main source of domestic heat in the UK, but it is expected that the future will be quite different, as heating electrification will be replaced by natural gas on a larger scale for both commercial and domestic use. By 2050, the UK is expected to meet up to 80% of the carbon reduction target, including the electrified supply of heat. The most common key technology will be heat pumps with the ability to deliver 80–90% of total heating [33].

As an end-user with an increased reliance on electricity, there will be an increase in the expectations of meeting the demand. End-users will have more expectations, and they will want a more efficient and responsive power supply service to meet their needs while understanding their demand priorities. For many domestic households, however, their needs will remain limited to the purpose of how to *'keep the lights on'*. For those who are interested in using the network, it is important to understand how they connect to it and how quickly they understand the system to take advantage of most of the known opportunities.

The major concern of household customers will be the pricing arrangement, which is why the adoption of LCTs will be more affordable. Most of the LCTs found in the UK are combined with renewable energies from solar panels and low-carbon heating supply from electric heat pumps. Table 1-1 illustrates the advantages and disadvantages associated with these technologies.

Table 1-1: Advantages and disadvantages of LCTs

| Technology | Advantages | Disadvantages |
|-------------------------|--|---|
| Heat Pumps | <ul style="list-style-type: none"> • Environment-friendly/lower carbon footprint than fossil fuel systems, i.e. boilers • Offers both heating and cooling with one system • Long lifespan (e.g., 20 years) • No fuel storage | <ul style="list-style-type: none"> • High demand for electricity • Unable to contract CO₂ savings without decarbonisation of grids • High initial cost and limited heat output |
| Solar PV | <ul style="list-style-type: none"> • Reduction in CO₂ generation/a typical solar PV system in a single UK house can save almost a tonne of CO₂ pollution every year [34]. • Long lasting and highly reliable • Provides clean, green energy[35] | <ul style="list-style-type: none"> • Consequently, intermittency and unpredictability of solar energy make solar PV panels a less reliable solution. • Solar energy panels require additional equipment (e.g., inverters) |
| Solar Thermal | <ul style="list-style-type: none"> • Commonly used by stable industries (UK) that use renewable energy sources • Affordable and simple | <ul style="list-style-type: none"> • Needs supplementary heating due to its seasonal demand |
| Solar PV Thermal | <ul style="list-style-type: none"> • Allows simultaneous production of electricity and heat • Efficient in generating electricity in hot climatic conditions • Requires minimal maintenance | <ul style="list-style-type: none"> • The payback period is long. • Expensive during installation, as it requires connections for thermal and electrical supply |

In the near future, an increase in the installation of LCTs is expected, most preferably in homes because they are already linked with LV distribution networks. The major concern is that the installation of new LCT systems in bulk, along with LV feeders, may cause some technical issues. For instance, it may cause overloading of transformers or cables or even a significant drop/rise in voltage levels in the network [36]. Typically, the method of *'fit and forget'* is applied by DNOs, and nowadays seems that there are a lot of difficulties in undermining the integration of domestic-level LCTs into traditional and conventional network systems due to the inactive and old features of these networks and a severe presumption that disregards change. Moreover, traditional systems are designed using the top-down approach, connecting electricity from generation to transmission to the end-user. Thus, the distribution system is designed without considering the bottlenecks. To this date, this approach is troublesome and may become burdened (e.g., reverse power flow from solar PV) by the increase in application and implementation of LCTs.

Therefore, it is essential to determine the uncertainties associated with the placement and size of microgeneration load at the domestic level to better understand behavioural patterns. A better method is to have a high-resolution representation of LCTs (e.g., air-sourced heat pumps), as it offers a foundation to better understand electricity grid connection to associated LCTs and thus, how they influence an electricity network.

1.4 INTEGRATED COMMUNITY ENERGY SYSTEMS

The growing demand for sustainable energy by domestic consumers has significantly impacted low-carbon energy systems after its importance was promoted by the local energy initiative agencies [37]. To increase the worth and importance of these energy systems, it is essential to combine multiple energy systems in the form of communities through the common means of renewable energy consumption at local levels. As such, an ICES scheme (Figure 1-8) is presented in this thesis, in which three levels are covered:

- i) Household Level
- ii) Community Level
- iii) Renewable Energy Level

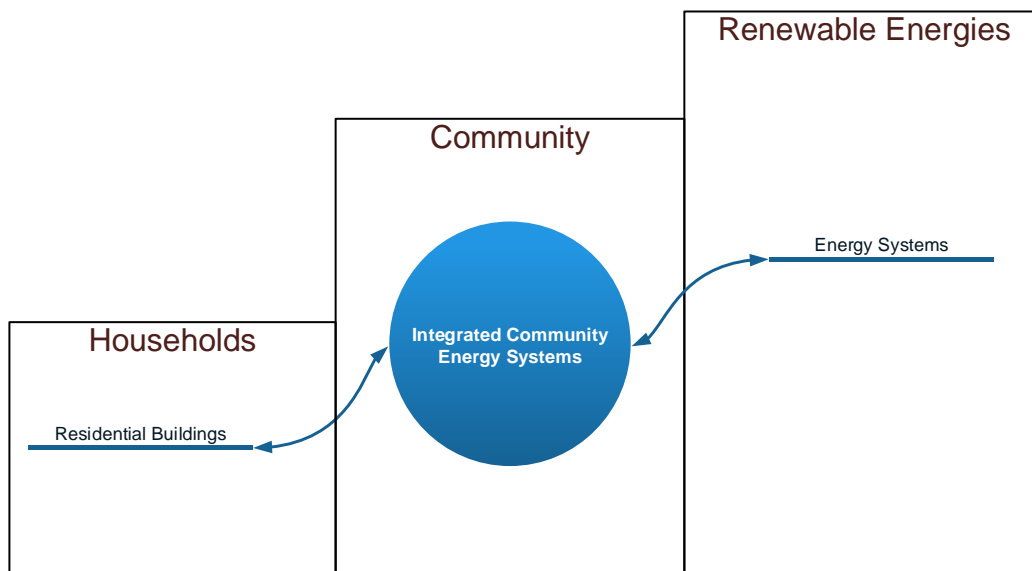


Figure 1-8: ICES scheme on three levels of an energy system

1.4.1 ICES Definition

In the context of this thesis, ICES is defined as a heterogenous approach to meet a local community's energy requirements by using technology capable of operating multiple energy systems simultaneously (i.e., electricity, hydrogen), coupling renewable energy technologies with energy storage solutions, and adopting electric vehicles and demand side measures. A more detailed concept of ICES has been demonstrated in **Chapter 5** with a real case study of a community in Levenmouth, Scotland.

Another feature of the ICES is that it can take advantage of cross-sectorial opportunities in areas of infrastructure, building, land, and transportation. This can increase energy security and reduce greenhouse gas emissions; this can also result in an enhancement of the quality of life of residents and a realisation of financial benefits for them [38].

1.4.2 Technical Integration

The ICES is different from other conventional energy systems because of its ability to engage local communities. It offers more bargaining power to the consumers by allowing communities to switch and purchase its energy and energy-related products collectively. It is easier to develop a local consumer–prosumer energy exchange platform in a liberalised market, pushing them to develop such energy systems that are based on community exchange [39]. It should be noted that the acceptance of an integrated energy system is directly dependent on the engagement of citizens as individuals and as a community. ICES can also help to fight for energy poverty, keeping local revenue for the local economy. Another social and economic benefit is that it does not only provide opportunities and jobs locally but also develops trust and identity among them, which is very important to ensure the prevalence of a sense of community among people to build stronger communities [40].

The development and installation of ICES involve planning, system designing, implementing the system, and finally, governing the developed energy system at the community level. It can maximise energy performance and cut costs, along with reducing bad environmental impacts [41]. The advancement in energy-related supply technologies also provides different viable options to integrate varied energy vectors to correspond to the demand and supply of energy in the form of ICES [42]. Energy should be supplied through cogeneration and trigeneration⁴, coupled with technologies that are capable of generating power with renewable energy systems. Figure 1-9 shows an example of how multiple energy systems can interact in communities.

Although many studies have been conducted on the shift in energy approach to the ICES system in recent years, only a handful of them has been integrated into practical application as compared to studies on isolated systems. Moreover, there is a severe need to investigate the role of domestic dwellings and communities in the present system in relation to its overall impact on multiple energy systems[43]–[45].

⁴ Cogeneration or combined heat and power is the use of a heat engine or power station to generate electricity and useful heat at the same time. Trigeneration or combined cooling, heat, and power (CCHP) is the process by which some of the heat produced by a cogeneration plant is used to generate chilled water for air conditioning or refrigeration.

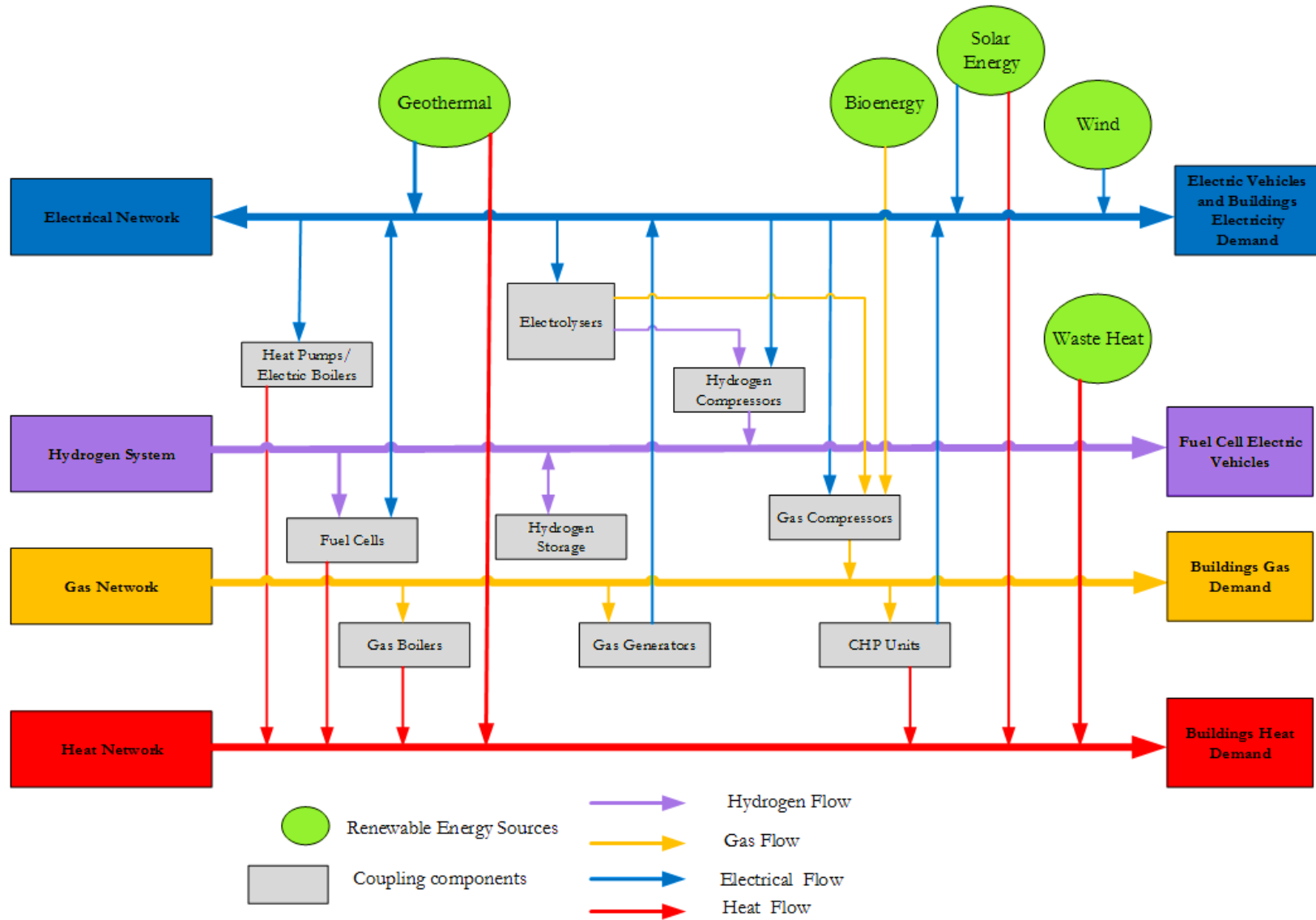


Figure 1-9: Interactions between energy vectors, coupling components, and renewable energy sources [46]

1.4.3 Energy Demand Flexibility: Concepts and Definition

1.4.3.1 Concepts

Energy demand flexibility is essential to manage the demand for energy from residential buildings based on user demands and requirements of energy grids. It can be attained in several ways, for instance, by equipping buildings with thermal mass to allow storing a certain amount of heat. In this case, thermal mass heat storage can be applied to change the demand-delaying active heating for a particular timeframe without affecting the thermal comfort in the building.

A typical method of storing energy that adds to energy demand flexibility is domestic hot water tanks. They can be pre-heated in abundance prior to a low-demand circumstance. The excess heat can also be used to heat space. In short, modelling buildings with heat storage methods, such as thermal water storage tanks combined with LCTs (heat pumps), is important to investigate their impact in ICES.

The awareness that energy demand flexibility can give seems to be of utmost significance in terms of developing community energy systems and buildings. Additionally, it is essential for utilities, policymakers, and government entities to work for the betterment of future community energy systems.

1.4.3.2 Definition

From the aforementioned concepts, it may be easy to define energy demand flexibility, but the same cannot be said for its quantification. **In this thesis, energy demand flexibility is defined as follows:**

“The quantity of energy demand that can be shifted during a period of time with the use of intrinsic heat storage in buildings for the provision of ancillary services without compromising the thermal comfort of the occupants in a community”.

Flexibility is significant for its ability to address several uncertainties that may occur within an energy supply system (e.g., a distribution network). In the framework of this thesis, energy demand flexibility was quantified by quantifying the consumed load that can be shifted during a certain period. Furthermore, the case studies presented in the thesis have looked into the association between the flexibility and thermal comfort of building occupants.

1.5 RESEARCH GAPS

1. After reviewing the literature on buildings (Zero Carbon Homes, Net and Nearly Zero Energy Buildings; and Zero Energy Bill Homess) in **Chapter 2**, it was found that in Net Zero Energy Buildings (NZEBS), there is a gap between energy savings and their cost that limits houses from becoming NZEBs. However, ZEBHs fill this gap by maximising FiT revenue streams for solar PV generating systems within customer premises. In this way, households can benefit from the UK's FiT system and achieve a ZEBH status by producing more electricity than they need. However, there was a lack of research on suitable techniques to evaluate the value of ZEBHs (i.e., benefits from the UK FiT). **Chapter 3** presents a model and simulation of a ZEBH, demonstrating the zero-bill status concept with the aid of an economic analysis.
2. In addition, in **Chapter 2**, building surveys and electrical networks with DER have been reported to achieve different objectives. However, the value of a ZEBH with the potential for electricity grid interaction and different LCTs in communities that consider renewable energy systems has not been explored. Therefore, this study investigates the benefits of a ZEBH with grid interaction capability and an energy demand flexibility option in a community energy system with DER (as presented in the **Chapter 4**).
3. It should also be noted that in **Chapter 2**, the benefits that energy vector interaction can provide have been identified as important in evaluating the benefits of renewable energies in integrated community energy systems. However, techniques to evaluate the benefit of a multi-period heuristic energy vector simulation for communities with distributed generation, electrical vehicles, and ZEBHs with and without energy demand flexibility were not explored. Therefore, in this thesis, operational benefits (in terms of voltage profiles) of a low-voltage distribution network and of maximising hydrogen fuel production for FCEVs in a community have been quantified and reported in **Chapter 5**. For this purpose, an optimisation technique was developed and simulated to evaluate these benefits. Evaluating the impact of optimised integrated community energy systems (with buildings, electrical networks, and FCEVs) can benefit distributed network operators, electrical vehicle owners, and households. However, in the surveyed literature, techniques to evaluate integrated community energy systems have only been explored from one perspective. Therefore, in this thesis, a linking procedure has been designed to evaluate the impact (in terms of building level, voltage profiles, and hydrogen production to dispense FCEVs) of an optimised energy system on a community (as presented in **Chapter 6**).

1.6 RESEARCH OBJECTIVES

The transformation of the UK's energy sector is being driven by technological innovation; however, disruptions are taking place at the intersection of distribution networks and households in communities. The objective of this thesis is to present an optimal integrated community energy system that considers the use of Fuel Cell Electrical Vehicles (FCEVs), hydrogen production, wind and solar power, LV electricity networks, and ZEBHs. The objective of this research has been detailed as follows:

- Assess and quantify how much energy demand flexibility the ZEBHs can provide to LV electricity networks and communities based on household demands and requirements of the electrical network while managing the needs of energy (electricity, heat, domestic hot water, and FCEV's fuel demand)

Furthermore, in an attempt to cater to energy demand flexibility studies focussing on communities, a gap was observed in integrated community energy systems that combine renewable energy supply systems, energy vectors, and buildings. As such, this thesis proposed an integrated model and analysis of buildings and community energy systems that incorporated the following core aspects:

- The modelling, validation, energy performance analysis, and feasibility study of ZEBHs
- The development of an optimisation approach that enables the quantification of energy demand flexibility of ZEBHs connected on LV electrical networks
- The development of an optimisation method to manage the energy demand flexibility of ZEBHs for a UK-based community's Hydrogen Energy System (HES), in which hydrogen storage, FCEVs, and an electrical distribution network were considered

1.7 THESIS OUTLINE

This thesis adheres to the structure of any fundamental research, as illustrated in

- **Chapter 1** – Introduction:

This chapter discusses the UK's energy system and carbon emission reduction targets. Furthermore, it introduces the concept of zero carbon homes and the role of the UK's distribution networks in the greenhouse gas emission reduction target. ZEBH has also been presented as a new notion in the UK's building sector. Finally, the concepts of ICES and energy demand flexibility of buildings have been highlighted.

– **Chapter 2** – Literature Review:

This chapter reviews the relevant literature related to this thesis. It presents the background and state of the art for studies presented in **Chapters 3, 4, and 5**. Furthermore, this chapter presents an overview of the following: (i) zero-carbon homes, zero energy buildings, and ZEBH, (ii) integration of DER into community energy systems, (iii) ICES, and (iv) modelling tools for integrated energy systems.

– **Chapter 3** –Energy Performance and Techno-Economic Analysis of Zero Energy Bill Homes:

The chapter elaborates on the building energy modelling of residential buildings in a community. Additionally, this chapter discusses the modelling of residential buildings, solar PV/T-assisted heat pumps, heat emitters, and occupant behaviour. Furthermore, a building modelling calibration method and a feasibility study are presented to confirm the hypothesis regarding ZEBH.

– **Chapter 4** –Analysis and Quantification of Energy Demand Flexibility in Low-Voltage (LV) Electrical Distribution Networks:

This chapter depicts the processes involved in developing a simulation platform that supports building modelling, control systems, and LV electrical networks. The link between the ZEBHs and LV network allowed the use of building energy models, inclusive of internal energy supply systems, in association with external energy supply systems such as an electrical grid. It, therefore, permitted the simulation of an integrated building and electricity network. The simulation of the system portrayed an environment for an air source heat pump's (ASHP) load shifting strategy that was tested on the platform to assess the energy demand flexibility of a ZEBH when the voltage drops in the network. In this case, the Institute of Electrical and Electronics Engineers' (IEEE) 33-node test feeder was considered.

The voltage profile was evaluated based on the 2002 UK Electricity Safety, Quality, and Continuity Regulations' distribution network's steady-state voltage statutory limits. These limits are + 10% (upper limit) and 230V – 6% (lower limit) [47].

– **Chapter 5** – ICES with Hydrogen Storage:

This chapter presents the optimal implementation of a hydrogen energy system to analyse the hydrogen system with local energy systems. The chapter demonstrates the operation of renewable energy technologies (a wind turbine and a solar PV system) integrated with HES in supplying electrical energy to ZEBH, energy storage using hydrogen, hydrogen fuel for FCEV, and an LV electrical network. The supply of power for hydrogen generation and to meet the load demand of ZEBH are derived from the intermittent electricity that is generated by a wind turbine and solar PV panel system. Thus, in some instances, there isn't sufficient fuel to operate FCEVs. Therefore, a ZEBH has thermal storage tanks that allow storing heat;

depending on the amount and speed of charging and discharging of the storage tanks, it is, indeed, possible to confine the functionality of the ZEBH's ASHPs for a certain period without impairing the thermal comfort in the building. This increases hydrogen generation from renewable energy sources and maximises its production upon high hydrogen fuel demand for FCEVs, apart from revealing its impact on an IEEE 33-node test feeder.

– **Chapter 6** – Concluding Observations and Recommendations for Future Work:

This study has been concluded with a summary of the outcomes derived from the previous chapters and the provision of several recommendations for future research on this topic.

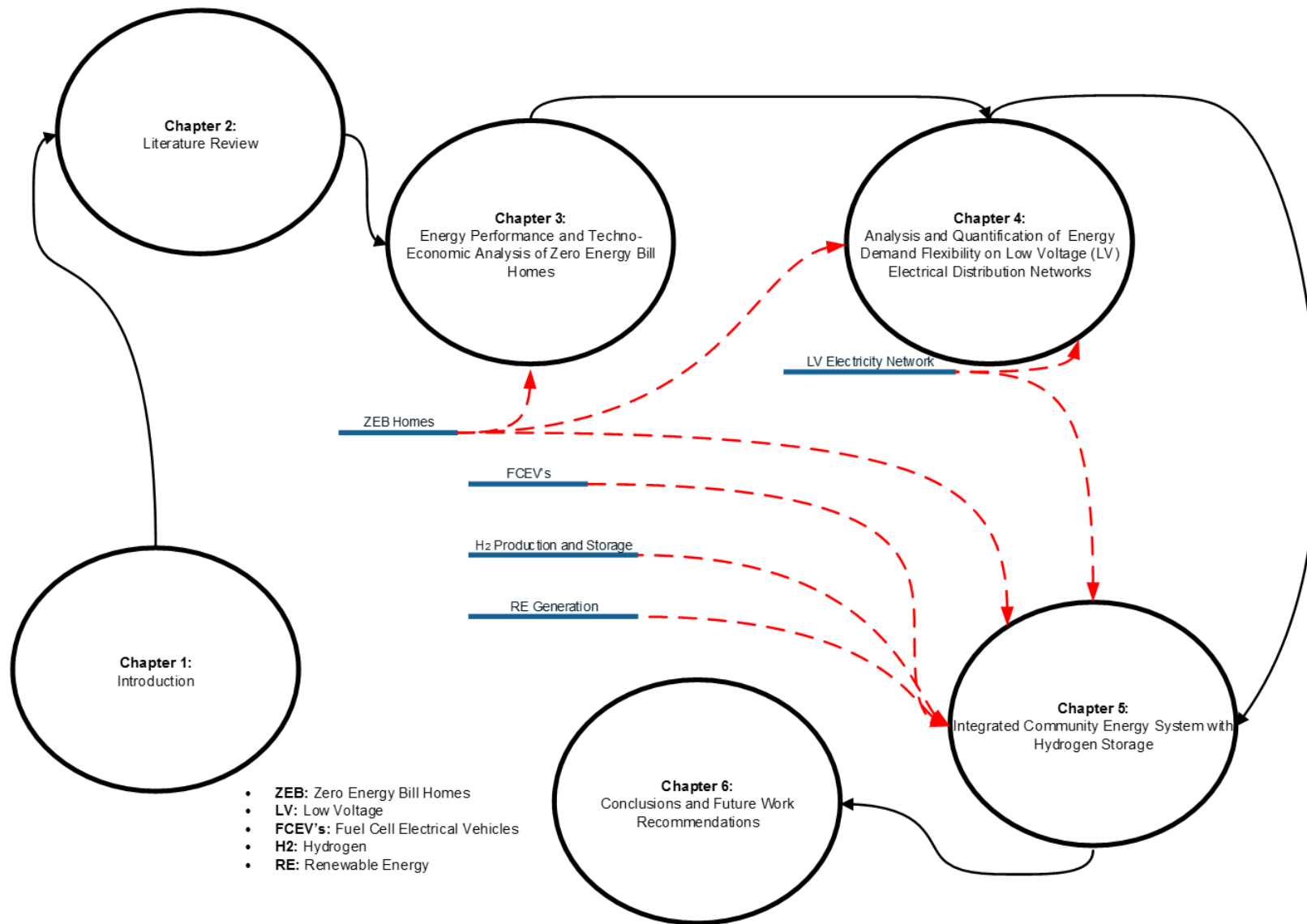


Figure 1-10: Integrated community energy system (ICES) model and thesis outline

CHAPTER 2 – LITERATURE REVIEW

2.1 BUILDINGS

2.1.1 Zero Carbon Homes

A zero-carbon home (ZCH) is a home with neutral or negative carbon dioxide (CO₂) emissions over a year. Such houses produce enough energy from zero-carbon sources such as solar photovoltaics (PV) to offset any fossil-fuel-derived energy [48]. However, definitions, broadly speaking, global definitions, of ZCH slightly vary. In the UK, ZCH is formally defined as follows:

“Homes whose net carbon dioxide emissions, taking account of emissions associated with all energy use in the home, including heating, lighting, hot water, is equal to zero or negative across the year” [49].

To achieve the status of a ZCH, a three-step approach is implemented:

1. The first step requires achieving a high level of energy efficiency in the building fabric and design, i.e. Fabric Energy Efficiency (FEE). This involves improving the U-values of the building fabric or investigating external and integral heat gains [50].
2. The second step requires meeting the minimum carbon reduction levels through on-site generation and implementation of other low-carbon technologies (LCTs); this is termed “carbon compliance”.
3. Finally, to achieve a zero-carbon status, a range of measures known as “allowable solutions”, which go beyond meeting the minimum carbon compliance requirements, must be implemented. These solutions include on-site measures such as installing smart appliances and off-site measures such as investing in energy-from-waste technology or retrofitting LCT in communal buildings. However, the scope of allowable solutions has been criticised as it continues to expand, allowing further field solutions to contribute to a ZCH [51] and raising the question of whether off-site investments should be considered during a zero-carbon evaluation of a home.

In response to criticism related to allowable solutions and the broadening definition of ZCH [52], the UK government conducted a consultation, the findings of which state that the government will provide a national framework for allowable solutions rather than leaving it to the local authorities to ensure national consistency and maximise chances of fulfilling the aims [53]. However, studies have shown that a significant portion (37–45%) of GHG emissions from domestic energy use is not controlled by the above three step approach[52][53].

The Code for Sustainable Homes is a voluntary national standard that guides the design and construction of sustainable dwelling to reduce emissions and energy use and to maintain the current UK building regulations. Reaching level 6 of this code results in obtaining a ZCH status [52]–[54].

2.1.2 Net Zero Energy Buildings

The net zero energy-building (NZEB) approach is a strategy to develop climate-neutral buildings, in addition to others, based on energy-efficient buildings combined with an almost carbon neutral grid supply. NZEBs are designed to overcome limitations through a non-100% “green” grid infrastructure. This strategy involves exploiting local renewable energy sources (RES) on-site and exporting surplus energy generated on-site to utility grids to increase the share of renewable energy within the grids, thereby reducing resource consumption and associated carbon emissions [55].

However, the wide diffusion of distributed generation, especially in the power grid, may result in problems pertaining to power stability and quality in today’s grid structures, mainly at the local distribution grid level. At present, “smart grids” are being developed to fully benefit from distributed generation in the context of reducing the grids’ primary energy and carbon emission factors, as well as operation costs [56]. Within a least-cost planning approach, on-site measures have to be compared with measures at the grid level, which take advantage of the economy of scale and equalisation of local peaks. However, it is clear that a mere satisfaction of the annual balance is not in itself a guarantee that a building is designed in a way that will minimise its (energy-use-related) environmental impact [57]. In particular, NZEBs should be designed – to an extent within the control of the designers – to ensure they work in synergy with the energy grids and do not place additional stress on their functioning.

However, a formal, comprehensive, and consistent framework that considers all relevant aspects characterising NZEBs and allows a consistent definition of NZEB in accordance with the UK’s political targets and specific conditions is missing. Thus, this section presents a framework based on concepts found in the literature and further developed in the context of Towards Net-Zero Energy Solar Buildings, a joint project of IEA (International Energy Agency) SHC (Solar Heating and Cooling programme) – Task40 and ECBCS (Energy Conservation in Buildings and Community Systems) – Annex 52 [58].

The underlying mechanism of defining an NZEB involves defining the boundary of a building system, including the on-site generation of energy [59]. Incorporated in this boundary is the energy consumed from all energy sources, conventional and renewable, as well as any renewable energy that is exported to the grid.

Following this, a weighted system of demand and supply is compared to assess whether a net-zero balance of the designer’s choice can be achieved with the given technological solution that graphically depicts this framework. The evaluator can choose the weighted metric to be energy, CO₂ emissions, cost, or even comfort levels, highlighting the benefit of a flexible definition. The sketch in Figure 2-1 provides an overview of the relevant terminology associated with energy use in buildings and the connection between buildings and energy grids [60].

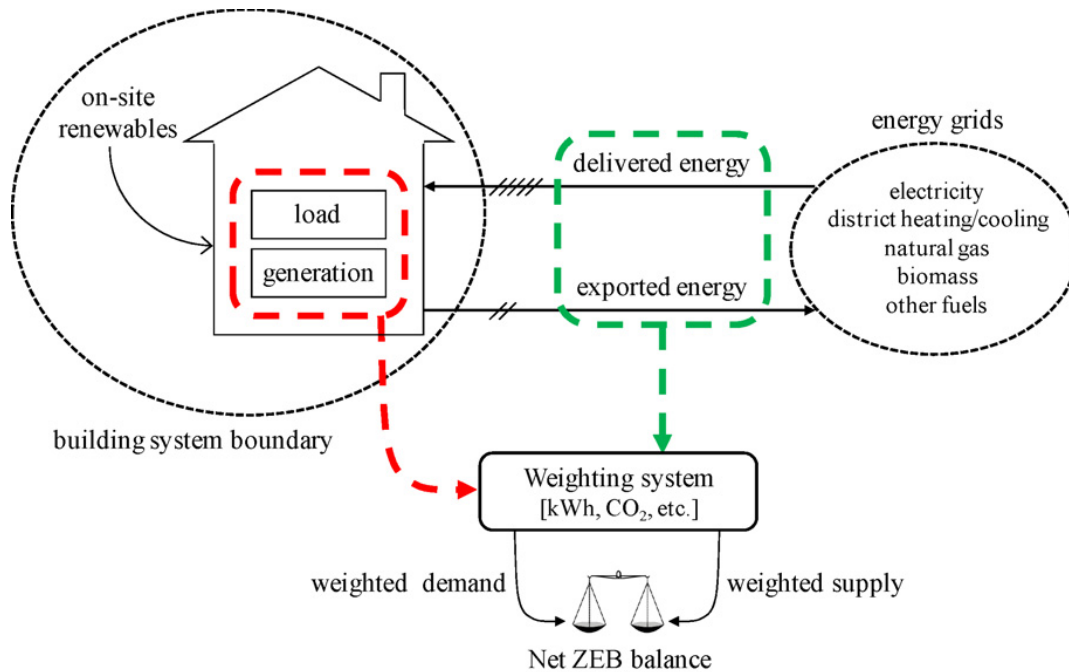


Figure 2-1: Schematic representation of important concepts in an NZEB, showing the connection between buildings and energy grid [55].

Reduction of emission from the domestic sector for NZEBs starts with insulation and fabric efficiency, followed by energy efficiency, and finally, micro-generation. While renewable generation is essential in an NZEB, a primary reduction in heating demand through increased fabric efficiency and the use of energy-efficient technology are also important [60].

2.1.2.1 Building Fabric Efficiency

Key areas of improvement included the U-values of building components (walls, roofs, floors, and windows), reducing thermal bridging, and increasing the airtightness of buildings. It also considered other possible measures such as energy-efficient ventilation and heat and wastewater recovery.

It should be noted that heat transfer and building performance are influenced by thermal conduction, convection, and radiation. The U-value, which is derived from the thermal resistances of building materials, represents the thermal conductance of a building component. It is an important value that represents the heat transfer coefficient of buildings.

Changing building materials or adding insulation can improve the U-value of walls, roofs, and floors; however, the feasible thickness of the space provided and thermal bridging must be accounted for [61]. An experimental analysis of housing development in the UK led to the finding that the overall effects of fabric efficiency such as insulation or double glazing aid in maintaining building performance for over at least the medium term (about 20 years) [62].

2.1.2.2 Technology Solutions

The transition of the domestic sector into an energy provider and not solely a consumer of heat and electricity will be necessary for the UK to meet both its renewable energy and carbon emission reduction targets [62].

A range of technologies to achieve the development of NZEB has been presented in Figure 2-2. It should be noted that research has indicated a gap between energy savings and the cost of energy-saving or generation systems, which limits houses from achieving an NZEB status [63]. This emphasises the need for renewable technologies to provide significant cost and performance benefits to an occupant as compared to conventional energy systems. It should be noted that the literature review presented here does not discuss all possible technologies; it only briefly discusses the domestic deployment of solar, micro-combined heat and power (CHP), and heat pump technologies.

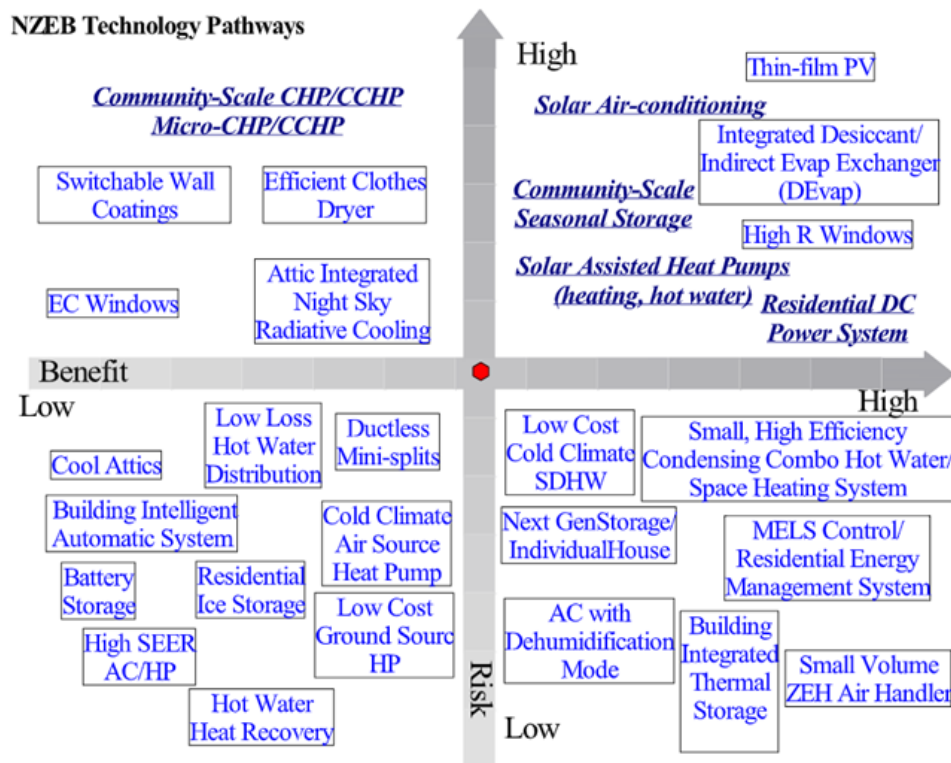


Figure 2-2: NZEB's technology pathways [63]

Solar PV systems is the most common renewable energy generation system installed domestically in the UK [64]. This technology is also commonly used when attempting to establish NZEBs on a global scale, as will be seen through case study reviews, with some studies stating PV generation is essential to establish an NZEB. Additionally, an optimisation review of trade-offs between house design and renewable energy generation has proposed 90% of roof coverage by solar PV to be an optimal parameter for an NZEB [65].

Solar thermal technology is another mature technology that has proven to be cost-effective as well as effective in reducing the environmental impact of water heating [66]. Although solar water heating systems are common in the UK [67], recent research on solar water heating systems has argued that in terms of life-cycle analysis, their contribution to GHG emission reduction is limited [68]. However, in terms of environmental performance, solar water heating is better than electric water heating, as the grid generates carbon-intensive electricity; this has been further discussed below. With respect to meeting domestic hot water (DHW) requirements, studies have shown that solar water heating could be the sole provider of water heating demands, even at latitudes of 50–60° [69].

Due to the issues with solar technologies, advancements in technology have led to the development of hybrid solar PV and thermal collectors (PV/T). They aid in overcoming the problem of efficiency reduction in PV generation as a result of increased temperatures through the inflow of cool water from behind the PV panel [70]. PV/T panels are becoming an increasingly attractive technology for NZEBs due to their ability to provide both electrical generation and DHW; however, they currently require a high capital cost. **Chapter 3** presents a set of PV/T models in domestic dwellings.

Micro-CHP technology has also been identified as a technology that can save energy and reduce GHG emissions [71]. Previous studies have found that appropriately sized micro-CHP systems can economically meet both the electrical and thermal demands of a home; however, to ensure profitability sizing, selection of the prime mover, the driver of the alternator, is essential. Further analyses have demonstrated that micro-CHPs have the potential to increase the efficiency of energy supply within the domestic sector by 3–10% [72].

Ground-, air- or water-source heat pumps are viewed as a key technology to achieve legislated emission targets and have been found to be highly efficient, contributing towards the successful deployment of NZEBs [73]. However, uncertainties relating to seasonal efficiency and instability in air temperatures [74] have reduced their overall installation.

It should be noted that although heat pumps may remain a carbon-intensive technology in the short term, their inclusion in new buildings highlights the importance of installing technology for the future, with decarbonisation of energy systems as a prominent agenda in government policy [75]. Recent analysis has shown that PV/T-assisted heat pumps can reduce the impact of variations in temperature and sunshine on a heat pump system, as well as provide the electricity necessary to upgrade the water temperature to the heating needs [76].

2.1.3 Nearly-Zero Energy Buildings

Article 2 of the Energy Performance of Buildings Directive (EPBD) states the following:

“A nearly-zero energy building is a building that has a very high energy performance. The nearly zero or very low amount of energy required should be covered to a very significant extent by energy from renewable sources, including energy from renewable sources produced on-site or nearby” [77].

As can be seen, the EPBD provides a qualitative, not quantitative, definition of an nZEB, which is different from the NZEB mentioned in the previous section [78].

In the UK, the term “nearly-zero carbon building” was introduced instead of the term “nearly-zero energy building”. Although the use of renewable technologies is not obligatory, in light of the recast EPBD, it is required to give proper consideration to the use of “high-efficiency alternative systems”, such as renewables, district heating, heat pumps, and CHP technology [79].

2.1.3.1 *Cost Optimality Method*

The EPBD recast requires establishing a comparative methodology framework for nZEBs using the cost optimality method, through which it specifies the level of minimum energy performance requirements for new buildings and renovations by developing a benchmark method to achieve cost-optimal levels [80]. The global cost (life-cycle cost) vs. primary energy consumption of different packages of measures (combinations of compatible energy efficiency and energy supply measures) can be assessed by calculating and comparing energy-related costs [81]. To establish a comprehensive overview, all combinations of commonly-used and advanced measures should be assessed as packages of measures to find the cost curve (Figure 2-3).

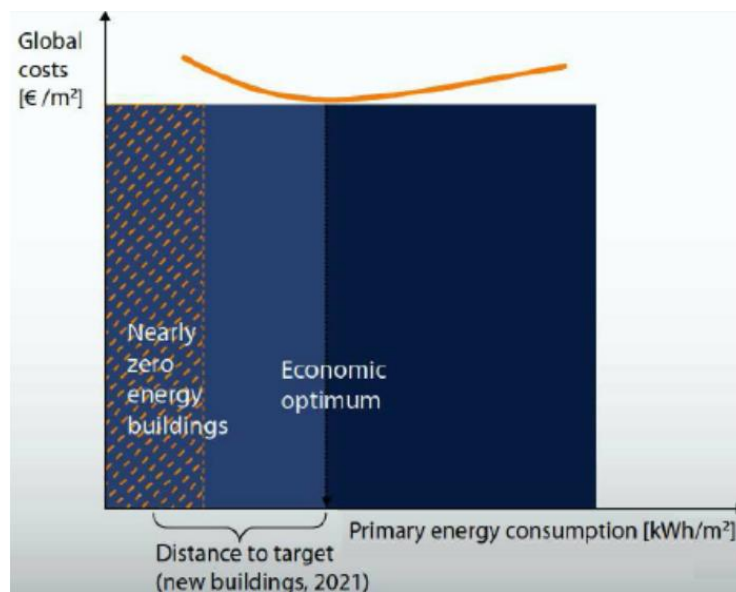


Figure 2-3: Minimum cost and distance to Nearly-Zero Energy [80]

The packages of measures start from compliance with the building regulations in force and extend to best practices in the building envelope and energy systems that realise nZEB. These packages can also include various options for local renewable energy generation. Although they need to suit national circumstances, experiences and solutions from other EU Member States can be also used [82].

The lowest part of the curve represents the economic optimum for the packages of measures. The part of the curve to the right of the economic optimum represents solutions that underperform in both aspects (environmental and financial) [83].

2.1.3.2 Drivers and Barriers

To meet the requirements of the building legislation, it is important to identify the main drivers and barriers with respect to nZEB’s level of performance.

Regarding the drivers of refurbishment that aid existing buildings in reaching the nZEB level, the first precondition is the transposition of the definition of nZEB into the national legislation [83].

Energy cost savings, lower dependence on energy suppliers, and improved comfort in buildings are the major common drivers of renovation and nZEB in several countries.

The inclusion of energy aspects in planned renovations seems to depend greatly on government support programmes, such as grants, tax deductions, and low-interest loans. The Energy Performance Certification database makes it easy for energy experts to choose potential buildings for major renovations [79]. With respect to the major common barriers, some specific technical issues were identified pertaining to the absence of a specific boundary in the nZEB’s balance definition. High initial investment costs together with the lack of financial instruments and limited technical skills can also be considered to be significant barriers [82]. Table 2-1 lists the identified drivers and barriers in the UK [84].

Table 2-1: nZEB’s driver and barriers

| Drivers | Barriers |
|---|---|
| <ul style="list-style-type: none"> • Energy Cost Savings • Lower dependence on energy suppliers • Improved comfort • Tax deductions • Low-interest loans • Best practices of building renovation • Energy Performance Certification database | <ul style="list-style-type: none"> • No numerical indicator for the energy demand of nZEBs • No indicator for nZEBs’ share of renewable energy sources • No specified boundary for nZEB balance • High initial investment costs • Long payback time • Uncertainties in measurement and verification • Low number of renovation projects involving the development of nZEB for demonstrations |

2.1.4 Zero Energy Bill Homes

The concept of a Zero Energy Bill Home (ZEBH) was first launched in March 2016 [85] at the Building Research Establishment (BRE) Innovation Park in Watford as an innovative response to the housing crisis [86].

The ZEBH incorporates integrated energy-generation facilities, demonstrating how investment needed for centralised national infrastructure could be reduced by becoming net exporters of renewable energy.

A ZEBH is a building that offsets energy bills, generating more electricity than what is needed in a year, considering the Feed-In Tariff (FiT) concept. These dwellings are built from building materials with high resistance levels. Furthermore, the rooves of these dwellings are fitted with solar PV panels.

The electricity generated by these PV panels earns revenues from the FiT scheme, which when combined with the surplus electricity generated by the PV panels leads to incomes and savings that exceed the residual cost of electricity. **Chapter 3** presents a set of ZEBHs that consider the installation of solar PV/T panels assisted by heat pumps. This type of home that integrates technology with huge potential helps in dealing with ever-rising energy bills and reducing fuel poverty; however, it requires a high capital cost during installation.

A ZEBH's thermal performance is balanced between insulation, thermal mass, and airtightness. Insulation aids in retaining heat inside the house while thermal mass stores the heat in the house, ensuring a stable internal temperature. The airtightness prevents undesired air exchange between the interior and exterior of the house. The ZEBHs presented in **Chapter 3** were modelled using real building fabric material data.

Although the thermal mass of buildings stores thermal energy that can be used to shift thermal demand for a period of time, this thesis (**Chapters 4 and 5**) considered water tanks as thermal storage with solar PV/T-assisted heat pumps as a load-shifting approach.

2.1.4.1 Concept

A ZEBH can consume approximately 50% of the energy generated by solar PV panels, reducing the export of electricity from the grid by 30%. The imported grid electricity constitutes approximately 20% of the annual energy load [86].

The FiT is crucial for a ZEBH to achieve an annual zero-cost bill status. The PV/T panels presented in **Chapter 3** are connected to the electricity grid to achieve maximum payback from the FiT for every unneeded kilowatt of energy. The excess electricity that is generated is exported to the grid to allow every surplus electricity unit to be used as an offset.

2.2 DISTRIBUTED ENERGY RESOURCES INTEGRATION IN COMMUNITY ENERGY SYSTEMS

The following Distributed Energy Resources (DER) technologies will be studied in this thesis:

- Wind turbine
- Solar PV
- Proton Exchange Membrane Electrolyser (PEM)
- Fuel Cell Electrical Vehicles (FCEV)
- Hydrogen Storage

2.2.1 Wind Turbines

A wind energy conversion system or turbine produces power by utilising the kinetic energy of an incident wind on the turbine rotor. The power that the turbine can extract from the wind is proportional to the cube of wind speed [87].

In **Chapters 4 and 5** of this thesis, wind power is considered for studies on community energy systems. Wind turbines can be classified as large onshore-offshore wind turbines or small-scale domestic wind turbines.

By 2050, 7% of DER technologies installed in the UK is expected to consist of domestic wind turbines – a total of approximately 1.4 GW [88].

2.2.2 Solar PV

Solar PV systems, despite having high installation costs, have high adoption rates. However, in some domestic buildings, this is largely driven by the FiT schemes in the UK [89].

Large-scale installations of these systems in the form of solar farms are also common due to favourable energy policies [90]. **Chapters 4 and 5** consider a large solar PV system (220 PV panels) for the case studies included in this thesis. The UK has low solar irradiance compared to countries in the southern part of Europe; however, even with this drawback, it is expected that approximately 2% of DER generation capacity in the UK by 2050 will be contributed by PV generation systems [91].

PV can benefit energy systems in terms of peak load and CO₂ emission reduction. However, these benefits are accompanied by challenges such as a mismatch between generation and load, reverse power flow, and a rise in voltage [92].

2.2.3 Proton Exchange Membrane Electrolysers

The prognostics to overcome the drawbacks of alkaline electrolysers changed when General Electric, in the 1960s, developed the first water electrolyser based on the concept of a solid polymer electrolyte [93]. This concept was idealised by the researcher named as Grubb [94], where a solid sulfonated polystyrene membrane was used as an electrolyte. This concept is also referred to as proton exchange membrane (PEM) or polymer electrolyte membrane (which also has the acronym PEM) water electrolysis and less frequently as solid polymer electrolyte water electrolysis.

Today, electrolysers have capacities up to m³/h based on the PEM electrolyser (Figure 2-4), as presented in this thesis (**Chapter 5**). PEM electrolysers follow the reverse process of a PEM fuel cell. **Section 2.2.4** provides more details on fuel cell systems. A PEM electrolyser works as follows:

1. The electrode (anode) splits water into hydrogen, protons, and electrons with the application of a Direct Current (DC) voltage higher than a thermoneutral voltage of 1.482 V[95].
2. Protons pass through the polymer electrolyte membrane, and on the cathode, they combine with electrons to form hydrogen.

In **Chapter 5**, PEM electrolysis is presented as a method to produce hydrogen from renewable energy sources.

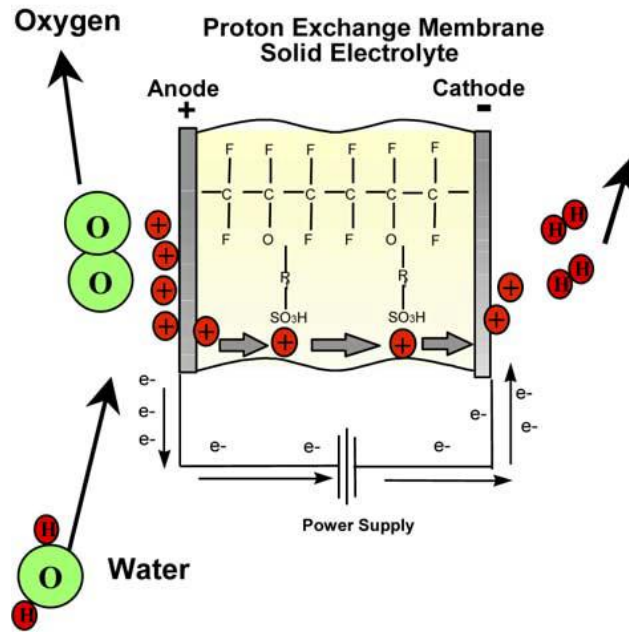


Figure 2-4: Schematic representation of a PEM electrolyser [96]

2.2.4 Fuel Cell Electrical Vehicles

Fuel Cells (FC) produce a current through electrochemical reactions. In an FC system connected to an electrolyser, hydrogen produced in the electrolyser system is used with oxygen in the FC unit to produce electricity and water. This can be used for an extended range of Fuel Cell Electrical Vehicles (FCEV). FCs, though expensive, are more efficient than thermal engines [97]. However, due to their high initial capital costs, they have not been extensively used as DER, but they have been extensively integrated with combined and heat power plants in microgrid systems [41].

In this thesis (**Chapter 5**), FCEVs are shown to be used in a community with hydrogen storage that dispenses fuel to the vehicles from a PEM electrolyser fed by renewable energies.

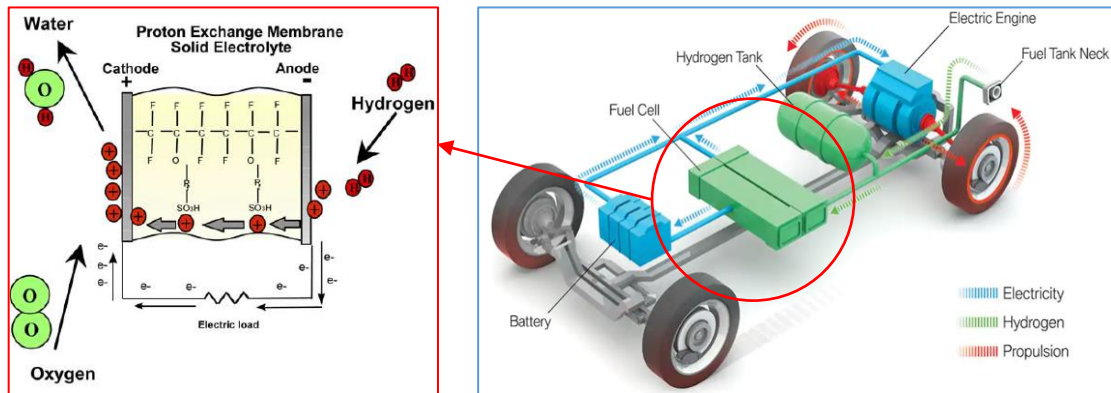


Figure 2-5: Schematic representation of a PEM fuel cell (left) and Fuel Cell Electrical Vehicle (right)

2.2.5 Hydrogen Storage

In the development of hydrogen energy, the storage of this energy for prevalent use in transportation and stationary power systems is considered to be a concern [98]. At present, the most common methods to store hydrogen include storing it as compressed hydrogen, cryogenic liquid, and metal hydride. **Chapter 5** discusses a compressed hydrogen storage system [99].

Rivard et al. summarised the storage methods of hydrogen, discussing forms of storage such as compressed hydrogen, liquefied hydrogen, metal hydride, carbon nanotubes, liquid organic hydrogen carrier, and metal-organic framework [100]. Hydrogen fuel can be stored in different forms, as presented in [101]. However, storage in the form of compressed gas is more popular due to its technical simplicity, high reliability, acceptable efficiency, and affordability. A storage vessel is the key technology that enables the widespread use of compressed hydrogen. The material used in a hydrogen storage vessel must be safe, reliable, cost-effective, and must prevent any strong interaction with hydrogen or other reactions [102].

2.3 INTEGRATED COMMUNITY ENERGY SYSTEMS

In this thesis, the concept of an “integrated community energy system” considers a whole-system approach for the evaluation and optimisation of a community. **Chapter 5** analyses case studies of expanding the system boundary beyond buildings, electricity and hydrogen systems, and FCEVs. Doing so provides a perspective to the analysis of a community energy system, particularly in the light of reducing issues of energy services subjected to an electricity network, hydrogen (H₂), and constraints of a building’s comfort level.

2.3.1 Building-to-Community-Level Perspective

From a building-to-community perspective, this thesis explores the concept of a multi-energy system. This is exemplified in Figure 2-6 that displays how multiple energy vectors can be relevant to buildings and communities. For instance, at the building level, natural gas and electricity can be used as input in different types of equipment such as boilers, air-source heat pumps, chillers, micro-CHP, and so on to produce electricity, heat, and cooling. It should be noted that such equipment can be optimally coordinated for various purposes. In this thesis (**Chapters 4, and 5**), a set of buildings with solar technology and air-source heat pumps have been represented in the context of a community.

Buildings can then also interact at the community level. For instance, in typical community energy systems, electricity networks are used to interface local generation. For instance, wind turbines and electrolysers, on the other hand, supply energy vectors such as electricity and hydrogen (for the purpose of fuelling electrical vehicles).

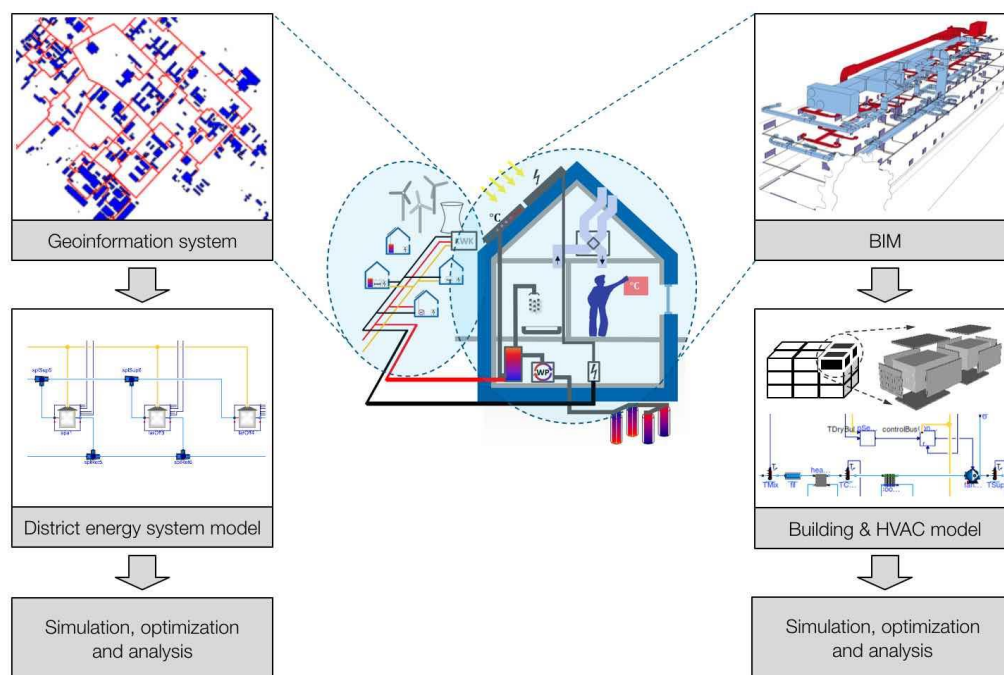


Figure 2-6: Building-to-Community level perspective concept [103].

A building-level energy system has been presented in [104] where an energy hub model approach has been proposed to describe the coupling of supply and demand in an integrated way to minimise electricity and gas costs among others.

Scaling it up from individual buildings to a higher level (communities), various works have been proposed to deal with the operational and planning analyses of community energy systems. Pioneering work on the comprehensive assessment of electricity and heat supply options was conducted by Karunathilake et al. in a case study of a new residential development [105].

2.3.2 Building and Energy Grid Systems

The significance of investigating the interactions between buildings that employ LCTs and grid system have been outlined by several researchers. Van Roy et al., along with the Modelica library, proposed the Integrated District Energy Assessment by Simulation (IDEAS) tool to assess the incorporation of district energy systems in buildings [106].

The study further probed into the benefits of incorporating Energy System Integration (ESI)⁵ into electrical modelling by evaluating electrical bottlenecks at the feeder level for a district that has implemented domestic dwellings, PV systems, and heat pumps on a radial IEEE 34-node test feeder. Additionally, the paper looked into the simultaneity between demand and supply (cover factors) but neglected to analyse the integration aspect.

In a similar manner, Verbruggen and Driesen studied the impact of an NZEB on an electricity grid [107]. The model, which also applied the Modelica library, investigated the control mechanisms via simulation to analyse the impact of a power exchange that took place in a building with its grid adjusted to set-point temperature for thermal energy storage tank of the heat pump, apart from determining the shift in local consumption to better coincide with local PV generation. Nevertheless, the simulations solely focussed on a single building and its impact on the grid while omitting its related network simulation.

Navarro-Espinosa et al. performed a probabilistic analysis based on Monte Carlo simulations in an attempt to evaluate the impact of a domestic dwelling's heat pumps and varied indoor temperatures on the UK's LV distribution networks [108]. They revealed that the electrification of heating via EHP technology and the alteration of indoor temperatures exhibited the potential to decarbonise the UK's energy sector. The paper, therefore, examined the aspects of voltage, congestion, and bottleneck percentages of three networks at diverse penetration levels by applying the Open Distribution System Simulator (DSS) software package. The article concluded that to successfully minimise the buildings negative impact on feeders, the heating temperature set-points should be reduced. However, the study dismissed the implications of building modelling and considered the model of Good et al. [109] in domestic energy consumption results to arrive at the outcomes.

Protopapadaki and Saelens [110] expanded the work of Navarro-Espinosa et al. [108] by employing Modelica software to assess the probabilistic grid impact of heat-pump-equipped buildings, including rural and urban feeder configurations and variations in building quality. Simultaneously, the proposed method provided a platform for further statistical analysis, as well as quantification of an Air-Source Heat Pump (ASHP) and PV systems implemented among Belgian residential feeders. The outcomes demonstrated that high rates of heat pump penetration lead to overload and voltage stability issues in feeders designed based on the present practice, particularly in rural areas. Therefore, the method of controlled ASHP load was omitted, and thus, the stability of the grid was not improvised.

⁵ ESI is the process of coordinating the planning and operation of energy systems across multiple pathways and/or geographical scales to deliver reliable, cost-effective energy services with minimal impact on the environment.

2.3.3 Building Energy Demand Flexibility

Energy demand flexibility is significant due to its ability to address several uncertainties that may arise within an energy supply chain (e.g., electric power systems). Therefore, upon exploiting it, one should comprehend defining the quantification of energy demand flexibility. In this thesis, energy demand flexibility is quantified by calculating the consumed load, which can be shifted or minimised without compromising the occupants' thermal comfort for ancillary services.

Researchers such as Finck et al. have investigated the optimal control to minimise operational electricity costs of a heat pump integrated with thermal energy storage on real-time power spot market prices [111]. The optimisation findings suggest that heat pumps need to be operated with a high rate of recurrence of on/off switching and display efficiency at partial load. As such, the study modelled a small-scale office building via a MATLAB toolbox to model a resistance-capacitance building; this model was validated using a building modelling software package. However, the study solely focussed on minimising the total operational costs of electricity usage, disregarding electrical network parameters (voltage, current).

Kelly et al. highlighted the load shifting of populations of buffered heat pumps wholly to off-peak periods by using the UK Economy 10 tariff, along with the building simulation tool ESP-r [112]. The study identified several forms of significance related to heat pump load shifting to off-peak periods for both end-users and electricity networks. However, the constriction of the ASHP population that only operated during off-peak hours was observed to increase the peak aggregate demand instead of minimising it. This occurred mainly due to limited optimum control of the ASHPs and because only the tariff-based method was employed. Meanwhile, Masy et al. analysed energy demand flexibility in Belgian buildings using heat pumps and thermal mass of buildings as storage [113]. The research suggested five control strategies for thermal comfort, consumption, and financial expenses. The Belgian buildings were equipped with air-to-water heat pumps to supply both space heat and DHW. The study also quantified flexibility based on shifted load volume by omitting electricity market costs. Nevertheless, the outcomes seemed to display some economic benefits of implementing the five control strategies for the occupants after shifting the peak load from peak to off-peak hours (13%), wherein electricity consumption was found to hike up to 20%.

Konsantin et al. investigated the quantitative potential of varied flexibility alternatives [114]. The study analysed and compared four flexibility and storage options for an office building (batteries, fuel switch, water tanks, and thermal building mass) in terms of load shifting. The initial aim of the flexible operation was to minimise electricity generation cost at the system level. Although the paper found that multiple flexibility and storage options can be considered, further price values are required to simulate load shifting because the considered electricity prices failed to prove adequate support for grid operation.

2.3.4 Integrated Energy Systems

Different energy vectors can be integrated together to provide multiple energy vectors such as electricity, heat, hydrogen, and transport in communities. This concept has been schematically illustrated in Figure 2-7, focussing on multiple outputs. In particular, the possibility of integrating the production of multiple services paves the way for improving system performance from techno-economic, energy, and environmental perspectives; for example, owing to the possibility of recovering wasted heat from CHP devices that are used to supply local thermal or cooling demands.

In this context, the most significant and widespread cases of integrated energy systems are the ones based on different generation sources, which can be defined as the combined production of multiple energy vectors (e.g., electricity, heat, and cooling) from a unique source of fuel. Different energy vectors in communities have the potential to provide significant economic, energy, and environmental benefits relative to the “conventional” way of separately producing the same energy vectors.

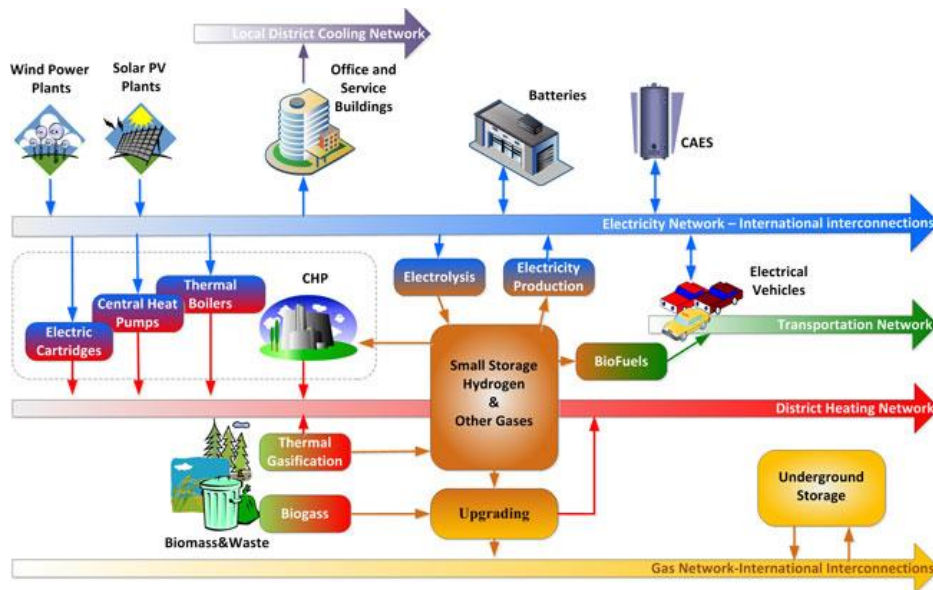


Figure 2-7: Integrated Energy Systems [115]

The simplest form of an integrated energy system plant is cogeneration or CHP technology, which has been comprehensively analysed from an economic and energy/exergy perspective in [116], as already mentioned. The “natural” extension of cogeneration is trigeneration or combined cooling heat and power (CCHP). A comprehensive energy and environmental assessment of CCHP can be found in [117]. In particular, in a “classical” trigeneration case, absorption chillers are coupled with a CHP plant to produce cooling, making up for the potential lack of thermal demand in summer when cooling might be required instead (seasonal trigeneration). Generalising the concept of trigeneration beyond the context of absorption chillers has been proposed in [118], where various solutions to deliver electricity, heat, and cooling have been analysed in detail. An example of a trigeneration scheme with CHP and absorption chillers has been depicted in Figure 2-8.

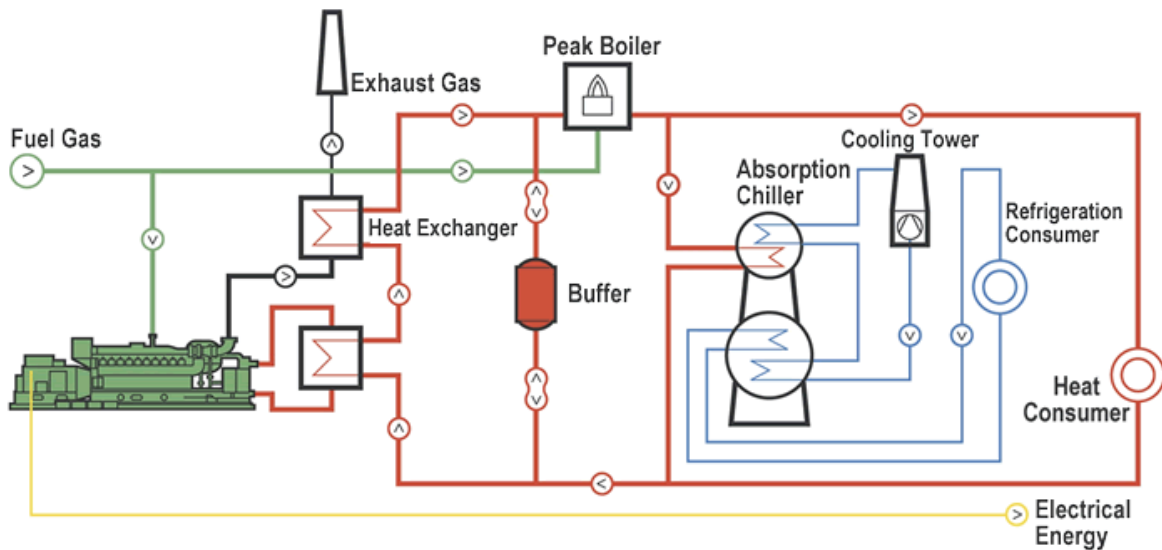


Figure 2-8: Combined Heat And Power With Absorption Chiller [118]

An integrated energy system with a storage model based on electricity, heat, and hydrogen has been presented in [119], with the results highlighting potential competitiveness under certain incentive spread conditions for hydrogen production relative to alternative options for better power grid regulation flexibility and economy instead of battery energy storage. Recent work on biomass, based on the production of hydrogen, has also been reported in [120], which indicates significant environmental benefits of multi-generation compared to both power-only and CHP cycles. Efforts to decarbonise the transport sector have become increasingly important in recent years, and the need to incorporate transport into an integrated energy system's thinking and analysis framework has recently been discussed in a number of studies [121]. Discussions on transport in the context of an integrated energy system are also relevant to the interaction with hydrogen as an energy vector (with excellent transportability characteristics such as electricity and storability). In this respect, a comprehensive analysis of synergies and interactions between electricity and hydrogen at the system level, with critical applications to transport, is available in [122].

2.3.5 Energy Networks

Interconnections take place through energy networks that carry different vectors, such as electricity, gas, heat, cooling, and so on. Energy networks can thus enable optimal management of multiple energy resource portfolios on the one hand and introduce further complexity in the system's operational and planning analysis on the other, for instance, relevant to what energy network type is most appropriate in a given integrated community energy system.

Figure 2-9 demonstrates the role of multi-vector energy networks. The local inputs are primarily based on distributed generations and renewable energies, whereas the external network's inputs are mainly from traditional energy vectors such as electricity and natural gas.

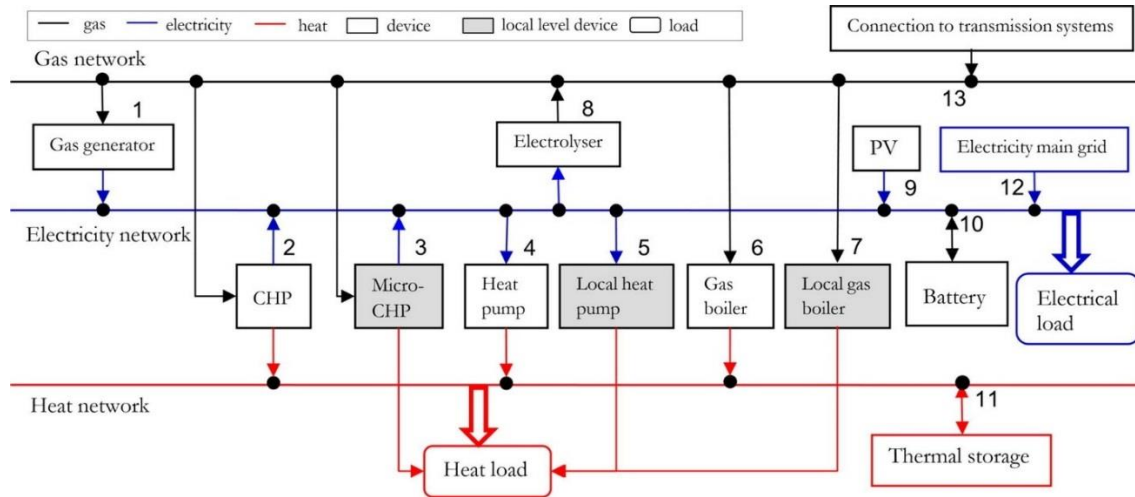


Figure 2-9: Energy Network Interactions [123]

Many studies on multi-vector energy systems from a network perspective have been conducted. For instance, a complex energy flow analysis of an integrated electrical and natural gas network has been conducted in [124] using a deterministic energy flow solution provided by the sample generated from the Monte Carlo simulation. In [125], a comprehensive theoretical framework for modelling the power flow of different energy networks in a multi-vector energy system based on the electric heating concept has been proposed. Furthermore, different types of energy infrastructure such as electricity, gas, and district heating systems are coupled. The power flow model includes the conversion and transmission of an arbitrary number of energy vectors. A detailed description of a framework comprising electric heating, interfaced for network participants and energy interconnectors, which transmit several forms of energy, has been provided in [126].

2.3.6 Modelling Tools

Different analysis aspects of integrated energy systems can be obtained using modelling tools. Some software tools and models have been reviewed by several studies. A summary of these reviews has been provided below:

- A review and survey of available tools to plan and analyse ICES has been presented in [127].
- A modelling tool selection method has been presented in [128] for the planning of community-scale energy systems, including storage and demand-side management. Findings from the capability categorisation process were highlighted, as well as the gaps to be addressed and future trends in the modelling of such systems.
- A review of software tools available to analyse the integration of renewable energy into various energy systems was undertaken in [129]. The study reviewed 37 tools in collaboration with the tool developers or recommended points of contact.
- A number of tools with the ability to model multi-energy systems applicable to a city-scale were reviewed in [130].

Table 2-2 provides a summary of the most commonly used modelling tools classified in [127]–[130].

Table 2-2: Types of tools reviewed

| Tool | Community Scale | Studies | | Design System | | Time Frequency | Optimisation | |
|---------------------------|-----------------|-----------|---------|---------------|---------|----------------|--------------|-----------|
| | | Buildings | Network | Electrical | Thermal | | Investment | Operation |
| RetScreen ¹ | √ | x | x | √ | √ | monthly | x | √ |
| EnergyPlan ² | x | x | x | √ | √ | hourly | √ | √ |
| HOMER ³ | √ | x | √ | √ | √ | minutes | √ | √ |
| H2RES ⁴ | √ | x | x | √ | √ | hourly | x | √ |
| MARKAL/TIMES ⁵ | √ | x | √ | √ | √ | hourly | √ | x |
| DERCAM ⁶ | √ | x | x | √ | √ | 5 minutes | √ | √ |

1. <https://www.nrcan.gc.ca/maps-tools-publications/tools/data-analysis-software-modelling/retscreen/7465>
2. <https://www.energyplan.eu/>
3. <https://www.homerenergy.com/>
4. <http://h2res.fsb.hr/>
5. <https://www.energyplan.eu/othertools/national/markaltimes/>
6. <https://building-microgrid.lbl.gov/projects/der-cam>

From Table 2-2, it can be noted that most of the commonly used tools do not consider design at the building level. The design or detailed modelling of buildings that considers the weather/environment, occupancy, appliance use, and LCTs (e.g., PV panels) can provide a more accurate outcome than a steady load demand. **Chapter 5 presents a developed tool that solves an operational optimisation objective function in a community, integrating buildings, electrical networks, and hydrogen storage/supply for electrical vehicles using 100% renewable energy sources (solar PV and wind turbine).** The tool was developed to solve an optimisation problem with a time resolution of 15 minutes.

2.4 OPTIMISATION METHODS

Optimisation techniques have traditionally been used to optimise schedules of large generators in power systems. The following sections present a review of various optimisation methods. In **Chapters 4 and 5**, a Mixed Integer Linear Programming (MILP) technique is applied to simulate the case studies presented in these chapters, since it is possible to define the power flow direction in electrical systems. Besides that, the MILP approach guarantees a global optimisation solution.

2.4.1 Problem Formulation

2.4.1.1 Function Optimisation

In case of any problem with optimisation, an objective must be fulfilled within certain boundaries, which are referred to as constraints. Figure 2-10 shows the sequence of finding a solution to an optimisation problem. To formulate an optimisation algorithm, the objective of the optimisation problem must be identified [131].

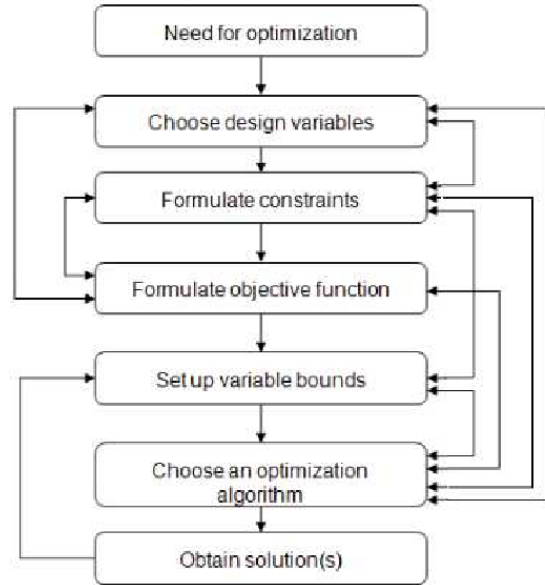


Figure 2-10: Optimal Design Procedure Flowchart [131]

2.4.1.2 Decision Variables

Decision variables, sometimes referred to as design variables, are the unknowns in an optimisation problem; they need to be determined by solving the problem. The speed and efficiency of optimisation simulation largely depend on the number of decision variables [132].

2.4.1.3 Constraints

Once the design variables have been identified, constraints or limitations to such a problem must be identified. Constraints express the relationship between the design variables and other parameters to meet the requirement of a physical phenomenon or limited resources [132].

Some examples of constraints include voltage boundaries in distribution networks, thermal or ratings of distribution network cables. Constraints may take the form of equality ($=$) or inequality (less or equal to \leq , or greater than or equal to \geq).

2.4.1.4 Objective Function

The next step after the selection of constraints is the formulation of the target objective, which is known as the objective function. There may be multiple objective functions in an optimisation problem; this phenomenon is known as multi-objective optimisation. The objective function may be minimised or maximised. The duality principle aids in converting minimisation into maximisation through multiplication with a factor of (-1) [133].

2.4.1.5 *Variable Bounds*

Variable bounds delineate the extent of the optimisation problem by selecting the minimum and maximum bounds of the decision variables.

2.4.2 Optimisation Methods

According to [132], there are two main categories of optimisation techniques:

1. Optimisation methods based on numerical and mathematical methods
2. Artificial Intelligence (AI) methods

The numerical methods can be summarised as follows [132]:

- Linear Programming (LP), and Interior Point:

Linear Programming aims to determine the best solution for problems that are modelled through linear equations. Thus, the objective function and the model restrictions needs to be linear functions of the decision variables. The model restrictions can be represented by equations in the form of equalities or inequalities [132].

Over the years, several methods were developed to solve LP problems as the Interior Point method developed by Kharmarkar, which presents a fast response over other methods. However, the Simplex Method is the most traditional method used due to its efficiency [132].

Despite the simplicity to resolve linear optimisation problems, linear mathematical models usually do not represent a real model, that is, they are simplified models of the actual cases.

- Non-LP (NLP):

The NLP model consists of optimising an objective function subject or not to restrictions, where the restriction functions can be non-linear and/or linear. This programming is characterised by not having a single algorithm to solve your problems.

The biggest problem with this type of programming is the uncertainty that the solution obtained for the problem is the best, that is, it is often possible to arrive at a great location instead of a global optimum, this being a fact inherent in nature not -linear of the problem; while its great advantage is the comprehensiveness, that is, once the mathematical model of the problem to be optimised has been elaborated, with its objective function and restrictions, usually no simplification will be necessary in terms of formulation.

The NLP algorithms do not necessarily achieve the exact solution, as with the Simplex Method of linear programming (LP). However, they generate a sequence of points whose limit converges to the optimum point. In practice, the optimisation process ends when a point is close enough to the solution point.

Non-linear programming problems come in many different forms and formats. Unlike the Simplex method for linear programming, there is no single algorithm capable of solving all these types of problems. Instead, algorithms have been developed for several individual classes of non-linear programming problems. Some of them are: linearly restricted optimisation, quadratic programming, convex programming, separable programming, non-convex programming, among others. Basically, they are classified according to the characteristics of non-linear objective and restrictive functions [132].

- Mixed Integer Linear Programming (MILP):

MILP can be understood as a specific linear programming case, where part of the variables must be integers (usually are used binary variables 0 or 1). MILP problems are generally more complex when compared to LP problems, and can be solved using methods such as “branch-and-bound”, “branch-and-bound-and-cut” and “branch-and-bound-and-cut- and-price ”among others [132].

The main characteristic that makes the MILP method widely used in energy management problems is the possibility of using binary variables in the formulation of problems, which, can model devices, elements, or systems that have a bidirectional power flow condition [133]. In a physical system, the simultaneous occurrence of power flows in opposite directions is not feasible, and the optimization models must guarantee a possible solution for power management. In this context, several works in the literature present solutions with binary variables to control the power flow direction.

- Dynamic Programming (DP):

Many efficient algorithms are based on the DP method. This method, or algorithm design strategy, is a kind of intelligent iterative translation of recursion. As in a recursive algorithm, each instance of the problem is solved by solving smaller, or better, sub-instances of the original instance. The distinguishing feature of DP is the table it stores as solutions for the various sub-instances. The time consumption of the algorithm is, in general, proportional to the size of the table. For the method of dynamic programming to be selected, the problem must have a recursive structure: the solution of every instance of the problem must contain solutions of sub-instances of the instance.

As advantages of dynamic programming, stand out the possibility of being used in many discrete optimization problems, it does not need much numerical precision, and it is useful to apply in problems that demand to test of all possibilities. On the other hand, it requires large memory space and the spatial complexity can be exponential.

2.5 SUMMARY

This chapter analysed the literature relevant to this thesis and described the concepts of a ZCH, ZEB, and ZEBH. Furthermore, it discussed the use of buildings in community energy systems. Additionally, user cases of LCTs (ASHPS) in electricity supply networks were analysed to provide a background to optimisation developed in **Chapter 4** for energy demand flexibility that ZEBHs can provide to an electrical network. The concept of DER was reviewed to provide a background to the key renewable energy technology presented in this thesis. DERs have been identified as key distributed resources in community energy systems. The following DERs were described in this chapter:

- (i) wind turbines,
- (ii) PV,
- (iii) PEMs,
- (iv) FCEVs, and
- (v) Hydrogen storage. Emphasis was placed on storing hydrogen in a compressed manner, as this has been studied in **Chapter 5**.

Buildings with on-site generation (e.g., PV) were identified as means to decarbonise the electricity sector to provide a background to the case studies simulated in **Chapter 4**. Buildings that are considered to be prosumers that impact distribution networks were reviewed. Voltage excursions were identified as a potential issue of integrating DER into distribution networks. This criterion was applied on a set of ZEBHs linked in an LV electricity network with DER, as developed in the **Chapter 4**.

Drivers and the challenges and opportunities of modelling ICES have also been highlighted in this chapter. Such modelling should be able to assess interactions between different energy vectors and networks to highlight the benefits and potential unforeseen or undesired drawbacks of integrated energy systems. Aspects such as choices to be made with respect to time resolutions, network representation, system operational details, and the link between buildings and energy grid systems have also been discussed. Finally, a coupling method was developed to assess the impact of a ZEBH on an LV distribution network, hydrogen production, and FCEVs' demand in a community in the UK.

CHAPTER 3- ENERGY PERFORMANCE AND TECHNO-ECONOMIC ANALYSIS OF ZERO ENERGY BILL HOMES

3.1 INTRODUCTION

In the past 12 years, the United Kingdom (UK) has made significant progress in making domestic dwellings more efficient. Presently, the domestic sector is required to meet the UK's net-zero target in new and renovated dwellings by 2050. As a measure in this on-going determination, the UK has constructed a number of Zero Energy Bill Homes (ZEBH) in Corby, Northamptonshire, which is currently a part of the European Union District of Future Project. For the effectiveness of a zero energy bill performance, a solar photovoltaic thermal-assisted heat pump (SPVTAH) was modelled, which represented building modelling, emphasising the essential outcomes through energy demand profiles (electricity, space heat, and domestic hot water), and occupant behaviour. To authenticate the building modelling, the baseline models were calibrated using the weekly electricity-use curve and validated using statistical indices. It is inferred that the evidence-based manual calibration technique has fairly validated the energy-use profiles of the chosen case studies and is found to be within acceptable tolerance levels. In addition, to verify the zero-energy bill status of the buildings, an economic analysis was extremely crucial. A feasibility assessment indicated that the ZEBH concept will be impractical if the UK government subsidies are withdrawn. Moreover, the Net Present Value analysis further signified that although SPVTAH seemingly generates revenues, the initial investment turned out to be the largest barrier to repay for the system. However, it was proven that the renewable energy technology operational in the domestic dwellings of the UK does offer major advantages, and reduction in costs appears to be the most significant one.

3.2 BUILDING MODELLING TOOL

The building modelling tool used in this study has certain unique attributes and specific applications. Such tools used for simulation purposes, such as modelling of building geometry, renewable energy systems, electrical/lighting equipment, and heating systems, include EnergyPlus and DesignBuilder [[134] [135]. EnergyPlus, developed by the U.S. Department of Energy (DOE) [135], is one of the most recognised and validated building energy simulation software tools. This tool employs dual energy simulation engines – DOE-2 and Building Loads Analysis and System Thermodynamics (BLAST) systems[136]. The BLAST indicates aggregation of programs developed to estimate energy consumption and the performance of energy systems using thermodynamic equations. Meanwhile, the DOE-2 uses the weighted heat balance approach. Nevertheless, the EnergyPlus is not equipped with any graphical user interface (GUI) that would allow its users to clearly visualise the building concept. Therefore, as the EnergyPlus software is not equipped with a GUI, DesignBuilder with a GUI[134] was utilised to complete the task of modelling the geometry of the ZEBHs. In order to do so, first, floor plans were built as per the CAD format using the AutoCAD software package. Afterwards, the CAD files were imported from the DesignBuilder software package to develop the ZEBHs 3D model whilst using the building fabric data.

3.3 ZERO ENERGY BILL HOMES DESCRIPTION

This study investigated four residential single-family homes, with the standard semi-detached ZEBHs, which are referred to as Electric Homes (EHs) 272, 273, 274, and 349. This novel concept has been recently adopted in the community of Corby, England, under a European Union project called ‘the District of Future’ (DoF)[3]. In this study, each dwelling, along with its own energy supply system, were modelled by featuring characteristics such as occupancy, activity profiles, building fabric materials, and weather profiles. Figure 3-1 illustrates the actual representation of the ZEBHs and the site plan indicating each EH with the designated plot numbers facing north-east direction.

These dwellings feature building materials with low U-values, storage systems (thermal), heat pumps, and solar PV panels on top of the roof. A zero-energy bill status can be achieved with the UK’s FiT and the export of excess electricity to the electricity distribution grid [19].

The target of ZEBHs is to produce sufficient energy that can fulfil their annual energy consumption need, and this target can perhaps be achieved using technologies such as photovoltaic thermal (PV/T) panels[137]–[139]. Since the UK has binding targets on energy demand and GHGs emissions reduction [140], it is expected that ZEBHs will become commonly used in the future [140].



Figure 3-1: Left- ZEBHs building aspect and Right - site plan highlighting the Electric Homes facing North-East

3.4 METHODOLOGY

This section presents an overview of the methodology used in the ZEBHs project at Corby, with an emphasis on the data measurement and calibration procedures as well as the building modelling/simulation approach, including economic analysis. Figure 3-2 displays the process used for this study.

As shown in the flow diagram, exhibiting the building modelling, initial simulations, and metered building electrical consumption data were used to create a calibrated simulation model from each ZEBH. In addition, an evaluation of the ZEBHs’ building performance was carried out using the measured data representing the buildings’ electricity consumption. Finally, a techno-economic analysis was performed to assess the feasibility of the SPVTAH installed in each dwelling and confirm whether ZEBHs can achieve a zero-energy bill status or not.

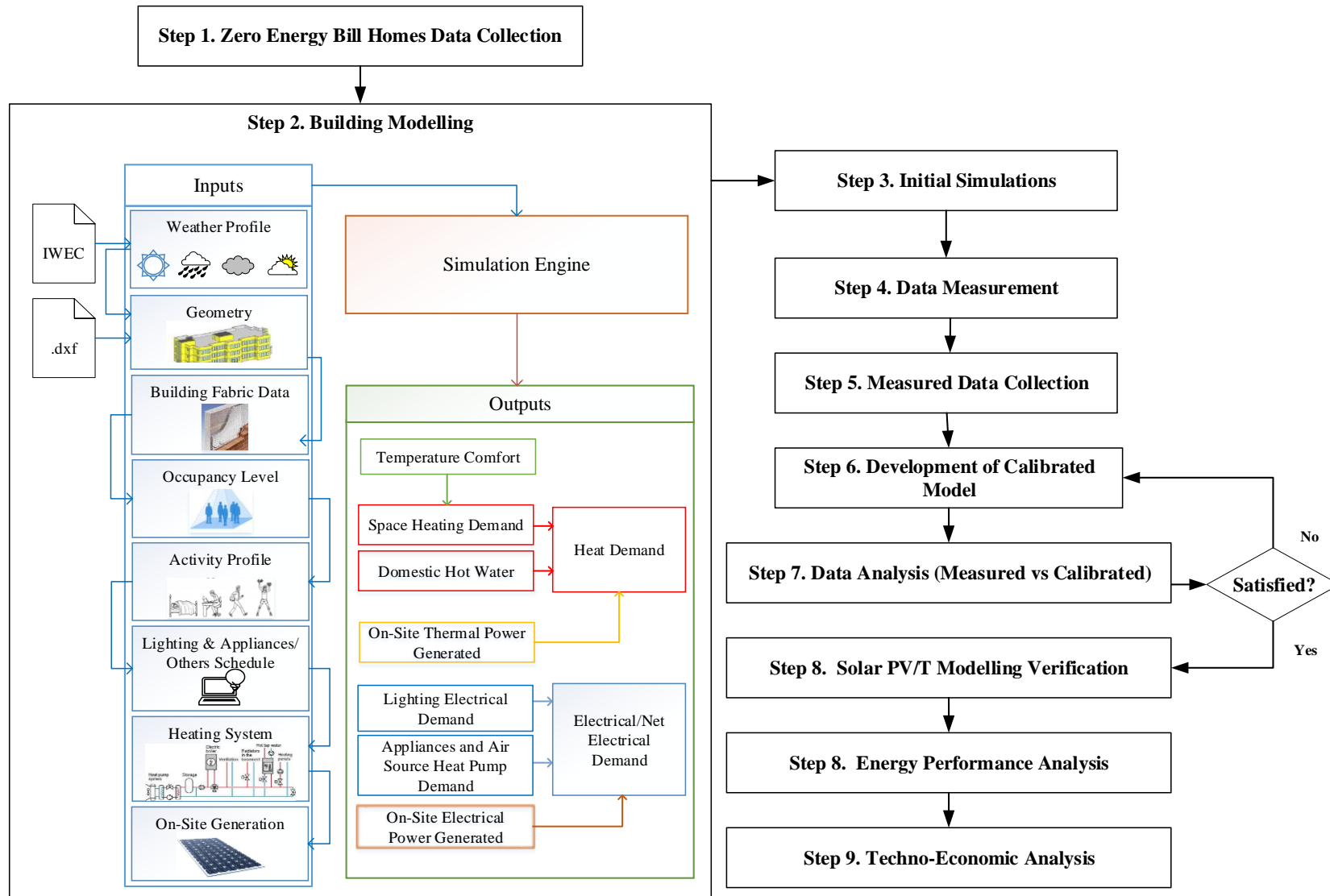


Figure 3-2: Overview of procedure used

3.4.1. Zero Energy Bill Homes Data Collection

The selected ZEBHs were visited, and except weather and climate data, all information pertaining to the buildings was collected, including building fabric materials data, floorplans, occupants information (e.g., total number, profession, etc.), and the SPVTAH system data. The site visit and data collection could be accomplished with the help of Electric Corby CIC. The company highly contributed to the energy use case analysis of the ZEBHs being built at Corby.

3.4.2. Building Modelling

The buildings, a previously mention in **Section 3.2**, were modelled using the GUI and simulated with EnergyPlus software. Figure 3-3 presents the final views on the developed 3D modelling of the studied dwellings. After completing the modelling, an initial simulation was performed to assess the electrical and space heat demand as well as the temperature comfort in each zone of the houses.

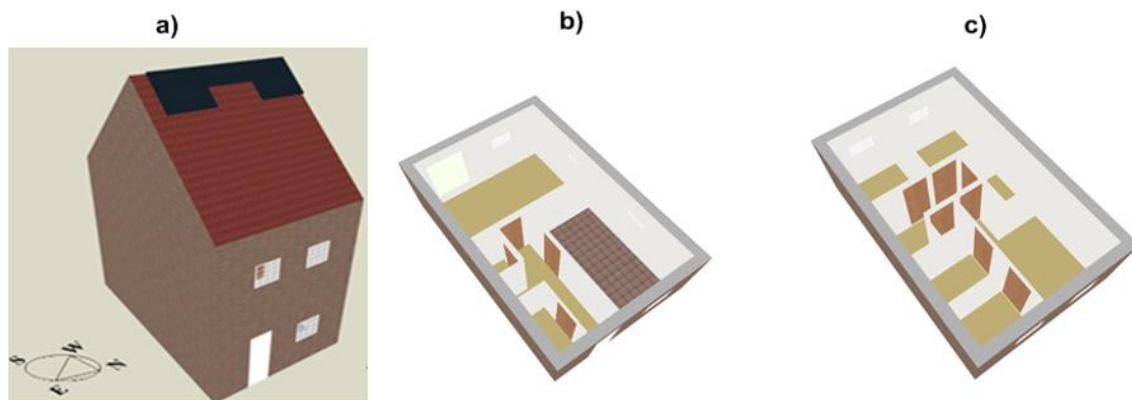


Figure 3-3: Representation of the building model. a) axonometric view. b) ground floor. c) first floor

3.4.3. Weather and Climate

Environmental factors affect domestic energy requirements in many ways, and since all geographical areas have their own weather and climate, a weather file profile for the ZEBHs simulation was considered. These data files provide information about factors such as global and diffuse solar radiation, outdoor temperature, barometric pressure, wind direction, and wind speed. Building energy simulation for the ZEBHs with the modelling tool, uses EnergyPlus Weather Files (EPW) weather conditions. Therefore, an EPW (Europe WMO Region 6 - United Kingdom - Birmingham 035340 file) was obtained from EnergyPlus official website [141] and modified with Corby's PVGIS [142] weather data for the period of 2015-2016. Figure 3-4 illustrates the weather variation as displayed by EnergyPlus throughout January 2015 after adapting PVGIS weather data in the EPW file.

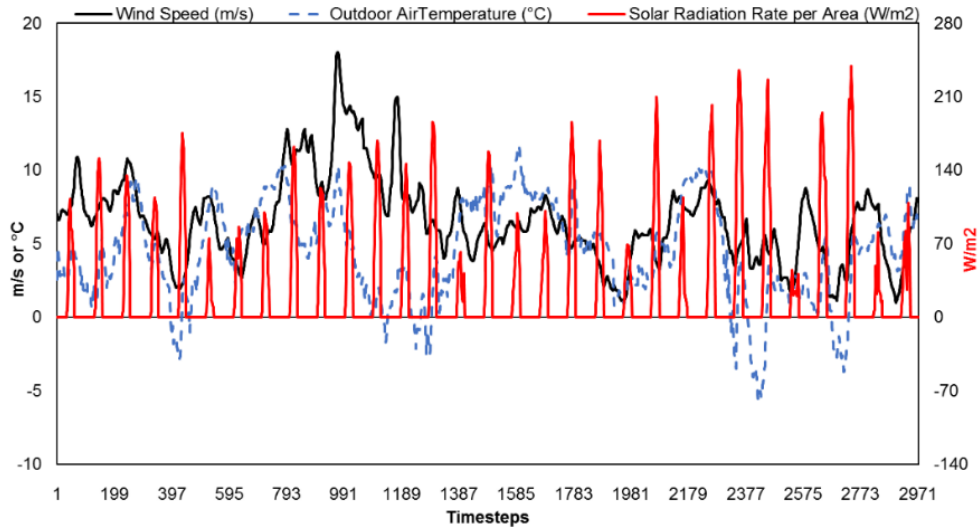


Figure 3-4: January winter month profile in EnergyPlus

3.4.4. Geometry and Buildings Envelope

The building structures of the selected domestic dwellings are in direct contact with the ground, and their external walls are adjacent to the neighbouring buildings. Hence, models of the dwellings were designed using their floor plans, while real building fabric data was employed to model the building envelopes.

Figure 3-5 illustrates the floor plan of the examined dwellings, which points out the building zones, inclusive of living room, kitchen/dining area, three bedrooms, bathroom, cupboard (cup'd), the ensuite-bathroom, electrical equipment room (A/C), and storage room. The types of structural materials used to build these domestic dwellings are bricks, insulation, and plaster/boards. More importantly, the overall heat transfer coefficients (U-values) were acquired from these materials. Air exchange between the environment and the dwellings creates natural ventilation and infiltration through the envelopes. The air exchange rate for ventilation and heat loss calculations can be determined through air changes per hour (ACH). It is worth noting that 0.50 ACH is the common value applied at most homes [143][144]. Table 3-1 presents the U-values and ACH considered for modelling domestic dwellings. The U-value is the reciprocal of all resistance of the materials found in each building elements (walls roof...etc). **Appendix A1** presents the type of materials used for the domestic dwellings

Table 3-1: Considered building standards for modelled domestic dwellings

| Parameters | Electric Homes |
|--------------------|----------------|
| Wall U-Value | 0.178 |
| Roof U-Value | 0.129 |
| Floor U-Value | 0.136 |
| Windows U-Value | 1.200 |
| Airtightness (ACH) | 0.50 |



Figure 3-5: Domestic dwelling floorplan views with defined zones. a) front view; b) cross-section view; c) first floor plan view; and d) and ground floor plan view.

3.4.5. Occupancy Levels and Activity Profiles

Table 3-2 tabulates the occupancy for each domestic dwelling. A set of monitoring data of all the domestic dwellings was collected to acquire knowledge regarding the realistic activities and behavioural profiles of the occupants in terms of electrical appliances, lighting, heating systems, and DHW usages. The simulation related to electrical appliances and lighting usages were calibrated to match the monitoring data results and consequently to validate the model. **Section 3.4.11** presents the calibration method.

Table 3-2: Occupancy information

| Home and Plot Number | Occupants |
|----------------------|-----------|
| EH Plot-272 | 4 |
| EH Plot-273 | 3 |
| EH Plot-274 | 5 |
| EH Plot-349 | 2 |

3.4.6. Electrical Appliances and Lighting

Details regarding the electrical appliances used in the domestic dwellings were also modelled based on Richardson et al [145]. These appliances include a computer, a monitor, a printer, a hairdryer, a television, a DVD player, and kitchen appliances. As for the lighting system, 12 We lights was in each building zone. Table 3-3 and Table 3-4 summarises the lighting and equipment data.

Table 3-3: Distributed lighting system in the residential buildings

| 12W _e lights | No. per room | Total |
|----------------------------|--------------|-------|
| Living | 3 | 36 |
| Bedrooms | 3 | 36 |
| Kitchen | 4 | 48 |
| Hall | 2 | 24 |
| Bathrooms | 1 | 12 |
| En-Suite | 1 | 12 |
| Storage Rooms | 1 | 12 |
| Electrical Equipment Rooms | 1 | 12 |

Table 3-4: Overview of considered household appliances and their required properties for the buildings modelling

| Appliance Category | Appliance Type | Mean Power (W) | Cycle | Power Factor |
|----------------------|-------------------------------|----------------|-------|--------------|
| Wet | Washer Dryer | 792 | | 0.8 |
| | Washing Mashing | 406 | | 0.8 |
| Cooking | Hob | 2400 | | 1.0 |
| | Oven | 2125 | | 1.0 |
| | Kettle | 2000 | | 1.0 |
| | Microwave | 1250 | | 1.0 |
| | Toaster (small cooking group) | 1000 | | 1.0 |
| Consumer Electronics | TV1/Monitor | 124 | | 0.9 |
| | TV 2 | 124 | | 0.9 |
| | Printer | 335 | | 0.9 |
| | Personal Computer | 141 | | 0.9 |
| | VCR/DVD | 34 | | 1.0 |
| Cold | Fridge-Freezer | 190 | | 0.8 |

3.4.7. Solar Photovoltaic Thermal Assisted Heat Pump

The primary function of the energy supply systems is to supply heat and electricity to cater to the demands and needs of each household. As a matter of fact, the studied domestic dwellings employed a solar photovoltaic thermal-assisted heat pump (SPVTAH) system, along with an under-floor heating system and fan-assisted radiators as heat emitters (see Figure 3-6).

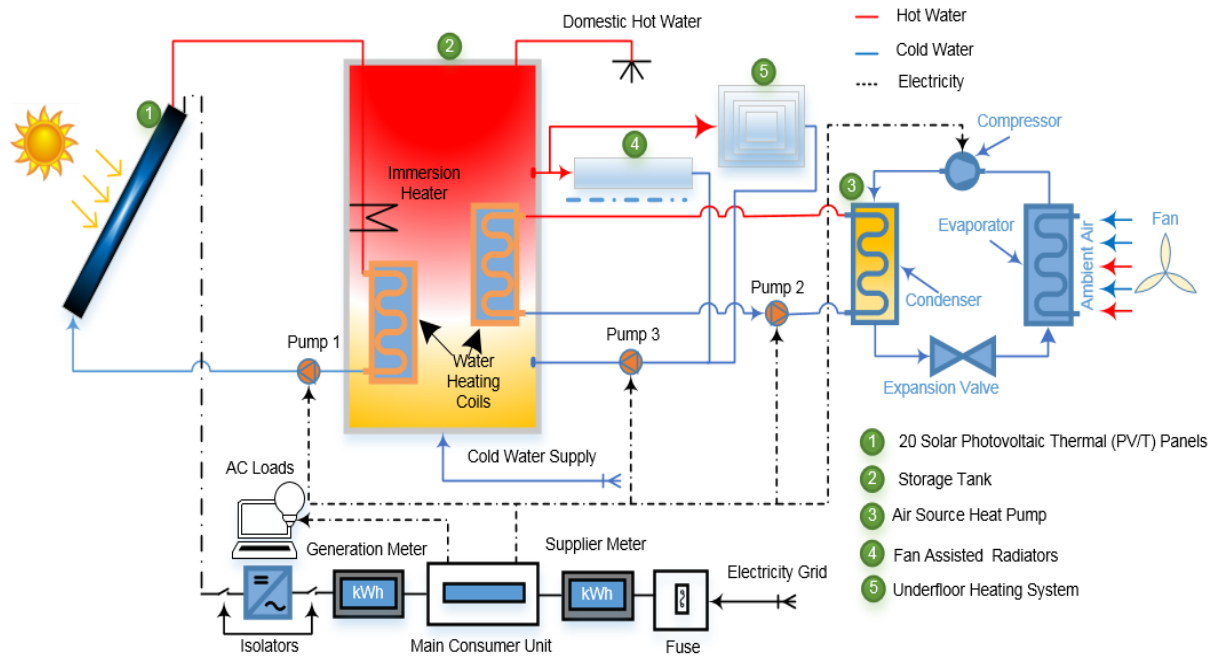


Figure 3-6: ZEBHs energy supply system

3.4.7.1. Solar Photovoltaic Thermal Panels

The main, as well as the primary source of energy, is the solar photovoltaic thermal (PV/T) panels that are used to generate electricity and heat. The electricity supplied caters to the household's electricity demand, whilst the heat generated is stored in the water tank for space and water purposes. However, the intermittent generation from the solar PV/T panels makes it complicated to maintain a steady temperature in the water tank, hence, requiring an air-source heat pump (ASHP) to be installed in the water tank as a back-up heat device for heating.

heating purposes. However, the intermittent energy generation from the solar PV/T panels makes maintaining a stable temperature in the water tank a little complicated; hence, an ASHP is needed to be installed in the water tank as a back-up heat device. The PV/T system produces electricity when solar radiation falls onto the surfaces of the PV panels; upon this electricity generation, the inverter switches from direct current (DC) to alternating current (AC). When the sunlight falls on the PV panels, the temperature of these panels increases, and the heat, thus generated, is absorbed by the absorber plate to heat the water inside the tubes, and this hot water supplies heat to the domestic dwellings. Figure 3-7 presents the modelled PV/T panels cross-section view.

The solar PV/T system modelled for the selected ZEBHs had 20 roof-mounted solar PV/T panels. Table 3-5 summarises the key parameters of the modelled solar PV/T collectors.

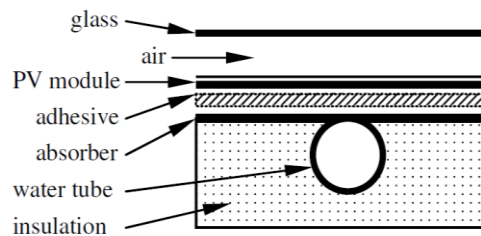


Figure 3-7: Cross section view of a PV/T collector [139].

Table 3-5: PV/T Key parameters [146]

| PV/T Parameters ^a | Value |
|--|-------|
| A_{surf} - Module area (m ²) | 1.37 |
| E_{σ} - Cell Efficiency (%) | 17.5 |
| E_{r} - Temperature coefficient of Cell efficiency (%/°C) | 0.045 |
| I_{mpp} -Nominal Current (A) | 5.43 |
| P_{mpp} -Nominal Power at maximum power point (W) | 200 |
| T - Module Temperature at Normal Operating Cell Temperature (°C) | 25 |
| V_{mpp} -Nominal Voltage maximum power point (V) | 36.8 |
| α - Collector Plate Absorptance | 0.70 |
| τ - Cover Transmittance | 0.91 |
| A_{abs} -Absorber Area (m ²) | 1.19 |
| FR- Heat Removal Factor | 0.86 |
| UL- Collector Thermal Loss Coefficient (W/m ² °C) | 0.30 |

^a Obtained from manufacturers. Source: <https://www.solimpeks.com/hybrid>

EnergyPlus currently has a model based on user-defined efficiencies. The solar PV/T models reuse the PV models for electrical production. The model calculates the outlet temperature based on the inlet temperature and the collected heat using the following equations:

$$Q_{therm} = A_{surf} f_{act} G_T \eta_{thermal} \quad (3.1)$$

The working fluid temperature leaving the solar PV/T panels is calculated as follows:

$$T_{out} = T_{in} + \frac{Q_{therm}}{\dot{m} C_p} \quad (3.2)$$

The usable electrical power produced by the PV/T panels surface is calculated using:

$$P_{el} = A_{surf} f_{activ} G_T \eta_{cell} \eta_{invert} \quad (3.3)$$

- Q_{therm} is the thermal energy collected in W
- A_{surf} is the net area of the surface in m^2
- f_{activ} is the fraction of surface area with active PV/T collector
- $\eta_{thermal}$ is the thermal conversion efficiency in %
- η_{invert} is the inverter efficiency in %
- T_{out} is the working fluid outlet temperature in $^{\circ}C$
- T_{in} is the working fluid inlet temperature in $^{\circ}C$
- \dot{m} is the mass flow rate of the working fluid through the PV/T panels
- C_p is the specific heat capacity of the working fluid in $J/kg^{\circ}C$
- G_T is the solar irradiance in W/m^2

3.4.7.2. Air Source Heat Pumps

The role of the ASHP is to maintain the temperature in water storage tank between $50^{\circ}C$ and $55^{\circ}C$ (for space heating and DHW) using on/off controls with a dead band $5^{\circ}C$ variance in temperature. The modelled ASHPs were directly attached to the water storage tank to support supply of heat for DHW usage and space heating. The ASHP was set to have a maximum thermal capacity of $4kW_{th}$ and a nominal coefficient of performance (COP) of 3.2 was also designated as the ratio of energy output to energy input. Figure 3-8 illustrates the details of the model key parameters. The configuration is inclusive of an evaporator, a compressor, a condenser, a valve, and a water circulation pump. The fan draws in outdoor air across the evaporator coil so that the refrigerant can absorb the heat. Next, the refrigerant compresses the air and increases its temperature. When air is compressed, temperature increases because temperature and volume of gas are inversely proportional to each other according to gas laws [147]. Afterwards, the heat generated from the compressed air is transmitted to the heat sink through the condenser coil. Table 3-6 represents the ASHP model parameters implemented as input for the EnergyPlus models.

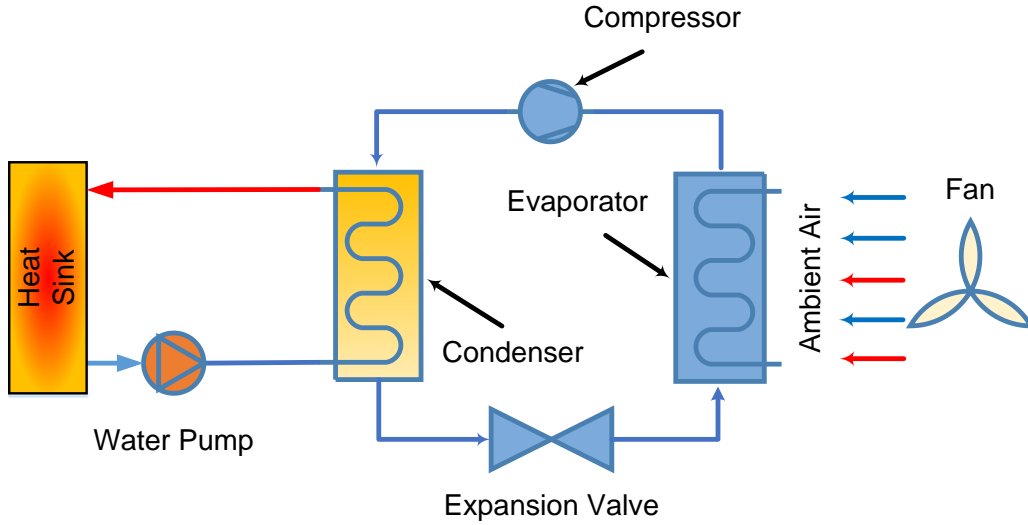


Figure 3-8: Illustration of an air source heat pump

Table 3-6: ASHP parameters description

| ASHP parameters | Value |
|---|-------|
| Max. rated heating capacity (kW) | 4 |
| Rated COP | 3.2 |
| Evaporator max. inlet air temperature (°C) | 29.44 |
| Condenser max. inlet water temperature (°C) | 55.73 |
| Condenser water pump power (kW) | 0.150 |
| Fan total efficiency (%) | 70 |
| Fan pressure (Pa) | 600 |

Based on the EnergyPlus ASHP model, the condenser heat capacity \dot{Q}_{cond} is calculated by using the following equation:

$$\dot{Q}_{cond} = \sum_{t_i}^{t_o} (\dot{m}_{fr} (b_{out} - b_{in})) \quad (3.4)$$

where,

- \dot{m}_{fr} is the mass flow rate of the refrigerant (kg/s), and
- b_{out} and b_{in} are the specific enthalpies of the refrigerant at the outlet and inlet of the condenser (kJ/kg).

The heat transferred to the heat sink (\dot{Q}_{hw}) can be determined by using the following equation:

$$\dot{Q}_{hw} = \sum_{t_i}^{t_o} (m_{hw} (T_{w,in} - T_{w,out})) \quad (3.5)$$

where,

- m_{hw} is mass flow rate of hot water (kg/s), and
- $T_{w,in}$ and $T_{w,out}$ are the inlet and outlet water temperatures in °C.

The ASHP power consumption (\dot{Q}_{hp}), as displayed in Equation 3.6, is equivalent to the total energy consumed by the compressor and the water pump, as follows:

$$\dot{Q}_{hp} = \sum_{t_i}^{t_o} (P_{comp} + P_{pump}) \quad (3.6)$$

where,

- P_{comp} and P_{pump} are the electrical power of compressor and pump (W)

Meanwhile, the nominal Coefficient of Performance of the ASHP is given as follows:

$$COP = \frac{\dot{Q}_{hw}}{\dot{Q}_{hp}} \quad (3.7)$$

3.4.7.3. Hot Water Tank and Domestic Hot Water Demand

The solar PV/T panels and ASHP serve the 250-L water storage tank at each dwelling by using a water heating coil. The water storage tank modelled in this study is a joule sequentially stratified thermal storage tank applied in medium-sized solar DHW heating systems (Figure 3-9). The temperature of the water storage tank was set between 45°C and 55°C, with a maximum temperature of 70°C. On top of that, the storage tank temperature was increased up to 60°C once every ten days using 3kW_e heater to prevent the growth of legionella [148]. In EnergyPlus, the model analytically solves the differential equation governing the energy balance of the water tank:

$$mC_{pT} \frac{dT_T}{dt} = \rho_T V_T C_{pT} \frac{dT_T}{dt} = q_{net} \quad (3.8)$$

where,

- m is the total mass of water in the tank (kg/s),
- ρ_T is the density of the water storage tank (kg/m³),
- V_T reflects the total volume of the tank (m³),
- C_{pT} stands for heat capacity of the storage fluid (J/Kg°C),
- T_T is the temperature of the water tank in °C,
- t is the time in s, and
- q_{net} is the net heat transfer rate to the tank water in W.

The net heat transfer rate q_{net} is the sum of gains and losses due to multiple heat transfer pathways:

$$q_{net} = q_{heater} + q_{oncyclepara} + q_{offcyclepara} + q_{oncycleloss} + q_{offcycleloss} + q_{use} + q_{source} \quad (3.9)$$

where,

- q_{heater} is the heat added by the heating element in W,
- $q_{oncyclepara}$ is the heat added due to on-cycle parasitic loads (zero when off) in W,
- $q_{oncycleloss}$ is the heat transfer to/from the ambient environment (zero when off) in W,
- $q_{offcycleloss}$ is the heat transfer to/from the ambient environment (zero when on) in W,
- q_{use} is the heat transfer to/from the heat use side connections in W, and
- q_{source} is the heat transfer to/from the source side connections in W.

$q_{oncycleloss}$ and $q_{offcycleloss}$ are defined as follows:

$$\begin{aligned} q_{oncycleloss} &= UA_{oncycle} (T_{air} - T_T) \\ q_{offcycleloss} &= UA_{offcycle} (T_{air} - T_T) \end{aligned} \quad (3.10)$$

where,

- U is the rate of transfer of heat through, divided by the difference in temperature in (W/(m²/°C))
- $A_{oncycle}$ is the external surface of the storage tank when heat is transferred from environment and load is on in m²,
- $A_{offcycle}$ is the external surface of the storage tank when heat is transferred from environment and load is off, and
- T_{air} and T_T are the ambient air and storage tank temperatures in °C, respectively.

q_{use} and q_{source} are defined as follows:

$$\begin{aligned} q_{use} &= \varepsilon_{use} \dot{m}_{use} C_p (T_{use} - T_T) \\ q_{offcycleloss} &= \varepsilon_{source} \dot{m}_{source} C_p (T_{source} - T_T) \end{aligned} \quad (3.11)$$

where,

- ε_{use} and ε_{source} are the heat exchanger effectiveness for the heat use and source sides in W
- \dot{m}_{use} and \dot{m}_{source} are the mass flow rates of fluid through the heat exchangers (kg/s),
- C_p is the heat capacity of the heat exchange fluid (J/Kg°C), and
- T_{source} and T_{use} are the source and use water tank temperatures in °C, and
- T_T is the water tank temperature in °C.

Incorporating equation 3.10 and 3.11 into the original differential equation 3.9, we obtain:

$$mC_p \frac{dT}{dt} = q_{heater} + q_{oncycle} + q_{offcycle} + UA_{oncycle} (T_{air} - T_T) + UA_{offcycle} (T_{air} - T_T) + \varepsilon_{use} \dot{m}_{use} C_p (T_{use} - T_T) + \varepsilon_{source} \dot{m}_{source} C_p (T_{source} - T_T) \quad (3.12)$$

Associating terms not dependent on temperature T_T and terms dependent to T_T , yields:

$$\frac{dT}{dt} = \left[\frac{1}{mC_p} \left(q_{heater} + q_{oncycle} + q_{offcycle} + UA_{oncycle} T_{air} + UA_{offcycle} T_{air} \right) + \varepsilon_{use} \dot{m}_{use} C_p T_{use} + \varepsilon_{source} \dot{m}_{source} C_p T_{source} \right] + \left[\frac{1}{mC_p} \left(UA_{oncycle} + UA_{offcycle} + \varepsilon_{use} \dot{m}_{use} C_p + \varepsilon_{source} \dot{m}_{source} C_p \right) \right] T_T \quad (3.13)$$

The differential equation now has the form:

$$\frac{dT}{dt} = a + bT_T \quad (3.14)$$

where,

$$a = \left[\frac{1}{mC_p} \left(q_{heater} + q_{oncycle} + q_{offcycle} + UA_{oncycle} T_{air} + UA_{offcycle} T_{air} \right) + \varepsilon_{use} \dot{m}_{use} C_p T_{use} + \varepsilon_{source} \dot{m}_{source} C_p T_{source} \right] \quad (3.15)$$

$$b = \left[\frac{-1}{mC_p} \left(UA_{oncycle} + UA_{offcycle} + \varepsilon_{use} \dot{m}_{use} C_p + \varepsilon_{source} \dot{m}_{source} C_p \right) \right]$$

The solution to the differential equation can be written in terms of a and b as:

$$T_T(t) = \left(\frac{a}{b} + T_i \right) e^{bt} - \frac{a}{b} \quad (3.16)$$

Where,

- $T_T(t)$ is the water tank temperature at time t in °C,
- T_i is the initial temperature tank at time $t=0$ in °C,

However, if $b=0$, the solution presented in Equation 3.16, becomes:

$$T_T(t) = at + T_i \quad (3.17)$$

Since the control algorithm must sometimes calculate the time needed to reach a specified temperature in the water tank, the equations above can also be rearranged to solve for t , as follows:

$$t = \frac{1}{b} \ln \left(\frac{a/b + T_f}{a/b + T_i} \right) \quad (3.18)$$

hence, if $b = 0$:

$$t = \left(\frac{T_f - T_i}{a} \right) \quad (3.19)$$

Where,

- T_f is the final temperature of the water tank at time t in $^{\circ}\text{C}$,

In the case where $b=0$ and $a=0$, and $T_f \neq T_i$, the time t is infinity.



Figure 3-9: Modelled Hot Water Storage Tank. Courtesy of Electric Corby and EDP Consulting Limited[149].

This study considered a maximum usage of 150L/day for nominal daily hot water demand based on the standard outlined by Department for Environment, Food and Rural Affairs [150][151]. The DHW consumption schedule of each ZEBH occupant was determined by the UK National Calculation Methodology templates [152]. When the occupants use DHW, each water tap draw has a nominal draw flow rate, as presented in Table 3-7 [142].

Table 3-7: DHW flow rate to calculate hot water demand

| Fixture | Flow rate (m ³ /s) | Flow rate (m ³ /day) |
|----------------|-------------------------------|---------------------------------|
| Basins | 0.00008 | 6.912 |
| Sink and baths | 0.00015 | 12.96 |
| Shower | 0.00050 | 43.20 |

The energy content of hot water is derived from the following equation:

$$E_{DHW} = \frac{C_{p,water} \rho_{water} V (T_{out} - T_{in})}{3600} \quad (3.20)$$

where,

- E_{DHW} is the domestic hot water load in kWh/day,
- $C_{p,water}$ is the specific heat capacity of water (4.187kJ/kg°C),
- V is the daily volume of hot water draw (m³/day) and
- T_{out} and T_{in} are, respectively, the output and input mains supply water temperatures in °C.

3.4.8. Space Heating Demand

The heaters installed in the selected dwellings offer indoor temperature comfort to their occupants at a set temperature of 19 °C for the entire dwelling space, except in the living room where the thermostat temperature is set at 21 °C. Heat load within domestic dwellings is dictated by the indoor heat gain values and heat losses that vary over time. **Appendix A2** presents an example on how to calculate the heat losses in a building.

Heat load within the domestic dwellings was dictated by the indoor heat gain values and heat losses that vary over time. The heat load of any building is simply determined using the differences between heat gains and heat losses. To determine the space heating demand, the Heating Degree Days (HDD) for a building should be measured. The HDD is a value that corresponds to the difference between baseline temperature (15.50 °C in the UK) and the actual outdoor temperature, multiplied by the number of annual days [153]. However, HDD is set to zero in the case temperature exceeds the baseline temperature. Finally, the space heating demand is measured by subtracting the heat gains from the product of heat losses and HDD, as follows:

$$\dot{Q}_{bd} = \left[(\dot{Q}_{hl} HDD) - \left(\int_{\tau_1}^{\tau_2} \dot{Q}_{hg} dt \right) \right] = (\dot{Q}_{vent/inf} + \dot{Q}_{trans}) HDD - \int_{\tau_1}^{\tau_2} (\dot{Q}_{sirr} + \dot{Q}_p + \dot{Q}_{app/light}) dt \quad (3.21)$$

where,

- \dot{Q}_{bd} is the space heating demand in W
- \dot{Q}_{hl} is the total heat losses in W

- \dot{Q}_{bg} is the total heat gains in W
- $\dot{Q}_{vent/inf}$ is the heat losses due to the infiltration and ventilation losses in W
- \dot{Q}_{trans} is the transmission losses associated to building envelope materials in W
- \dot{Q}_{sirr} is the heat gains caused through the windows in W
- \dot{Q}_p is the heat gains from human beings in W, and
- $\dot{Q}_{app/light}$ is heat generated from the electrical equipment and lighting in W.

The *HDD* was weighed in this study to determine the space heating demand within the buildings as follows:

$$HDD = \begin{cases} \sum_{i=1}^N (t_{base} - t_o), & t_o < t_{base} \\ 0, & t_o > t_{base} \end{cases} \quad (3.22)$$

where,

- t_o is the outdoor temperature variances that vary over time in °C
- t_{base} is the baseline temperature in °C. In the UK t_{base} for heating is commonly been set at 15.5°C [154].

The transmission losses (\dot{Q}_{trans}) are associated to fabric heat losses that can be determined by the conductive and convective heat transfer rates of the layers within the building components (walls, roof, windows, doors and ground), and is calculated using the following equation:

$$\dot{Q}_{trans} = \sum_{i=1}^n U_i A_i (t_r - t_o) \quad (3.23)$$

The heat transfer coefficient or U-value is calculated by:

$$U_i = \frac{1}{\frac{1}{h_0} + \frac{\delta_1}{k_1} + \frac{\delta_2}{k_2} + \frac{1}{h_r}} \quad (3.24)$$

For calculating the heat losses through the ground, the following equation is applied:

$$\dot{Q}_{ground} = \sum_{i=1}^n U_i A_i (t_r - t_g) \quad (3.25)$$

where,

- \dot{Q}_{ground} is the heat loss through the ground in W
- h_0 : heat transfer coefficient for external conditions, dependent on convection and radiation $\sim 12-20 \text{ W/m}^2\text{K}$,
- t_o and t_r are the indoor and outdoor temperatures ($^{\circ}\text{C}$) respectively,
- U_i is the overall heat transfer coefficient ($\text{W}/(\text{m}^2/^{\circ}\text{C})$), and
- A_i is the surface area (m^2) connected to the overall heat transfer coefficient.
- h_i : heat transfer coefficient for internal conditions, dependent on convection and radiation $\sim 8-12 \text{ W/m}^2\text{K}$,
- δ : thickness of the material layer (m), and
- k : thermal conductivity of the material layer ($\text{W}/(\text{mK})$).
- t_g stands for the ground temperature in $^{\circ}\text{C}$.

The approach for calculating the heat loss due to infiltration and ventilation is the ACH , as follows:

$$\dot{Q}_{vent/inf} = \left[\left(\frac{V(ACH)}{3600} \right) \rho_{air} C_{p,air} (t_r - t_o) \right] \quad (3.26)$$

where,

- V is the volume of the house (m^3),
- ρ_{air} the density of air (kg/m^3) at indoor temperature;
- $C_{p,air}$ represents the specific heat capacity of the air ($\text{J}/(\text{kg}/^{\circ}\text{C})$).
- ACH , is the air changes per hour for the minimum fresh air requirements.

The amount of heat generated by occupants when they are within their dwellings highly depends on their activities and the level of occupancy level, but the heat gain caused by \dot{Q}_{sirr} through the windows, is given as follows:

$$\dot{Q}_{sirr} = F_r G_T \sum_{i=1}^n A_{windows,i} \quad (3.27)$$

where,

- F_r is the fraction of radiation transmitted through the windows, typically less than 80%,
- G_T is the solar irradiance (W/m^2),
- $A_{windows}$ is the windows area in m^2 , and
- n is the total number of window areas.

Heat generated from electrical equipment is calculated according to the operating hours, and several load factors. Meanwhile, heat generated by the lighting system depends on the electricity levels and on the light emitted from the source. Heat gained from appliances and lighting (Q_{app}) is calculated as follows:

$$\dot{Q}_{app/light} = \left[\left(\sum_{i=1}^n (P_{a,i} F_{UA,i} F_{LA,i}) \right) + \left(\sum_{i=1}^n ((3.41 P_{l,i}) (F_{UL,i} F_{SL,i})) \right) \right] \quad (3.28)$$

where,

- P_a is the rated electrical power (W),
- F_{UA} is the equipment use factor and
- F_{LA} the equipment load factor,
- P_l is the installed light wattage (W),
- F_{UL} is the light use factor and F_{SL} is the light special allowance factor for fluorescent fixtures and/or fixtures that are ventilated.
- 3.41 is British thermal unit/hour to Watts conversion factor

3.4.9. Electrical and Net Electrical Demand

Electricity demand for every studied dwelling was determined in order to calculate the energy load to be adequately supplied by considering the varied energy usage activity profiles.

Total electricity demand denotes the sum of the building loads, the electric heating loads from ASHPs, and the water tank immersion heaters.

The net electrical demand refers to the variances between the demand for electricity in buildings and the electric power generated on-site. As revealed in this study, electricity is exported from grids when its demand exceeds the electricity generated from the solar PV/T panels.. Hence, as depicted in Equation 3.29, the total electricity demand (P_{dmd}) refers to the sum of the building loads ($P_{bldg, dmd}$), the electric heating loads from ASHPs, and the water tank immersion heaters ($P_{elecbeat, dmd}$).

$$P_{dmd} = P_{bldg, dmd} + P_{elecbeat, dmd} \quad (3.29)$$

where,

- P_{dmd} is the total electricity demand in kW_e
- $P_{bldg, dmd}$ is the sum of the building loads in kW_e and
- $P_{elecbeat, dmd}$ is the electric heating loads from the ASHP and water tank immersion heater in kW_e

Equation 3.30 presents two relevant values weighed in for the concept of ‘net’ electricity demand, which are:

- i) the amount of power generated by the PV/T panels, and
- ii) the building electricity demand by its occupants.

$$P_{net} = P_{dmd} - P_{PV/T,gen} \quad \text{where, } P_{net} = \begin{cases} P_{net} < 0, & \text{for } P_{dmd} < P_{PV/T,gen} \\ P_{net} > 0, & \text{for } P_{con} > P_{PV/T,gen} \\ P_{net} = P_{con}, & \text{for } P_{PV/T,gen} = 0 \end{cases} \quad (3.30)$$

where,

- P_{dmd} is the electricity demand in kW
- P_{con} is the actual power consumed by the PV/T panels in kW
- $P_{PV/T,Gen}$ is the power generated by the solar PV/T panels in kW
- P_{net} is the net electrical demand in kW

3.4.10. Data Measurement

To validate the actual electrical energy performance of each ZEBH, measured data from each building was needed to be collected. This data includes the Uniq solutions EM21 energy meter and Live View Pack [155] where the electricity consumption (appliances and lighting) for a period of one winter week (10th to 17th of December 2015) with a time frequency of 15 min was measured. Furthermore, the metered data only considered the electrical demand and not the net electrical demand.

3.4.11. Calibration Method

The calibration process required several manual iterations on the appliances and lighting usage before obtaining a model with acceptable accuracy. The limit proposed by the American Society of Heating, Refrigerating and Air-Conditioning Engineers (ASHRAE) Guideline 14 [ASHRAE, 2002] was selected for this study. Accordingly, the Normal Mean Bias Error (NMBE) should be inside +/- 10% and the Coefficient of Variation of the Root Mean Square Error CVRMSE lower than 30% when evaluated on hourly time intervals. This entails determining the two dimensionless indicators of errors, NMBE and CVRMSE values using the following equations:

$$NMBE = \frac{\sum_{i=1}^{N_i} (M_i - S_i)}{\sum_{i=1}^{N_i} M_i} \quad (3.31)$$

$$CVRMSE = \frac{\sqrt{\frac{\sum_{i=1}^{N_i} [(M_i - S_i)]^2}{N_i}}}{\frac{1}{N_i} \sum_{i=1}^{N_i} M_i} \quad (3.32)$$

where:

- M_i and S_i are respective measured and simulated data at instance i , and
- N_i is the count of the number of values used in the calculation.

3.4.12. Solar PV/T Model Verification Method

It was not possible to model the functionality of ZEBHs solar PV/T panels using the DesignBuilder; hence, solar PV panels were modelled instead, and subsequently, the EnergyPlus model code files were modified in order to adapt solar PV/T panels for each home.

In this case, no reliable data could be measured using monitoring devices on the ZEBHs for validation purposes; therefore, the MATLAB software was used to replicate the EnergyPlus solar PV/T panels. This permitted the analysis of the solar PV/T panels performance, which consequently helped verify whether or not the EnergyPlus simulations results were accurate. Therefore, the PV/T model's performance was verified on a summer day (1st of June). The performance of a solar PV/T collector depends on design parameters and weather and operating conditions (e.g., irradiance, ambient temperature, absorber plate temperature, etc.).

Thus, in order to complete the analysis with MATLAB, the parameters of the PV/T collector described in Table 3-5 were applied, considering a fluid inlet temperature (T_i) of 40°C and a tilt angle of 45°. **Appendix A3** presents the results, the steps followed, and equations used in MATLAB and EnergyPlus to attain this.

3.4.13. Techno-Economic Study

This section outlines the methodology adopted for accomplishing the economic study. Based on the outcomes derived from the building energy simulations using EnergyPlus, a techno-economic assessment was performed on the SPVTAH of the dwellings over the course of a year. The three key parameters that helped determine the economic benefit include Feed-in Tariff (FiT), exported tariff price, and electricity cost (including standing charges).

The UK price tariffs directed by the Office of Gas and Electricity Markets (Ofgem) for the generation and export of electricity were adopted in this study. The electricity cost included the standing charges for providing electricity by the actual energy retailer (BritishGas) to the dwellings. Table 3-8 depicts the parameters embedded in the economic analysis. The parameters from Table 3-8 were retrieved from Ofgem Standard Large Solar PV system charge export tariff, and FiT, whilst Table 3-9 represents cost of the Solar PV/T panels (obtained from the manufacturer), and total cost of installation and maintenance by the installation company-Convert Energy Ltd.

Table 3-8: Tariffs used for feasibility calculations

| Tariffs | Price |
|--------------------|--------------------------|
| FiT | 0.0034£/kWh ^a |
| Export Tariff | 0.054£/kWh ^a |
| Electricity Tariff | 0.12£/kWh ^b |
| Standing Charge | 0.25£/day ^b |

^aOfgem- Standard large solar PV systems (1000-5000kW) [156]

^bBritishGas [157]

Table 3-9: Energy supply system cost parameters

| Parameter | Value |
|---|-----------|
| 20 x Solar PV/T panels cost ^a | £6600 |
| 20 x Solar PV/T panels installations cost ^a | £4200 |
| ASHP cost ^a | £5500 |
| ASHP installations cost ^a | £1800 |
| 20 x Solar PV/T panels and ASHP maintenance cost ^a | £220/year |
| Discount rate (d) | 10% |
| System life ^b | 25 years |

^aObtained from supplier. Source: <https://www.convertenergy.co.uk/>

^bObtained from manufacturers. Source: <http://www.solimpeks.com/>

The total cost incurred to operate the 20 solar PV/T panels and an ASHP at each dwelling is calculated as the total electricity cost minus the cost of displaced electricity imported from grid, including the revenue accumulated from the electricity exported to the grid. The following equation represents this notion at each time step (t):

$$SPVTAH_{cost(t)} = \left[\left((Elec_{dmd} - PVTElec_{out}) Cost_{Elec} \right) + (SC_{Elec} d) \right] - \left[(PVTElec_{out} FiT_{price}) + (Elec_{Exp} TariffElec_{price}) \right] \quad (3.33)$$

Now, the annual costs for SPVTAH can be calculated by summing each time step over a year, with:

$$\sum_{t=1}^{t=N} TotalSPVTAH_{(t)} \quad (3.34)$$

where,

- $SPVTAH_{cost}$ is the solar PV/T assisted by the ASHP system total cost in £,
- $PVTElec_{out}$ refers to the electrical output from the PV/T panels (kWh_e),
- $Cost_{Elec}$ is defined as the imported electricity cost £/kWh_e,
- SC_{Elec} stands for the electricity standing charge cost (£/day),
- t is the time step,
- N is the total number of time steps,
- $Elec_{dmd}$ is the electricity demand from the households (kWh_e),
- FiT_{price} is the electricity tariff in £/kWh_e, $TariffElec_{price}$ is the exported electricity price (£/kWh),
- $Elec_{Exp}$ is the electricity exported to the grid in kWh_e, and the term d is the number of days.

The present value of each annual cash flow can be discounted back to it. The Net Present Value (NPV), as displayed in Equation 3.25, can be determined by summing the cash flow for each year, starting from year 0 (investment) until the lifetime of the SPVTAH system (25 years).

$$NPV \sum_{n=0}^{25} \frac{R_n}{(1+d)^n} \quad (3.35)$$

where,

- NPV refers to the net present value in £,
- R_n is the cash flow (£), and
- d reflects the discount rate (10%).

3.5. RESULTS AND DISCUSSION

3.5.1. Measured Data Analysis

Before attempting to generate highly detailed building energy models, the measured data from each ZEBH was analysed, as illustrated in Figure 3-10 to Figure 3-13. This information was considered in the input activity schedules of the energy model. Moreover, it was important to get a reliable and predictable set of measured data to calibrate the model.

The EH-Plot 272 graph shows, at a glance, that there is a high consumption level between the 12th and 13th of December in the winter, especially in the mornings. The EH-Plot 273 had 3 occupants, and it can be noted that there were high peaks in the mornings when they woke up; however, a large power demand occurred in the evenings between 03:00h and 06:00h. Although EH-Plot 274 had 5 occupants in their dwelling, most of the time, the power demand remained only between 320 W and 480 W. EH-Plot 349 had been occupied by only 2 residents, differing from the total number of occupants in the other homes, the electrical power demand there was between 240 W and 480 W.

3.5.2. Measured Data vs Initial and Calibrated Model

After obtaining the calibrated building energy models, an analysis to compare the measured and initial model simulation was conducted. First of all, operation schedules were compared using a 15-minute time stamp for a week, as shown in Figure 3-14 to Figure 3-17. The figures enabled a quick visual inspection of the measured data against the initial and calibrated model values and the statistical variations, such as the maximum and minimum peaks, the total consumed energy, and the average power demand. From the initial model results, it can be noted that electrical consumption from appliances and lighting is more closely related to occupant activity, which deviates (randomly) from the deterministic occupancy initially used in the EnergyPlus model. The electricity consumptions of the buildings during winter weeks were 275 kWh, 392 kWh, 309 kWh, and 372 kWh in EHPlots 272, 273, 274, and 349, respectively, and the final calibrated models produced a sum of 286 kWh, 369 kWh, 338 kWh, and 363kWh in the similar order. From the individual results in each ZEBH it can be seen that EH-Plot 274 carries the highest accumulation of errors (9%) from the final calibrated model.

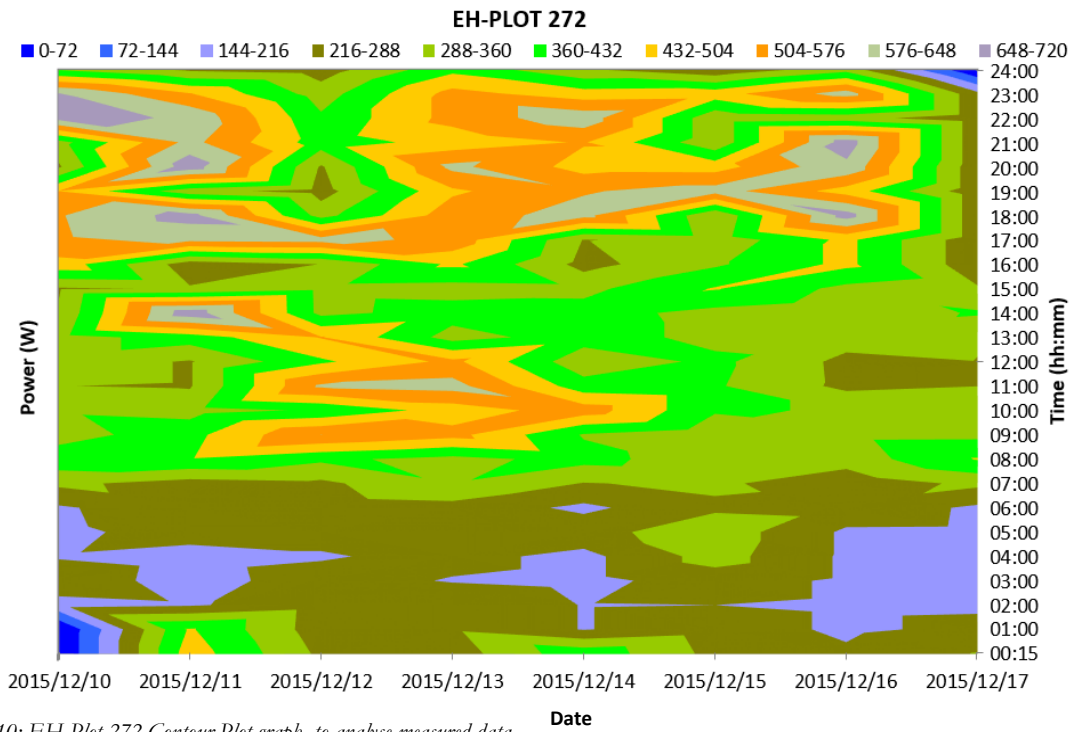


Figure 3-10: EH-Plot 272 Contour Plot graph to analyse measured data

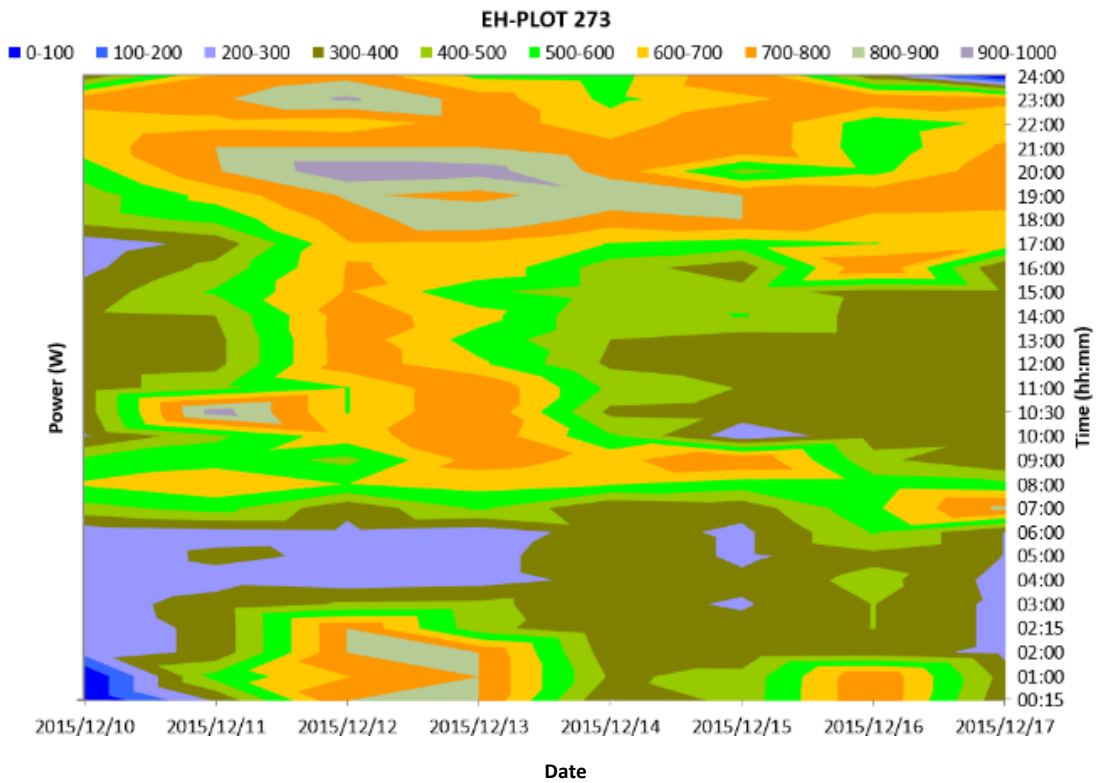


Figure 3-11: EH-Plot 273 Contour Plot graph to analyse measured data

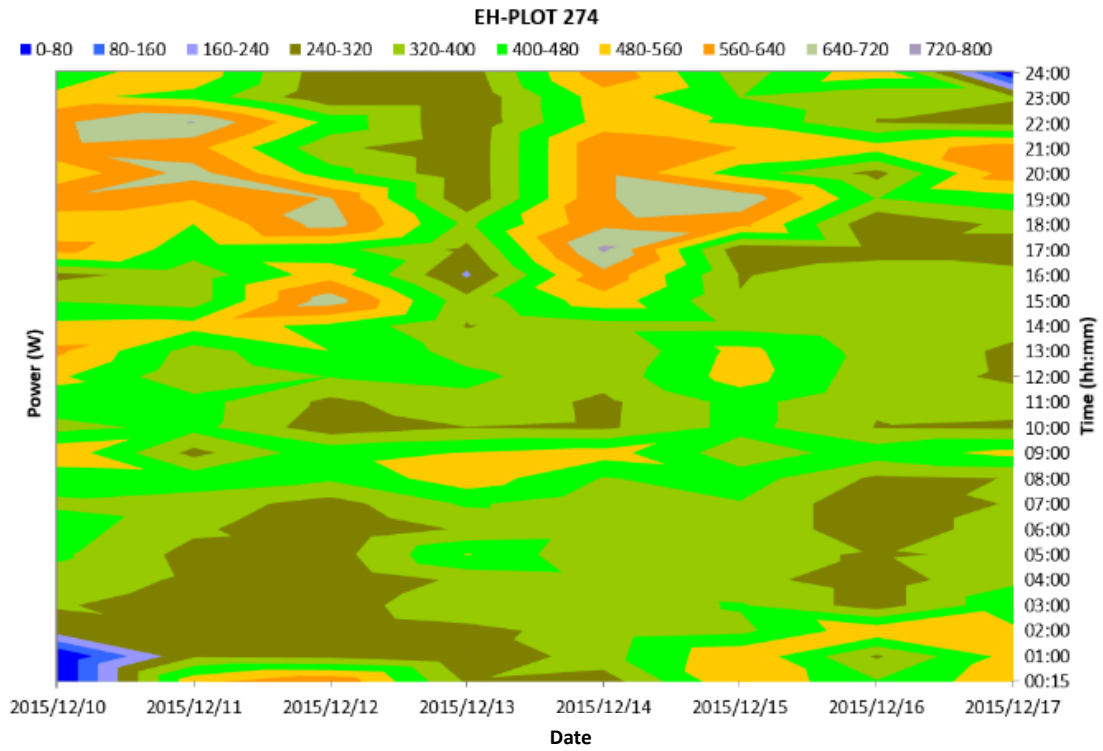


Figure 3-12: EH-Plot 274 Contour Plot graph to analyse measured data

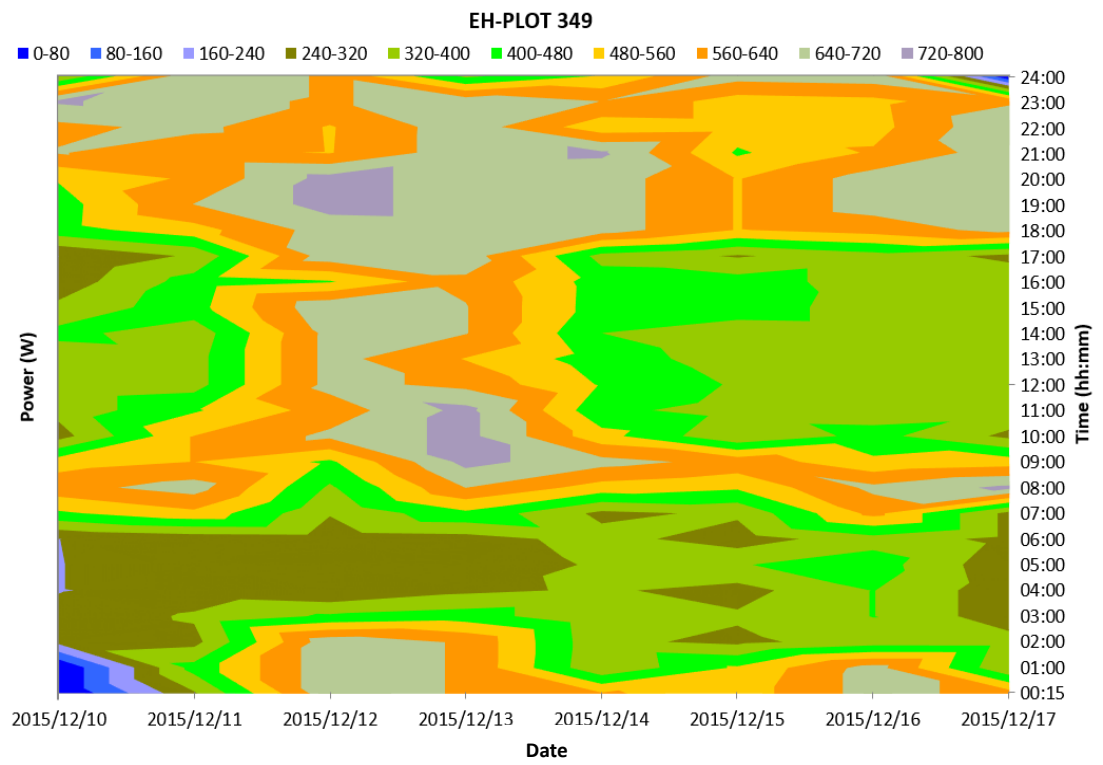
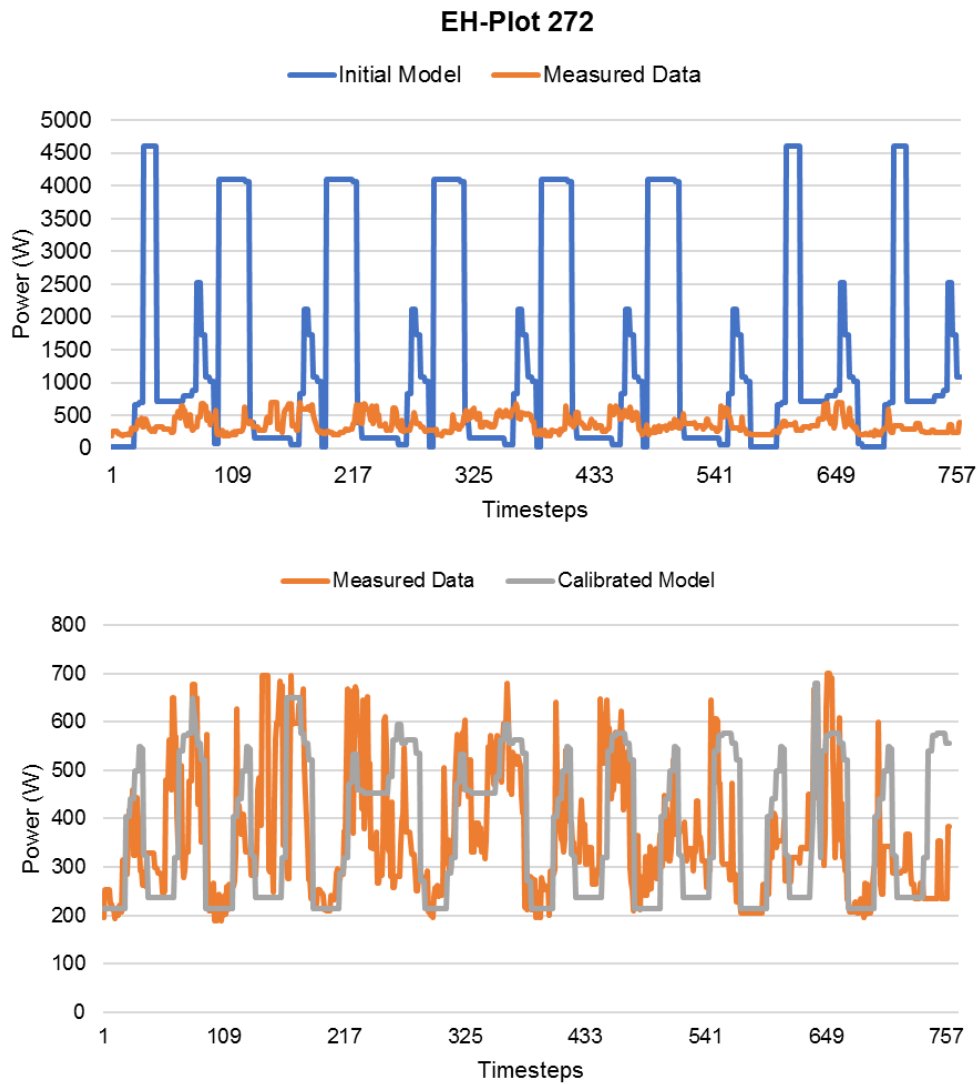
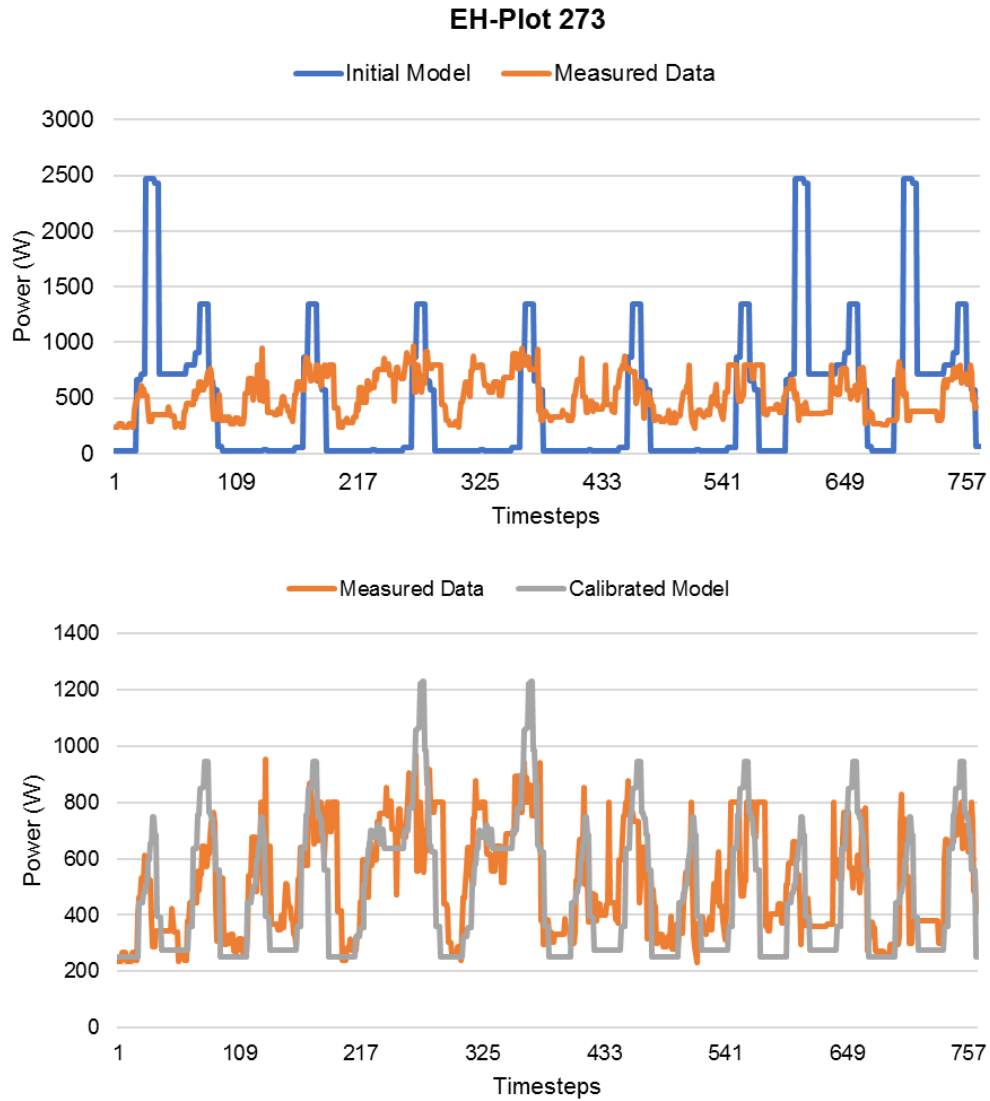


Figure 3-13: EH-Plot 349 Contour Plot graph to analyse measured data



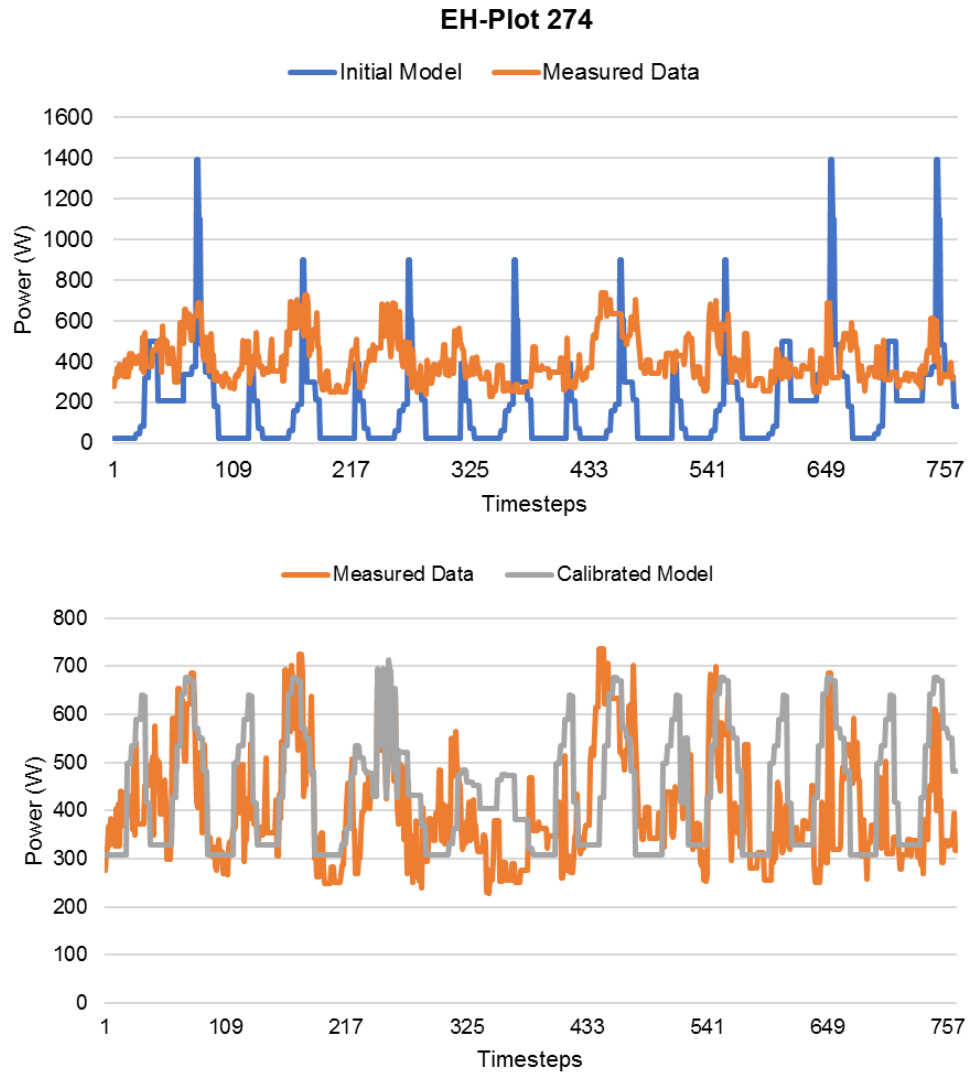
| | Measured | | Calibrated | | Difference Error |
|-----------|----------|----------|------------|--------------|------------------|
| Average | 362 | W | Average | 377 W | |
| Maximum | 699 | W | Maximum | 680 W | |
| Minimum | 190 | W | Minimum | 215 W | |
| Summation | 275 | kWh/week | Summation | 286 kWh/week | |

Figure 3-14: EH-Plot 272 Measured vs Initial and Calibrated model



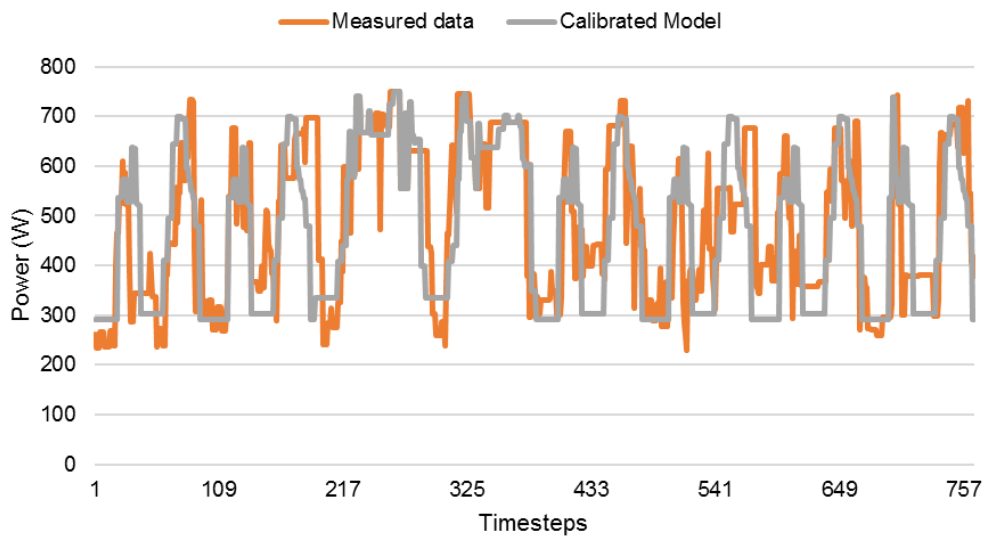
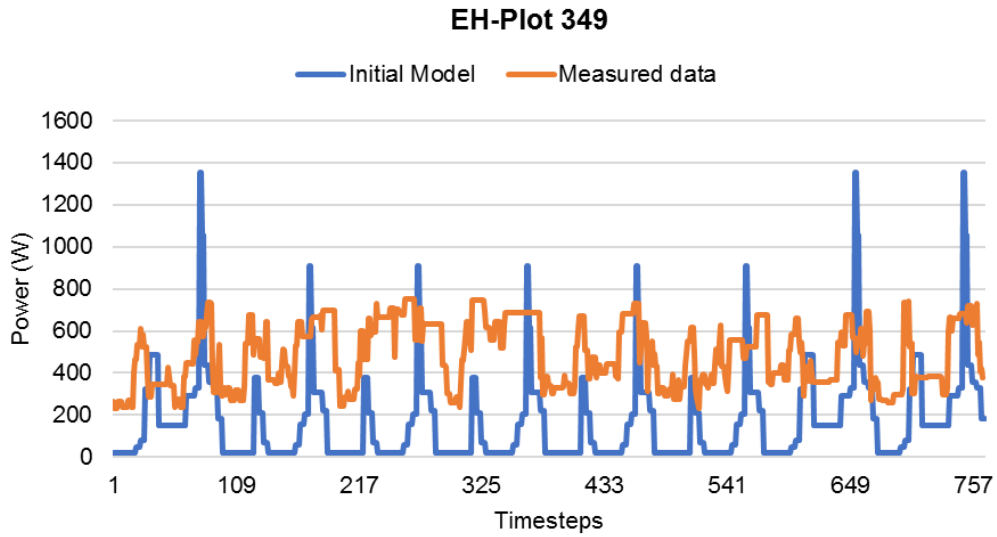
| | Measured | | Calibrated | | Difference Error |
|-----------|----------|----------|------------|--------------|------------------|
| Average | 513 | W | Average | 482 W | |
| Maximum | 968 | W | Maximum | 1230 W | |
| Minimum | 230 | W | Minimum | 253 W | |
| Summation | 392 | kWh/week | Summation | 369 kWh/week | |

Figure 3-15: EH-Plot 273 Measured vs Initial and Calibrated model



| | Measured | | Calibrated | | Difference Error |
|-----------|----------|----------|------------|-----|------------------|
| Average | 404 | W | Average | 442 | 9% |
| Maximum | 736 | W | Maximum | 714 | |
| Minimum | 227 | W | Minimum | 308 | |
| Summation | 309 | kWh/week | Summation | 338 | |

Figure 3-16: EH-Plot 274 Measured vs Initial and Calibrated model



| | Measured | | Calibrated | | Difference Error |
|-----------|----------|----------|------------|--------------|------------------|
| Average | 486 | W | Average | 473 W | |
| Maximum | 749 | W | Maximum | 749 W | |
| Minimum | 230 | W | Minimum | 292 W | |
| Summation | 372 | kWh/week | Summation | 363 kWh/week | |

Figure 3-17: EH-Plot 349 Measured vs Initial and calibrated model

3.5.3. Statistical Index Evaluations

Figure 3-18 to Figure 3-21 show the NMBE and coefficient of variance of CVRMSE for the calibrated simulation model generated by the hourly simulation program. The calibration results could meet the limits of model calibration accuracy directed in ASHRAE Guideline 14-2014.

The calibration models demonstrated accuracies for 26% (EH-Plot273), 29% (EH-Plot 273), 25% (EH-Plot274), and 21% (EH-Plot 349) over the full-week cycle.

Each of the NMBE and CVRMSE values each provide a different set of insights. NMBE possess the drawback of cancellation and hence might under-report the magnitude of the errors, as observed for instance in electrical calibration where the overall NMBE value of 5.9% was identical in EH-Plot 273 and EH-Plot 274, however, this concealed much larger CVRMSE errors in EH-Plot 273 (Figure 3-19). Within this work the CVRMSE in EH-Plot 273 carried the largest error and was the greatest source of uncertainty in the model energy prediction. This mostly affected the simulated electricity value. In contrast, the CVRMSE values provided a better indication in EH-Plot 349.

Interestingly, the difference error result from EH-Plot 274 (Figure 3-16) was higher than the CVRMSE results of EH-Plot 273 (Figure 3-19) . This might be due to the different study approaches between CVRMSE and difference error. The CVRMSE is defined as the ratio of the root mean square error to the mean values, whereas the difference error is the difference between the measured data and calibrated model, divided by calibrated model results.

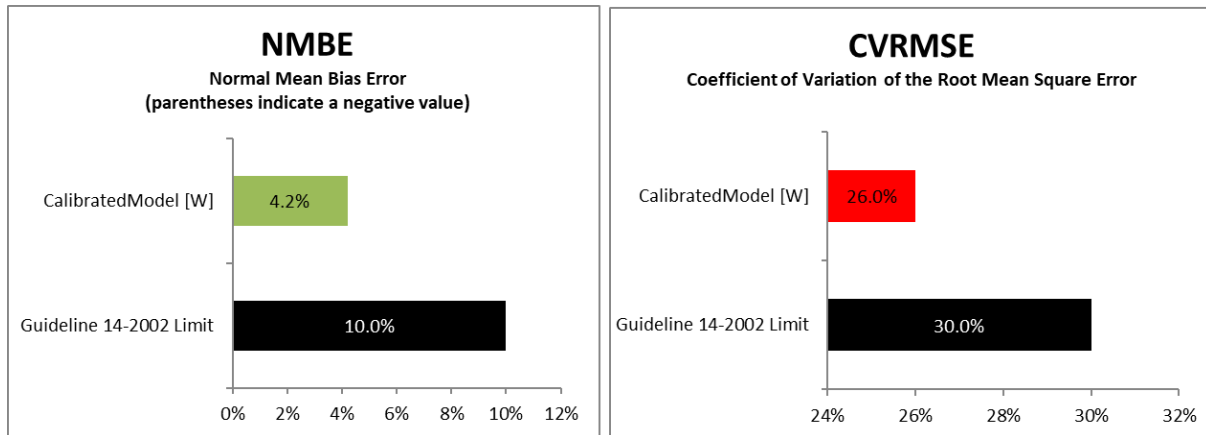


Figure 3-18:EH-Plot 272 NMBE and CV(RMSE) calibration results

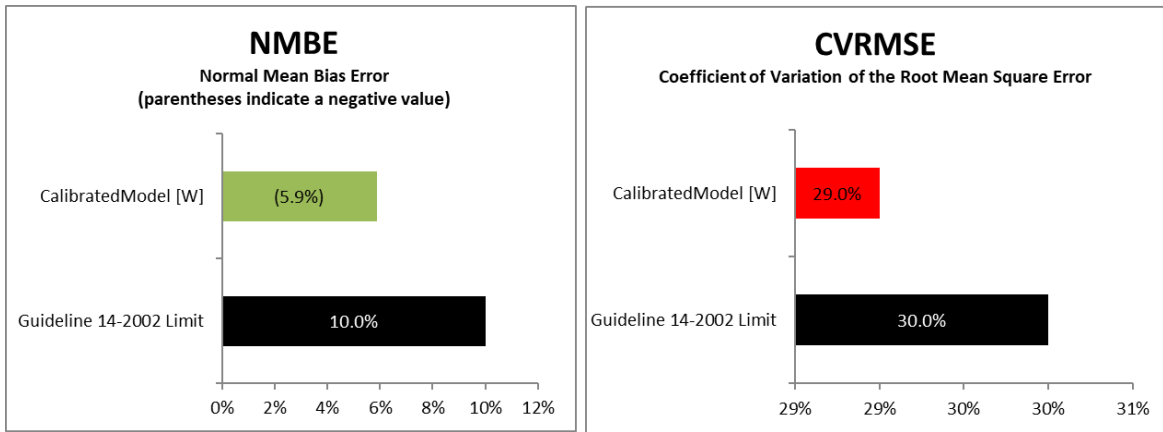


Figure 3-19: EH-Plot 273 NMBE and CV(RMSE) calibration results

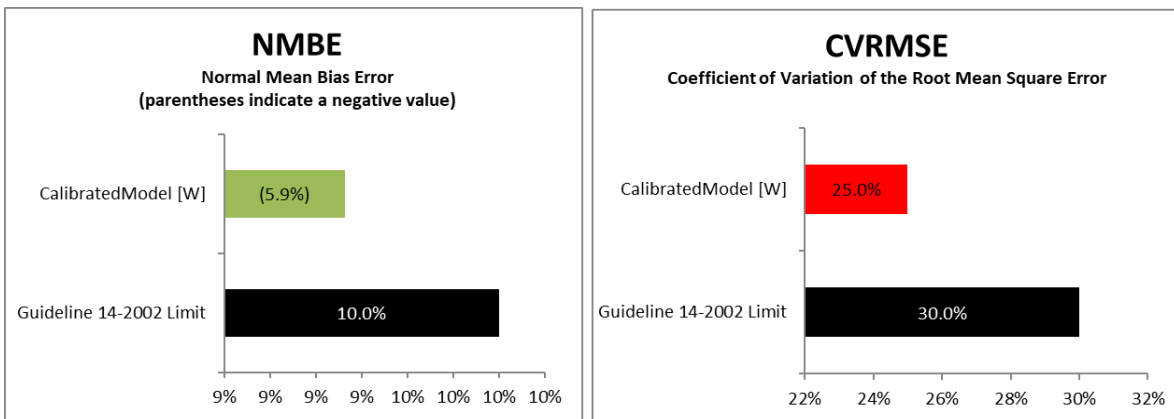


Figure 3-20: EH-Plot 274 NMBE and CV(RMSE) calibration results

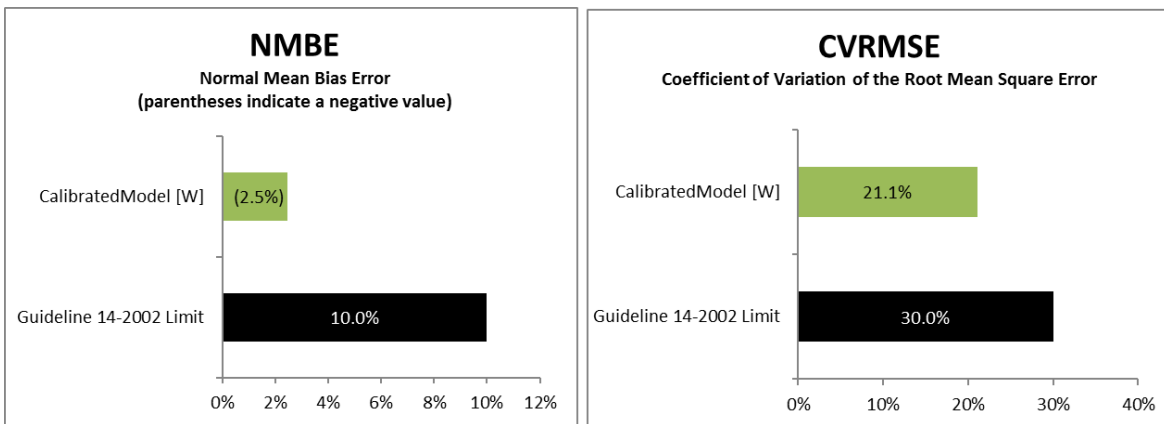


Figure 3-21: EH-Plot 274 NMBE and CV(RMSE) calibration results

3.5.4. Building Energy Performance

3.5.4.1. Electrical Energy Demand

This section presents the values of electricity end-use. Figure 3-22 illustrates the total electrical energy consumption broken down each month to emphasise the aspects related to appliances, lighting, and ASHP energy use.

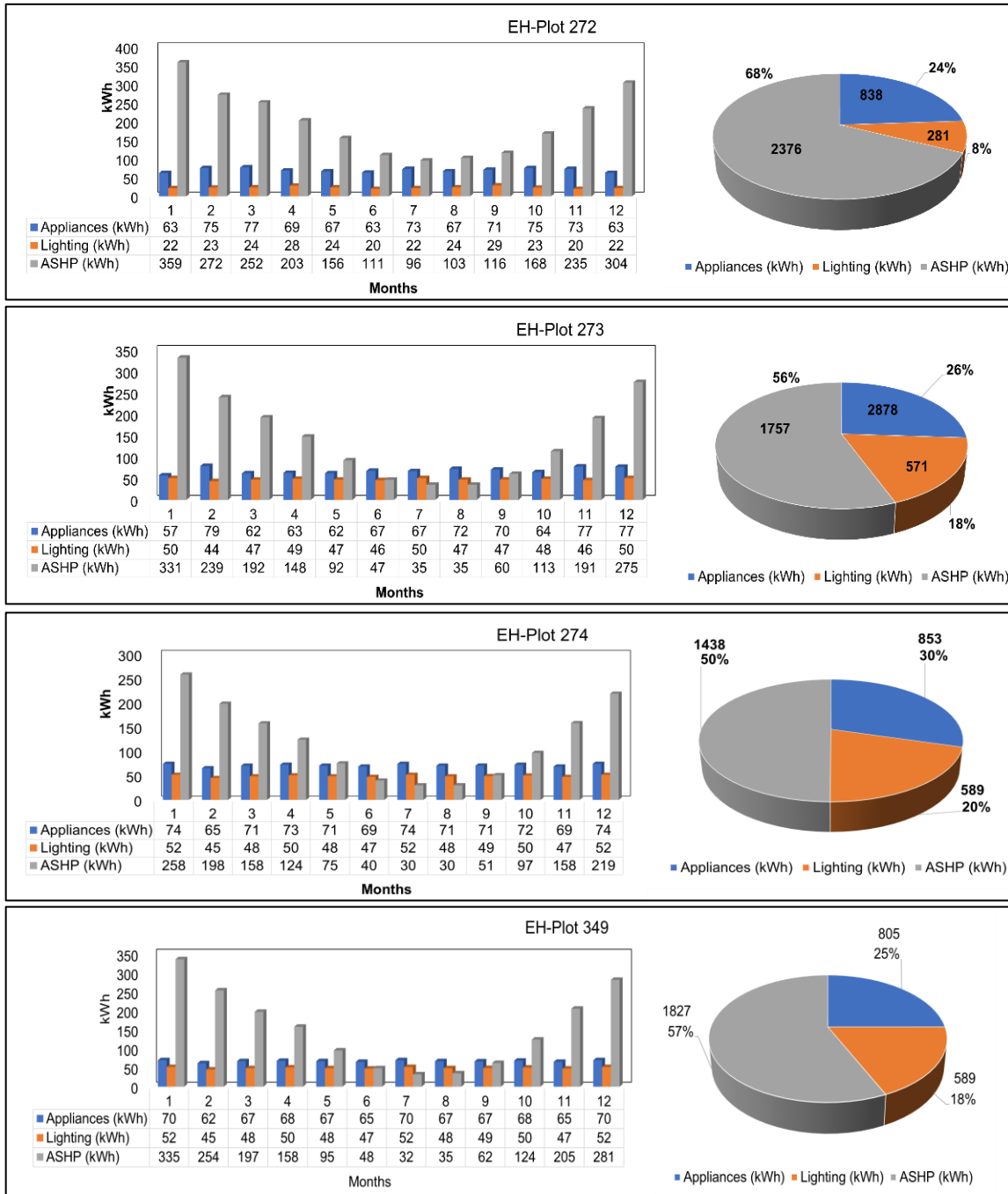


Figure 3-22: Annual breakdown of electricity use in the Electric Homes

The EH Plot-272 had the highest electrical consumption (3495 kWh_e /year), primarily due to the high operation of ASHP in meeting the building's space heating demand. Furthermore, the maximum monthly electrical energy consumption for all domestic dwellings was found for the months of December and January, while it was the most minimum for July and August. Thus, it is obvious that variation in electrical energy consumption is linked to seasons, mainly due to the ASHP application.

3.5.4.2. Thermal Energy Demand

Thermal energy was also stimulated with EnergyPlus over the course of a year. The outcomes yielded for monthly required (kWh_{th}) energy for heating, DHW, and ASHP thermal power have been presented in Figure 3-23.

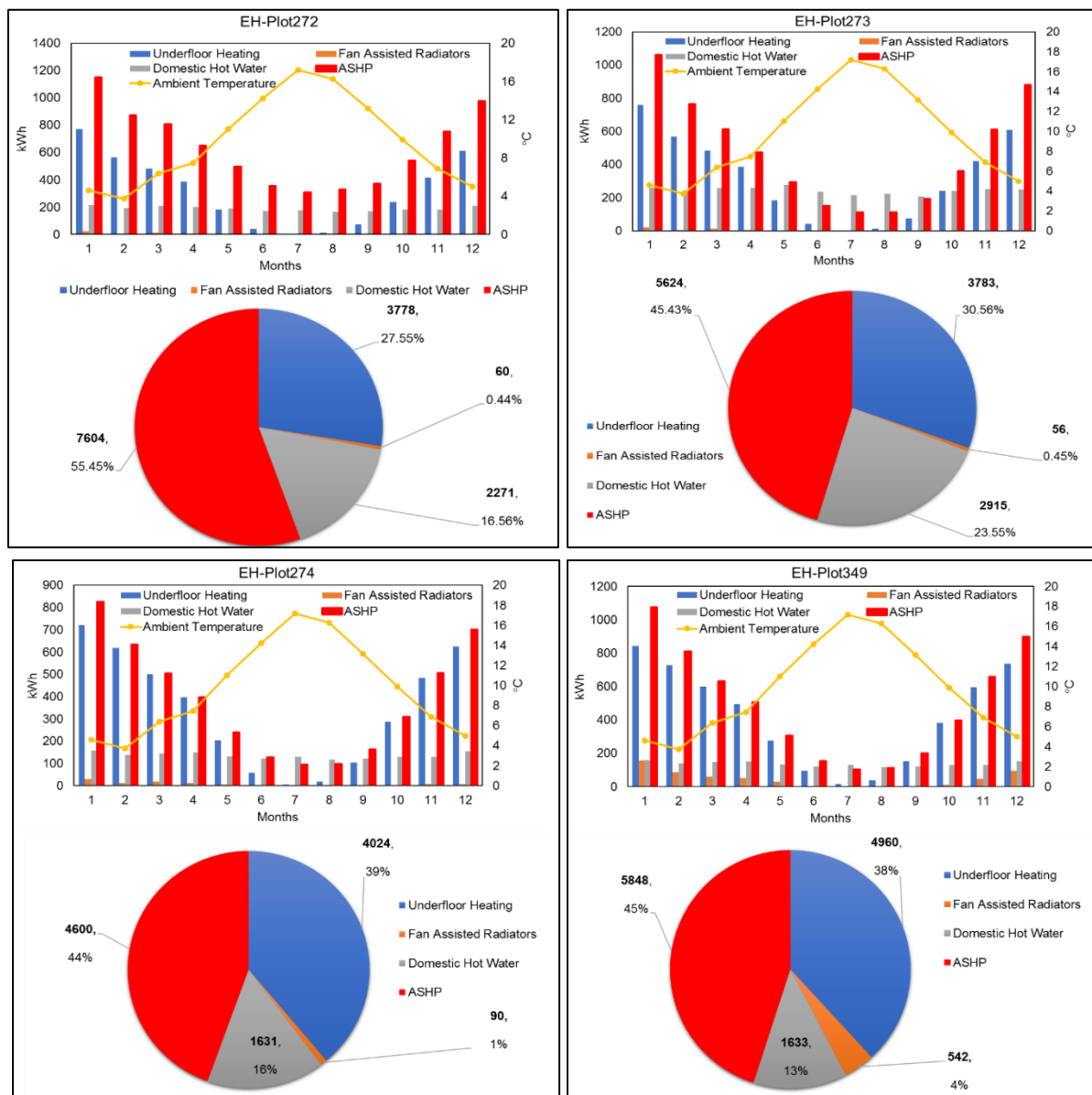


Figure 3-23: Annual breakdown of thermal energy use in the Electric Homes

The findings exhibited variation in terms of space heat demand over the course of a year, especially with only a little or nil heating energy consumption in summers, and high usage during the winter. Moreover, the consumption of heat energy seemed to vary amongst the dwellings, as portrayed in the outputs of the building modelling while considering the occupants and their activities.

The space heating demand and related deviations during winter months, usually occur in the mornings as well as in the evenings. The largest ASHP demand was recorded for EH-Plot 272, indicating that the activities and demand of the four occupants have a clear impact on the final ASHP thermal energy consumption. The study results also assessed the heating demand of underfloor heating and fan assisted radiators. Notably, the type of heat emitter operated most in these homes is the under-floor heating system. The under-floor heating systems were modelled on the ground floor, whereas the fan-assisted radiators on the first floor.

The usage discrepancies between the two types of heat emitters confirmed the notion that the under-floor heating can meet the space heating requirements on both floors most of the time; this is due to the fact that heat flows from ground to the upper floor. Furthermore, it is important to highlight that the heating system usage discrepancies amongst buildings are related to the space heating demand when heat loss occurs; thus, the buildings' air infiltration and ventilation have a major impact on the total heat loss. It is obvious that the main factors affecting heat loss are climate, environment data, and infiltration. Another factor considered in EnergyPlus was the transfer of heat across the rooms, especially due to the opening and closing of doors by the occupants. Heat loss occurs when the door of a heated room is opened to a colder one.

On the other hand, during summertime, solar heat gains seemed to have contributed to the decrease in heating system usage and the outcomes of heat losses. The discrepancies in outputs amongst the buildings exhibited an influence on the direction in which the buildings were facing, and hence, the extent of solar gains through the windows. Additionally, the lighting system appeared to have affected the discrepancies due to a decrease in operation during the summer period when there are more daylight hours. The number of occupants and their activities (metabolic rates) also had an effect on the heat gains, as the ZEBHs models incorporated variables such as the occupants' rising time in the morning, activities (e.g., cooking), and leaving home for school/work.

In short, upon analysing the outcomes and the variations noted in DHW consumption amongst the dwellings, the most highly influential factors in determining consumption of hot water are the climate, the number of occupants and their activities.

3.5.5. Solar PV/T Panels Energy Generated

Figure 3-24 to Figure 3-27 illustrated in this section present a breakdown of the monthly PV/T panels performance. The generation of electricity in every dwelling appeared to exhibit rather good performances during the summer. Nevertheless, only 20–40% of the electricity power expectation was generated during the four coldest months – November through February. This is almost exclusively due to low solar radiation and possible snow accumulation on the surfaces of the PV/T panel during those months. For instance, the maximum electricity generated in each dwelling was approximately 477 kWh_e for July (month with the highest solar radiation), while the total annual electrical energy generated from the 20 PV/T panels in each domestic dwelling was 3243 kWh_e/year.

Thus, timing is very critical for the performance of the PV/T panels, as thermal energy is only useful if it is used immediately or stored for future use. While total thermal energy outputs were relatively similar in magnitude over the course of a year (3710 kWh_e/year), it varies significantly by month, peaking in the summer months. Moreover, there is a seasonal mismatch between supply and demand, as the supply increases significantly in the shoulder season and summer months. Hence, the most reasonable method is to use seasonal storage in order to take advantage of the excess of thermal energy generated during this period. This indicates that without the use of heat pumps, effective PV/T performance is limited to warmer months.

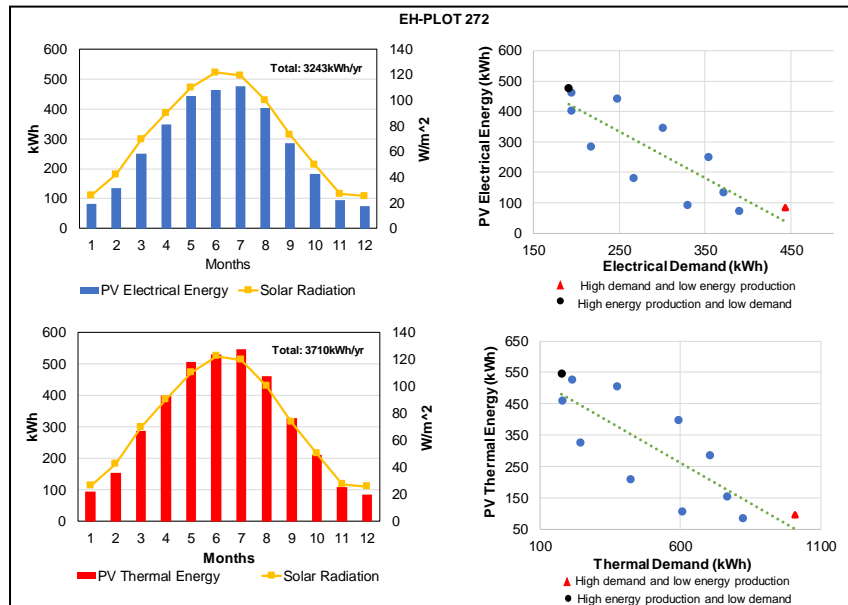


Figure 3-24: Annual PV electrical and thermal energy generated in EH-Plot 272

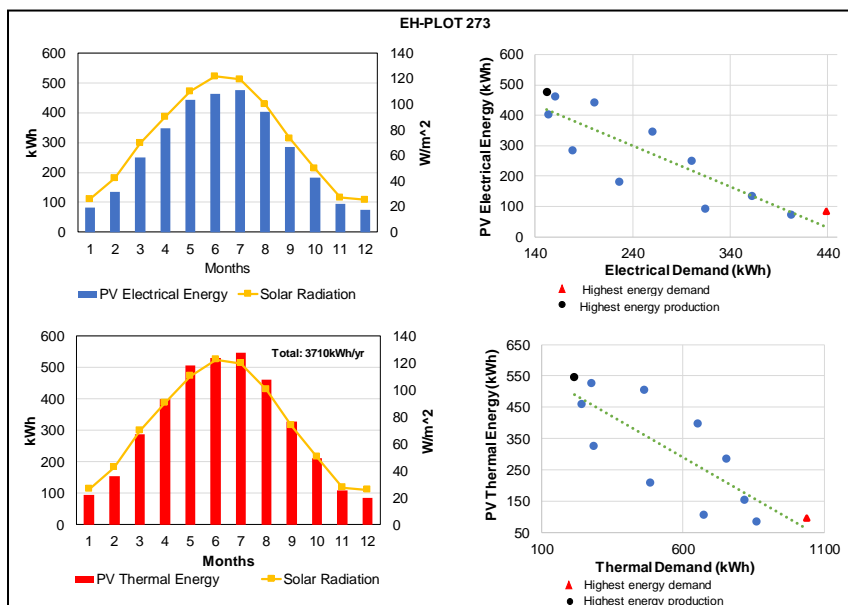


Figure 3-25: Annual PV electrical and thermal energy generated in EH-Plot 273

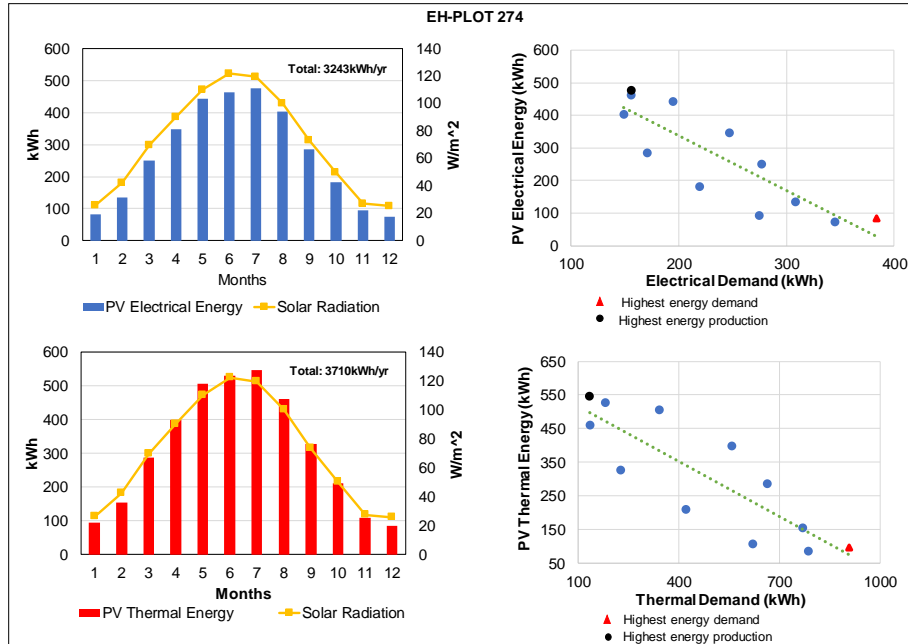


Figure 3-26: Annual PV electrical and thermal energy generated in EH-Plot 274

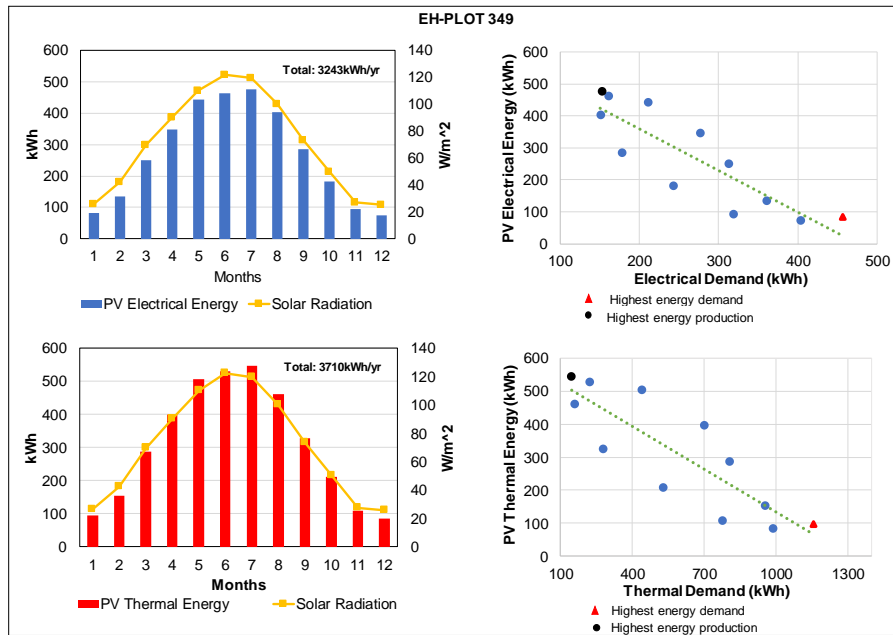


Figure 3-27: Annual PV electrical and thermal energy generated in EH-Plot 349

3.5.6. Techno-Economic Analysis

3.5.6.1. Zero Energy Bill Assessment

This section provides a detailed appraisal to assess the economic viability of the selected ZEBHs. The economics of homes is mainly driven by the running cost of the ASHP and the revenue generated by the exported electricity from the solar PV/T panels to the grid. Besides, the economics of the heating system, together with the SPVTAH system, is highly dependent on the magnitude of energy consumption, or, in particular, thermal demand. Figure 3-28 to Figure 3-31 portray the related monthly electricity costs in each ZEBH over a year, with and without the FiT scheme. The outcomes showed that the status of the energy bill had been met. The simulation performed using EnergyPlus indicated that the zero-energy bill status may be attained when coupled with positive net income.

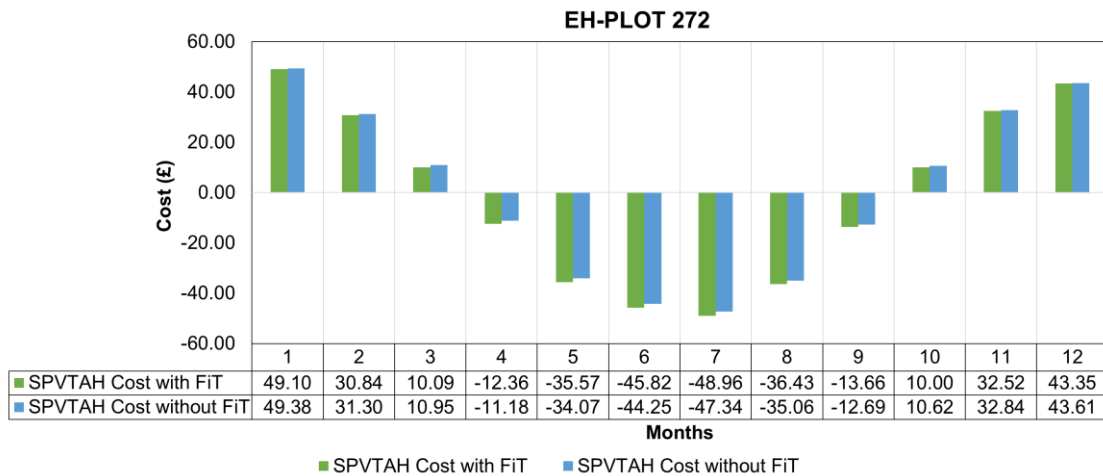


Figure 3-28: EH-Plot 272 Economic analysis monthly plot

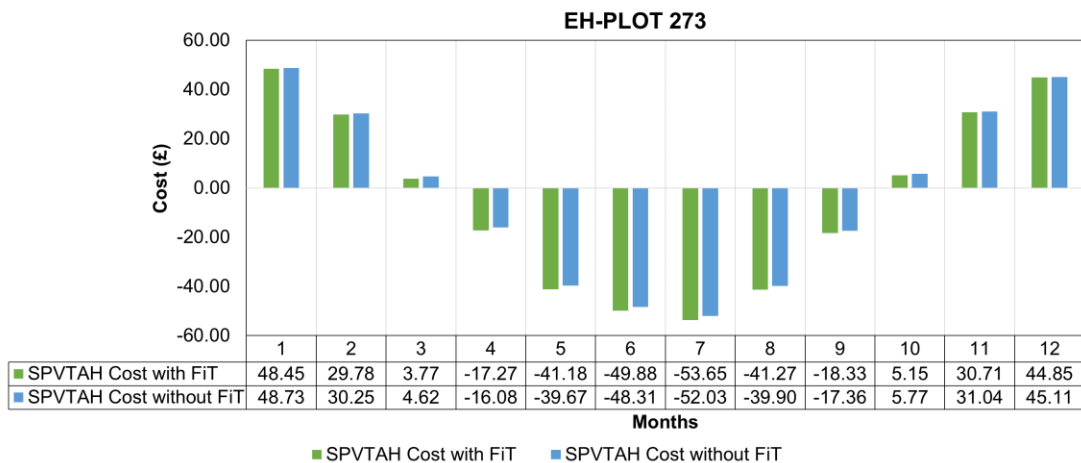


Figure 3-29: EH-Plot 272 Economic analysis monthly plot

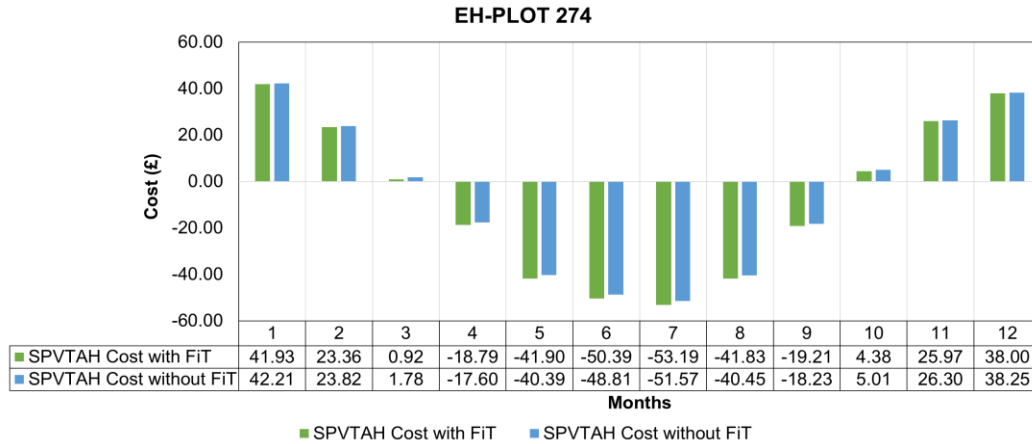


Figure 3-30: EH-Plot 274 Economic analysis monthly plot

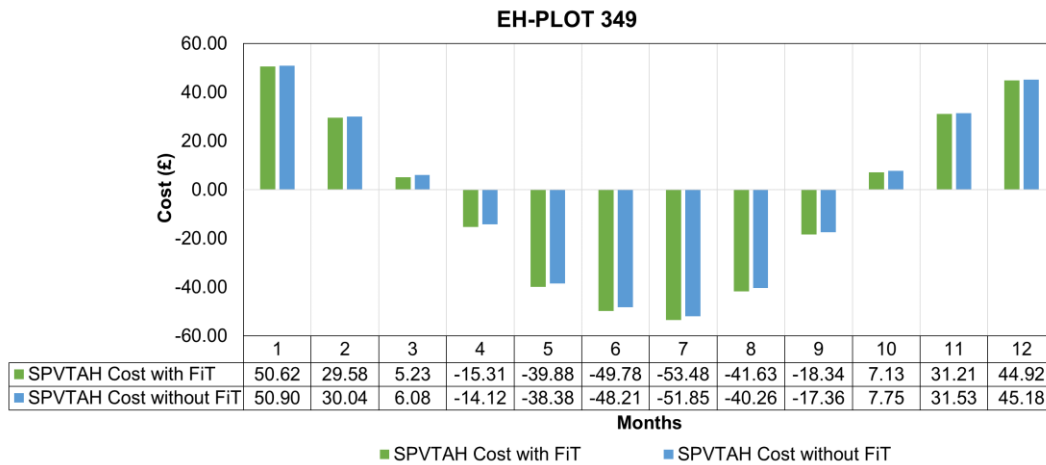


Figure 3-31: EH-Plot 274 Economic analysis monthly plot

Table 3-10 presents the implementation of the ZEB status through the SPVTAH system at the selected dwellings. The results highlight the significance of enabling an exceptional grid interaction between the SPVTAH system and the support mechanisms from the UK government, such as the FiT scheme, in generating higher profitable returns. The outcomes have been summarised as comparative economic appraisals on the SPVTAH system with the FiT against the SPVTAH without the FiT. In addition, the electricity consumption of the ASHP, appliances, and lighting was also incorporated.

Table 3-10: Economic analysis results

| ZEB home | SPVTAH with FiT* | SPVTAH without FiT* | Difference |
|--------------|------------------|---------------------|------------|
| EH-Plot 272 | -£16.91 | -£5.88 | -£11.03 |
| EH-Plot 273 | -£58.86 | -£47.83 | |
| EH- Plot 274 | -£90.73 | -£79.70 | |
| EH-Plot 349 | -£49.73 | -£38.70 | |

*The negative value means that the annual energy bill ends with net incomes.

3.5.6.2. NPV Analysis

An NPV analysis was conducted at the condition of 10% interest. In fact, the cash flows in the analysis included the cost of the ASHP and 20 solar PV/T panels, along with installation cost, annual servicing, energy cost, and the revenues gained from FiT as well as the export tariffs. The values of these parameters were assumed to be constant for the entire 25-year NPV assessment period. See Figure 3-32.

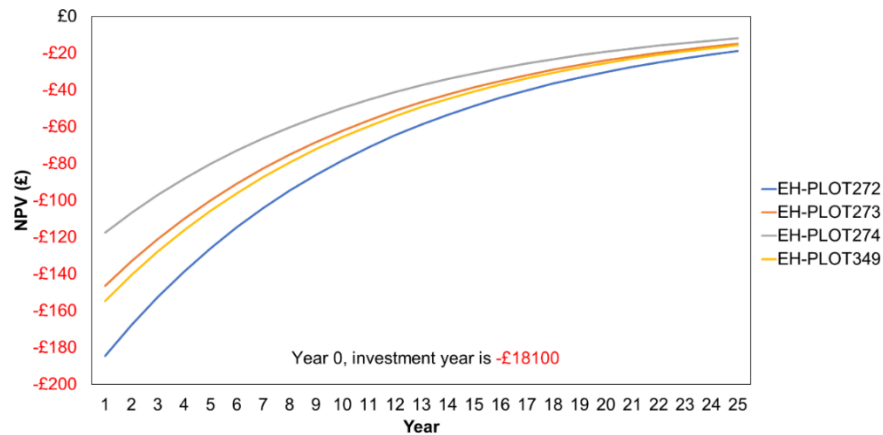


Figure 3-32: NPV analysis results

Table 3-11 presents a summary of the comparative results for the NPV analysis of the SPVTAH system against each ZEBH. Over the period of 25 years, assuming no escalation in maintenance costs or electricity prices, it was noted that increment of years led to a slump in the PV of each cash flow. The NPV at each home was -£19,943, -£19,563, -£19,273, and -£19,646 for EH-Plots 272, 273, 274, and 349, respectively. Notably, a higher NPV of the SPVTAH system was exhibited in EH-Plot 349.

Table 3-11: Summary of 25 years NPV analysis results

| ZEB Home | NPV (£) * |
|--------------|-----------|
| EH-Plot 272 | -£19943 |
| EH-Plot 273 | -£19563 |
| EH- Plot 274 | -£19273 |
| EH-Plot 349 | -£19646 |

* The negative values mean an outgoing of cashflow

3.6. SUMMARY

This chapter implemented a building modelling approach by incorporating SPVTAH in ZEBHs. Thus, the modelling and the energy performance, of the UK-based community ZEBHs were analysed. The modelling offered a baseline to assess energy performance of UK-based community ZEBHs had been analysed. The modelling offered a baseline to assess energy performance as it had been imminent to identify the parameters that influenced energy demand and calibration method. Furthermore, a comparison of the modelling outputs by employing the measured data verified the performed assessments.

Modelling and simulation are still essential tools for conducting energy performance analysis of the ZEBHs. Pervasive-logged metered data offered information with focus points from the behaviour of the building occupants to the exploitation of the actual values facilitated by the calibrated model with accuracy. The following summarises the main findings of this work:

- Calibration should be conducted over an annual cycle with the use of hourly energy data, where impractical hourly primary data could be collected for shorter cycles (weekly or monthly) to ‘validate’ the simulation results.
- Local weather files should be measured and used for the models to be considered calibrated. Otherwise, any other weather type of weather file may assist in validating the models.
- The NMBE and CVRMSE calibration results when presented in weekly intervals will allow an assessment of daily and hourly variations.
- The tolerated error levels of the models should be dictated by the function of the ZEBH models and primary data availability. There is scope for further work in defining the required levels of model accuracy for efforts such as optimisation and control studies.
- To that end, further refinement of the calibration guidelines should first reflect the model purpose. As demonstrated in this work, the models calibrated according to the limitations of the ASHRAE guideline can more confidently predict actual prevailing results within the building. The existing NMBE and CVRMSE values of $\pm 10\%$ and $\pm 30\%$, respectively, can still be adhered even when complete annual hourly data is not available to the analyst. In this case, such a model can be considered ‘validated’.

The primary reason for integrating the measured data was to establish a benchmark for ZEBHs energy performance, including occupancy behaviour in terms of appliance use and lighting. Therefore, the comparison outputs amongst the ZEBHs point out the significance of the occupancy elements as a factor that can influence thermal and electrical demand. In addition, several key variances for the representation of the parameters influencing the ASHP thermal power demand have been determined. These variances seem to have mainly arisen due to the difference in occupant behaviours, DHW consumption, internal heat gains, and heat losses.

Furthermore, this chapter also highlighted the production of energy mapping on-site electrical/thermal power generation under various climatic conditions (e.g.: irradiation). In fact, it has been proven that PV/T is a clear optimum solution for such houses with zero-energy target. However, this study has emphasised the importance of back-up energy supply devices, such as ASHPs.

As the dwellings and their energy systems are part of the technical and economic subsystems, the aspect of cost-effective quantification at the level of each single building unwittingly externalised the costs. This notion certainly applies to the implementation of ASHPs, along with solar PV/T panels, as an energyefficient method in providing space heating and/or domestic hot water. The economic analysis, prices, and tariffs is absolutely crucial. This is especially true since fluctuation in prices may affect the status of the ZEBHs, particularly when space heat demand increases. Moreover, the feasibility assessment indicated that the zero energy bill concept would be impractical if the UK government subsidies are withdrawn.

Additionally, the NPV analysis further signified that even though the SPVTAH might generate revenues, repayment of the initial investment of £18100 in 25 years would turn out to be the largest barrier.

However, it cannot be denied that operating renewable energy technology in ZEBHs offers vast advantages, among which reduction in costs appears to be the most significant one. Nevertheless, the implementation of the SPVTAH systems grid interaction is essential for significant electricity cost reductions and the achievement of the ZEBH status. In addition, at present, the capital cost of the SPVTAH system has a stretched payback period (+25 years).

Excluding these attributes seemingly underestimates the overall societal cost of possible the future low carbon systems, resulting in a disproportionate trade-off between various viable policy measures. In this context, the primary objective of this study was to offer an initial estimate of the energy performance in ZEBHs with a presentation of a technical subsystem based on comprehensive building modelling, calibration, and energy simulations.

Future works for this study presented in **Chapter 4**, includes the integration of ZEBHs and low voltage (LV) electrical networks. The link would allow the use of building energy models, inclusive of internal energy supply systems, in association with external energy supply systems, such as the electrical grid. This can, therefore, permit the simulations of integrated building and electricity network. The simulation of those systems can also portray an environment for ASHP load shifting strategy to be tested on the platform and assess energy demand flexibility of ZEBHs, especially when the intrinsic heat storage in the building can be used for provision of ancillary services in LV networks.

CHAPTER 4- ANALYSIS AND QUANTIFICATION OF ENERGY DEMAND FLEXIBILITY ON LV ELECTRICAL DISTRIBUTION NETWORKS

4.1 INTRODUCTION

The United Kingdom (UK) has a maritime climate, with a heating season of about eight months. These climate circumstances are ideal for the effective operation of air source heat pumps (ASHP), whose efficiency is inversely proportional to the temperature difference between the heated space and the outdoor environment. The inexorable heat strategy set by the UK power networks encourages the adoption of heat pumps as they (heat pumps) have a strategic role in reducing greenhouse gas emissions and are a key component of the transition to a low carbon economy[147]. UK power networks support this transition and are investing in the UK network to ensure that they can safely and reliably meet the increase in electricity demand required to support these technologies.

Ground-source heat pumps are typically installed in new, detached dwellings whereas air source is generally more suited for retrofit applications [158]. The coefficient of performance (COP), which is the heat produced per unit of electrical energy consumed, is typically in the range 3.0–4.0. If the supply generation is predominantly fossil fuel, with a thermal efficiency of about 35%, the heat produced by the heat pump is little more than what could be obtained directly from the fossil fuel.

Often the choice is between an oil-fired central heating boiler with an efficiency of about 70% and a heat pump with under-floor heating. The economic and climate change arguments are now converging, with the result that heat pumps are likely to become more popular for new, detached dwellings [159]. In addition, a significant heat pump load brings a number of benefits to power system operators. In particular, the thermal inertia of water tank storage is such that the heat pump attached to it, can be switched off for several hours with minimal effect on temperature [160]

This improves generation load factor, and also offers the possibility of heat pump motor inertia helping to stabilise the system at times of significant renewable generation.

However, the growth of heat pump load poses a challenge for distribution networks. These include supply overload, damage to supply equipment, power quality issues or adequacy of earthing[161]. There may even be the possibility of voltage collapse.

One way to address the abovementioned issues is by installing the optimal ASHP control upon drop of voltage. However, this may have negative impacts on supplying both acceptable indoor and domestic hot water temperatures (DHW). As such, implementation of heat pumps should have low negative impacts on the occupant thermal needs.

This chapter have assessed the energy demand flexibility that by the Zero Energy Bill Homes (ZEBHs) can offer to the electricity network considering the dynamic effects of varying heat pump deployment on a low voltage (LV) distribution network.

In this framework, a load shifting strategy is presented to assess the impact in respect of the network, especially considering the presence of manageable loads like ASHPs. Currently, the development and application of load shifting in buildings are still at the beginning stage. Most of the articles present in literature have their special focuses with limited attention on buildings ASHPs load shifting [162]. The aim of this chapter is to show the advantage of the suggested ASHP load shifting method based on community level viewpoint, by adopting an optimisation approach that manages the ASHPs load whilst improving an IEEE-33 node LV network voltage drop levels.

The suggested approach upgrades the ZEBHs qualification with multiple goals:

- Quantify how much energy flexibility they can provide to the network when the voltage drops below the UK statutory limits, without reductions in comfort for the users;
- Control ASHP load profile to reduce voltage drop impact on the network, improving the exploitation of the water tanks thermal inertia, which is part of the solar photovoltaic thermal assisted heat pump (SPVTAH) systems.
- Link the electric network with a unique point of connection and a common distribution system for the a ZEBHs at community level.
- Manage the ASHPs of the buildings according to the network voltage profile with an ASHP load shifting algorithm whilst adopting an optimisation approach

4.2 OBJECTIVES

This chapter presents a developed integrated building and electricity network model. To achieve this, an IEEE - 33 node test feeder was incorporated into a system that comprised of 100 modelled ZEBHs (from **Chapter 3**). As described in **Chapter 3**, the dwellings were equipped with 20 solar PV/T panels as the primary heat energy source, along with ASHP that serves as the back-up to supply energy.

Additionally, the models had an external interface that offered two-way communication between the ZEBHs, also referred as Electric Homes (EHs) and the feeder. This interface allowed the EnergyPlus software package to be integrated with MATLAB/Simulink software program. Hence, the software was employed to simulate building modelling, whilst MATLAB/Simulink was applied to study the electrical network load over a 24-hour period, and an optimum ASHP control action that was determined by an algorithm when voltage drops below a limit occurred in the electrical network. **Section 4.3.2** provides more details in regards of the interface and coupling method.

The ASHP load-shifting contributed in minimising the peak demand upon voltage drop at the electrical distribution level by constraining the operation of ASHP loads. Hence, several factors concerning energy performance of building at the community level shed light on the expected feeder voltage profiles. The requirements of the model for each sub-system are elaborated in the following sections.

4.3 METHODOLOGY

Figure 4-1 illustrates the system investigated in this research. The system was comprised of the following ZEBHs primary components: the existing solar photovoltaic thermal (PV/T) generation system, the proposed domestic hot water (DHW) storage, the electricity loads demanded by occupants (including ASHP); and on the other hand, a LV electricity grid. The dashed line arrows represent the electrical interactions between the appliances/lighting, ASHP, and solar PV/T exported electricity with the external electrical grid (IEEE- 33 node test feeder). The blue arrows show the connections between each component of the SPVTAH system in the ZEBHs. The system control here represents the ASHP load shifting approach (with an optimisation model) that is executed to switch off the ZEBHs heat pumps when there are voltage drops below the UK statutory limits.

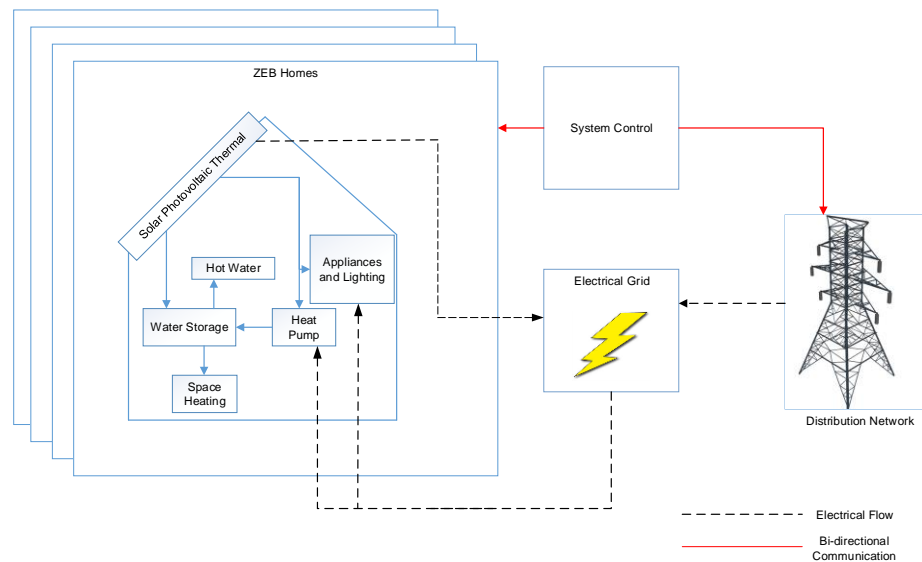


Figure 4-1: Illustration of integrated building and electricity network model

4.3.1 Scenarios

By employing the model described above, two different scenarios were presented for comparison analysis purposes.

- **Scenario 1- Continuous Heating Strategy:**
 - In this strategy, the heating temperature was set to be constant at 19°C for the entire building, except for the living room where the temperature was set at 21°C.
- **Scenario 2- ASHP Load Shifting Algorithm:**
 - The load-shifting strategy constrained the ASHP operation only upon voltage below limits. This strategy is based on optimisation model which is presented in **Section 4.4**.

4.3.2 Interface and Coupling Method

Coupling between EnergyPlus and MATLAB/Simulink was carried out by using a JAVA language interface, which was Building Control Virtual Test Bed (BCVTB). It received inputs from EnergyPlus and BCVTB interface [163], which subsequently sent signals back to E+. The Lawrence Berkeley National Laboratories [164] developed the BCVTB as EnergyPlus was not equipped with any control function. Figure 4-2 displays the integrated building and electricity network framework. The system is as follows:

1. EnergyPlus sends water tank and indoor temperatures of the building models to BCVTB interface and receives signals to control ASHP functions.
2. MATLAB accepts the electrical consumption data from BCVTB for the network power flow simulation with MATPOWER 6.0, as well as to send ASHP ON/OFF-time control signals to EnergyPlus via Simulink block, upon voltage drops below the limits. However, constraints conditions were included, and this include- water tank and indoor temperature range value limits.

Figure 4-3 portrays the Simulink model controller, where the voltage parameter is fed into the Simulink function code from the MATPOWER 6.0.

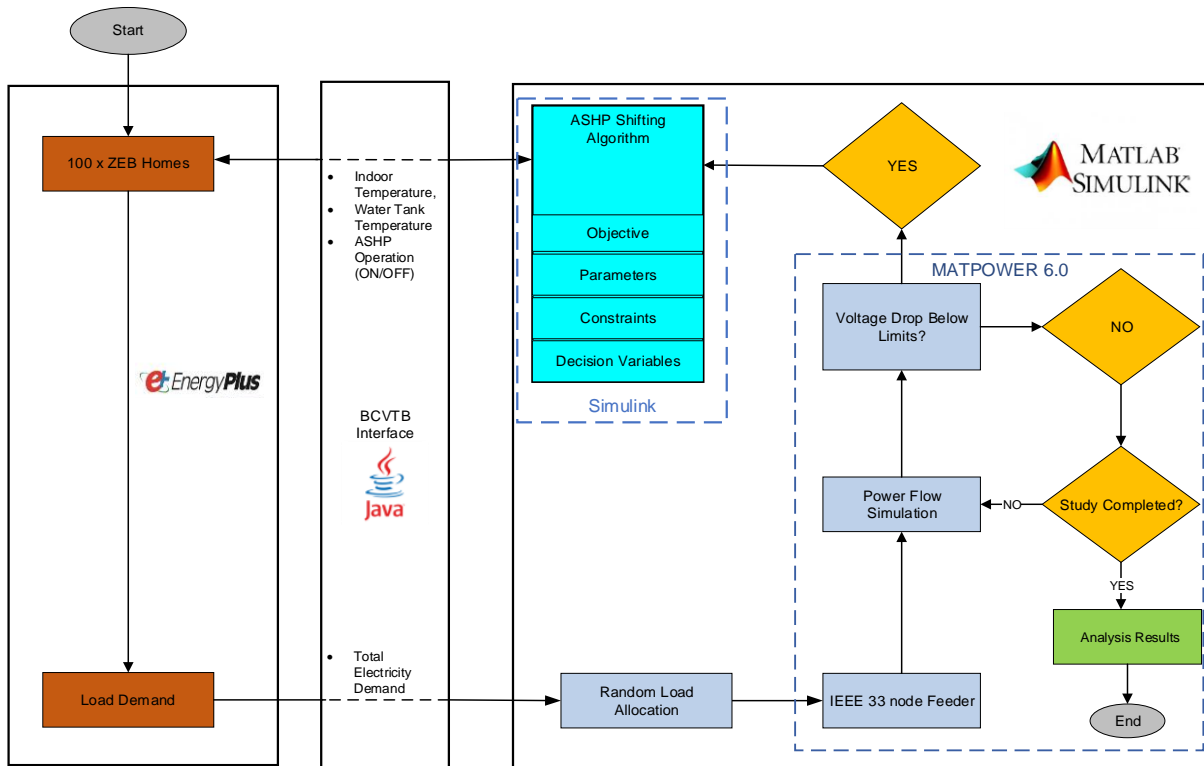


Figure 4-2: Integrated Buildings and Electricity Network Framework

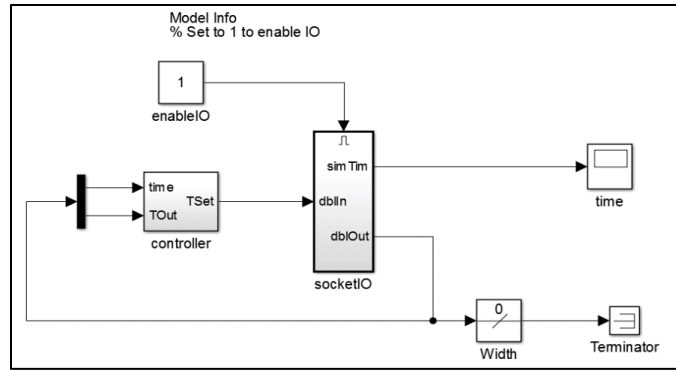


Figure 4-3: Controller in MATLAB/Simulink

In matching the simulation step time for EnergyPlus and MATLAB/Simulink, the BCVTB interface was set along with a simulation clock based on seconds to send data to both software programs. In this case, a winter day was considered with a 15-minute time frequency, hence making the total configured simulation time 86400 seconds. During the simulation process, BCVTB pauses one program until the other one finishes simulation and sends it back for a simulation step. Figure 4-4 illustrates the model interface for the coupled simulation.

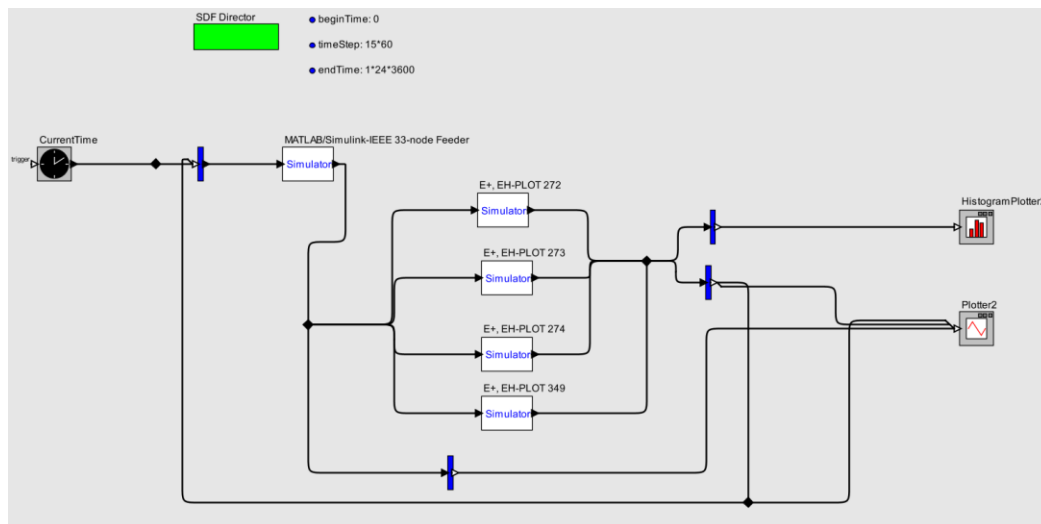


Figure 4-4: System model for coupled simulation in BCVTB

The two different software programs were connected by BCVTB via XML⁶ file configuration meant for exchange of data. The file script was set into each E+ model (see Figure 4-5). The variable that reflected the E+ ASHP had an input vector, which was computed by the interface (derived from MATLAB/Simulink) and sent to E+. Meanwhile, the three output vectors, which are: (i) indoor, and (ii) water tank temperature elements, as well as (iii) electrical demand, were computed by E+ and sent to MATLAB/Simulink using the interface.

⁶ Extensible Mark-up Language (XML) is used to describe data. The XML standard is a flexible way to create information formats and electronically share structured data.

```

1 <?xml version="1.0" encoding="ISO-8859-1"?>
2 <!DOCTYPE BCVTB-variables SYSTEM "variables.dtd">
3 <BCVTB-variables>
4 <!-- The next element receive the water tanks temperature from E+ to MATLAB/Simulink -->
5 <variable source="EnergyPlus">
6 <EnergyPlus name="AUX HW LOOP HP WATER HEATER" type="Water Heater Tank Temperature"/>
7 </variable>
8 <!-- The next element receive the indoor temperature from E+ to MATLAB/Simulink-->
9 <variable source="EnergyPlus">
10 <EnergyPlus name="Whole Building" type="Zone Mean Air Temperature"/>
11 </variable>
12 <!-- The next element send the ASHP operation control signal from MATLAB/Simulink to E+ -->
13 <variable source="Ptolemy">
14 <EnergyPlus schedule="BCVTB-SP-TH"/>
15 </variable>
16 <!-- The next element receive the schedule value as an output from E+ from MATLAB/Simulink-->
17 <variable source="EnergyPlus">
18 <EnergyPlus name="Whole Building" type="Facility Total Purchased Electric Power"/>
19 </variable>
20 </BCVTB-variables>

```

Figure 4-5: XML file script

4.3.3 Zero Energy Bill Homes Load Demand

In order to assess building energy performance and to analyse the dynamic simulation outputs, several elements, such as building fabric, ambient conditions, user behaviour, and renewable energy supply system, had been weighed in.

The assessment and analysis gave information regarding indoor and water storage tanks temperature, as well as their dynamic variations over a period of time. It was found that the efficiency of ASHP device relied on ambient temperature, while the internal hot water flow and indoor temperature depended on both heating system and water storage tank.

The resulting electrical demand of the appliances was also embedded in the model because internal heat generated by these appliances also appears to have an impact on the indoor temperature.

The load demand of the ZEBH was allocated randomly in the network through the interface from E+ software to MATLAB/Simulink (where the network was modelled). The maximum loads selected was 100, while the power factor was set to 0.95. In this case, 100 ZEBHs were randomly allocated to the network using MATLAB's uniformly distributed random numbers syntax: $X = rand(sz)$. The syntax returns an array of random numbers where size vector sz specifies $size(X)$. In this case, the vector size is determined during the electrical network modelling and power flow simulation method (i.e. Newton Raphson). **Section 4.3.4** provides more details.

Figure 4-6 and Figure 4-7 illustrate the total energy demand and the average demand for each type of ZEBHs incorporated in the IEEE 33-node test feeder for a winter day (7th of January). Consumption of energy during the day is the sum of all electrical consumption of each building, whereas average demand refers to the total energy consumed by each type of building and divided by the total number of hours in a day. Figure 4-8 portrays the maximum demand of each dwelling.

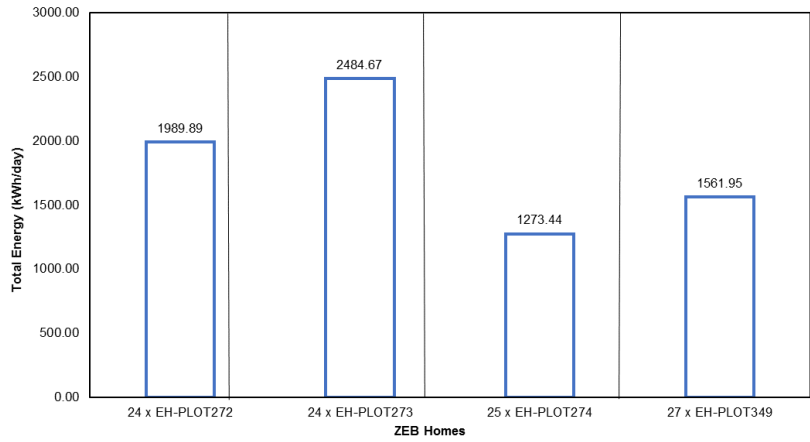


Figure 4-6: Total energy demand of modelled ZEBHs comprised by building type in a winter day (7th of January)

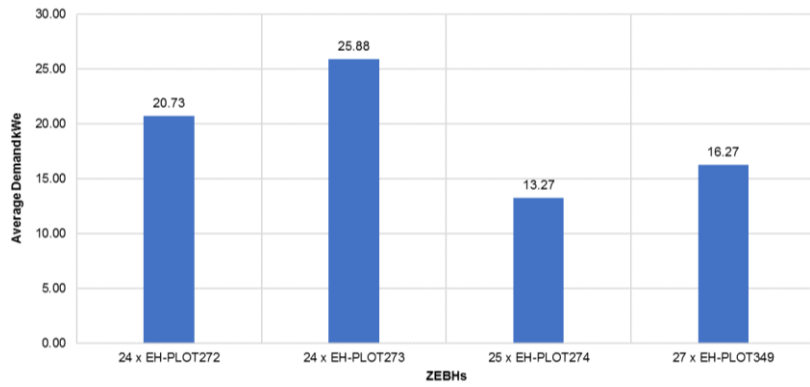


Figure 4-7: Total average demand of modelled ZEBHs comprised by building type in a winter day (7th of January)

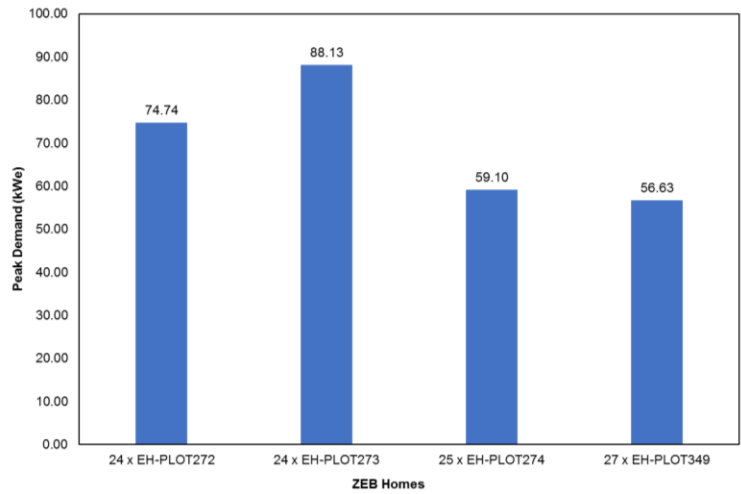


Figure 4-8: Peak demand of ZEBHs comprised by building type in a winter day (7th of January)

The distribution transformer serves the building cluster via feeders. The sum of the allocated load demand for each time interval within 24 hours reflects the diversified demand for each type of building within the time interval. Figure 4-9 displays the diversified demand for the winter day.

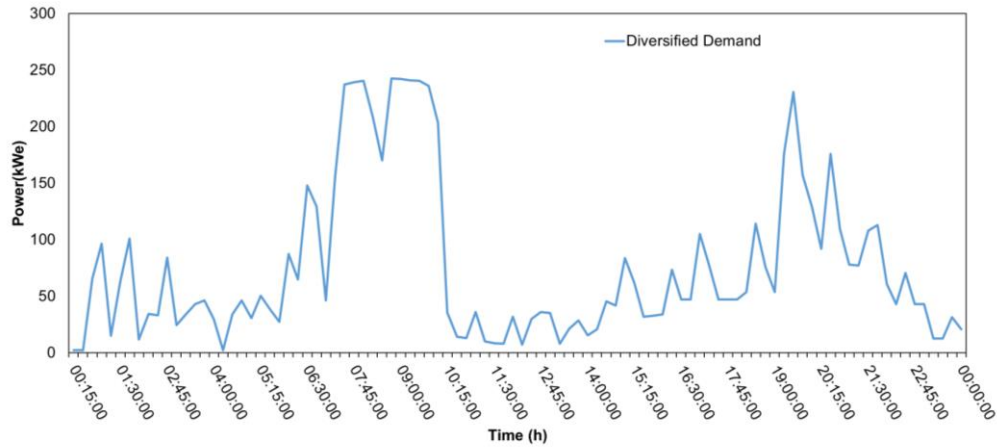


Figure 4-9: Building clusters diversified demand in a winter day- 7th of January

4.3.4 Benchmark Test Feeder Model

The developed model incorporated the LV electrical network supplied to residential dwellings. This is because the investigation of control algorithm required inputs from both internal and external conditions of the buildings. Therefore, a steady-state representation of the electrical network was considered, as the electrical network was modelled and simulated using the steady state power flow software-MATPOWER 6.0⁷, which refers to a power system analysis toolbox based on MATLAB.

The IEEE 33-node test feeder simulated in this chapter had been based on the data derived from [165] and [166]. The reference radial network, as shown in Figure 4-10 including the transformer were modelled using MATPOWER 6.0.

4.3.4.1 Transformer and Network Data

The transformer parameters was adopted from reference [166] and the transformer was connected to the electrical grid at 11kV to 0.416kV level. The transformer parameters and the network cable data are tabulated **Appendix B1**, respectively. The transformer was a 500 kVA, 11/0.416 kV with an impedance of 0.0190+ j 0.0408 p.u. The connection group of the transformer was Dyn11, which corresponded to delta-connected primary and wye-connected secondary winding.

⁷ MATPOWER 6.0 is a package of MATLAB® M-files for solving power flow and optimal power flow problems.

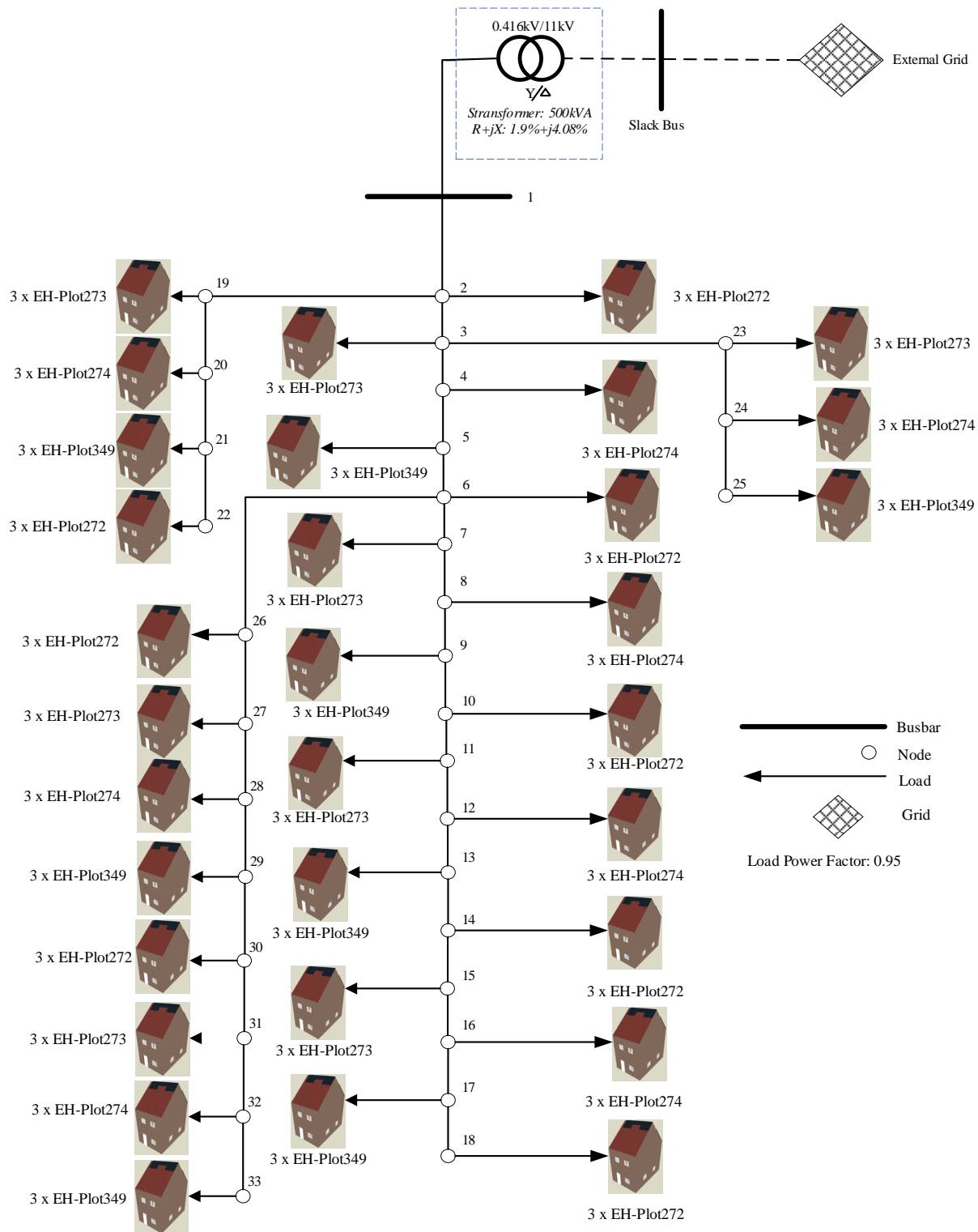


Figure 4-10: Configuration of the IEEE-33 node Feeder with 100 ZEBHs

4.3.4.2 IEEE 33-Node Test Feeder Model

Electrical network modelling is the basis of power system analysis performed to investigate power flow. Typically, networks constitute of lines, transformers, generator, and impedances, or they may be even represented by a nodal admittance matrix. **Appendix B2** presents the power flow formulation method, nodal formulation and admittance matrix, and solution of electrical power flow by Newton-Raphson method. In addition, further details regarding calculation of voltage for IEEE 33-node radial network is presented in **Appendix B3**.

Based on the above network description, by considering Kirchoff's current law (KCL), Kirchoff's voltage law (KVL), and electricity flow constraints for network systems, the current injected into the network at node I is given by:

$$[I_{node}] = [Y_{node}][V_{node}] \quad (4.1)$$

where,

- I_{node} is the vector injected nodal currents
- Y_{node} is the nodal admittance matrix, and
- V_{node} is the vector nodal magnitude voltages measured with respect to the slack node.

The current that flows through the electrical networks is initially unknown, thus determined from power equation. This forms a correlation between nodal currents and voltages. The net nodal power injection at node I can be determined as follows:

$$S_I = P_I \pm jQ_I = V_I(I_I)^* \quad (4.2)$$

where,

- I_I^* is the complex conjugate number of the current injected at node I
- j is the imaginary number
- $V_I, P_I, Q_I,$ and S_I are the voltage, active, reactive, and apparent power at node I .

After determining the values of power and voltage from the above equation, the current injected through the line from busbar I , is calculated as follows:

$$I_I^* = \frac{P_I \pm jQ_I}{V_I} = V_I \sum_{n=1}^N (V_n Y_{In})^* \quad (4.3)$$

where,

- Y is the admittance matrix ($1/Z$)
- Z is the impedance ($R + jX$) in Ω
- V is the voltage in v
- N is the total number of nodes in the electricity network
- n is the number of nodes

4.3.5 Energy Demand Flexibility Analysis

This section presents the developed quantification indicators to evaluate the performance of ASHP shifting algorithm amongst ZEBHs and its network, which were applied in winter day simulation. Data from the voltage grid were applied by the indicators to assess the control technique. Grid voltage, load demand, as well as indoor and water tank temperatures, are some of the essential indicators that dictate the interaction between grid voltage levels and load consumed by the dwellings. Index scores are presented for each indicator to offer a notion of the ASHPs load shifting aim, for which the indicator is adequate for quantification analysis. The energy demand flexibility is considered for the amount of time in which the ASHP load can be constraint without compromising the occupants thermal comfort when voltage drops below the limit occurs.

4.3.5.1 Flexibility

In assessing the flexibility of ZEBHs thermal energy demand, the water tank temperature indices were incorporated. This is because space heating and DHW gain their sources of heat from the water tank that serves as thermal storage. The function of water tank is integral for flexibility assessment as the coupled ASHP operations are constrained upon drop of voltage below limit (VBL), as long as the constrains of thermal storage temperature are respected.

Flexibility was quantified based on the outcomes derived from water tank temperatures depicted in the results. The temperature profiles were determined for each ZEBH, while the related flexibility was estimated based on percentage variances between the two scenarios. **In this thesis, the flexibility is defined as the amount of time in which the ASHPs load can be shifted without compromising the occupants thermal comfort.** This, was quantified by the water tanks temperature difference error, expressed as follows:

$$flexibility_{t,tank}(\%) = \left(\frac{|t_{tank,base}(t) - t_{tank,ASHPs\ shifting\ algorithm}(t)|}{\frac{(|t_{tank,base}(t)| + |t_{tank,ASHPs\ shifting\ algorithm}(t)|)}{2}} \right) \times 100 \quad (4.4)$$

where,

- $t_{tank,base}$ is the base temperature of the hot water tank (°C), and
- $t_{tank, ASHPs\ shifting\ algorithm}$ is the tank hot water temperature when the ASHP shifting algorithm is applied in °C.

4.3.5.2 Voltage Below Limits

The VBL, refers to the percentage of time the voltage profile drops below the limits, seemed to be a crucial indicator in determining the effectiveness of ASHP load shifting. This indicator appeared to be essential in analysing the limiting voltage constrains on the network based on the stipulated UK LV limits. Based on the following equation, $V < V_{min}(t)$ denotes the moment when the feeder voltage profile is below the limit in terms of time percentage, as following:

$$VBL(\%) = \left(\frac{|V(t) < V_{min}(t)|}{\Delta t} \right) \times 100 \quad (4.5)$$

where,

- VBL is voltage below the limit in %, and $V(t)$ is the voltage network over a period of time t , in v .
- $V_{min}(t)$ is the minimum voltage over a period of time t , in v .

4.4 OPTIMIZATION MODEL

In this thesis, the mixed integer linear programming (MILP) method to solve the optimization model was used. As mentioned in **section 2.4.2**, the MILP presents a great advantage for power management problems since it is possible to define the power flow direction in the devices or systems. Besides that, the MILP approach guarantees a global optimisation solution.

In this study, the optimization model was built by the software MATLAB/Simulink and solved by the MATLAB's "*intlinprog*" solver script (solver-based optimization problem). The model involves the following decision variables:

- P_{Dj} and Q_{Dj} are the power consumption connected to the branch j at time t in kW and kVAr.
- V_s is the voltage at the secondary side of the transformer in v .
- $P_{ASHP,operation}$ operation of the ASHP (ON/OFF).
- t_{ind} is the indoor temperature in °C and T_{tank} is the water tank temperature in °C.
- P_{net} is the net electrical demand in kW_e and P_{dmd} is the total building electrical demand in kW_e.

The objective of the proposed optimization is to implement a control strategy in order to investigate the network support solution provided by the ZEBHs energy demand flexibility. The controller will schedule the operation of the ASHPs connected to the electricity network. The objective of the ASHP load shifting algorithm implemented is to minimise the voltage drops on the network during a UK winter day. In summary, the controller sends signals to control the heat pumps when the when VBL condition is met. Furthermore, the ASHPs are coupled to the water storage tanks, hence, the water storage tank and indoor temperatures will be also considered to remain within a temperature range limit. In addition to the constraints related to the individual buildings, network constraints were considered in the optimization model.

4.4.1 Objective Function

Objective function (OF) minimises voltage drop in the grid upon considering that the 100 ZEBHs are connected to the network. The optimisation model is indexed by sets (t) , while t_x refers to the set that denotes 15-minute period per day ($1 \leq t_x \leq 96$). Equation 4.6 depicts the mathematical formulation of the OF at time, t .

$$OF = \min \sum_{t=1}^H V_{drop}(t) \Delta t \quad (4.6)$$

The calculation of the voltage drop is as follows:

$$V_{drop} = V_s + IR \cos \theta + IX \sin \theta - \sqrt{V_s^2 - (IX \cos \theta - IR \sin \theta)^2} \quad (4.7)$$

where,

- V_{drop} is the voltage drop in v
- Δt is the OF time steps over time horizon H , here, 15 minutes, and
- H is the time horizon, here, ($1 \leq t_x \leq 96$).
- V_s is the source voltage at the secondary side of the transformer in v
- I is the line (load) current in A
- R_i is the branch resistant in p.u
- X_i is the branch reactance in p.u
- $\cos \theta$ is the power factor load
- $\sin \theta$ is the reactive factor load

4.4.2 Constraint Conditions

In the optimisation model, the variation of the parameters in the model should be within a certain range. Their constraint conditions are given in the following subsections.

4.4.2.1 Voltage Constraint

The voltage constraints kept the voltage across the LV feeder within the permissible voltage range, which was 230 volts +10% and -6%. Since the network was passive, it was adequate to implement voltage constraints for only one node: at the beginning of the feeder (bus 1). The constraint, as modelled in Equation 4.8, determines that the voltage should be maintained above 0.95p.u, when the signal is sent to the building clusters to shift the ASHPs load.

$$V_{\min} \leq V_s - \frac{\left[\sum_{i=1}^n \left(R_i \sum_{j=i}^n P_{Dj} \right) (t) + \sum_{i=1}^n \left(X_i \sum_{j=i}^n Q_{Dj} \right) (t) \right]}{V_s} \quad (4.8)$$

as such,

$$Q_{Dj}(t) = \left[\tan(\cos^{-1}(\text{power factor})) \right] P_{Dj}(t) \quad (4.9)$$

where

- i is the index of the branch section across the feeder,
- n is the number of branches on the feeder,
- P_{Dj} and Q_{Dj} are the power consumption connected to the branch j at time t in kW_e and kVA_r.
- X_i is the branch reactance in p.u.
- R_i is the resistance in p.u.
- V_s is the voltage at the secondary side of the transformer in V.
- V_{\min} is the voltage limit for the LV network in V.

4.4.2.2 ZEBHs Water Tank Constraints

The water tanks temperature (t_{tank}) constraints should be within the following range:

$$t_{\text{tank},\min}(t) \leq t_{\text{tank}}(t) \leq t_{\text{tank},\max}(t) \quad (4.10)$$

Based on the reference [167], the limits for water tank temperatures are:

- $t_{\text{tank},\min}$ is the minimum water tank temperature in °C, is 30°C, while
- $t_{\text{tank},\max}$ is the maximum water tank temperature in °C. Here, 70°C.

4.4.2.3 Indoor Temperature Constraints

The operational constraints for the indoor temperature (t_{ind}) include the maximum and minimum temperatures. They are given by:

$$t_{\text{ind},\min}(t) \leq t_{\text{ind}}(t) \leq t_{\text{ind},\max}(t) \quad (4.11)$$

Based on the UK CIBSE Knowledge Series-Comfort [168], the limits for indoor temperatures are:

- $t_{\text{ind},\min}$ the minimum indoor temperature is 17°C, while
- $t_{\text{ind},\max}$ the maximum indoor temperature is 25°C.

4.4.2.4 ASHP ON Mode Constraint

The ASHPs should be limited to operated only when when the following conditions are met:

$$V_s - \frac{\left[\sum_{i=1}^n \left(R_i \sum_{j=i}^n P_{Dj} \right) (t) + \sum_{i=1}^n \left(X_i \sum_{j=i}^n Q_{Dj} \right) (t) \right]}{V_s} \leq V_{min}(t) \quad (4.12)$$

$$t_{tank}(t) \leq t_{tank,min}(t)$$

$$t_{ind}(t) \leq t_{ind,min}(t)$$

4.4.2.5 ASHP OFF Mode Constraint

The ASHPs should be switched off when following conditions are met:

$$V_{min}(t) \leq V_s - \frac{\left[\sum_{i=1}^n \left(R_i \sum_{j=i}^n P_{Dj} \right) (t) + \sum_{i=1}^n \left(X_i \sum_{j=i}^n Q_{Dj} \right) (t) \right]}{V_s} \quad (4.13)$$

$$t_{tank,min}(t) \leq t_{tank}(t)$$

$$t_{ind,min}(t) \leq t_{ind}(t)$$

4.5 RESULTS AND DISCUSSION

Impact from occupant behaviour, environment and network voltage level on the 100 ZEBHs performance is presented in this section. The analysis of the influence of the mentioned factors included analysis of the following: ASHP thermal power demand, indoor and water tank temperature and electricity and grid interaction. Result comparison of both scenarios is also given in the section.

4.5.1 Solar Photovoltaic Thermal Assisted Heat Pump

Figure 4-11 illustrates scenario 1 outcomes recorded from the building modelling simulation for a winter day (7th of January), so as to represent the dynamics between the SPVTAH system, as well as indoor and outdoor air temperatures. The ASHP at each ZEBH were directly attached to the water storage tank to support DHW and space heating supply, hence retaining the temperature of the water tank between 50°C and 55°C [169]. The ASHP cycles appeared to occur more at nights and evenings (as the outdoor temperature decreases) in order to maintain the water tank temperature due to higher space heating demand.

The maximum output of thermal power generated by ASHP in each dwelling was approximately $3.30\text{kW}_{\text{th}}$, while the average electrical demand of 1.10kW_{e} was noted for outdoor temperature at -2°C . The thermal/electrical behaviour of the simulated ASHP appeared to be in accordance with BRE and the British Standards EN14511 Part 3-standard rating conditions, which stipulated that typical domestic ASHPs can convert 1kW_{e} of electrical energy to between 3 and 4kW_{th} of thermal heat [170][171].

Figure 4-12 shows that scenario 2 results had an effect using ASHP's load shifting approach with the heat pumps operating to charge the water tanks, which is then discharged to meet dwellings space heating and DHW demands. The heat pump operation is constrained during times in which the feeder is under voltage limit condition. The discharge of the tanks is evident, especially when they experience sudden reductions in temperature variations during the simulation. This is due to the optimisation approach, and hence, the constraint of the heat pumps can also be identified in the net electrical demand results.

4.5.2 Water Tank and Indoor Temperatures

Indoor and water tank temperatures are very important to consider in the ZEBHs, since it provides relevant information about human perception in the investigated 100 buildings. The indoor and water temperatures are two important factors among many explaining indoor temperature comfort values. Scenario 1 (Figure 4-11) shows the continuous heat strategy results while scenario 2 (Figure 4-12) present changes due to the optimisation approach, especially on the water tank temperatures. In scenario 2, the water tank temperatures dropped up to 30°C to maintain the thermal comfort requirements by the residents. The simple fact that the water tanks revealed a 3-hour time period (08:00h to 11:00h) thermal inertia it proved the temperature step-change allowed for a temporal ASHPs load constrained operation.

4.5.3 Net Electrical Demand

As for the outcomes of net electrical demand, the maximum demand on both scenarios was noted at the investigated homes during mornings when the occupants began to start their day, as well as in the evenings when they were back to their dwellings and performed activities that included electrical appliances such as kettles, lights, and electric ovens. Electricity supply produced by the 20 PV/T panels did cater to the electrical demand, and the net electrical demand dropped substantially from 11.00h until 14.00h. It was observed that the electricity supply generated by PV/T panels was insufficient in catering to the electrical demands. This is because electricity production was minimal and unable to compensate the extreme demand caused by the ASHP's.

Figure 4-11 (scenario 1) net electricity demand use is for the continuous heat strategy model. The results for scenario 2, as shown in Figure 4-12 considered the ASHP load shifting and this resulted on a load demand reduction at times where the ASHPs operation were constrained. The difference in the net electricity demand between both scenarios was depicted. The total electricity use for scenario 1 model was 17% higher than scenario 2.

Scenario 1

24 × EH-Plot 272

24 × EH-Plot 273

25 × EH-Plot 274

27 × EH-Plot 349

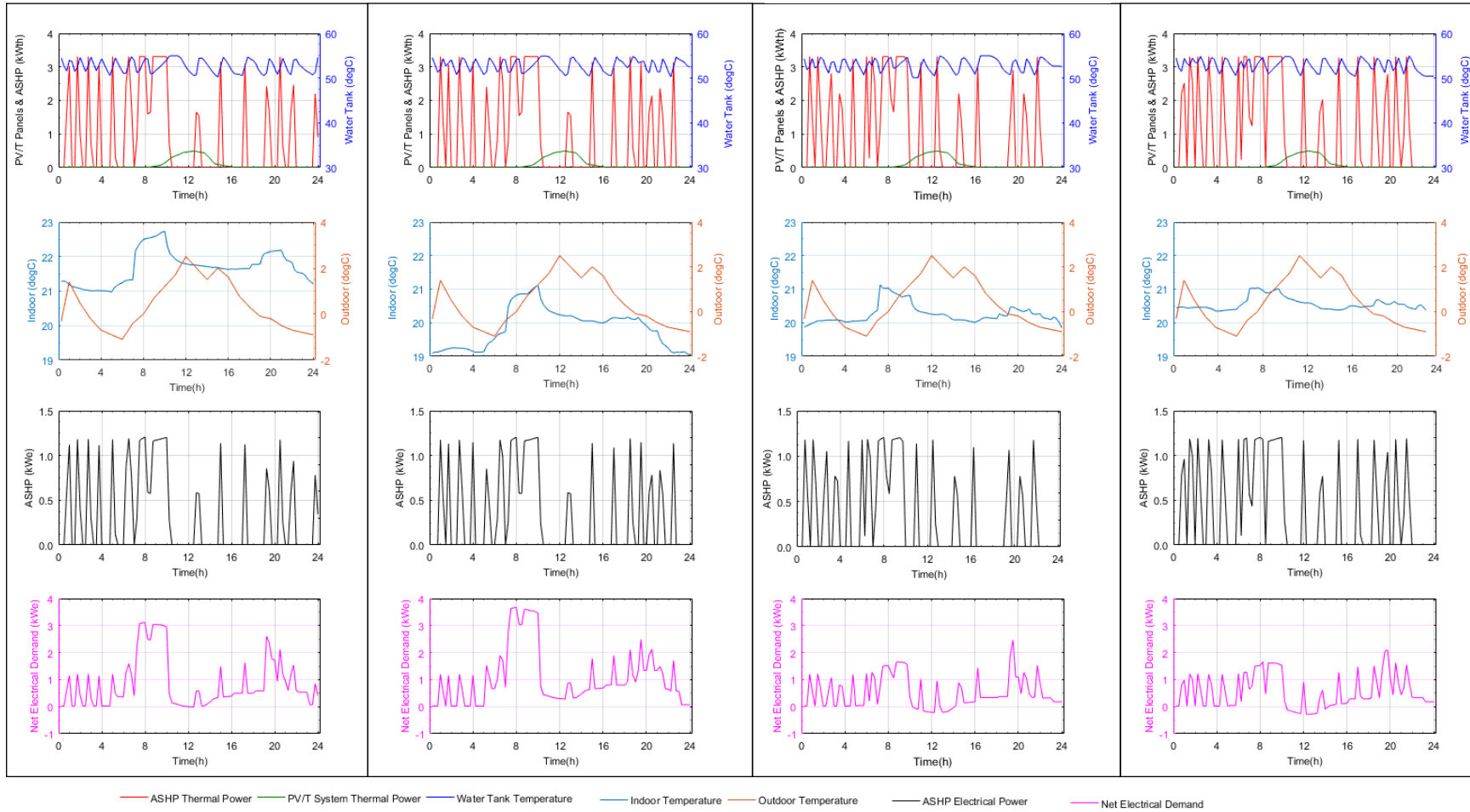


Figure 4-11: Scenario 1-Buildings connected in the test feeder. From top to bottom the water tank dynamic (water tank temperature, ASHP thermal power, PV/T thermal power), indoor and outdoor temperatures, ASHP electrical power and net electrical demand.

Scenario 2

24 X EH-PLOT 272

24 X EH-PLOT 273

25 X EH-PLOT 274

27 X EH-PLOT 349

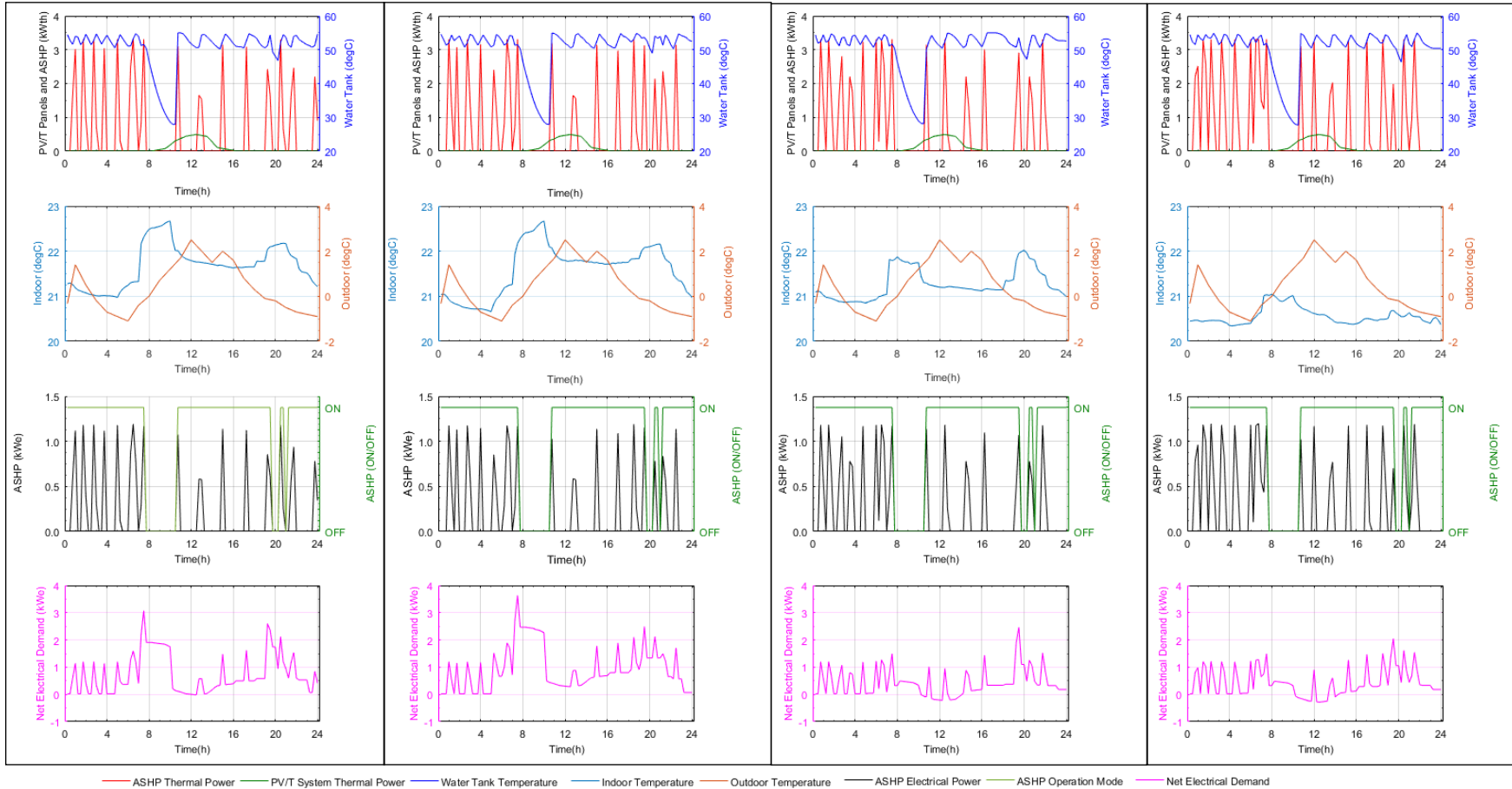


Figure 4-12: Scenario 2-Buildings connected in the test feeder. From top to bottom the water tank dynamics (water tank temperature, ASHP thermal power, PV/T thermal power); indoor and outdoor temperatures; ASHP electrical power, and control operation; and net electrical demand.

4.5.4 IEEE 33-Node Test Feeder

This section presents the voltage profiles for both scenarios, which had been evaluated based on the 2002 UK Electricity Safety, Quality, and Continuity Regulations distribution network voltage statutory limits. Figure 4-13 illustrates the outcomes of the voltage profiles. The voltage variations at the IEEE 33-node test feeder appeared to be visible. It can be seen from the figure that although the proposed ASHP control algorithm scheme is effective to keep the system voltage below the demand limit during the ASHP shifting period, it creates a rebound voltage drop at 11:15h right after the shifting algorithm event ends. Besides, the system voltage was stable for most of the days. Large voltage drops normally began from 07.00h and lasted until 09.45h (0.94 to 0.91 p.u), as well as in the evenings (19.30-20.15 hours). The dashed line shows the minimum bus voltage in the distribution network over time wherein the minimum bus voltage is below the voltage rating during the peak hours.

The simulated voltage profile of the feeder in scenario 2 is represented by red line. It is important to note that the ASHP control algorithm only controlled the demands of ASHPs when the feeder voltage was lower than V_{min} . This is due to the controller signal that is required to trigger the optimisation model from MATLAB/Simulink to E+ through the interface. The load profile upon end of the ASHP control algorithm had been based on the optimisation model generated by the proposed control scheme, and the households may adhere to the optimal ASHPs load demand schedules or otherwise. Hence, the proposed ASHP control algorithm can effectively manage the ASHP loads of the households within the distribution network, apart from maintaining the bus voltage levels within the permissible range for a period of time, only when the network sends the signal to the buildings.

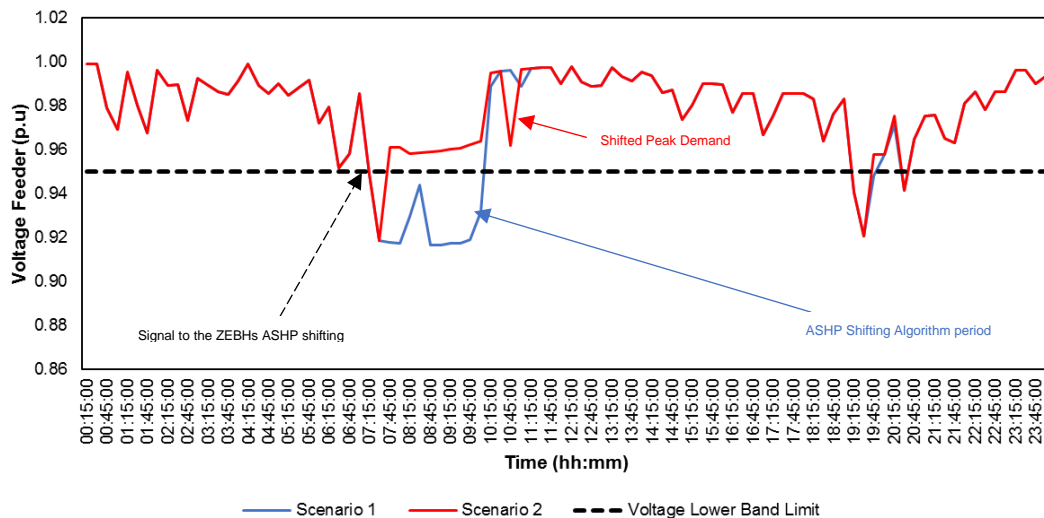


Figure 4-13: Feeder voltage profile on scenarios 1 and 2

Figure 4-14 portray the variations of the real and reactive line flows, in near branches 2 and 5 (from the feeder) and Figure 4-15 represent the line flow results at more distant branches- 22 and 27 for scenarios 1 and 2. It can be seen that the distant branches (22 and 27) from the feeder, contributed more than those closer to the feeder primarily due to reduction in demand implementing the ASHP load shifting algorithm technique. Both power loss and voltage drop along the distribution line had been linked to not only load level, but also at the length of each branch. With increment in distribution line length, its impedance increases, which leads to higher power loss and voltage drop. Thus, the location of load seemed to signify a potential fairness issue in optimal control schedule, mainly because the impact of ASHP shifting on each ZEBH was dissimilar. The optimisation approach (scenario 2), hence, may need to set incentives for the households in a dissimilar manner based on their locations within the network.

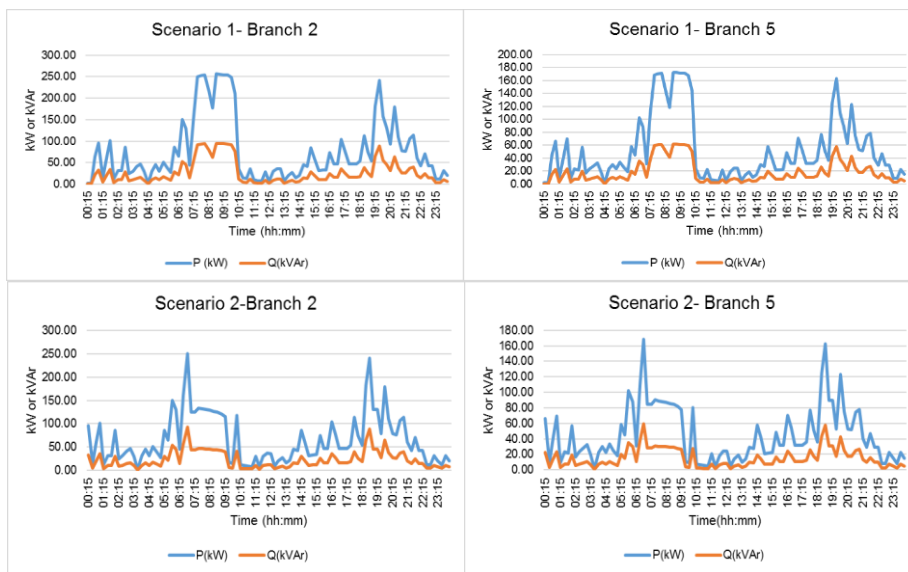


Figure 4-14: Branches 2 and 5 active and reactive power flows for scenario 1 (top) and scenario 2 (bottom)

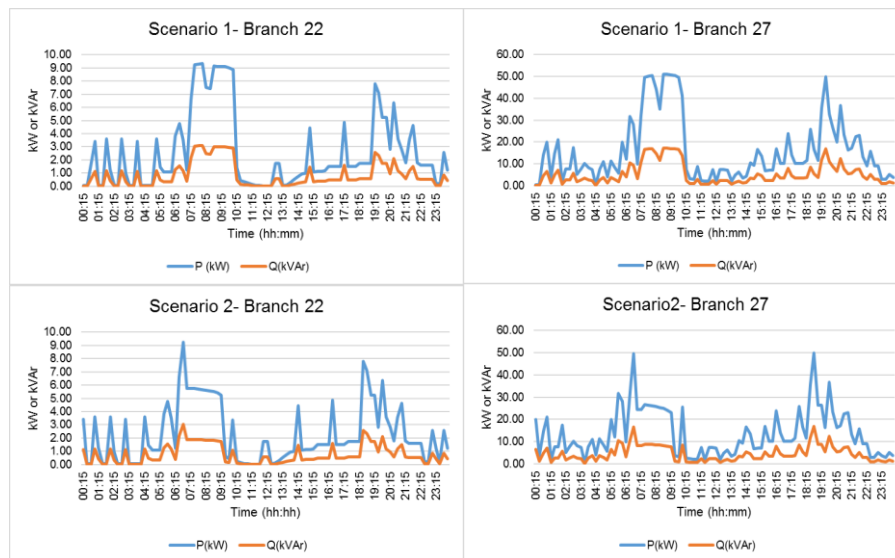


Figure 4-15: Branches 22 and 27 active and reactive power flows for scenario 1 (top) and scenario 2 (bottom)

4.5.5 Energy Demand Flexibility Analysis

This section presents the results of both scenarios to evaluate the energy demand flexibility provided by the buildings. In this thesis, the energy demand flexibility is defined as the period of time in which the ASHP load can be constraint without compromising the occupants thermal comfort when voltage drops below the limit occurs. Figure 4-16 shows that the highest percentage flexibility was experienced the 27 x EH-Plot349 type ZEBHs . This resulted in 51% value of energy demand flexibility. The lowest flexibility percentage was 40% from the 24 x EH-Plot 272 type ZEBHs.

The overall estimation of investigated parameters showed that the change in occupant behaviour models resulted in flexibility variance in the range of 40% to 51%. The results showed that the occupant behaviour regarding the appliances and lighting use were highly relevant when the ZEBHs were analysed. The extensive analysis of the ZEBHs considering energy demand flexibility will lead to proper design of LV electricity networks system for the ZEBHs and guarantee that a voltage dip would not happen during the peak hours.

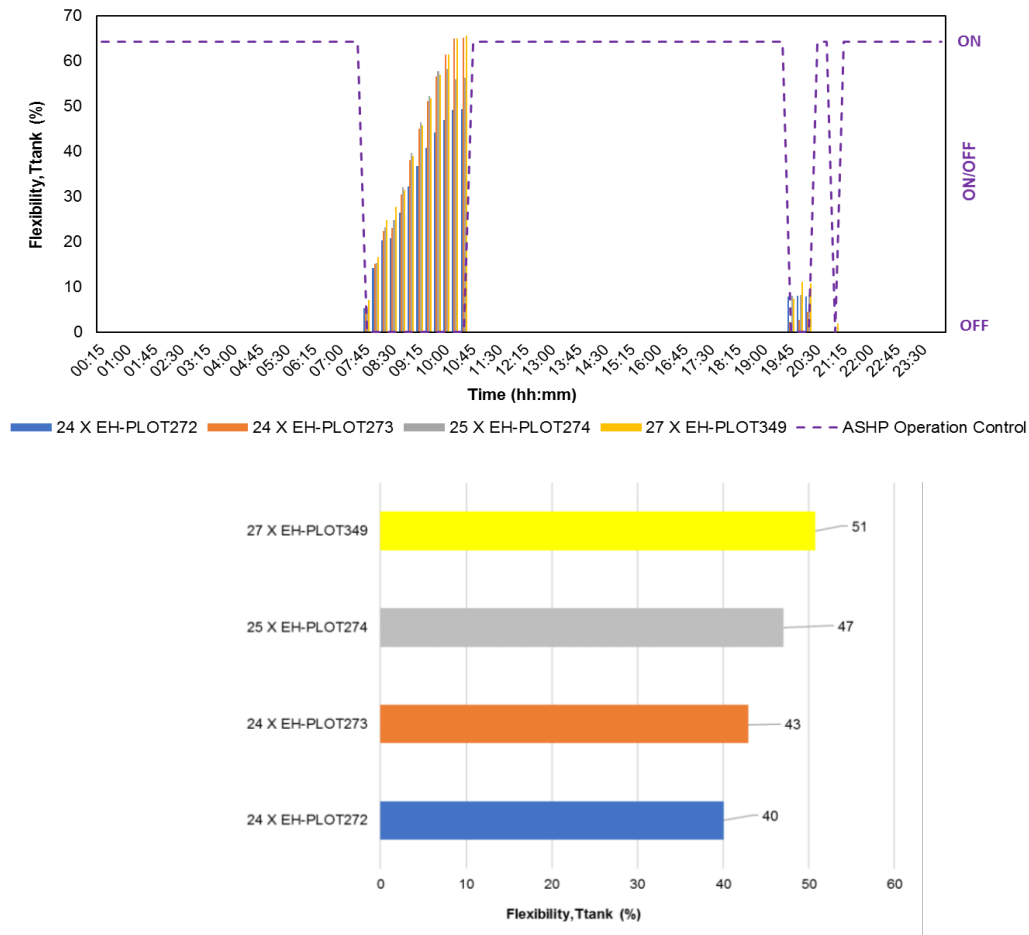


Figure 4-16: Top- flexibility provided by each type of ZEB home and Bottom- average flexibility provided.

Figure 4-17 presents the time for the exchange to exceed the limit, which was quantified as a percentage value. The indicator had been beneficial as scenario 2 results reduced voltage drops, while simultaneously meeting the thermal requirements of the dwellings. The outcomes showed that scenario 2 was 10.60% lower on time percentage below the limit.

The optimization model effectively limited the voltage drop on the LV grid at the transformer secondary side, which was equal to its voltage rating, hence sufficient to keep the voltage within its operational limits when signal was sent to the buildings to constraint the operation of the ASHPs.

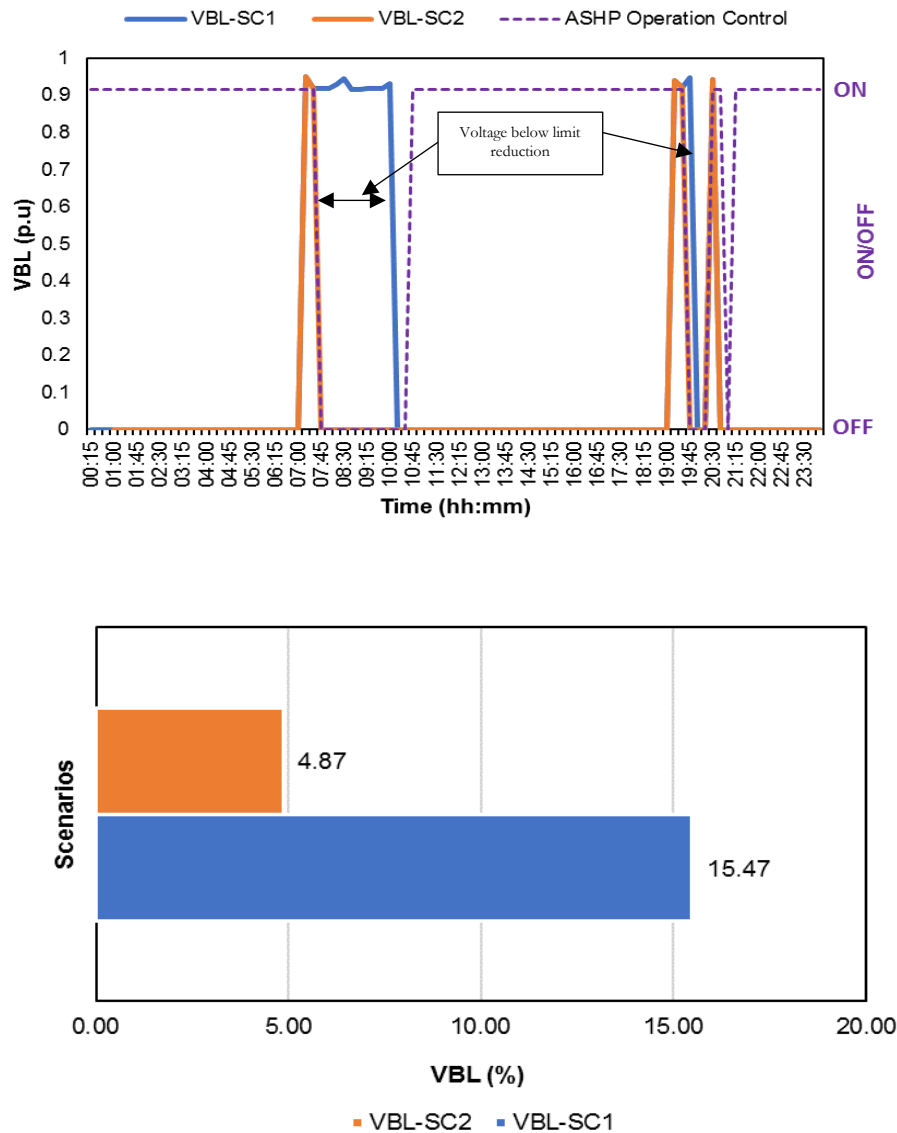


Figure 4-17: Top- VBL during a winter day (7th of January) and Bottom- VBL time percentage for scenarios 1 and 2

4.6 SUMMARY

This chapter presents an integration between building and electricity network model with the capability to study the interactions between the selected dwellings and LV electricity networks. This facilitated in assessing the effective heat pumps load shifting in ZEBHs, hence taking advantage of the thermal storage tanks inertia when voltage drops below the statutory limits in an IEEE 33-node test feeder.

The primary objective was to assess the ZEBHs energy demand flexibility potential without neglecting voltage, and temperature constraints (water tanks and indoor) by employing a control algorithm in the ZEBHs, thus, enhancing the electricity network voltage performance.

The building modelling generated dynamic simulation results, wherein occupants and their activities, internal heat generation, building envelope thermal properties, and environment had been weighed in. The employed models were simulated to evaluate the performances of both the semi-detached domestic dwellings and heating system, while taking into consideration the activities of the occupants.

The outcomes demonstrated that the number of buildings connected to the network and the high load consumption in the feeder sparked voltage issues. Therefore, the capability of controlling the heat pumps installed in the building clusters appeared to be beneficial for the IEEE 33-node test feeder. Nevertheless, the consequences have proven that in order to meet thermal demand, the water tanks experienced massive temperature drops. Subsequently, the ASHP increased its operation during those ON-times.

The optimisation model that can limit voltage drops to the grid has been inspired by the statutory UK LV network voltage limits. The ASHP shifting algorithm (scenario 2) exhibited that optimising the load demand of ASHP based on voltage profiles reduced VBL by 10.60%, in comparison to scenario 1. In particular, an important potential for ASHP load shifting was revealed in this study in association to the circumstances of the network.

At optimum (scenario 2), the percentage flexibility resulted, respectively, on ZEBHs, as given in the following: EH-Plots 272, 273, 274, and 349, as 40%, 43%, 47%, and 51%. The accuracy and flexibility of the presented approach in this chapter, rendered that is suitable for systematic assessment of building-related energy policies, and distribution grid constraints.

CHAPTER 5- INTEGRATED COMMUNITY ENERGY SYSTEM WITH HYDROGEN ENERGY STORAGE

5.1 INTRODUCTION

The call to minimise GHGs and to be more environmental-friendlier has led to the adoption of renewable energy (RE), as well as decarbonisation of road transport [172]. The intermittent nature of renewable sources, nevertheless, has brought about several challenges to the provision of steady power supply and grid balance. At the same time, alternatives to conventional carbon fuel vehicles are faced with several challenges, such as costing, driving range, performance, refuelling access, and safety issues, prior to projecting the attractive options. In the attempt to address these barriers, multiple energy generation and storage technologies are being investigated under the state-of-the-art research approaches and techniques so as to mitigate the impacts of renewable fluctuations and their incorporation into energy grids [173], apart from providing a cleaner and more efficient alternative to power vehicles. With that being depicted, hydrogen (H₂) has emerged to be an attractive alternative mainly because it serves as an energy carrier, it can store energy produced from renewable sources, and it can be used to power vehicles in substitution of conventional fuels.

Hydrogen, like any fuel, has safety risks and must be handled with caution. The society is familiar with gasoline, but handling compressed hydrogen is a new challenge for the society. Therefore, safe storage systems must be developed, while consumers become familiar with its properties and risks. Hydrogen is not toxic, yet extremely flammable [174]. Its laminar burning, n velocities are significantly higher than those of other fuels [175]. Meanwhile, its flame temperature at the presence of ambient oxygen content is almost the same as that of the others. However, its vapor-from-liquid-generation-speed is much higher than that of any fossil based liquid or liquefied fuel.

Hydrogen is a material with high sensitivity to detonation, and as previously earlier, its wide oxygen mixture range of ignition and detonation [176] clarifies how delicate its storage is.

Hydrogen infrastructure continue to be developed in areas where vehicle manufacturers, hydrogen providers, and governments share an interest in paving the way for greater fuel cell vehicle deployment[177]. Most of the existing hydrogen infrastructure was developed in the past several years. In most cases, station developers have sought to estimate local fuel cell vehicle deployment numbers as a means to forecast fuel demand. The UK has 15 hydrogen stations in operation since 2017, and at least five more in the planning stages. Infrastructure development is a public-private partnership among the national and local governments, and fuel cell, industrial gases, energy, and auto industry companies. The UK H₂ Mobility consortium has provided estimates for hydrogen infrastructure to match fuel cell vehicle goals through 2030[178]. An initial set of 65 stations is estimated to be able to support the development of an early market of 10,000 fuel cell vehicles by 2020. Subsequent station construction depends on the demand for hydrogen.

The mobility group has projected approximately 1.6 million FCEVs by 2030 in the UK with annual sales soaring up to 300,000 vehicles. Additionally, interest towards hydrogen as a fuel technology to power vehicles has spread across the world [179]. The primary car manufacturers in the US, Europe, and Asia have begun building fuel cell electric vehicle (FCEV) models to penetrate the market between 2013 and 2015 [180].

Hydrogen generation and storage is being explored at present as part of building energy management strategies towards embedding distributed renewable generation system into the electricity network, hence offering grid balancing and mitigating renewable intermittency. For instance, the Levenmouth Community Energy Project (LCEP) was established as an initiative of the Scottish hydrogen local energy system project that involved Bright Green Hydrogen Ltd. [181], Fife Council, Toshiba's Telecommunications Research Laboratory, and the Leven Valley Development Trust. This project demonstrated the readiness of hydrogen infrastructure to power a fleet of FCEVs. Toshiba deployed its hydrogen energy management system (H₂ EMS) that had been devised to ascertain optimal production and storage of hydrogen based on electricity supply and demand forecasts. In fact, Toshiba managed the overall system control, which allowed the collection of functional data from the entire system, including H₂ EMS, water electrolysis systems, and FCEVs[182].

In particular, the project installed a wind turbine, a solar PV power generation facility, water electrolysis system, hydrogen storage tanks, hydrogen stations, and FCEVs. The RE generated by both the wind and solar power systems had been applied to power the facility and the electrolysed water for hydrogen production. After that, the stored hydrogen was supplied to FCEVs via hydrogen stations. Primarily, the ultimate goal is to display the application of hydrogen technology integrated with renewable generation, as well as hydrogen production and storage, towards achieving zero-carbon alternative.

5.2 OBJECTIVES

This chapter elaborates the ICES model with H₂ storage (ICES-H₂), which is based on the LCEP project and focused on several critical system performance metrics. This study had been based on Toshiba's Telecommunications Research Laboratory analytical model[183], along with incorporation of practical system parameters and real weather data. Moreover, the objectives of this chapter are to:

- Depict the operation of RE technologies (a wind turbine and a solar PV system) integrated with IEEE 33-node test feeder (elaborated in **Chapter 4**), hydrogen energy system, to ZEBHs (presented in **Chapters 3 and 4**), energy storage using hydrogen, and fuel for FCEVs.
- Cater power supply for generation of H₂ and load demands from ZEBHs by wind turbine and solar PV panels system.
- Constrain the operation of the dwellings ASHPs for a certain period without impairing building thermal comfort, based on the demand required, as well as the speed of both temperature increase and decrease from the installed storage tanks.
- Increment the H₂ generation from RE sources and maximising its production upon high demand from FCEVs and evaluate its effect upon the IEEE 33-node test feeder power flow.

5.3 ICES-H₂ MODEL DESCRIPTION

Figure 5-1 illustrates the deployment of the hydrogen energy system (HES) model, in which all components were modelled in MATLAB/Simulink, except the ZEBHs which were modelled with EnergyPlus software. However, the ZEBHs were coupled to the HES model through the BCVTB interface. EnergyPlus was employed to present the building modelling simulation and MATLAB/Simulink to especially study the electrical network load flow and hydrogen energy system over one-week period. **Section 5.5** describes this method.

Hydrogen is generated via green electricity (wind turbine and solar PV system), hydrogen storage tanks, dispensing units, ZEBHs, and FCEVs. In this analysis, the LCEP actual weather data had been applied by using a monitoring device that stored the weather data in a database repository, which were retrievable via online portal [184]. The power for hydrogen generation and ZEBHs load demands were supplied by wind turbine (maximum output power of 750kW_e), and solar PV system (618 monocrystalline PV panels of 255W_p).

In precise, the supply of green electricity was prioritised for ZEBHs, and the electricity excess was used to generate hydrogen. It is noteworthy to highlight that the studied domestic dwellings are equipped with micro-generation systems (solar PV/T panels) to supply their load demand, wherein electrical demand that exceeds power supplied by solar PV/T panels is satisfied by the power generated from green technology. Nonetheless, in the case of insufficient green electricity, electricity is imported from grid to cater to the power demand. Thus, when electricity (from solar panels and green electricity) is generated exceeding the required demand, the surplus power is exported to the grid.

The storage units for FCEVs refer to the buffer tank of 30 bars (40 bars maximum) and 0.85m³; as well as a hydrogen storage tank of 450 bars with the capacity of 1.03m³ for the tank. The design of the buffer tank reflects the Proton Exchange Membrane (PEM) electrolyser of 60kW_e of rated power. The main function of this compressor is to raise the pressure from the 30-bar buffer tank to 450-bar hydrogen tank. In precise, the compressor has 10kW_e maximum power capacity and 80% motor-drive efficiency, whereas the FCEVs are equipped with Hyundai ix35 with maximum fuel consumption of 0.97 L/100km. The ICES-H₂ model was further divided into seven sub-sections as follows:

- i.* Green electricity generation,
- ii.* Inverters and rectifier,
- iii.* ZEBHs,
- iv.* LV Electrical distribution network,
- v.* H₂ refuelling station,
- vi.* H₂ demand (FCEVs), and
- vii.* Operation strategy.

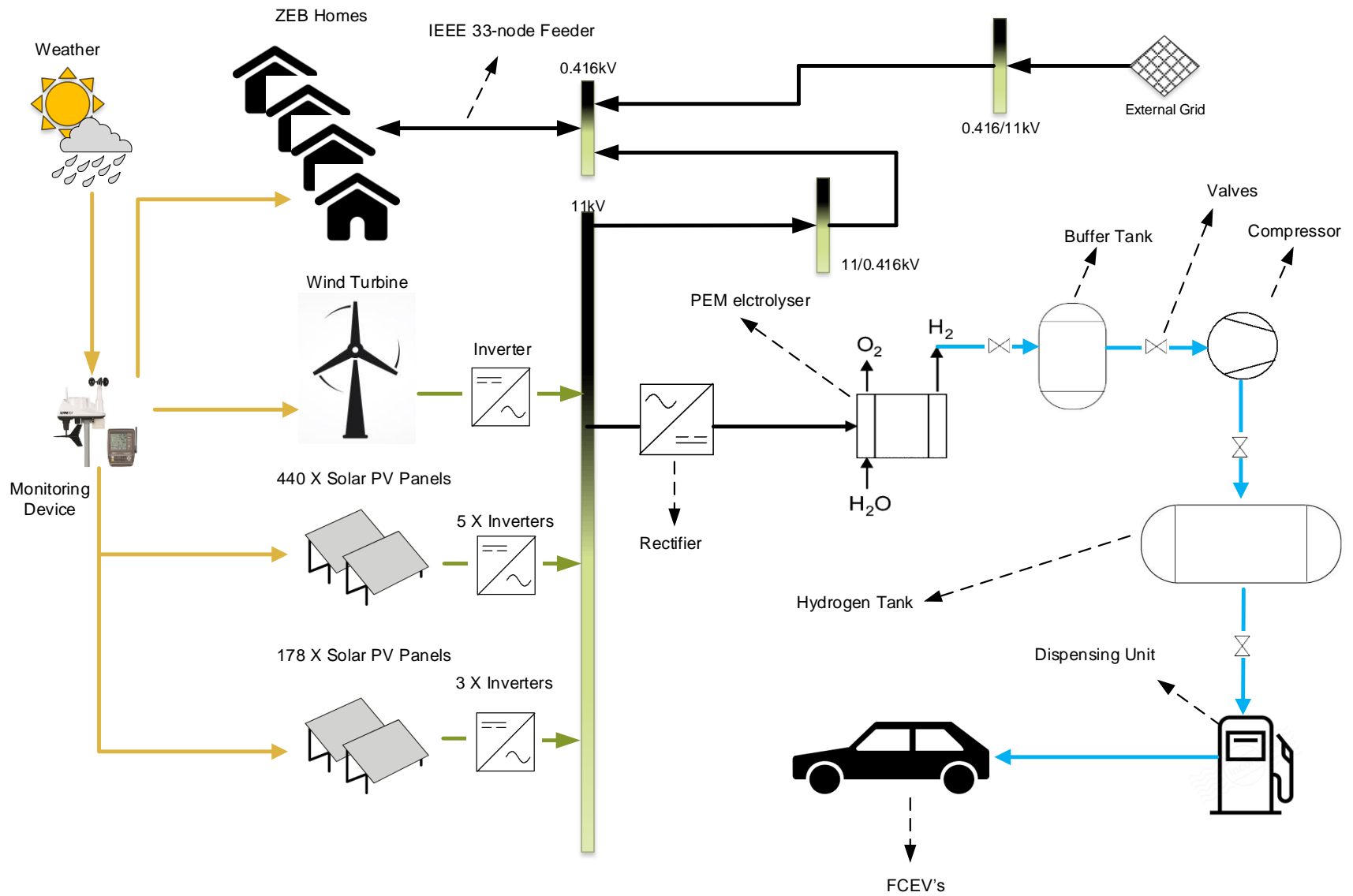


Figure 5-1:HES model

5.3.1 Wind Turbine and Solar PV Panels

The generation of hydrogen via water electrolysis driven by wind/solar-generated electricity has emerged to be a promising method that promotes community energy systems. With that, this thesis employed a *GWP47* and *GreenTriplex PM060P600* type as the wind turbine and the solar PV panels model. Additionally, Fonus Symo inverters were included in this study to convert DC power generated from the PV panels to AC electrical power. **Appendix C1** presents the technical characteristics of the selected components employed in this analysis.

5.3.1.1 Wind Turbine Model

The GWP47-750kW wind turbine used is a Horizontal-Axis Wind Turbine (HAWT) wind turbine with rotor diameter of 47m. The turbine uses LM 21.0P blades from LM Glasfiber (Figure 5-2). The blades can be turned to obtain optimal operational settings at both low and high wind speeds. The wind turbine utilise the best characteristics of both stall and pitch regulated wind turbines, it has the same regulation potential as a pitch regulated turbine; but by using the stall properties of the blades, the large load and power fluctuations that are typical for a pitch regulated machine are avoided. In line with the wind speed, data pertaining to solar radiation and ambient temperature were gathered from a monitoring device to complete the modelling of the wind turbine and 618 solar PV panels.

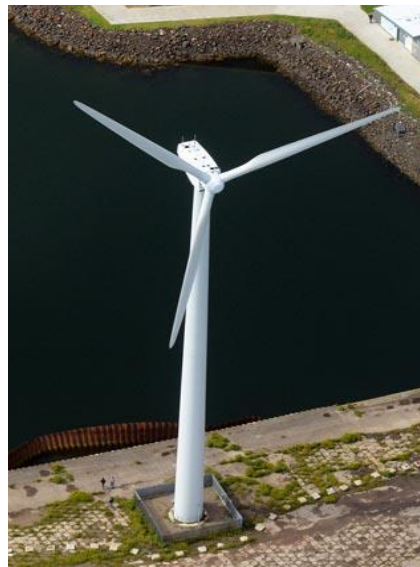


Figure 5-2: Aerial image of the LCEP wind turbine. Courtesy of Bright Green Hydrogen

The primary function of a wind turbine is to convert wind kinetic energy into AC or DC power based on power curve, in which the graph illustrated in Figure 5-3 depicts power output versus wind speed at the height of the hub.

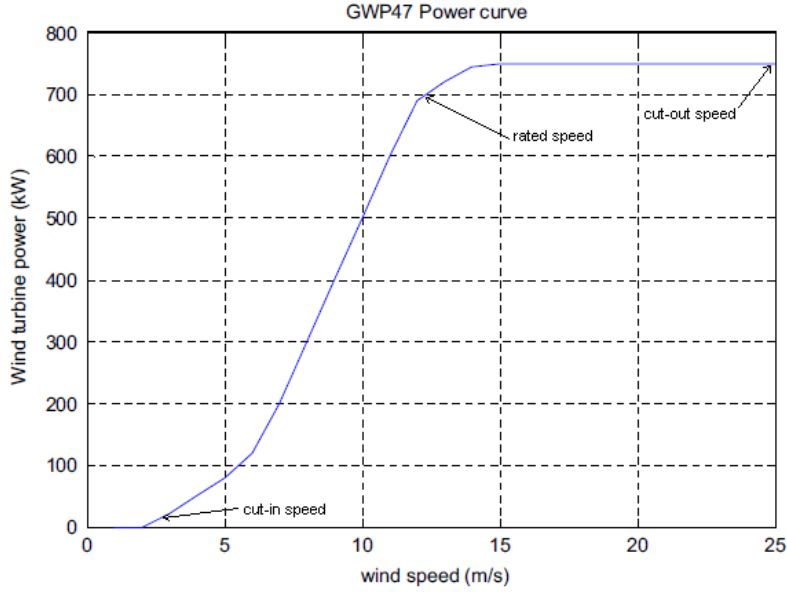


Figure 5-3: Power curve of the GWP47 wind turbine [185]

Wind turbine models can be categorised into detailed (or dynamic) models and simplified (or static) models. Detailed models [186] are useful to study the real turbine behaviour in the time frame of seconds while simplified models are more practical for the simulation of hours or days. The wind turbine model developed in this thesis is a parametric model⁸. The relationship between power output and wind speed the wind turbine between cut-in and rated speed is nonlinear, and this is given as follows:

$$P_{WT}(v) = \begin{cases} 0, & v < v_{ci} \\ P_R \left(\frac{v - v_{ci}}{v_R - v_{ci}} \right)^3, & v_{ci} \leq v \leq v_R \\ P_R, & v_R \leq v \leq v_{co} \\ 0, & v_{co} < v \end{cases} \quad (5.1)$$

where,

- P_R refers to rated power output of wind turbine generator (kW_e)
- v stands for wind speed in m/s
- v_{CI} denotes cut-in speed in m/s
- v_{CO} reflects cut-out speed in m/s
- and v_R is defined as rated wind speed in m/s.
- P_{WT} is the wind output power in kW_e

⁸ A parametric model defines the relationship between input and output by a set of mathematical equations with a finite number of parameters.

5.3.1.2 Solar PV Panels Model

Figure 5-4 shows the fitting of 178 panels on the roof of FIFE⁹ Renewable Energy Centre located at Methill, and additional 440 panels installed at an empty ground next to the East Fife Football Club located at the Bayview stadium. The schematics of the solar PV panels connection and arrangement can be seen in **Appendix C2**.



Figure 5-4: LCEP installed solar PV panels. 178 PV panels on roof of FIFE centre (left) and 440 PV panels on stadium ground. Courtesy of Bright Green Hydrogen

The output power of the PV panels (P_{PV}) relies on not only solar radiation, but also system and inverter efficacy, as modelled in the following:

$$P_{PV} = N_{PV} (I_{rad} \eta_{eff,system} \eta_{eff,inverter}) \quad (5.2)$$

and,

$$\eta_{eff,system} = E_o (1 - E_t (T - T_{air})) P.F \quad (5.3)$$

also,

$$P.F = \frac{A_{cells} N_{cell}}{A_{panels}} \quad (5.4)$$

where,

- $P.F$, reflects PV panel area fraction covered by solar cells; also called cell packing factor,
- E_o stands for PV cell efficiency, while E_t is temperature coefficient of solar cell efficiency in %,
- T denotes module temperature at standard conditions, while T_{air} is ambient temperature in °C,
- I_{rad} is the solar irradiance power per unit area (W/m^2)
- $\eta_{eff,system}$ is defined as PV system efficiency (%),
- $\eta_{eff,inverter}$ represents inverter efficiency (%),
- N_{PV} refers to the total number of PV panels, whereas N_{cell} is the total number of cells,
- A_{cells} and A_{panels} are the areas of the cells and PV panel in m^2 , respectively.

⁹ Fife refers to a council area located at a historic county in Scotland.

5.3.2 Inverters and Rectifier

The function of an inverters is to convert electrical power from DC to AC, whereas a rectifier converts AC power to DC at the desired load frequency. The efficiency of an inverter indicates how much DC power is converted to AC power and otherwise for a rectifier. Some of the power can be lost as heat, and also some stand-by power is consumed for keeping the inverter and rectifier in powered mode. In this thesis, sine wave inverters and rectifier were modelled using MATLAB. The efficiency should be constant throughout the working range for the inverter and rectifier, in this case, 94.8%[187].

There total power of the inverters (8 in total) is calculated as follows:

$$P_{inv,load} = P_{GreenElec} \eta_{eff, inverter} \quad (5.5)$$

In order to determine rectifier power, which is required to power up the electrolyser, the following equation is applied:

$$P_{rect,electrolyser} = P_{GreenElec} \eta_{eff, rectifier} \quad (5.6)$$

where,

- $\eta_{eff, inverter}$ is the inverter efficiency in %
- $\eta_{eff, rectifier}$ is the rectifier efficiency in %
- $P_{inv,load}$ stands for electrical power converted from DC into AC for ZEBHs load in kW_e,
- $P_{rect,electrolyser}$ denotes electrical power converted from AC into DC for electrolyser in kW_e,
- $P_{GreenElec}$ refers to the total power generated from solar PV system and wind turbine ($P_{PV} + P_{WT}$) in kW_e,
- $\eta_{eff, inverter}$ and $\eta_{eff, rectifier}$ reflect the efficiency of both inverter and rectifier in %.

5.3.3 Buildings Load Demand and Residual Load Calculation

The ZEBHs load data functioned as input to the ICES-H₂ model. The data was represented with 15-minute time frequency in kW_e for the same 100 residences over a period of a winter week. The loads, as presented in **Chapter 4**, had been allocated with the same configuration in the electrical network via the BCVTB interface. The interface was also applied to link EnergyPlus and MATLAB/Simulink. In line with that presented in **Chapters 3 and 4**, the ZEBHs were modelled by using EnergyPlus except for a variation in the selection of weather profile that employed the recorded Levenmouth real weather data [188]. The power generated from wind turbine and solar PV panels (green electricity) is supplied to cater to the power demands of ZEBHs.

The green electricity supply, nonetheless, is treated as negative load due to its intermittent supply that is inconsistent. With that, the residual load supplied by the grid is determined as follows:

$$P_{Res,load} = P_{Load} - P_{GreenElec} \quad (5.7)$$

where,

- $P_{Res,load}$ denotes ZEBHs residual load in kW_e supplied by the grid,
- P_{Load} reflects ZEBHs load demand (kW_e). P_{Load} was only weighed in when power generated by 20-roof mounted solar PV/T panels failed to meet load demand,
- $P_{GreenElec}$ is defined as the total output electricity from wind turbine and 618 Solar PV panels in kW_e

5.3.4 Modified IEEE 33-Node Test Feeder

For the purpose of the analysis, the IEEE 33-node test feeder had been restructured, as illustrated in Figure 5-5. Additionally, the wind turbine and solar PV system were embedded into the network so as to weigh in green electricity. Both the RE generation systems were operated at 0.95 power factor, especially after having to consider reactive power for the power flow simulation in MATPOWER 6.0.

Appendix B1 present the transformer 1 and the network parameters data, respectively. The maximum voltage of the wind turbine-GWP47 was 0.690kV, while the maximum power from the wind turbine and solar PV system was 750kW_e and 200kW_e (0.950MW_e in total). Therefore, an additional 11kV transformer and 1MVA of apparent power was selected (transformer 2). The technical specifications of the transformer 2 ($S_{transformer,2}$) are detailed in [189].

5.3.5 H₂ Refuelling Station

Figure 5-6 presents the principle of hydrogen refuelling subsystem. In this study, the subsystem was integrated with a 60kW_e PEM electrolyser that employed green electricity to generate hydrogen via water electrolysis. The buffer tank temporarily stored the hydrogen and regulated the fluctuations in the rate of hydrogen generation.

Hydrogen generated from the electrolyser was stored in the buffer until the pressure hit its limit. As a result, the compressor raised the hydrogen from 30 bars to 450 bars to the final storage system that supplied power to the FCEVs through a dispenser unit. **Appendix C3** summarises the technical description of the parameters.

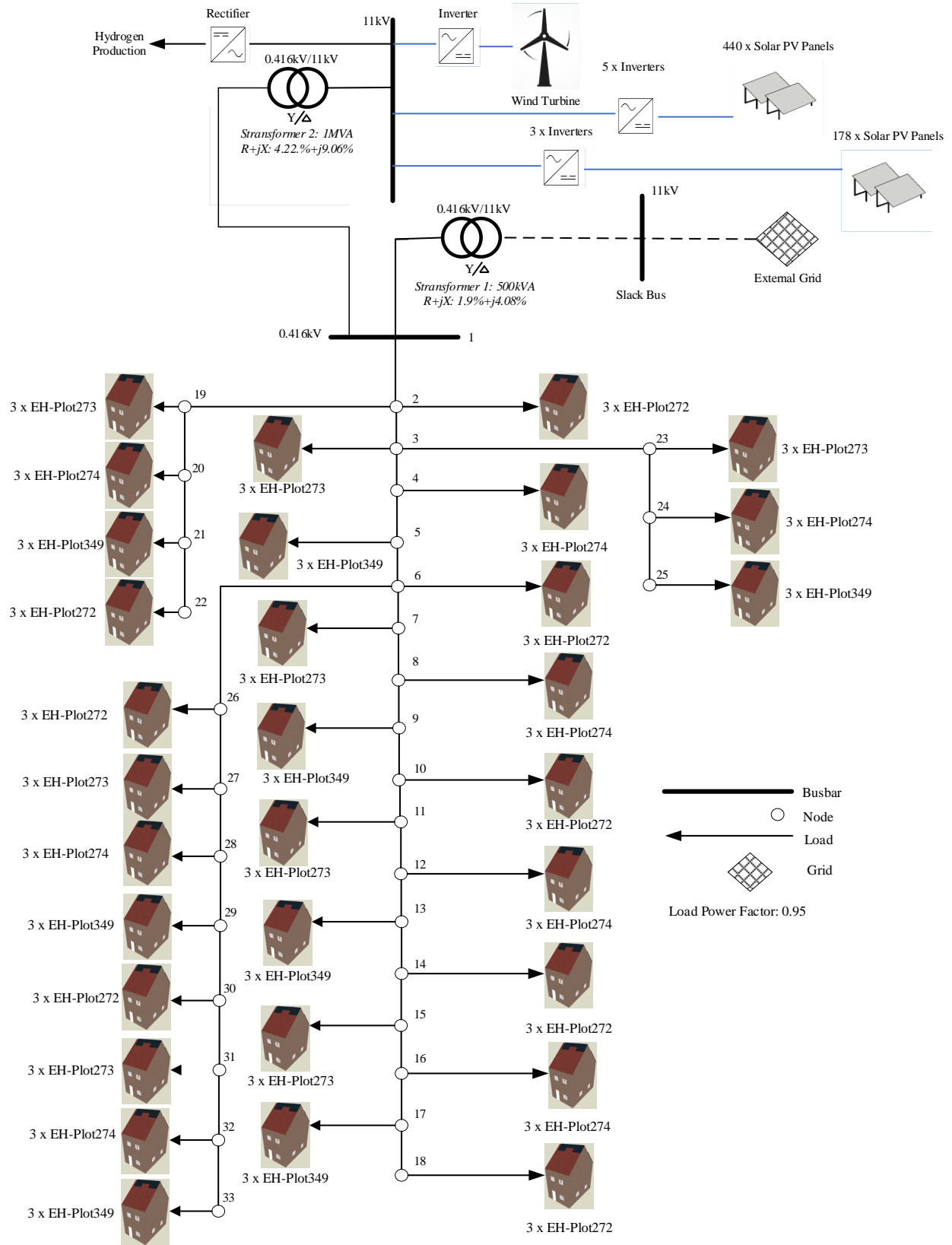


Figure 5-5: Modified IEEE 33-node test feeder

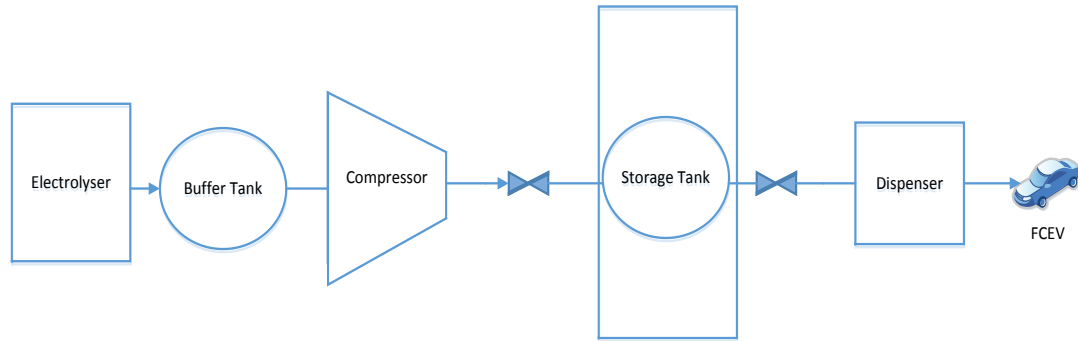


Figure 5-6: Schematic of H₂ refuelling station

5.3.5.1 Proton Exchange Membrane Electrolyser

The electrode kinetics of an electrolyser cell can be modelled using empirical current-voltage (I-V) relationships. Figure 5-7 portrays the PEM electrolyser modelled in this study implemented in LCEP that was made in Canada by Hydrogenic [190]. For the PEM cell the I-V characteristic, given by Equation 5.8, was found in [191] through experimental data fitting method. As in the case of PEM cell, the first element of the Equation 5.8 is the reversible cell voltage (V_0). The second element of the sum, V_1 , considers the influence that the pressures of the gases and water have on the overvoltage. The third element, V_2 , considers the plates and membrane resistance. Only the membrane resistance was included in this study, as its resistivity is significantly higher than that of plates and electrodes [4]. While the last element of Equation 5.11, V_3 , models the activation overvoltage.



Figure 5-7: Hydrogenic PEM electrolyser installed in the LCEP. Courtesy of Bright Green Hydrogen

$$V_{electrolyser} = V_0 + V_1 + V_2 + V_3 \quad (5.8)$$

and,

$$V_1 = \frac{RT_{cell}}{F} \ln \left(\frac{pb_2 p_{o_2}^{1/2}}{pb_2 o} \right) \quad (5.9)$$

$$V_2 = \left(R_{eq,an} + R_{eq,cat} + \left(\frac{\delta_m RT_{cell}}{F^2 AC_{H^+} D_{H^+}} \right) \right) i \quad (5.10)$$

$$V_3 = \left(\frac{RT_{an}}{a_{an} F} \operatorname{arcsinh} \left(\frac{i / A}{2i_{o,an}} \right) \right) + \left(\frac{RT_{cat}}{a_{cat} F} \operatorname{arcsinh} \left(\frac{i / A}{2i_{o,cat}} \right) \right) \quad (5.11)$$

where,

- $V_{electrolyser}$ refers to electrolyser cell terminal voltage (V),
- V_0 stands for reversible cell voltage (V),
- V_1 represents overvoltage from gas and water pressure (V),
- V_2 , is defined as the voltage from plate membrane (V),
- V_3 is activation overvoltage in V,
- R stands for ideal gas constant (8.3144J/mol/K),
- T_{cell} , T_{cat} , and T_{an} are cell, cathode, and anode constant temperatures (353K), respectively,
- pb_2 and p_{o_2} refer to anode and cathode partial pressures (bars),
- $R_{eq,an}$ and $R_{eq,cat}$ are anode and cathode resistances in Ω ,
- F refers to Faraday's constant in Ah/mol,
- A represents electrolyser cell area in m^2 ,
- δ_m denotes PEM membrane thickness in cm,
- C_{H^+} is the concentration of H_2 ions in PEM membrane (mol/m^3),
- D_{H^+} reflects diffusivity of H_2 ions in PEM membrane in m^2/s ,
- α_{an} and α_{cat} stand for anode and cathode transfer coefficients,
- $\operatorname{arcsinh}$ represents the inverse of hyperbolic sine function,
- $I_{o,an}$ and $I_{o,cat}$ are the exchange current density of anode and cathode in A/cm^2 , and
- I refer to cell current in A.

According to Faraday's law, the production rate of hydrogen in an electrolyser cell is directly proportional to the transfer rate of electrons at the electrodes, which in turn is equivalent to the electrical current in the external circuit. Hence, the total hydrogen production rate in the electrolyser, which consists of several cells connected in series, is expressed as:

$$n_{H_2} = n_s \left(\frac{n_F n_{cells} i}{z F} \right) \quad (5.12)$$

and,

$$n_s = \frac{P_{rated, electrolyser}}{P_{stack}} \quad (5.13)$$

In this context the Faraday efficiency in Equation 5.14 is defined as the ratio between the actual and theoretical maximum amount of hydrogen produced in the electrolyser. The Faraday efficiency, η_F , accounts for the parasitic currents and depends on the temperature and current.

The Faraday efficiency decreases with the increase of temperature and the decrease of the current through the cell. An empirical expression that accurately depicts these phenomena is the non-linear relationship, as follows:

$$n_F = a_1 \exp \left(\left(\frac{a_2 + a_3 T_{cell} + a_4 T_{cell}^2}{i / A_{cell}} \right) + \left(\frac{a_5 + a_6 T_{cell} + a_7 T_{cell}^2}{(i / A_{cell})^2} \right) \right) \quad (5.14)$$

where,

- n_{H_2} is hydrogen produced in mols/s,
- n_s is total number of stacks,
- n_F is efficiency of electrolyser in %,
- $P_{rated, electrolyser}$ and P_{stack} are electrolyser and stack electrical powers in W, respectively,
- n_{cells} is the total number of cells,
- I is the cell current in A,
- z is the electrons transferred per ion in H_2 (2),
- F is Faraday's constant (Ah/mol),
- T is cell temperature (353K),
- A_{cells} is cell area in m^2 , while $a_1 \dots a_7$ refer to empirical parameters.

5.3.5.2 Compressor

The function of the modelled compressor is significant in generating gas flow between the buffer and the hydrogen tank. In this case, the energy required for the compression process is situated between the energy required for an isothermal process as a lower boundary and that of an adiabatic process as the upper boundary. The polytropic process occurs with an interchange of both hydrogen gas pressure and volume during the operation of the compressor[192].

The compressor operates in two stages by modelling a polytropic process, at the first stage, the compressor increases the hydrogen inlet pressure, P_1 , to an intermediate value, P_2 . The process is repeated at the second stage, wherein the gas leaves at the discharge pressure, P_3 . The energy required for the compression process refers to the energy required for isothermal process at the lower boundary and that of an adiabatic process at the upper boundary.

The polytropic index relies on the nature of the gas and the details of the compression. As such, the following had been calculated:

$$W = \frac{\gamma RT}{\gamma - 1} \left[\left(\frac{P_2}{P_{1,buffer}} \right)^{\frac{\gamma-1}{\gamma}} - 1 \right] + \frac{\gamma RT}{\gamma - 1} \left[\left(\frac{P_{3,H2tank}}{P_2} \right)^{\frac{\gamma-1}{\gamma}} - 1 \right] \quad (5.15)$$

also,

$$P_2 = \sqrt{P_{1,buffer} P_{3,H2tank}} \quad (5.16)$$

Finally, hydrogen flow through the compressor, a (moles/s), was determined as follows:

$$a = \frac{\eta_c P_c}{W} \quad (5.17)$$

where,

- W is the work done by the compressor in Joules,
- γ is the polytropic index, for an isothermal process γ is 1.
- P_2 stands for optimal intermediate pressure in bars,
- $P_{1,buffer}$ is pressure from buffer tank, while $P_{3,H2tank}$ is pressure of the hydrogen storage tank in bars,
- R refers to universal gas constant $8.3144621e^{-5}$ (mol³/molK), whereas T is temperature (300K),
- η_c denotes both mechanical and motor drive efficiency (%), and
- P_c is compressor rated power in kW_e.

5.3.5.3 Buffer and Hydrogen Storage Tanks

The hydrogen storage system is inclusive of storage tank; both buffer and hydrogen tank, as well as compressor. In order to determine optimum compressor operation, the hydrogen tank is filled when the pressure within the buffer tank reaches the pressure of electrolyser outlet. In this study, the electrolyser outlet pressure was fixed at 80 bars, while the maximum pressure for the hydrogen tank pressure was set at 450 bars. Figure 5-8 illustrates the modelled storage tank.



Figure 5-8: LCEP H₂ Tank. Courtesy of Bright Green Hydrogen

The mathematical model that describes both buffer and hydrogen storage are given by the Van der Waals equation [193][194], which associates variables pressure (P), temperature (T), and volume (V) for real gases. The Van der Waals equation has been reckoned to be an accurate mathematical model as it incorporates the interaction between the molecules, as given in the following equation:

$$P = \frac{nRT}{V - nb} - a \frac{n^2}{V^2} \quad (5.18)$$

a and b are constants given by

$$a = \frac{27R^2T_{cr}}{8P_{cr}}, \quad b = \frac{RT_{cr}}{8P_{cr}}, \quad (5.19)$$

where,

- n refers to the number of mol of H₂ accumulated in the tanks,
- R stands for universal gas constant $8.3144621e^{-5}$ (mol³/molK),
- T is temperature of tanks (300K),
- T_{cr} and P_{cr} are hydrogen critical temperature and pressures (32.97K and 12.93Pa), and
- V denotes volume in m³.

The values of volume for both buffer and storage tank are presented in Normal Meter Cubic (Nm³), which were converted into m³ by using the following formula of conversion:

$$V(m^3) = V(Nm^3) \frac{P_{atm}}{P_{abs}} a \frac{25^\circ C + T_{std}}{T_{std}} \quad (5.20)$$

where,

- P_{atm} is the standard atmosphere pressure in bars,
- P_{abs} denotes buffer and H₂ tanks absolute pressures (80bars and 450 bars),
- T_{std} is the ideal gas standard temperature in Kelvin (K), and
- V reflects volume in m³.

5.3.6 Hydrogen Demand for Fuel Cell Electrical Vehicles

This study had employed the Hyundai ix35 equipped with an on-board tank capacity of 144 L and maximum fuel consumption of 9.7 L/100 Km (Figure 5-9). The Hyundai vehicle was also considered in another case study [183] for the UK Island Hydrogen project that probed into technical and economic analyses of hydrogen refuelling with on-site hydrogen generation [195].



Figure 5-9: Hyundai ix35 FCEV [196]

As for this study, the hydrogen demand had been modelled based on two primary aspects: i) random arrival of the vehicles at the refuelling station, and ii) the state of the tank in the cars at arrival.

The features of random arrival are given as follows: distance travelled, time of the day when the first vehicle arrives at the station, interval time between arrival of cars, and the total number of vehicles arriving in one day. As for this study, cars arrival time for fuelling had been selected based on random and uniform distributions between 09:00h and 18:00h. The total number of vehicles that arrived at the station per day was determined by using the Poisson Probability Distribution, as given in the following:

$$P_x(k) = \frac{\lambda^k e^{-\lambda}}{k!} \quad (5.21)$$

The interval time between two consecutive arrivals is given in the following exponential distribution:

$$P_x(k) = \gamma e^{-\gamma k} \quad (5.22)$$

where,

- λ is the average number of cars (40 cars),
- γ refer to car arrival rate,
- e is Euler's number (2.71828...),
- k stands for the number of times a car arrives at the refuelling station in the interval; and k can take values 0, 1, 2, ..., and
- $k!$ is the factorial number of k

The initial state of the car tanks when they arrived at the fuelling station was determined from the daily driving distance average of the vehicle. The daily driving distance had been based on the UK Department of Transport for daily average distance travelled by length trip in Great Britain [197]. The mean value for the travelled distance appeared to be 30.5 miles (49Km), as depicted in Figure 5-10.

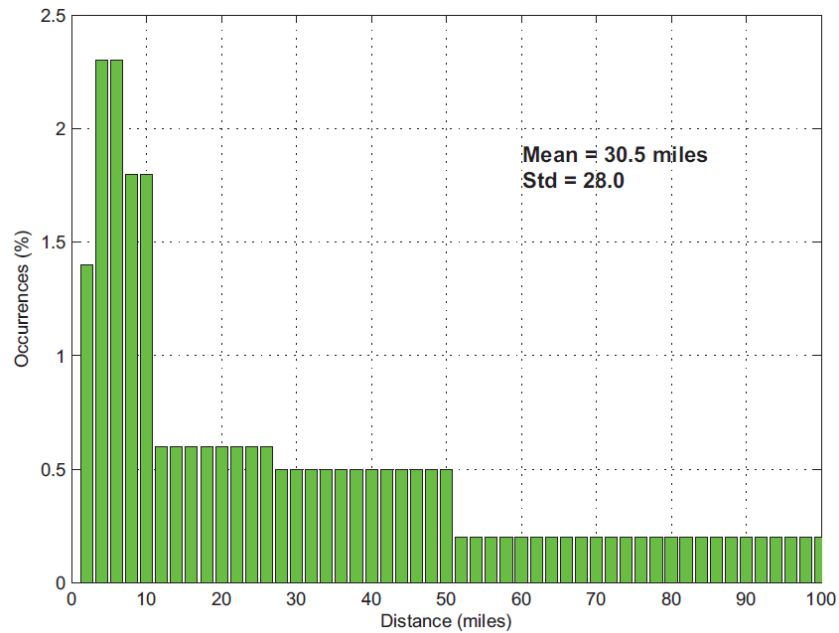


Figure 5-10: Daily driving distance distribution in the UK [197]

5.3.7 Operation Strategy

The strategy of system operation is according to the following rules (see Figure 5-11):

Electricity

- If $P_{GreenElec}(t) = P_{Load}(t) / \eta_{eff, inverter}$, then whole power generated by the wind turbine and solar PV system is injected to the ZEBHs load through the inverters.
- If $P_{GreenElec}(t) > P_{Load}(t) / \eta_{eff, inverter}$, then the surplus power is delivered to the electrolyser.
- If $P_{GreenElec}(t) > P_{rated, electrolyser}$, then the excess of energy will circulate to the grid.
- If $P_{GreenElec}(t) < P_{Load}(t) / \eta_{eff, inverter}$, then the shortage power for the ZEBHs is supplied by the grid.
- If $P_{PV/T, gen}(t) > P_{Load}(t) / \eta_{eff, inverter}$, then the excess of electricity generated by the ZEBHs PV/T panels is exported to the grid.

Hydrogen

- If $10\text{bars} \leq P_{1, buffer} < 30\text{ bars}$, then the produced n_{H2} , is injected to the buffer tank
- If $P_{1, buffer} = 30\text{ bars}$, then $P_{rated, electrolyser} = 0$. Hence, no more n_{H2} is injected to the buffer tank.
- If $P_{1, buffer} = 30\text{ bars}$, and $P_{1, H2tank} < 450\text{ bars}$; then the compressor will work (*Joules*) and hydrogen (*mols/s*) will flow through it in order to fill the H_2 tank.
- If $10\text{ bars} \leq P_{1, buffer} < 30\text{ bars}$, then the compressor power, P_c will be equal to zero. Therefore, it will not work (*Joules*) and hydrogen (*mols/s*) will not flow through it.
- If $P_{3, H2tank} = 450\text{ bars}$, then the compressor will not work (*Joules*) and hydrogen (*mols/s*) will also not flow through it.

FCEVs

- If $360\text{bars} \leq P_{3, H2tank} \leq 450\text{ bars}$, then the refuelling station is available to supply hydrogen to the vehicles.
- If $P_{3, H2tank} \leq 360\text{bar}$, then the refuelling station will not allow vehicles to be fuelled with hydrogen.

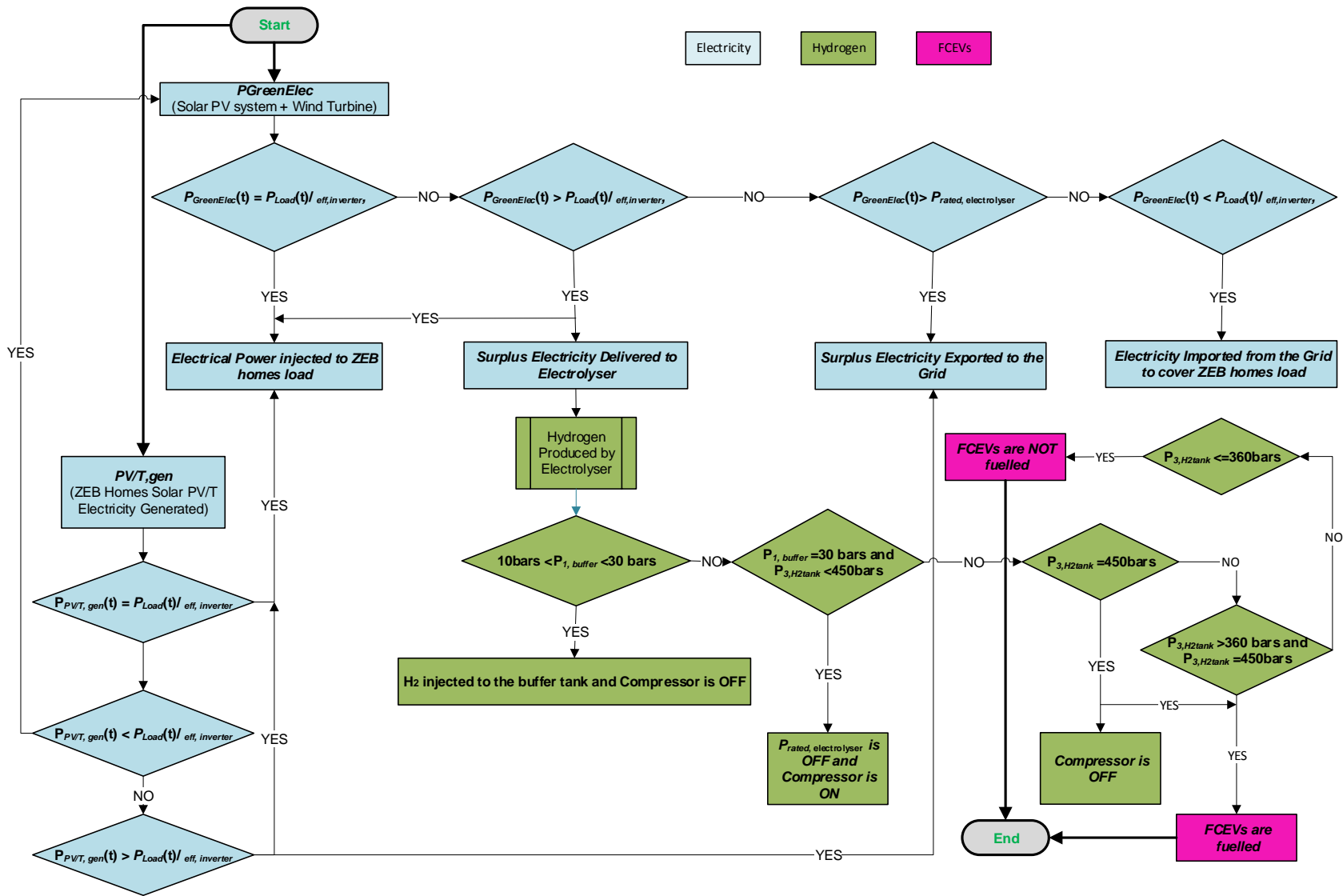


Figure 5-11: ICES-H2 Operation Strategy

5.4 OPTIMIZATION MODEL

The primary goal of the optimization model is to maximise hydrogen production by decreasing pressure from dropping in the hydrogen storage tank. Thus, the ZEBHs ASHPs load required a control algorithm that was applied to schedule the operation, particularly to constrain the operation of heat pumps in ZEBHs upon high demand for hydrogen to fuel the FCEVs.

Furthermore, the ASHPs are coupled to the water storage tanks, hence, the water storage tank and indoor temperatures considered to remain within a temperature range limit. Additionally, to the constraints related to the ZEBHs, hydrogen supply constraints were considered in the shifting algorithm.

Similar to **Chapter 4**, this chapter also implemented a **mixed integer linear programming (MILP) method to solve the optimization model**. This was built by MATLAB/Simulink and solved by the MATLAB's "*intlinprog*" solver script (solver-based optimization problem). The following deviation variables (unknown) were involved:

- n_{H_2} is the hydrogen produced in mols/s,
- α is the flow of hydrogen through the compressor (moles/s),
- $FCEV$ (fuelled and non-fuelled),
- $P_{Buffer,Tank}$ is the buffer tank pressure in bars
- P_{H_2Tank} is the H_2 tank pressure in bars,
- $V_{electrolyser}$ (V) and I (A) are the voltage and current of the cell,
- V_s is the voltage at the secondary side of the transformer in V.
- $P_{ASHP,operation}$ operation of the ASHP (ON/OFF).
- t_{ind} is the indoor temperature in °C.
- T_{tank} is the water tank temperature in °C.
- P_{net} is the net electrical demand in kW_e, and P_{dmd} is the total building electrical demand in kW_e.

5.4.1 Objective Function

The objective function (OF) was to ultimately maximise the generation of hydrogen, especially when the electricity supplied to ZEBHs derives from green electricity (wind turbine and 618 solar PV panels), which were connected to the IEEE-33 node test feeder. The optimisation model was indexed by sets (t), in which t_x refers to the set that represents 15-minute period per week ($1 \leq t_x \leq 672$). The mathematical formulation of (OF) at time t is given in Equation 5.23.

$$OF = \max \sum_{t=1}^H n_{H_2}(t) \Delta t \quad (5.23)$$

where,

- m_{H_2} is the hydrogen produced in mols/s,
- Δt is defined as the OF time steps over time horizon H , in this case, 15 minutes, and
- H is the time horizon, in this case, ($1 \leq t_x \leq 672$).

5.4.2 Constraint Conditions

The process of optimizing the OF with respect to the variables was completed with the presence of constraints on those variables. Their constraint conditions are given in the following subsections.

5.4.2.1 Hydrogen and Buffer Tank Constraints

The constraints of the hydrogen and buffer tank pressure are to keep the pressure across the tanks within a defined range as follows:

$$H_2TankPressure_{min} \leq P_{H_2Tank} \quad (5.24)$$

For the buffer tank:

$$BufferTankPressure_{min} \leq P_{BufferTank} \leq BufferTankPressure_{max} \quad (5.25)$$

- $BufferTankPressure_{min}$ is the minimum buffer tank pressure at 10 bars, and
- $BufferTankPressure_{max}$, depicts the maximum buffer tank pressure at 30 bars.
- $H_2TankPressure_{min}$ is defined as the minimum pressure at 360 bars,
- P_{H_2Tank} denotes hydrogen tank pressure in bars,
- $P_{Buffer,Tank}$ is the actual buffer tank pressure in bars,

5.4.2.2 ZEBHs Water Tank Constraints

The water tanks temperature (t_{tank}) constraints should be within the following range:

$$t_{tank,min}(t) \leq t_{tank}(t) \leq t_{tank,max}(t) \quad (5.26)$$

Based on the reference [167], the limits for water tank temperatures are:

- $t_{tank,min}$ is the minimum water tank temperature in °C, is 30°C, while
- $t_{tank,max}$ is the maximum water tank temperature in °C. Here, 70°C.

5.4.2.3 Indoor Temperature Constraints

The operational constraints for the indoor temperature(t_{ind}) include the maximum and minimum temperatures. They are given by:

$$t_{ind,min}(t) \leq t_{ind}(t) \leq t_{ind,max}(t) \quad (5.27)$$

Based on the UK CIBSE Knowledge Series-Comfort [168], the limits for indoor temperatures are:

- $t_{ind,min}$, the minimum indoor temperature is 17°C, while
- $t_{ind,max}$, the maximum indoor temperature is 25°C.

5.4.2.4 ASHP ON Mode Constraint

The ASHPs should be limited to operated only when the following conditions are met:

$$\begin{aligned} P_{H_2Tank} &\leq H_2TankPressure_{min}(t) \\ t_{tank}(t) &\leq t_{tank,min}(t) \\ t_{ind}(t) &\leq t_{ind,min}(t) \end{aligned} \quad (5.28)$$

5.4.2.5 ASHP OFF Mode Constraint

The ASHPs should be switched off when following conditions are met:

$$\begin{aligned} H_2TankPressure_{min}(t) &\leq P_{H_2Tank} \\ t_{tank,min}(t) &\leq t_{tank}(t) \\ t_{ind,min}(t) &\leq t_{ind}(t) \end{aligned} \quad (5.29)$$

5.5 INTERFACE AND COUPLING METHOD

Similar to the method elaborated in **Chapter 4**, the coupling of EnergyPlus and MATLAB/Simulink platforms had been crucial in this study to represent the model. Figure 5-12 illustrates the ICES-H₂ model integrated the software packages via BCVTB interface.

The Simulink model controller is identical to the controller portrayed in Chapter 4. However, for this particular analysis, the pressure of the hydrogen storage tank was embedded into Simulink function from the MATLAB Code.

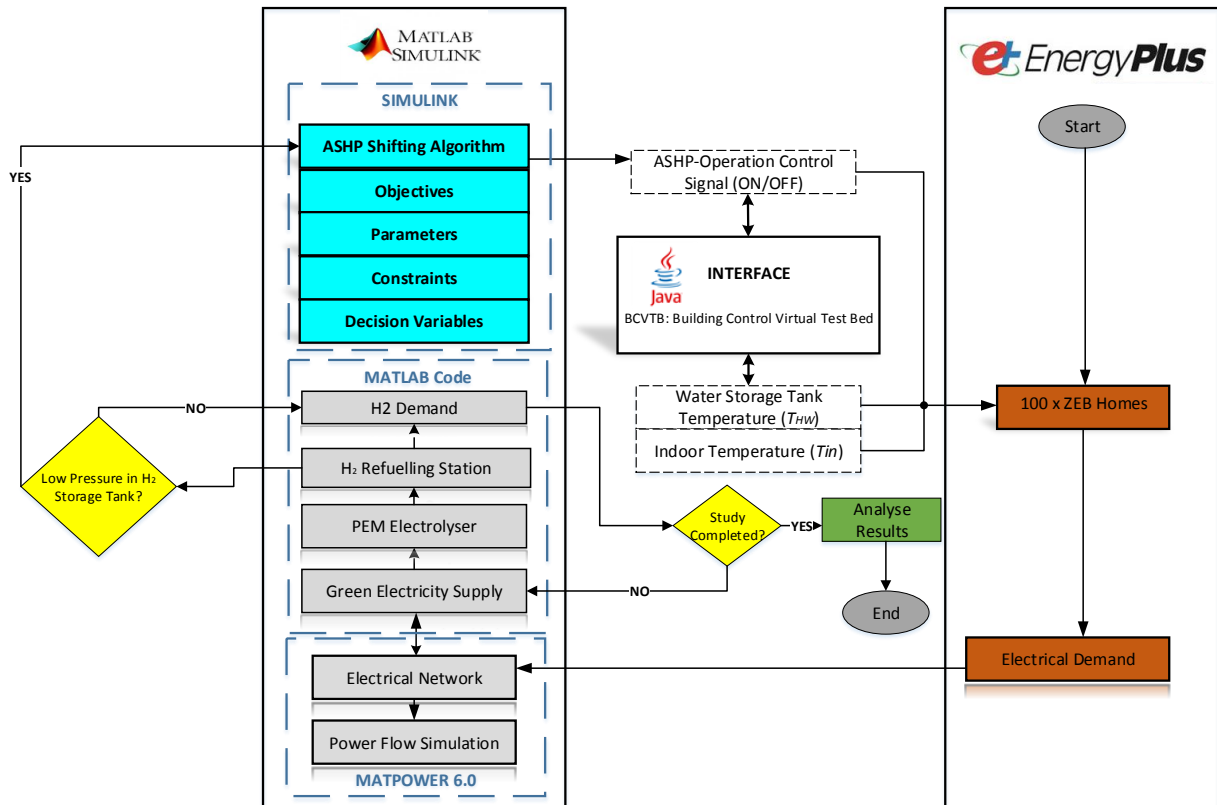


Figure 5-12: ICES-H₂ framework

The above figure defines the interface and coupled simulations as follows:

1. The 100 ZEBHs are first simulated in EnergyPlus
2. MATLAB accepts the building electrical consumption from the BCVTB to carry out network power flow and hydrogen system simulations.
3. The green electricity (wind turbine and solar PV panels) generated supplies the PEM electrolyser, and if any excess, is sent back to the electrical network as exported electricity
4. Once the hydrogen produced is available in the refuelling station to meet the H₂ demand, the H₂ tank pressure is then monitored

5. If H₂ tank pressure is below the limit, the ASHPs shifting algorithm sends ASHP ON/OFF-time control signals to EnergyPlus via Simulink block upon pressure drop hitting below the limit in the hydrogen storage tank.
6. EnergyPlus transmits the building water tank models and indoor temperatures to the BCVTB interface, and then, receives signals to control ASHP functionality.
7. Now, the optimisation model monitors start considering all variables and constraints.
8. The simulation continues for a period of 1-week until it ends.

A 15-minute time frequency was applied, in which the total configured simulation time was in this case 604800 seconds. Figure 5-13 illustrates the interface model for the coupled simulation.

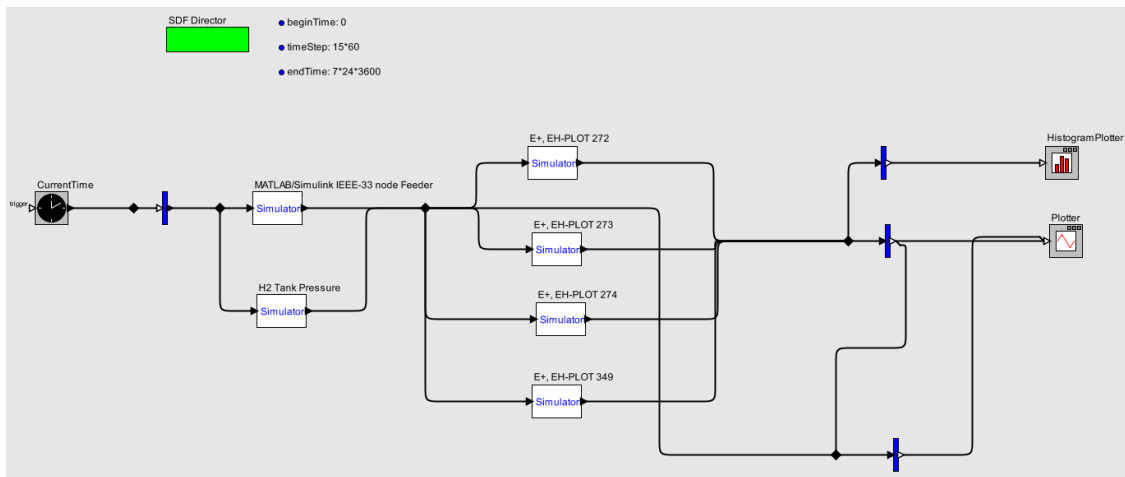


Figure 5-13: ICES-H₂ system model for coupled simulation in BCVTB interface

The XML file configuration had been arranged at each EnergyPlus model for data exchange, as portrayed in Figure 5-14. The parameters seem identical to the parameters depicted in **Chapter 4**. As for this analysis, the ASHPs control signal element referred to the hydrogen tank pressure instead of network voltage variation.

```

1 <?xml version="1.0" encoding="ISO-8859-1" ?>
2 <!DOCTYPE BCVTB-variables SYSTEM "variables.dtd">
3 <BCVTB-variables>
4 <!-- The next element receive the water tanks temperature from E+ to MATLAB/Simulink -->
5 <variable source="EnergyPlus">
6 <EnergyPlus name="AUX HW LOOP HP WATER HEATER" type="Water Heater Tank Temperature"/>
7 </variable>
8 <!-- The next element receive the indoor temperature from E+ to MATLAB/Simulink-->
9 <variable source="EnergyPlus">
10 <EnergyPlus name="Whole Building" type="Zone Mean Air Temperature"/>
11 </variable>
12 <!-- The next element send the ASHP operation control signal from MATLAB/Simulink to E+ -->
13 <variable source="Ptolemy">
14 <EnergyPlus schedule="BCVTB-SP-TH"/>
15 </variable>
16 <!-- The next element receive the schedule value as an output from E+ from MATLAB/Simulink-->
17 <variable source="EnergyPlus">
18 <EnergyPlus name="Whole Building" type="Facility Total Purchased Electric Power"/>
19 </variable>
20 </BCVTB-variables>

```

Figure 5-14: ICES-H₂ XML file script

5.6 SCENARIOS

In order to demonstrate the effectiveness of the proposed model, two scenarios are presented:

- **Scenario 1- Continuous Heating Strategy:**
 - In this strategy, the ZEBHs heating temperature was set to be constant at 19°C for the entire building, except for the living room where the temperature was set at 21°C.
- **Scenario 2- ASHP Load Shifting Algorithm:**
 - This strategy is based maximising the hydrogen production, as presented by the optimisation model that was built by incorporating an ASHP load shifting method, upon pressure drops below the limit in the hydrogen tank (360bars).

5.7 RESULTS AND ANALYSIS

5.7.1 Green Electricity Generation

Figure 5-15 illustrates the models output power of wind turbine and solar PV systems including wind speed and solar radiation over a winter week. As previously mentioned, the models employed 15-minute wind speed and solar resource data retrieved from Levenmouth from 1st until 7th January 2017, which served as wind and solar resource input data for wind and solar power generation [184].

The wind speed ranged from 3m/s to 9m/s with a maximum peak wind power generation of 612kW_e. When the wind speed is less than the wind turbine cut-in speed (3 m/s), there is no wind power generated.

The measured solar irradiance on horizontal surface (W/m²) functioned as input data for the solar PV system model. The maximum solar radiation was recorded on Friday, 5th of January, with a peak value of 180W/m². It can be noted that day, the maximum power was generated by the solar PV system. During this timeframe, the results depicts that the solar radiation was high and low wind speeds occurred (less than 3m/s).

The variation of electrical power produced by the solar and wind produced minimal peak 180kW_e for the wind turbine and 25kW_e for the solar PV system. The maximal peak value is during the week of January (1st to 7th) was 70kW_e for the solar PV system and 575kW_e for the wind turbine.

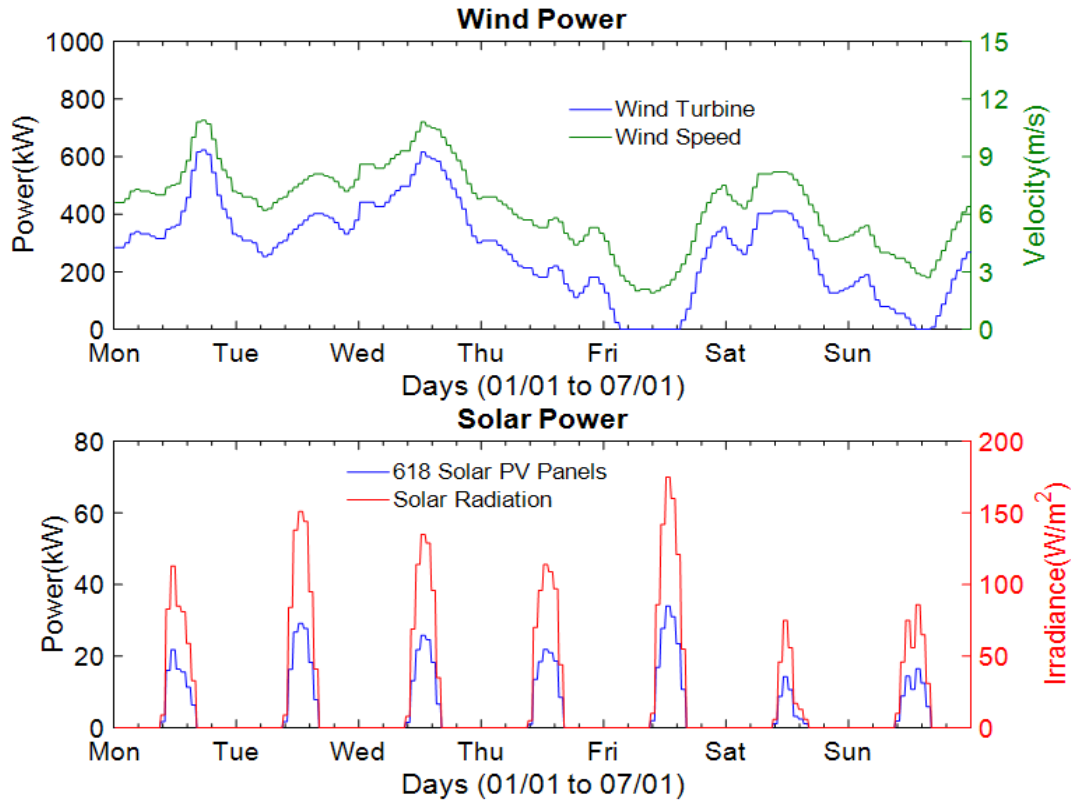


Figure 5-15: Wind turbine and solar PV system electricity generated during a winter (top) and a summer week (bottom)

5.7.2 Scenario 1

The first scenario evaluated the performances of ZEBHs, its technologies, and the operating mode of hydrogen energy simulation system as the base case scenario. Figure 5-16 shows that the water tank temperatures of the buildings were maintained at an average temperature of 50-55°C throughout the simulation period. The ASHP thermal power was approximately 2.8kW_{th} for each home. Meanwhile, the indoor temperatures ranged between 20 and 22°C for each home, except for EH-Plot 349 ZEBHs, which recorded a drop in the temperature up to 19°C. The ASHP electrical power appeared to vary for every home based on space heating and DHW demand aspects. Thus, one can say that the ASHPs operation was higher in the EH-Plot 273 ZEBHs. Higher net electrical consumption was also observed for EH-Plot 272 ZEBHs, mainly due to high usage of electrical appliances.

Based on the outcomes obtained from the hydrogen system (Figure 5-17), the green electricity output supplies served as priority in catering to ZEBHs load demand, and subsequently, it supplied the available electricity to PEM electrolyser to generate hydrogen. The model outcomes displayed that upon insufficient green electricity to satisfy ZEBHs load demand, electricity was imported from the grid. However, when there was excess of electricity generated by the ZEBHs solar PV/T panels and wind-solar PV system, this was exported to the grid.

The PEM electrolyser was modelled with a maximum power capacity of 60kW_e, and hence, any excess of electricity from the wind turbine and solar PV system that was not required to supply the electrolyser it was exported to the grid. The cell efficiency of the electrolyser was 100% whenever it operated to generate hydrogen (see Figure 5-18). Such efficiency (100%) is comparable to other studies depicted in the literature that reported values exceeding 95% [198]. The cell maximum voltage and current (I-V) were 1.5V and 200A. Based on prior studies, typically, the PEM electrolyser cell I-V should range as follows; 1.5 to 2.30V and 200 to 350A, respectively [96].

The hydrogen production process started once the DC source from rectifier was connected to the anode and cathode plate of the PEM electrolyser. The values of parameter such as voltage, current and power of the electrolyser while starting to operate can be seen in Figure 5-19. It was shown that at the electrolyser level the voltage and current for electrolyser were 1.55V and about 200A respectively.

It was observed that the voltage, current and efficiency decreased to almost zero due to low wind speed as a result of the produced power, while the solar PV system was the only source of energy for the electrolyser. The current from the electrolyser decreased as the voltage was dropped as a function of time and solar radiation as well as wind conditions.

The generated hydrogen was stored in the buffer tank (see Figure 5-19), and when the pressure of the buffer tank hit 30 bars, the compressor began its function to flow hydrogen into the hydrogen tank. The production of hydrogen varied greatly throughout the week. This shown how its production depends directly on the availability of the wind and solar radiation hydrogen energy system. As depicted in Figure 5-19 the accumulated H₂ in the tank is low on Friday due to the low production. From this figure, it appears that highest amount of daily hydrogen production is 1250 during Monday and Tuesday. The least hydrogen production ends with the value of 245mols, which has the lower wind density.

The accumulated hydrogen has a clear correlation with the pressure in the buffer and H₂ tanks. The results highlight that the pressure drops below 360 bars when there is H₂ demand. In addition, the compressor operation performance was depicted. The results show the amount of hydrogen that flows when it operates. The compressor was modelled as such does not need a constant operation but only when is required to supply between the buffer and H₂ tank.

The outcomes highlighted the total distance recorded by the FCEVs, the demand for hydrogen, and fuelling (see Figure 5-20). Pressure drop equivalent to or below 360 bars had been noted for almost every day (except on Monday) due to high fuel demand from vehicles. Figure 5-20 pointed out the total number of cars fuelled and non-fuelled over the period of a UK winter week. As for this scenario, the cars were not fuelled when the hydrogen tank pressure was 360 bars, thus leading to a total number of 250 fuelled cars and 72 non-fuelled.

24 x EH-Plot 272

24 x EH-Plot 273

25 x EH-Plot 274

27 x EH-Plot 349

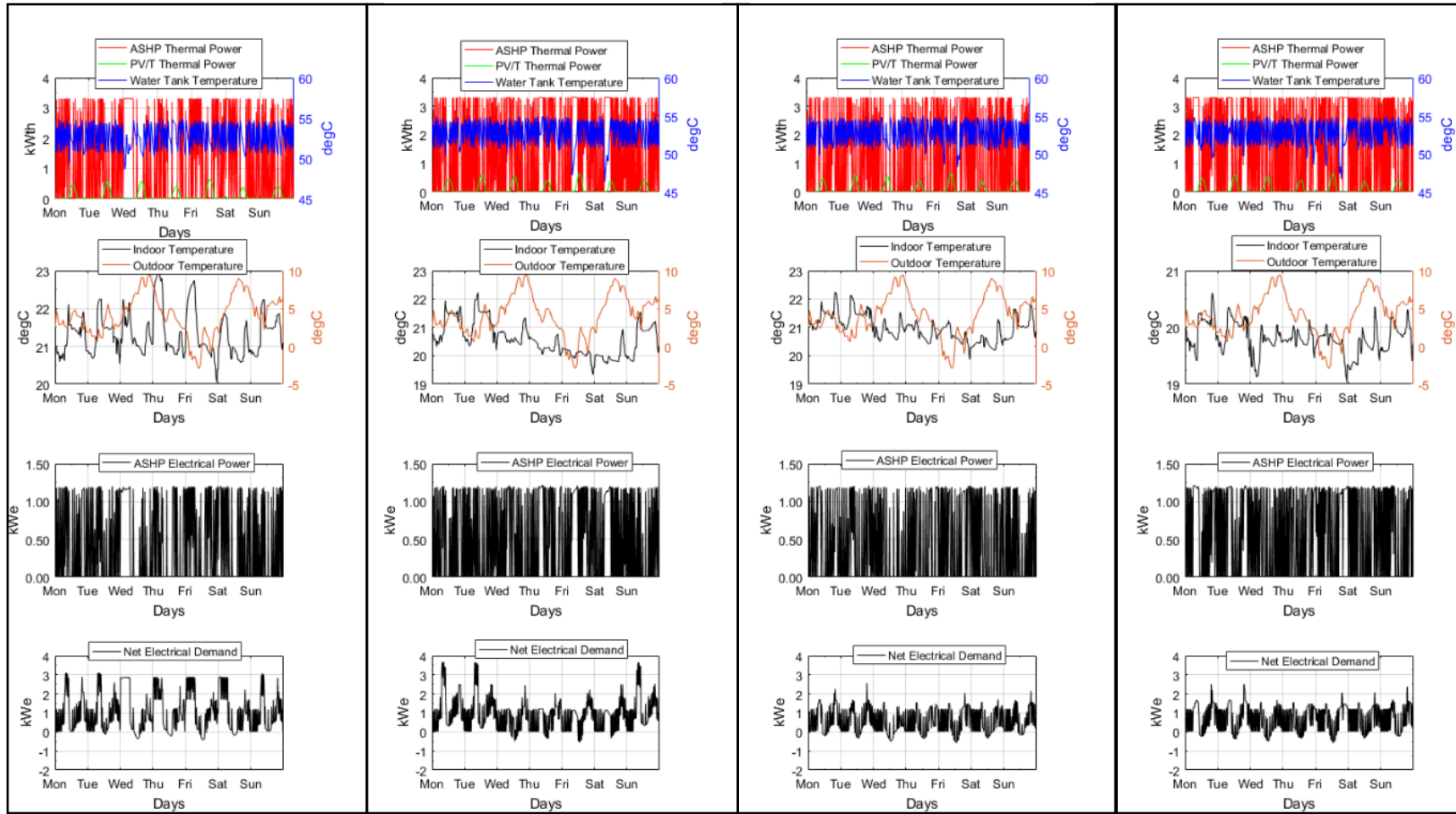


Figure 5-16: Scenario 1-Buildings connected in the test feeder. From top to bottom the water tank dynamics (water tank temperature, ASHP thermal power, PV/T thermal power), indoor and outdoor temperatures, ASHP electrical power and net electrical demand.

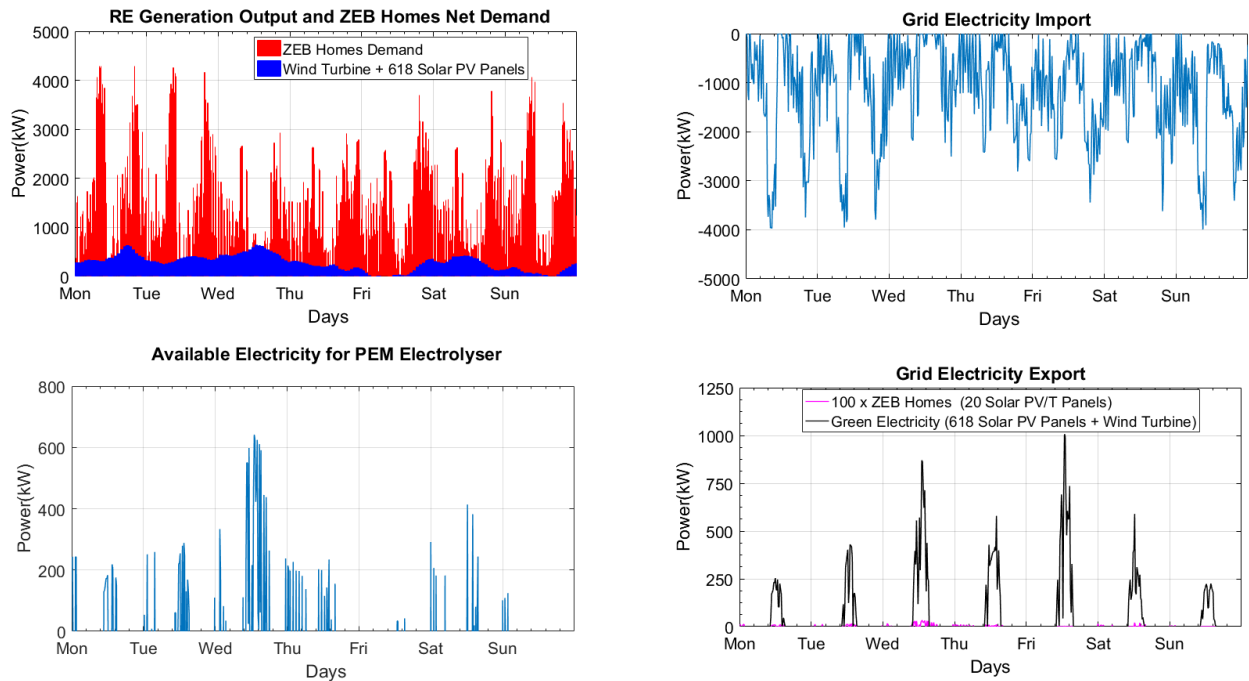


Figure 5-17: Scenario 1- RE generation output, ZEBHs demand, grid electricity import/export

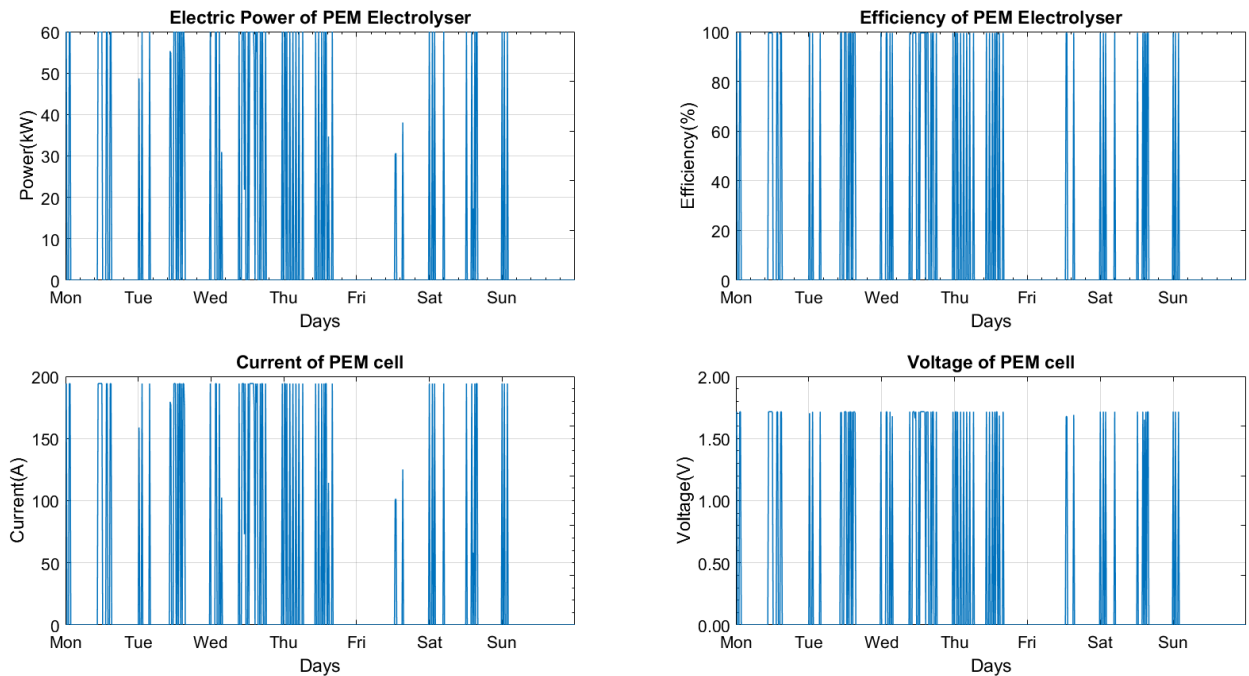


Figure 5-18: Scenario 1- PEM electrolyser power, efficiency current and voltage

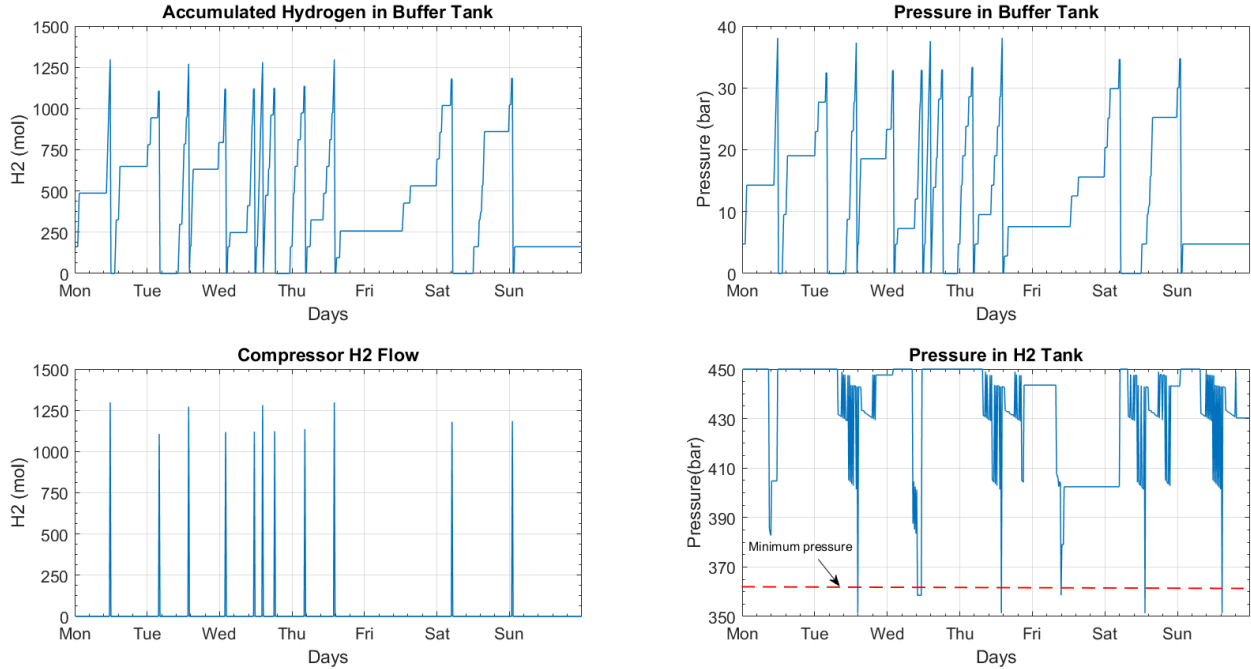


Figure 5-19: Scenario1- Buffer tanks accumulated hydrogen and pressure, compressor H₂ flow and H₂ tank pressure level

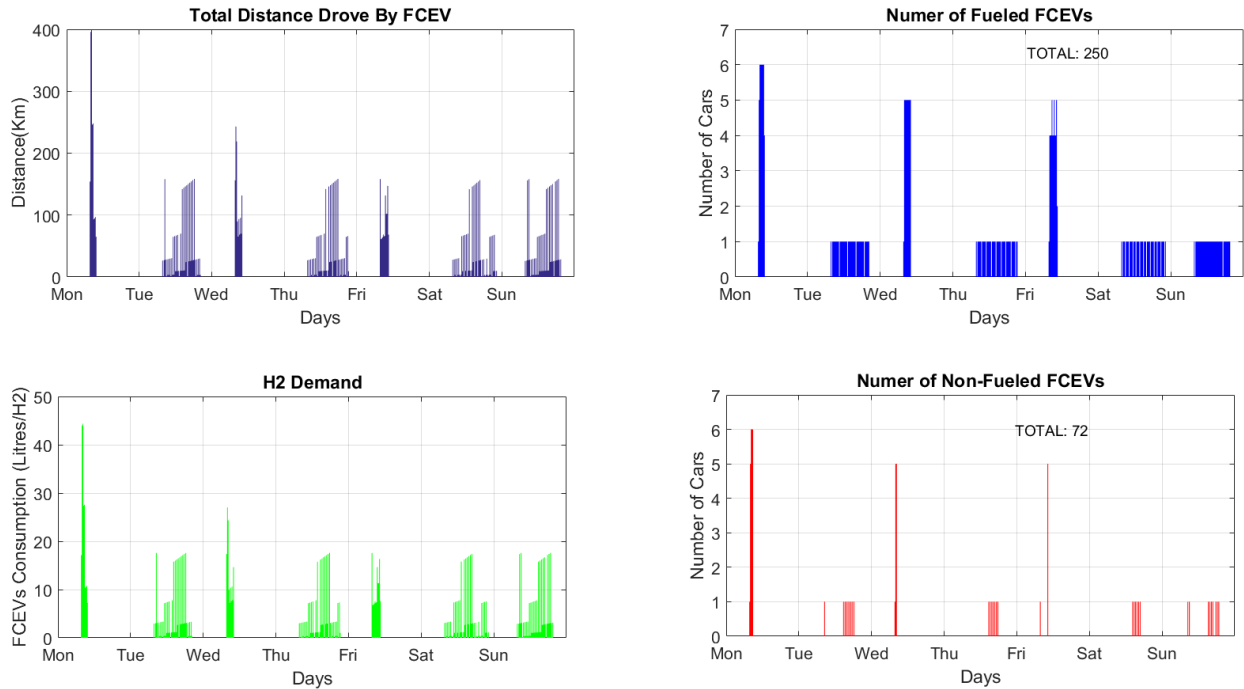


Figure 5-20: Scenario 1- FCEV's distance drove, consumption and fueled and non-fueled cars

5.7.3 Scenario 2

In this scenario, the performance of the ICES-H₂ system is evaluated for the ASHPs load shifting strategy. This strategy has been specifically carried out to check out the number of increased cars that can be fuelled when the H₂ production was maximised.

Figure 5-21 illustrates the ZEBHs simulation outcomes for scenario 2. The indoor temperatures appeared to be lower in this case due to the constrained ASHPs operation when the hydrogen tank pressure was equivalent or below 360 bars. This portrays a vivid picture regarding the dynamic water tank behaviour (thermal inertia). The indoor temperatures, as set on the constrain conditions, were retained between 17°C and 25°C throughout the analysis period.

The available electricity for PEM electrolyser hiked with decreased ZEBHs load demand, especially when high hydrogen fuel demand was noted (see Figure 5-23). Thus, this appeared to increase the operation of PEM electrolyser. It can be observed that the electrolyser is activated on Friday when there is excess of wind and solar power. The control ZEBHs ASHPs load profile causes the frequent switch ON and OFF, and hence, the increase on available green electricity. In contrast, in scenario 1 the electrolyser has a very low or no production of H₂ on the same day. In this case, the electrolyser operation increases, and as a result, the power, current, and voltage results on the worst day.

Figure 5-24 portrays increment of hydrogen that accumulated in the buffer tank. This had been observed particularly on a Sunday, 7th of January, where the buffer tank pressure stayed constant at approximately 29 bars for almost a whole day. The ZEBHs ASHP load shifting displayed an effective impact on the hydrogen tank pressure, which was retained above 360 bars.

The H₂ tank pressure level increase, is explained by the increase on intermittent operation of the PEM electrolyser during the ASHPs load shifting. Although the hydrogen consumed by the FCEVs causes the tank level to decrease, it was maintained above the limits.

The optimisation model therefore enables the increase on number of fuelled vehicles. Figure 5-25 illustrates the FCEV performance, in which the total number of fuelled cars increased to 284, while non-fuelled cars decreased to 38 cars.

These results indicate that the higher hydrogen amount and electrical energy production can be obtained by constraining the ZEBHs ASHPs for when there is low pressure in the H₂ tank, without compromising the occupant needs. The hydrogen produced can be used either as a fuel for transportation or if any excess, can be sold by storing to the hydrogen market.

24 × EH-Plot 272

24 × EH-Plot 273

25 × EH-Plot 274

27 × EH-Plot 349

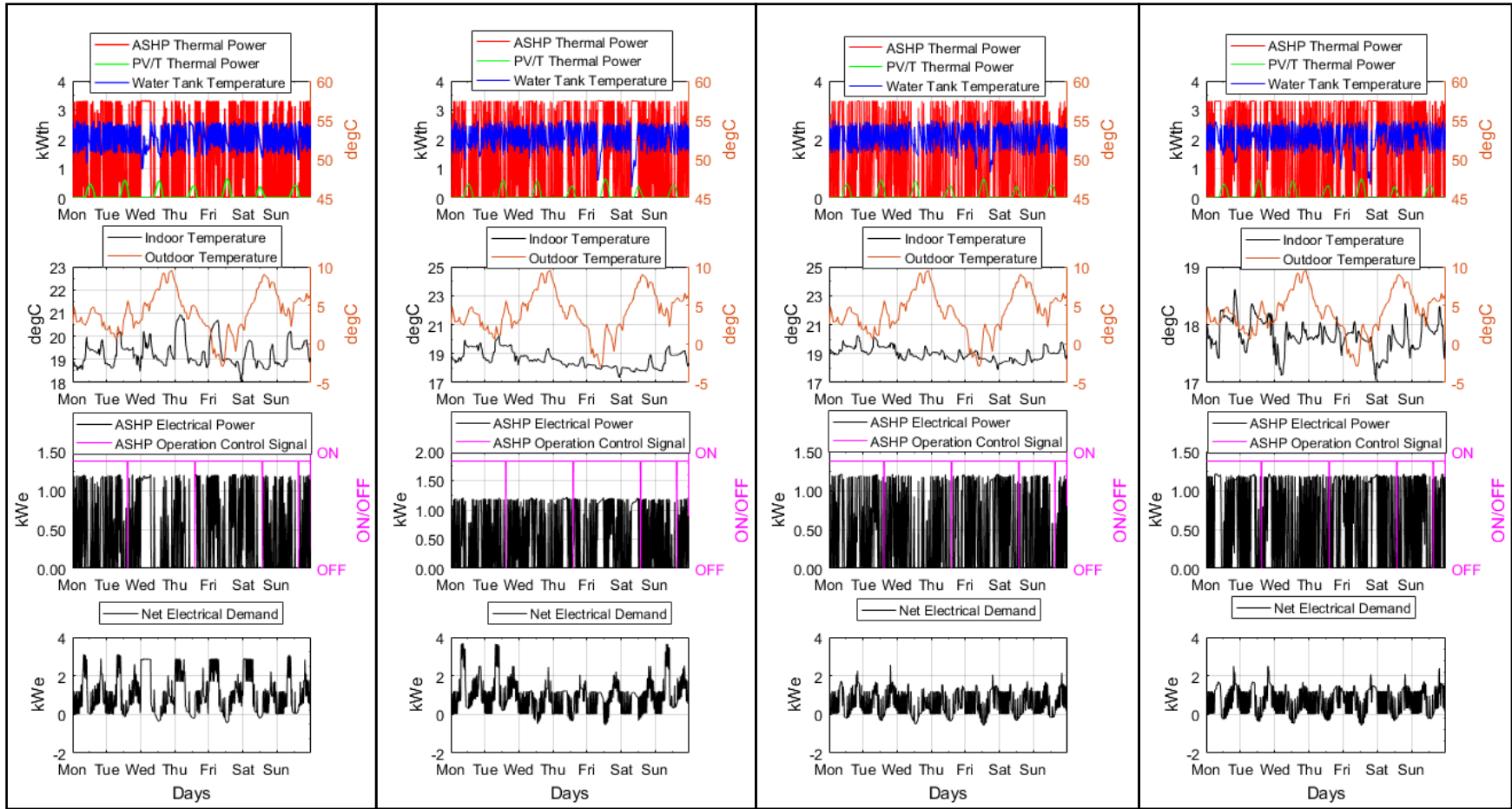


Figure 5-21: Scenario 2-Buildings connected in the test feeder. From top to bottom the water tank dynamics (water tank temperature, ASHP thermal power, PV/T thermal power), indoor and outdoor temperatures, ASHP electrical power and net electrical demand.

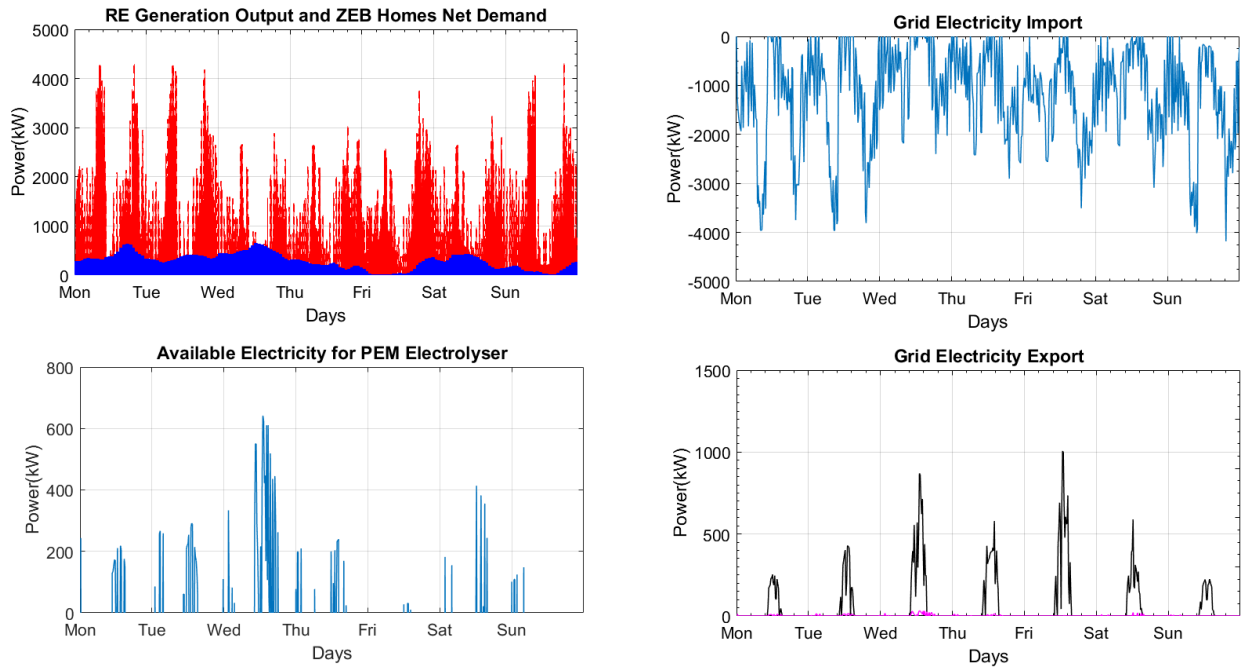


Figure 5-22: Scenario 2- RE generation output, ZEBHs demand, grid electricity import/export

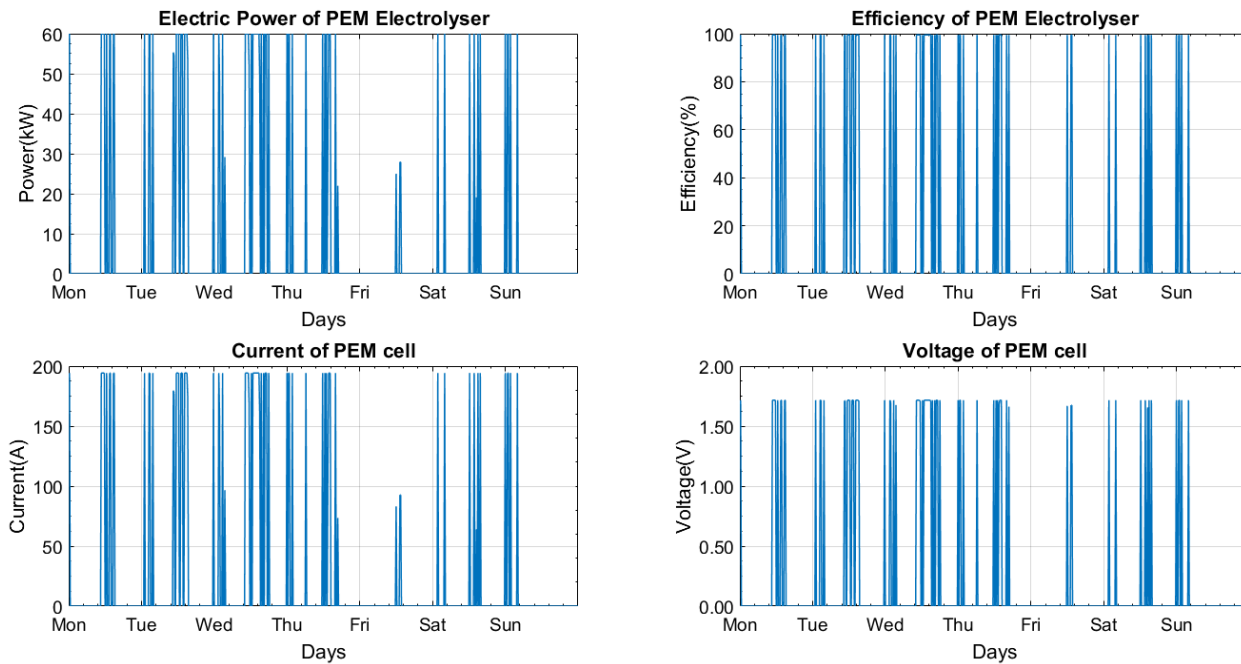


Figure 5-23: Scenario 2- PEM electrolyser power, efficiency current and voltage

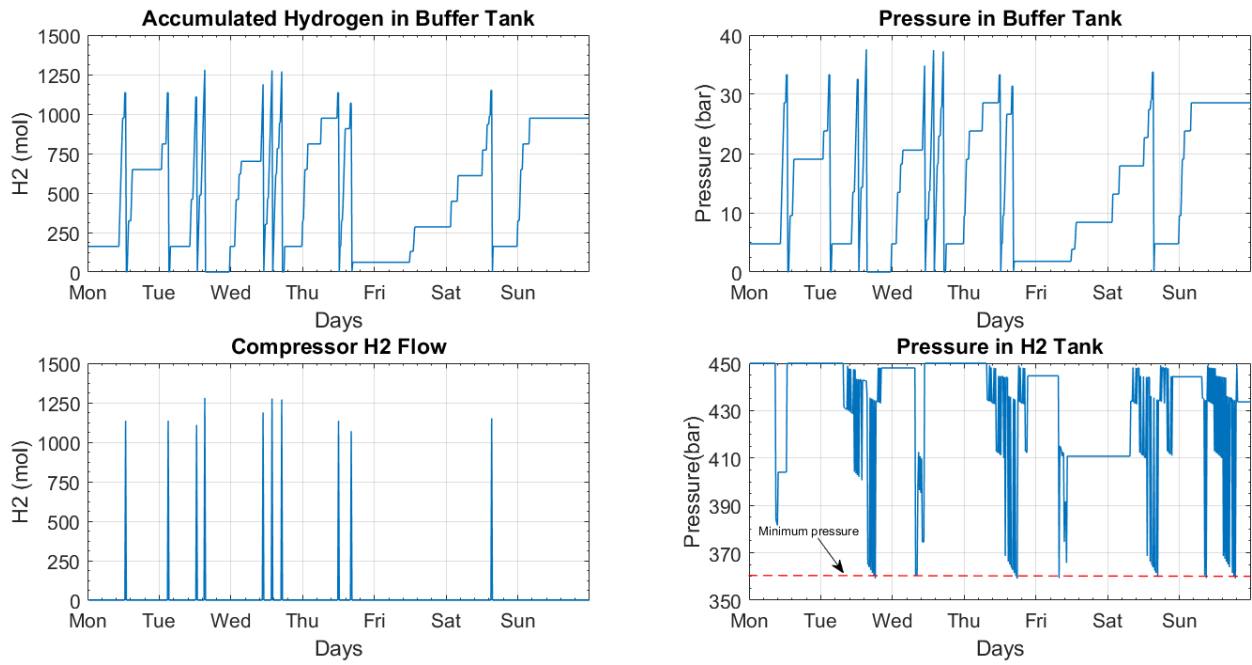


Figure 5-24: Scenario 2- Buffer tanks accumulated hydrogen and pressure, compressor H₂ flow and H₂ tank pressure level

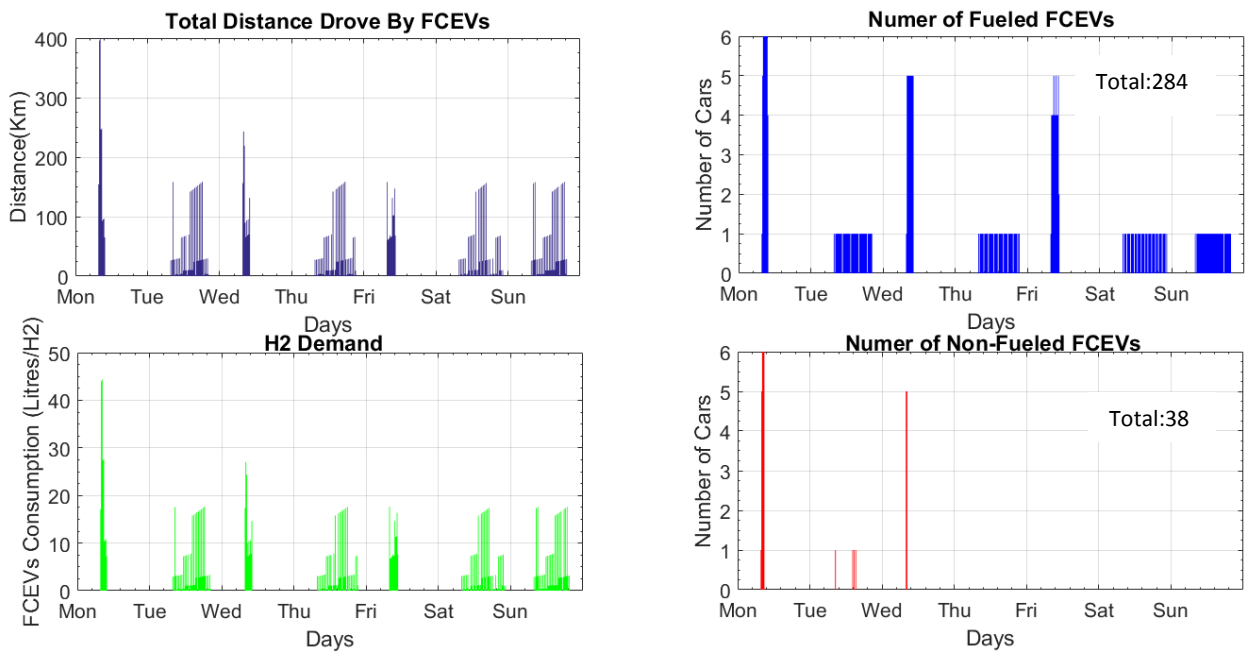


Figure 5-25: Scenario 2- FCEV's distance drove, consumption and fuelled and non-fuelled cars

5.7.4 Comparison of Results Under Different Scenarios

This section presents the comparison outcomes for hydrogen tank pressure, voltage network, total hydrogen generated, and FCEVs performance between scenarios 1 and 2.

Figure 5-26 illustrates the variation in pressure levels during winter week (672-time-steps). The optimal load control algorithm (scenario 2) had successfully controlled the pressure in hydrogen tank to always be equivalent to or above 360 bars.

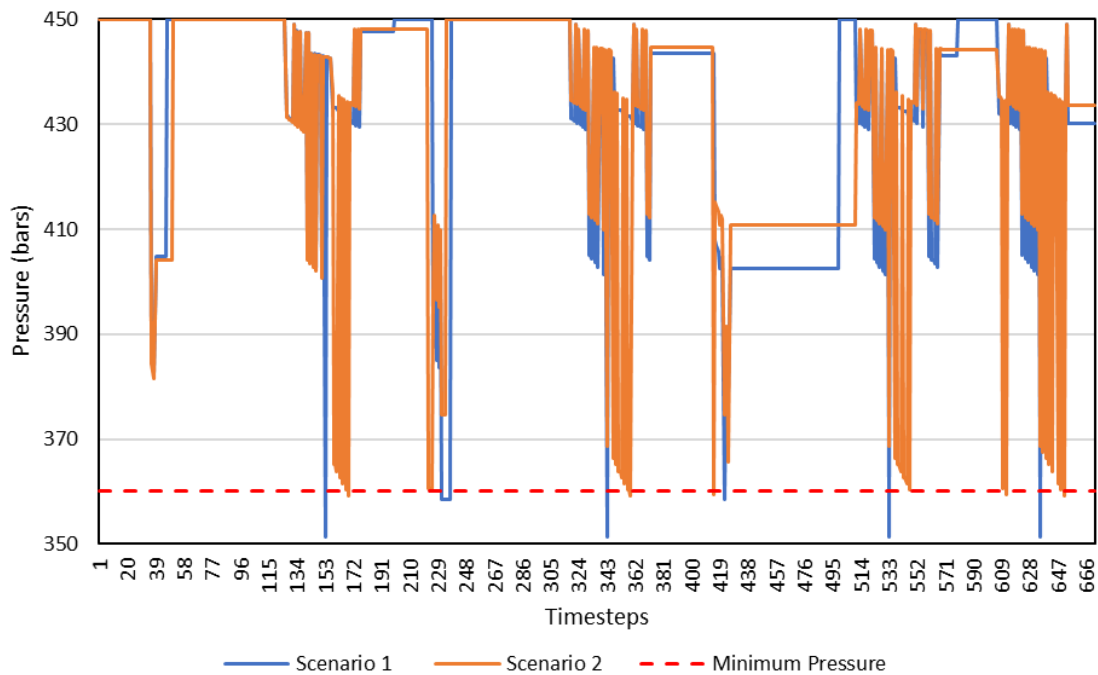


Figure 5-26: H₂ tank pressure levels from scenarios 1 and 2

On the other hand, Figure 5-27 portrayed that the IEEE 33-node test feeder did not exhibit significant variances between the two scenarios. A closer view to the network voltage variation was plotted (between 133 and 177 time-steps), and as displayed in the graph, when the ZEBHs ASHP operation control signal is OFF in scenario 2 from time-step 155 until 157 (30 minutes), the variation appeared to be minor, in comparison to that recorded for scenario 1. This concludes that in this case there is low evidence on the interaction between the hydrogen produced and electrical network voltage.

It only draws a slight deviation based on the two scenarios, which seemed to derive from the selected minimum pressure of the hydrogen tank. However, higher minimum hydrogen tank pressure setting (e.g.: 400 bars) could lead to higher pressure deviation, thus resulting in a dissimilar impact on the test feeder.

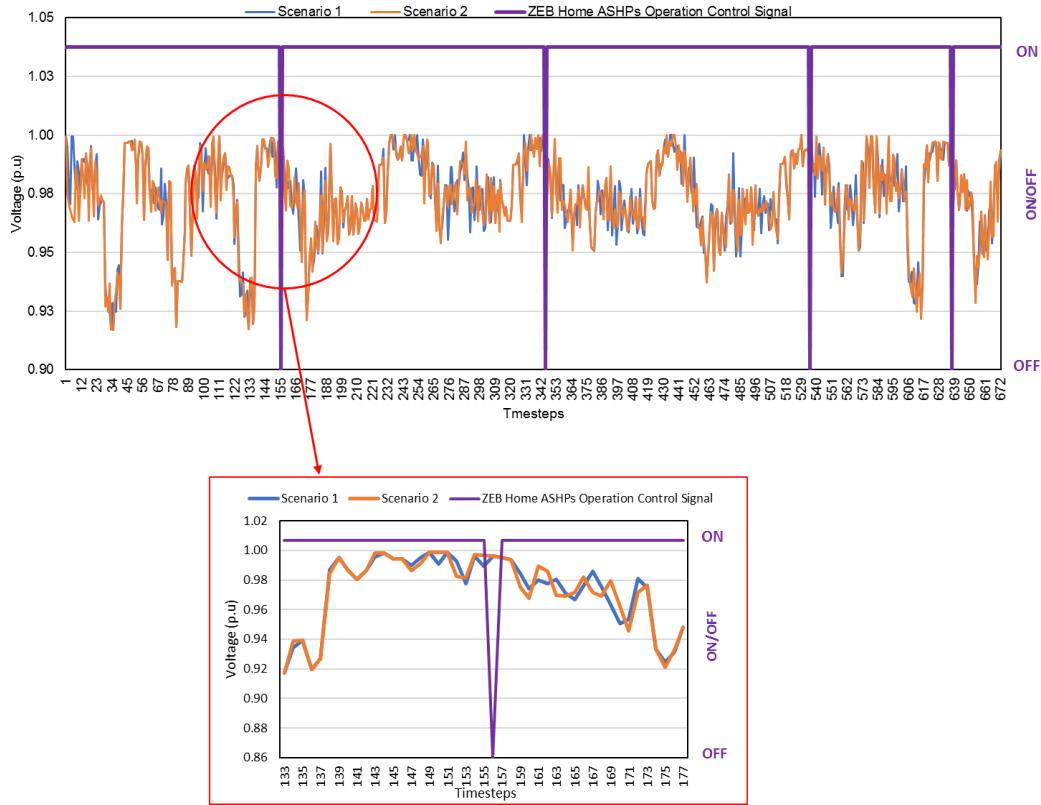


Figure 5-27: Comparison of IEEE 33-node test feeder voltage variations between scenarios 1 and 2

Figure 5-28 illustrates the total hydrogen that was generated during a winter week, as well as the total number of cars fuelled and non-fuelled for both scenarios. Therefore, scenario 2 increased the production of hydrogen during the tested winter week to 229 mols/week (1.73%). Subsequently, one can say that increment of 229 mols/week for hydrogen production led to an increase in the total number of fuelled cars by 34 FCEVs in a week.

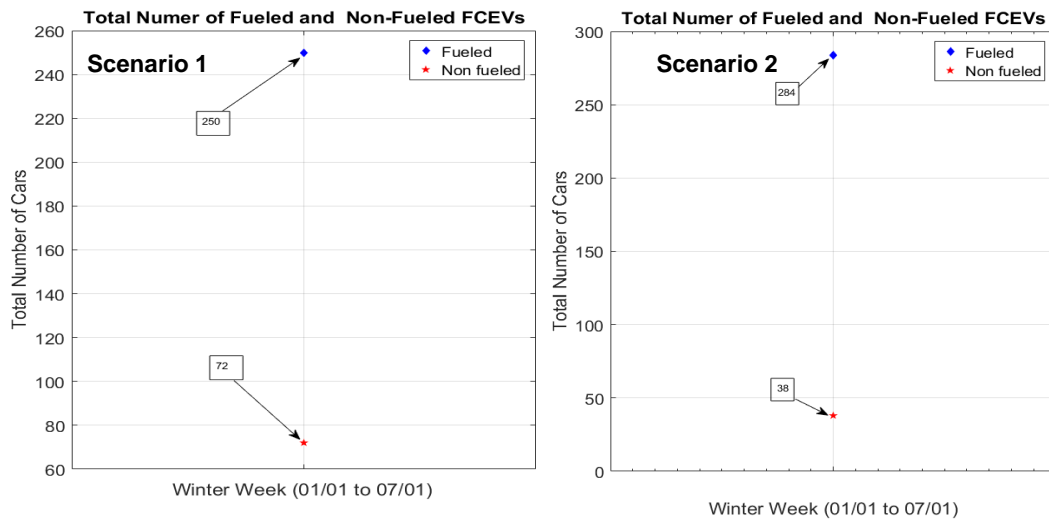


Figure 5-28: a) Total H₂ produced and b) FCEV's performance in scenarios 1 and 2

SUMMARY

This chapter presented the hydrogen energy storage system integrated with renewable generation to dispense hydrogen for FCEVs, LV electrical network, and ZEBHs. The system configuration had been based on a real system deployed in Scotland as part of its Levenmouth Community Energy Project. The power generated by the renewable sources had been applied by the ZEBHs and an electrolyser was installed to generate hydrogen, which was stored in a reservoir tank system to attend to the hydrogen demand for FCEVs. Each essential element of the system, inclusive of their interactions, were discussed in this chapter: renewable generation (wind and PV), ZEBHs, IEEE 33-node test feeder, PEM electrolyser, hydrogen storage tank and dispensing unit, as well as hydrogen demand for FCEVs.

In particular, this chapter looked into the ICES-H₂ model of the full system. The related simulations were carried out to examine the system performance based on two scenarios by incorporating ZEBHs load demand and actual weather data. The findings displayed that the weather aspect did substantially affected hydrogen generation and demand level, which in turn, influenced the pressure in reservoir tank.

The related model that was built based on MATLAB and EnergyPlus platforms, along with BCVTB interface, reflected the model employed for an integrated community energy system that embedded hydrogen refuelling. An optimisation technique (MILP) was incorporated to determine maximum hydrogen output. This approach seemed to have successfully decreased the number of non-fuelled FCEVs.

A comparison between both scenarios exhibited that the hydrogen component could be increased when a group of ZEBH ASHPs were controlled to limit their operation as soon as the hydrogen tank status turned critical (low pressure). The performance of PEM technology was efficient (100%), which reflected the sufficient electricity production component for hydrogen. Another comparison made between both operating modes of the refilling station showcased that although the hydrogen production increased when the ASHPs load shifting approach was applied, the electrical network voltage variation from each scenario was minimal.

The essential components of the refilling station were operated only using green electricity (wind and solar). The combined RE and grid-connected station is preferred to benefit from the RE supply and the high utilisation offered by the grid connection. The intermittency of wind and solar resources suggests that not all energy from renewable energy is captured by the refueler. As such, increasing the size of hydrogen storage tank may be an alternative solution.

CHAPTER 6- CONCLUSIONS AND FUTURE WORK

This chapter presents an outline of the research accomplished, the conclusion remarks and future work

6.1 CONCLUSIONS

Inside the context of zero energy bill homes, this research presented a means to evaluate the ZEBHs, their energy demand flexibility assessment, and optimal operation through the analysis of the buildings and energy in an integrated community. The literature review, presented in **Chapter 2-Literature Review**, covers all the fundamental theories to support the proposed integrated model and analysis.

Chapter 3- Energy Performance and Techno-Economic Analysis of Zero Energy Bill Homes presented a building modelling approach incorporating a SPVTAH in ZEBHs. The modelling offered a means to evaluate energy performance in order to identify the parameters that influenced the energy demand and the calibration method. The modelling and the simulation results were validated by comparing the model's outputs with the data obtained through measurement. Thus, through the integration of the measured data, it was possible to establish a reference for the energy performance of the ZEBHs. However, the calibration must be conducted over an annual (monthly or weekly) cycle using hourly energy data. On the contrary, the model results could present considerable differences. The calibration technique can be improved using other approaches, such as Monte –Carlo simulations. In addition, it is worth emphasizing the importance of economic analysis and the consideration of prices and tariffs. These factors have a significant impact on the viability of the ZEBHs, especially when there is an increase in space heat demand. In this context, mention is made of the dependence on the concept of zero energy bill being dependent on UK government subsidies.

Chapter 4- Analysis and Quantification of Energy Demand Flexibility on LV Electrical Distribution Networks presented the integration between the buildings and the electrical network model with the ability to analyze the interactions between specific dwellings and the low voltage network. The models used were simulated to evaluate the performance of the semi-detached dwellings and the heating system, taking into account the occupants' activities, the internal heat generation, the thermal properties of the building envelope, and the environment. The simulation results showed that the number of buildings connected to the grid, and the high load consumption on the feeder caused voltage problems. Although the control capacity of the heat pumps installed in the building clusters is beneficial for the IEEE 33-node test feeder, this action has the consequence of significant variations in temperature due to the need to maintain thermal demand. Due to the simulation results' precision and flexibility, the proposed approach is suitable for the systematic assessment of energy policies related to buildings and distribution network restrictions.

6.1.1 Integrated Community Energy Systems with Hydrogen Storage

Chapter 5- **Integrated Community Energy Systems with Hydrogen Storage** presented the integration of a hydrogen storage system with renewable generation to meet FCEVs demands, supporting the LV electrical network and ZEBHs. The simulations results, which included ZEBHs load demand and actual weather data, demonstrated that the weather significantly impacted hydrogen production. However, the implementation of an optimization algorithm (MILP) shows that the energy flexibility in ZEBHs can maximize H₂ production in communities. Despite the contribution of renewable generation in the system, the refueler can not absorb all the energy produced due to the intermittency of these sources.

Finally, the defined objectives of this research were achieved. The model and analyses presented to evaluate buildings and energy in a community could provide enough data to discuss the potential and limitations of ZEBHs within a community with an integrated energy system. It can be seen that although the concept of a zero-energy bill depends on government subsidies, the advantages of implementing this type of structure in the community are clear. Also, several points were raised to serve as themes for future work, which will be exposed in the following section.

6.2 FUTURE WORK

- The building approach to modelling the ZEBHs with EnergyPlus may be enhanced by including:
 - Stochastic occupant behaviour programming techniques that can be utilised to account for more uncertainty in load demand.
 - Whilst modelling is important to predict and provide a baseline for energy performance evaluation, monitoring the dwellings could be essential to develop comprehension pertaining to the parameters that influence heating demand, particularly occupancy. Hence, other calibration techniques using certain approaches, such as Monte-Carlo simulations to match simulation and monitoring data results could be implemented.
- The ICES-H₂ models used for the RE energy system, hydrogen, and distribution network may be extended by:
 - The inclusion of district heating/cooling, absorption chillers, and tri-generation for schemes with significant space heating and/or cooling demand in ZEBHs.
 - An extension of the model to include biomass conversion technologies, such as biomass boilers, with integration of heat and power units.
 - The model could be used to determine the use of sustainable local resources in meeting the set UK energy emissions reduction targets.

- Develop an optimal ASHP load control algorithm that includes voltage network constraints.
- Present different case scenarios based on varied seasons, such as the summer period.
- Future work could include lowering the 15-minute resolution to 1-minute resolution in order to capture variation of parameters, such as power quality at the busbar where the refuelling station is connected to green technologies (wind and solar).
- Another technical improvement that could be further investigated is simulating the generation of the excess heat resulting from chemical reactions of the PEM electrolyser for any possible utilisation on supplying heat to ZEBHs.
- Further work may include economic analysis to provide operational insight through tight coupling of technical models of physical processes and economic models. This allows the dynamic relationships of the system to be captured and analysed so as to provide short/medium term analytical capability to further support the system design, the planning, and the financing aspects.

REFERENCES

- [1] UK Committee on Climate Change, ‘Carbon budgets: how we monitor emissions targets - Committee on Climate Change’. [Online]. Available: <https://www.theccc.org.uk/tackling-climate-change/reducing-carbon-emissions/carbon-budgets-and-targets/>. [Accessed: 05-Jun-2018].
- [2] Y. Al Harbi, N. N. Eugenio, and S. Al Zahrani, ‘Photovoltaic-Thermal Solar Energy Experiment in Saudi Arabia’, *Renewable Energy*, vol. 15, pp. 483–486, 1998.
- [3] Department for Business Energy and Industrial Strategy, ‘2018 UK Greenhouse Gas Emissions, Provisional Figures’, London, 2019.
- [4] Department for Business Energy and Industrial Strategy, ‘Digest of United Kingdom Energy Statistics 2018’, London, 2018.
- [5] United Nations Framework Convention on Climate Change, ‘Global action on climate change - Committee on Climate Change’. [Online]. Available: <https://www.theccc.org.uk/tackling-climate-change/the-legal-landscape/global-action-on-climate-change/>. [Accessed: 05-Jun-2017].
- [6] M. Qadrdan, M. Abeysekera, J. Wu, N. Jenkins, and B. Winter, ‘The Operation of Gas Networks in the Presence of a Large Capacity of Wind Generation’, in *Springer Briefs in Energy*, 74th ed., New York: Springer, 2020, pp. 23–36.
- [7] G. Rentier, H. Lelieveldt, and G. J. Kramer, ‘Varieties of Coal-Fired Power Phase-Out Across Europe’, *Energy Policy*, vol. 132, pp. 620–632, Sep. 2019.
- [8] Department of Energy and Change of Climate, ‘2011 UK Greenhouse Gas Emissions, Final Figures’, 2013.
- [9] J. Prime, E. Wilkes, and S. Khan, ‘Energy Consumption in the UK’, London, 2012.
- [10] Her Majesty Government, ‘Climate Change Act 2008’, *UK Government Legislation*, 2008. [Online]. Available: <http://www.legislation.gov.uk/ukpga/2008/27/contents>. [Accessed: 30-May-2015].
- [11] Energy Performance of Buildings Directive, ‘Implementing the Energy Performance of Building Directive’, Porto, 2013.
- [12] ‘Concerted Action | Energy Performance of Buildings Directive’. [Online]. Available: <http://www.epbd-ca.eu/>. [Accessed: 28-May-2015].
- [13] K. Voss, E. Musall, I. Sartori, and R. Lollini, ‘Nearly Zero, Net Zero, and Plus Energy Buildings – Theory, Terminology, Tools, and Examples’, in *Transition to Renewable Energy Systems*, 1st ed., P. D. Stolten and P. D. -Ing. V. Scherer, Eds. Belgium: Wiley, 2013, pp. 875–889.
- [14] P. Woods, ‘Implementation of the EPBD in England and Wales , Scotland and Northern Ireland Status in November 2010’, 2010.
- [15] Department for Communities and Local Generation, ‘Next steps to zero carbon homes – Allowable Solutions - Government response and summary of responses to the consultation’, 2014.
- [16] ‘Building profiles | Zero Carbon Hub’. [Online]. Available: <http://www.zerocarbonhub.org/building-profiles>. [Accessed: 16-Mar-2015].

- [17] Zero Carbon Hub, ‘Zero Carbon Homes and Nearly Zero Energy Buildings UK Building Regulations and EU Directives’, 2014. [Online]. Available: www.zerocarbonhub.org.
- [18] Zero Carbon Hub, ‘Carbon Compliance - Setting an Appropriate Limit for Zero Carbon New Homes - Findings & Recommendations’, 2011.
- [19] X. Li, J. Patterson, E. Coma Bassas, and P. Jones, ‘A Feasibility Study to Evaluate the Potential Replication of an Energy Positive House in the UK’, *IOP Conference Series: Earth and Environmental Science*, vol. 329, no. 1, p. 012049, Oct. 2019.
- [20] Intergovernmental Panel on Climate Change, ‘Task Group on Data Support for Climate Change Assessments (TG-Data)’, *IPCC*, 2019. [Online]. Available: <https://www.ipcc.ch/data/>. [Accessed: 24-Jul-2019].
- [21] Digest of UK Energy and Statistics, ‘UK Energy in Brief 2018’, 2018.
- [22] Department of Trade and Industry, ‘The Electricity Safety, Quality and Continuity Regulations 2002’, London, 2002.
- [23] N. Jenkins, J. Ekanayake, G. Strbac, B. M. Weedy, and B. J. Cory, *Electric Power Systems*, 5th ed. London: Wiley, 2012.
- [24] M. Ndawula, S. Djokic, and I. Hernando-Gil, ‘Reliability Enhancement in Power Networks under Uncertainty from Distributed Energy Resources’, *Energies*, vol. 12, no. 3, p. 531, Feb. 2019.
- [25] R. Atia, N. Yamada, R. Atia, and N. Yamada, ‘Distributed Renewable Generation and Storage System Sizing Based on Smart Dispatch of Microgrids’, *Energies*, vol. 9, no. 3, p. 176, Mar. 2016.
- [26] M. Rowe, S. Haben, C. Singleton, W. Holderbaum, and B. Potter, ‘A Peak Reduction Scheduling Algorithm For Storage Devices On The Low Voltage Network’, *IEEE Transactions on Smart Grid*, vol. 5, no. 4, 2014.
- [27] M. A. Tamayol, H. R. Abbasi, and S. Salmanipour, ‘Distributed Generation Optimization Strategy Based on Random Determination of Electric Vehicle Power’, in *Springer*, Singapore: Springer, Singapore, 2019, pp. 655–665.
- [28] M. Qadrdan, N. Jenkins, and J. Wu, ‘Smart Grid and Energy Storage’, in *McEvoy’s Handbook of Photovoltaics*, Academic Press, 2018, pp. 915–928.
- [29] A. Ehsan and Q. Yang, ‘Optimal Integration and Planning of Renewable Distributed Generation in the Power Distribution Networks: A Review of Analytical Techniques’, *Applied Energy*, vol. 210, pp. 44–59, Jan. 2018.
- [30] E. O’Dwyer, I. Pan, S. Acha, and N. Shah, ‘Smart Energy Systems for Sustainable Smart Cities: Current Developments, Trends and Future Directions’, *Applied Energy*, vol. 237, pp. 581–597, Mar. 2019.
- [31] E. Liapopoulou and T. Theodosiou, ‘Energy Performance Analysis and Low Carbon Retrofit Solutions for Residential Buildings’, *IOP Conference Series: Earth and Environmental Science*, vol. 410, no. 1, p. 012026, Jan. 2020.
- [32] Department of Energy and Climate Change, ‘The Energy Efficiency Strategy: The Energy Efficiency Opportunity in the UK’, London, 2012.
- [33] P. Ekins, N. Strachan, W. Usher, J. Skea, and G. Anandarahjah, ‘The UK Energy System in 2050: Comparing Low-Carbon, Resilient Scenarios’, London, 2013.

- [34] S. Friggens, 'How much CO2 Pollution do Solar Panels Save?', *ethex*, 2013. [Online]. Available: https://www.ethex.org.uk/how-much-co2-pollution-do-solar-panels-save_479.html. [Accessed: 05-Oct-2017].
- [35] S. Kanteh Sakiliba, A. Sani Hassan, J. Wu, E. Saja Sanneh, and S. Ademi, 'Assessment of Stand-Alone Residential Solar Photovoltaic Application in Sub-Saharan Africa: A Case Study of Gambia', *Journal of Renewable Energy*, vol. 2015, pp. 1–10, Nov. 2015.
- [36] R. A. Walling, R. Saint, R. C. Dugan, J. Burke, and L. A. Kojovic, 'Summary of Distributed Resources Impact on Power Delivery Systems', *IEEE Transactions on Power Delivery*, vol. 23, no. 3, pp. 1636–1644, Jul. 2008.
- [37] F. Avelino, R. Bosman, and N. Frantzeskaki, 'The (Self-)Governance of Community Energy: Challenges & Prospects Natural gas studies View project Stimulating sustainable energy View project', no. February, 2014.
- [38] M. Harcourt *et al.*, 'Building Smart Energy Communities: Implementing Integrated Community Energy Solutions', Ottawa, 2012.
- [39] B. Koirala and R. Hakvoort, 'Integrated Community-Based Energy Systems: Aligning Technology, Incentives, and Regulations', in *Innovation and Disruption at the Grid's Edge*, Fereidoon Sioshansi, Ed. San Francisco: Academic Press, 2017, pp. 363–387.
- [40] B. P. Koirala, E. Koliou, J. Friege, R. A. Hakvoort, and P. M. Herder, 'Energetic Communities for Community Energy: A Review of Key Issues and Trends Shaping Integrated Community Energy Systems', *Renewable and Sustainable Energy Reviews*, no. 56, pp. 722–744, 2016.
- [41] S. J. W. Klein and S. Coffey, 'Building a Sustainable Energy Future, one Community at a Time', *Renewable and Sustainable Energy Reviews*, vol. 60, pp. 867–880, 2016.
- [42] Knowledge Transfer Network, 'The Role of Community Energy Systems in the UK Resilient Energy Supply', 2013.
- [43] J. C. Rogers, E. A. Simmons, I. Convery, and A. Weatherall, 'Public Perceptions of Opportunities for Community-Based Renewable Energy Projects', *Energy Policy*, vol. 36, no. 11, pp. 4217–4226, 2008.
- [44] G. Walker and N. Simcock, "'Community Energy Systems'", vol. 1, pp. 194–198, 2012.
- [45] C. Rae and F. Bradley, 'Energy autonomy in sustainable communities—A review of key issues', *Renewable and Sustainable Energy Reviews*, vol. 16, no. 9, pp. 6497–6506, Dec. 2012.
- [46] M. Abeysekera, J. Wu, and N. Jenkins, 'Integrated Energy Systems: An Overview of Benefits, Analysis Methods, Research Gaps and Opportunities', *HubNet Position Paper Series*, p. 3, 2016.
- [47] British Standards Institution. and Institution of Electrical Engineers., 'The Electricity Safety, Quality and Continuity Regulations', UK Legislation , London, 2002.
- [48] E. Heffernan, W. Pan, X. Liang, and P. de Wilde, 'Zero carbon homes: Perceptions from the UK Construction Industry', *Energy Policy*, vol. 79, pp. 23–36, Apr. 2015.
- [49] I. Catto, 'Carbon Zero Homes UK Style', *Renewable Energy Focus*, vol. 9, no. 1, pp. 28–29, Jan. 2008.
- [50] M. Faber, 'Zero Carbon Strategies - For Tomorrow's New Homes (UK)', London, 2019.
- [51] M. Panagiotidou and R. J. Fuller, 'Progress in ZEBs—A Review of Definitions, Policies and Construction Activity', *Energy Policy*, vol. 62, pp. 196–206, Nov. 2013.

- [52] Department for Communities and Local Government, 'Next Steps to Zero Carbon Homes – Allowable Solutions', London, 2014.
- [53] Department for Communities and Local Government, 'Next Steps to Zero Carbon Homes - Small Sites Exemption', London, 2015.
- [54] Technical Guide, 'Code for Sustainable Homes', 2010.
- [55] I. Sartori, A. Napolitano, and K. Voss, 'Net Zero Energy Buildings: A Consistent Definition Framework', *Energy and Buildings*, vol. 48, pp. 220–232, 2012.
- [56] L. Belussi *et al.*, 'A Review of Performance of Zero Energy Buildings and Energy Efficiency Solutions', *Journal of Building Engineering*, vol. 25, p. 100772, Sep. 2019.
- [57] W. Feng *et al.*, 'A Review of Net Zero Energy Buildings in Hot and Humid Climates: Experience Learned from 34 Case Study Buildings', *Renewable and Sustainable Energy Reviews*, vol. 114, p. 109303, Oct. 2019.
- [58] V. Karsten and R. Mark, 'IEA Joint Project: Towards Net Zero Energy Solar Buildings (NZEBs)', 2009.
- [59] S. Attia, *Net Zero Energy Buildings (NZEB) : Concepts, Frameworks and Roadmap for Project Analysis and Implementation*. Oxford: Butterworth-Heinemann, 2018.
- [60] I. Sartori, A. Napolitano, and K. Voss, 'Net zero energy buildings: A consistent definition framework', *Energy and Buildings*, vol. 48, pp. 220–232, May 2012.
- [61] M. Ferrara, V. Monetti, and E. Fabrizio, 'Cost-Optimal Analysis for Nearly Zero Energy Buildings Design and Optimization: A Critical Review', *Energies*, vol. 11, no. 6, p. 1478, Jun. 2018.
- [62] J. Ling-Chin *et al.*, 'UK Building Thermal Performance from Industrial and Governmental Perspectives', *Applied Energy*, vol. 237, pp. 270–282, Mar. 2019.
- [63] R. Anderson and D. Roberts, 'Maximizing Residential Energy Savings : Net Zero Energy Home Technology Pathways', 2010.
- [64] E. McKenna, J. Pless, and S. J. Darby, 'Solar Photovoltaic Self-Consumption in the UK Residential Sector: New Estimates from a Smart Grid Demonstration Project', *Energy Policy*, vol. 118, pp. 482–491, Jul. 2018.
- [65] Y. Che, S. Xue, W. He, L. Liu, and J. Jia, 'Optimal Energy Allocation of Net-Zero Energy Building', *Ekoloji*, vol. 28, no. 107, pp. 1425–1436, 2019.
- [66] Z. Ma, H. Bao, and A. P. Roskilly, 'Feasibility Study of Seasonal Solar Thermal Energy Storage in Domestic Dwellings in the UK', *Solar Energy*, vol. 162, pp. 489–499, Mar. 2018.
- [67] M. Herrando, A. M. Pantaleo, K. Wang, and C. N. Markides, 'Solar Combined cooling, Heating and Power Systems Based on Hybrid PVT, PV or Solar-Thermal Collectors for Building Applications', *Renewable Energy*, vol. 143, pp. 637–647, Dec. 2019.
- [68] M. Milousi, M. Souliotis, G. Arampatzis, and S. Papaefthimiou, 'Evaluating the Environmental Performance of Solar Energy Systems Through a Combined Life Cycle Assessment and Cost Analysis', *Sustainability*, vol. 11, no. 9, p. 2539, May 2019.
- [69] J. Hong, N. J. Kelly, I. Richardson, and M. Thomson, 'Assessing heat pumps as flexible load', *Proceedings of the Institution of Mechanical Engineers, Part A: Journal of Power and Energy*, vol. 227, no. 1, pp. 30–42, 2012.

- [70] R. W. Moss, P. Henshall, F. Arya, G. S. F. Shire, T. Hyde, and P. C. Eames, 'Performance and Operational Effectiveness of Evacuated Flat Plate Solar Collectors Compared with Conventional Thermal, PVT and PV Panels', *Applied Energy*, vol. 216, pp. 588–601, Apr. 2018.
- [71] A. Arsalis, 'A Comprehensive Review of Fuel Cell-Based Micro-Combined-Heat-and-Power Systems', *Renewable and Sustainable Energy Reviews*, vol. 105, pp. 391–414, May 2019.
- [72] M. Ebrahimi and E. Derakhshan, 'Design and Evaluation of a Micro Combined Cooling, Heating, and Power System Based on Polymer Exchange Membrane Fuel Cell and Thermoelectric Cooler', *Energy Conversion and Management*, vol. 171, pp. 507–517, Sep. 2018.
- [73] T. Sweetnam, M. Fell, E. Oikonomou, and T. Oreszczyn, 'Domestic Demand-Side Response with Heat Pumps: Controls and Tariffs', *Building Research & Information*, vol. 47, no. 4, pp. 344–361, May 2019.
- [74] G. Dermentzis and F. Ochs, 'Detailed Monitoring Analysis of two Residential NZEBs with a Ground-Water Heat Pump with Desuperheater', *International High Performance Buildings Conference*, Jul. 2018.
- [75] A. Navarro-Espinosa and P. Mancarella, 'Probabilistic Modeling and Assessment of the Impact of Electric Heat Pumps on Low Voltage Distribution Networks', *Applied Energy*, vol. 127, pp. 249–266, 2014.
- [76] M. A. Obalanlege, Y. Mahmoudi, R. Douglas, E. Ebrahimi-Bajestan, J. Davidson, and D. Bailie, 'Performance Assessment of a Hybrid Photovoltaic-Thermal and Heat Pump System for Solar Heating and Electricity', *Renewable Energy*, Oct. 2019.
- [77] D. D'Agostino and L. Mazzarella, 'What is a Nearly Zero Energy Building? Overview, Implementation and Comparison of Definitions', *Journal of Building Engineering*, vol. 21, pp. 200–212, Jan. 2019.
- [78] A. Brambilla, G. Salvalai, M. Imperadori, and M. M. Sesana, 'Nearly Zero Energy Building Renovation: From Energy Efficiency to Environmental Efficiency, a Pilot Case Study', *Energy and Buildings*, vol. 166, pp. 271–283, May 2018.
- [79] E. Duce *et al.*, 'Accelerating Energy Renovation Solution for Zero Energy Buildings and Neighbourhoods', Leuven, 2018.
- [80] R. Simson, E. Arumägi, K. Kuusk, and J. Kurnitski, 'Redefining Cost-Optimal nZEB Levels for New Residential Buildings', *E3S Web of Conferences*, vol. 111, no. 201 9, p. 03035, 2019.
- [81] D. D'Agostino and D. Parker, 'Data on Cost-Optimal Nearly Zero Energy Buildings (NZEBs) Across Europe', *Data in Brief*, vol. 17, pp. 1168–1174, Apr. 2018.
- [82] K. Loukaidou, A. Michopoulos, and T. Zachariadis, 'Nearly-zero Energy Buildings: Cost-Optimal Analysis of Building Envelope Characteristics', *Procedia Environmental Sciences*, vol. 38, pp. 20–27, Jan. 2017.
- [83] M. Hamdy, A. Hasan, and K. Siren, 'A Multi-Stage Optimization Method for Cost-Optimal and Nearly-Zero-Energy Building Solutions in Line with the EPBD-Recast 2010', *Energy and Buildings*, vol. 56, pp. 189–203, Jan. 2013.
- [84] A. Karlsson *et al.*, 'Common Barriers and Challenges in Current nZEB Practice in Europe', Oslo, Debegsa, Eibar, Ville de Grenoble, and Malmo, 2013.

- [85] J. Skandamoorthy, ‘BRE Innovation Park Shaping the Future of the Built Environment and Sustainable Communities’, London, 2012.
- [86] I. Mulheirn, ‘Tackling the UK Housing Crisis: is Supply the Answer?’, London, 2019.
- [87] S. Scott *et al.*, *Wind Energy*. John Wiley & Sons, 2017.
- [88] M. Harper, ‘The RSPB’s 2050 Energy Vision’, London, 2016.
- [89] E. McKenna, E. Webborn, P. A. Leicester, and S. Elam, ‘Analysis of International Residential Solar PV Self-Consumption (forthcoming)’, *Proceedings of the European Council for an Energy Efficient Economy Summer Study*, pp. 707–716, 2019.
- [90] J. D. Mondol and G. Jacob, ‘Commercial Scale Solar Power Generation (5MW to 50 MW) and its Connection to Distribution Power Network in the United Kingdom’, *Solar Energy Research Updates*, vol. 44, no. 0, pp. 25–38, 2018.
- [91] A. Fragaki, T. Markvart, and G. Laskos, ‘All UK Electricity Supplied by Wind and Photovoltaics – The 30–30 Rule’, *Energy*, vol. 169, pp. 228–237, Feb. 2019.
- [92] B. Singh and N. M. Pindoriya, ‘Impact Assessment of Distributed Solar PV Integration in Low-Voltage Unbalanced Distribution Network: A Case Study’, in *2018 5th IEEE Uttar Pradesh Section International Conference on Electrical, Electronics and Computer Engineering (UPCON)*, 2018, pp. 1–6.
- [93] L. J. Nuttall, A. P. Fickett, and W. A. Titterington, ‘Hydrogen Generation by Solid Polymer Electrolyte Water Electrolysis’, in *Hydrogen Energy*, Boston, MA: Springer US, 1975, pp. 24–40.
- [94] W. T. Grubb, ‘Batteries with Solid Ion Exchange Electrolytes’, *Journal of The Electrochemical Society*, vol. 106, no. 4, p. 275, Apr. 1959.
- [95] P. Sapkota, C. Boyer, R. Dutta, C. Cazorla, and K.-F. Aguey-Zinsou, ‘Planar polymer electrolyte membrane fuel cells: powering portable devices from hydrogen’, *Sustainable Energy & Fuels*, 2020.
- [96] M. Carmo, D. L. Fritz, J. Mergel, and D. Stolten, ‘A comprehensive Review on PEM Water Electrolysis’, *International Journal of Hydrogen Energy*, vol. 38, no. 12, pp. 4901–4934, 2013.
- [97] Y. Haseli, ‘Maximum conversion efficiency of hydrogen fuel cells’, *International Journal of Hydrogen Energy*, vol. 43, no. 18, pp. 9015–9021, May 2018.
- [98] D. Guilbert, B. Yodwong, W. Kaewmanee, and M. Phattanasak, ‘Power Converters for Hybrid Renewable Energy Systems with Hydrogen Buffer Storage: A Short Review’, in *2018 International Conference on Smart Grid (icSmartGrid)*, 2018, pp. 28–33.
- [99] H. Dagdougui *et al.*, ‘Hydrogen Storage and Distribution: Implementation Scenarios’, *Hydrogen Infrastructure for Energy Applications*, pp. 37–52, Jan. 2018.
- [100] E. Rivard, M. Trudeau, and K. Zaghbi, ‘Hydrogen Storage for Mobility: A Review’, *Materials*, vol. 12, no. 12, p. 1973, Jun. 2019.
- [101] R. Moradi and K. M. Groth, ‘Hydrogen Storage and Delivery: Review of the State of the Art Technologies and Risk and Reliability Analysis’, *International Journal of Hydrogen Energy*, vol. 44, no. 23, pp. 12254–12269, May 2019.
- [102] H. Barthelemy, M. Weber, and F. Barbier, ‘Hydrogen storage: Recent Improvements and Industrial Perspectives’, *International Journal of Hydrogen Energy*, vol. 42, no. 11, pp. 7254–7262, Mar. 2017.

- [103] M. Wetter and C. Van Treeck, 'New Generation Computational Tools for Building and Community Energy Systems: Annex 60 Final Report', Birmingham, 2017.
- [104] A. A. Bayod-Rújula, Y. Yuan, A. Martínez-Gracia, J. Wang, J. Uche, and H. Chen, 'Modelling and Simulation of a Building Energy Hub', *Proceedings*, vol. 2, no. 23, p. 1431, Nov. 2018.
- [105] H. Karunathilake, P. Perera, R. Ruparathna, K. Hewage, and R. Sadiq, 'Renewable Energy Integration into Community Energy Systems: A Case Study of New Urban Residential Development', *Journal of Cleaner Production*, vol. 173, pp. 292–307, Feb. 2018.
- [106] J. Van Roy, B. Verbruggen, and J. Driesen, 'Ideas for Tomorrow', *IEEE Power and Energy Magazine*, vol. 11, pp. 75–81, 2013.
- [107] B. Verbruggen and J. Driesen, 'Grid Impact Indicators for Active Building Simulations', *IEEE Transactions on Sustainable Energy*, vol. 6, no. 1, pp. 43–50, Jan. 2015.
- [108] A. Navarro-Espinosa, N. Good, L. Zhang, P. Mancarella, and L. F. Ochoa, 'EHP in Low Voltage Networks: Understanding the Effects of Heat Emitters and Room Temperatures', *2015 IEEE Eindhoven PowerTech, PowerTech 2015*, 2015.
- [109] N. Good, L. Zhang, A. Navarro-Espinosa, and P. Mancarella, 'High Resolution Modelling of Multi-Energy Domestic Demand Profiles', *Applied Energy*, vol. 137, pp. 193–210, 2015.
- [110] C. Protopapadaki and D. Saelens, 'Heat Pump and PV Impact on Residential Low-Voltage Distribution Grids as a Function of Building and District Properties', *Applied Energy*, 2016.
- [111] C. Finck, R. Li, and W. Zeiler, 'Operation of Heat pumps for Smart Grid integrated Buildings with Thermal Energy Storage', in *12th International Energy Agency Heat Pump Conference*, 2017, pp. 2–8.
- [112] N. J. Kelly, P. G. Tuohy, and A. D. Hawkes, 'Performance Assessment of Tariff-Based Air Source Heat Pump Load Shifting in a UK Detached Dwelling Featuring Phase Change-Enhanced Buffering', *Applied Thermal Engineering*, vol. 71, no. 2, pp. 809–820, Oct. 2014.
- [113] G. Masy *et al.*, 'Smart Grid Energy Flexible Buildings Through the Use of Heat Pumps and Building Thermal Mass as Energy Storage in the Belgian Context', *International High Performance Buildings Conference*, vol. 4731, no. August, pp. 800–811, 2015.
- [114] K. Klein, S. Herkel, H. M. Henning, and C. Felsmann, 'Load Shifting Using the Heating and Cooling System of an Office Building: Quantitative Potential Evaluation for Different Flexibility and Storage Options', *Applied Energy*, vol. 203, pp. 917–937, 2017.
- [115] A. Arabkooshar, A. Hajizadeh, and A. Moghaddam, 'Intelligent Energy Systems and Active Networks', *Alborg University*, 2018. [Online]. Available: <https://www.et.aau.dk/research-programmes/intelligent-energy-systems-and-active-networks/>. [Accessed: 28-Nov-2019].
- [116] B. Bidar and F. Shahraki, 'Energy and Exergo-Economic Assessments of Gas Turbine Based CHP Systems: A Case Study of SPGC Utility Plant', *Iranian Journal of Chemistry and Chemical Engineering*, vol. 37, no. 5, pp. 209–223, 2018.
- [117] J. G. Usack, L. G. Van Doren, R. Posmanik, J. W. Tester, and L. T. Angenent, 'Harnessing Anaerobic Digestion for Combined Cooling, Heat, and Power on Dairy Farms: An Environmental Life Cycle and Techno-Economic Assessment of Added Cooling Pathways', *Journal of Dairy Science*, vol. 102, no. 4, pp. 3630–3645, Apr. 2019.

- [118] T. Ma, J. Wu, L. Hao, W.-J. Lee, H. Yan, and D. Li, ‘The Optimal Structure Planning and Energy Management Strategies of Smart Multi Energy Systems’, *Energy*, vol. 160, pp. 122–141, Oct. 2018.
- [119] T. Yun, W. Zedi, L. Yan, M. Qian, H. Qian, and L. Shubin, ‘A Multi Energy Storage System Model Based on Electricity Heat and Hydrogen Coordinated Optimization for Power Grid Flexibility’, *CSEE Journal of Power and Energy Systems*, Jun. 2019.
- [120] F. Safari and I. Dincer, ‘Development and Analysis of a Novel Biomass-Based Integrated System for Multigeneration with Hydrogen Production’, *International Journal of Hydrogen Energy*, vol. 44, no. 7, pp. 3511–3526, Feb. 2019.
- [121] J. Cao, C. Crozier, M. McCulloch, and Z. Fan, ‘Optimal Design and Operation of a Low Carbon Community Based Multi-Energy Systems Considering EV Integration’, *IEEE Transactions on Sustainable Energy*, vol. 10, no. 3, pp. 1217–1226, Jul. 2019.
- [122] C. Yang, ‘Hydrogen and Electricity: Parallels, Interactions, and convergence’, *International Journal of Hydrogen Energy*, vol. 33, no. 8, pp. 1977–1994, Apr. 2008.
- [123] X. Liu, Z. Yan, and J. Wu, ‘Optimal Coordinated Operation of a Multi-Energy Community Considering Interactions Between Energy Storage and Conversion Devices’, *Applied Energy*, vol. 248, pp. 256–273, Aug. 2019.
- [124] Q. Hu, B. Zeng, Y. Zhang, H. Hu, and W. Liu, ‘Analysis of Probabilistic Energy Flow for Integrated Electricity-Gas Energy System with P2G Based on Cumulant Method’, in *2017 IEEE Conference on Energy Internet and Energy System Integration (EI2)*, 2017, pp. 1–6.
- [125] M. Geidl and G. Andersson, ‘Optimal Power Flow of Multiple Energy Carriers’, *IEEE Transactions on Power Systems*, vol. 22, no. 1, pp. 145–155, Feb. 2007.
- [126] P. Favre-Perrod, ‘Hybrid Energy Transmission for Multi-Energy Networks’, ETH, 2008.
- [127] G. Mendes, C. Ioakimidis, and P. Ferrão, ‘On the Planning and Analysis of Integrated Community Energy Systems: A Review and Survey of Available Tools’, *Renewable and Sustainable Energy Reviews*, vol. 15, no. 9, pp. 4836–4854, Dec. 2011.
- [128] A. Lyden, R. Pepper, and P. G. Tuohy, ‘A Modelling Tool Selection Process for Planning of Community Scale Energy Systems Including Storage and Demand Side Management’, *Sustainable Cities and Society*, vol. 39, pp. 674–688, May 2018.
- [129] D. Connolly, H. Lund, B. V. Mathiesen, and M. Leahy, ‘A review of Computer Tools for Analysing the Integration of Renewable Energy into Various Energy Systems’, *Applied Energy*, vol. 87, no. 4, pp. 1059–1082, Apr. 2010.
- [130] I. van Beuzekom, M. Gibescu, and J. G. Slootweg, ‘A Review of Multi-Energy System Planning and Optimization Tools for Sustainable Urban Development’, in *2015 IEEE Eindhoven PowerTech*, 2015, pp. 1–7.
- [131] P. S. C. J. Neetu Agarwal, Kushboo Gupta, Shailesh Porwal, *A Survey: Spider Monkey Optimization Algorithm*, vol. 4, no. 11. San’ei, 2019.
- [132] S. S. Rao, *Engineering Optimization : Theory and Practice*, Fifth. Florida: Wiley, 2019.
- [133] D. Han, W. Sun, and X. Fan, ‘Dynamic Energy Management in Smart Grid: A Fast Randomized First-Order Optimization Algorithm’, *International Journal of Electrical Power & Energy Systems*, vol. 94, pp. 179–187, Jan. 2018.

- [134] A. Tindale and S. Potter, 'DesignBuilder', 2005. [Online]. Available: <http://www.designbuilder.co.uk/>. [Accessed: 02-Jun-2015].
- [135] D. B. Crawley *et al.*, 'EnergyPlus: Creating a new-generation building energy simulation program', *Energy and Buildings*, vol. 33, no. 4, pp. 319–331, 2001.
- [136] K. Ellington, 'EnergyPlus: The Merger of BLAST and DOE-2'. [Online]. Available: http://eetd.lbl.gov/newsletter/cbs_nl/nl18/cbs-nl18-energyplus.html. [Accessed: 25-Nov-2015].
- [137] Electric Corby, 'Zero Energy Bill Homes - Electric Corby'. [Online]. Available: <http://www.electriccorby.co.uk/projects/zeb/>. [Accessed: 21-Jan-2016].
- [138] A. Ibrahim, M. Y. Othman, M. H. Ruslan, S. Mat, and K. Sopian, 'Recent advances in Flat Plate Photovoltaic/Thermal (PV/T) Solar Collectors', *Renewable and Sustainable Energy Reviews*, vol. 15, no. 1, pp. 352–365, 2011.
- [139] P. G. Charalambous, G. G. Maidment, S. a. Kalogirou, and K. Yiakoumetti, 'Photovoltaic Thermal (PV/T) Collectors: A Review', *Applied Thermal Engineering*, vol. 27, no. 2–3, pp. 275–286, 2007.
- [140] X. Nan, M. Abeysekera, and J. Wu, 'Modelling of Energy Demand in a Modern Domestic Dwelling', *The 7th International Conference on Applied Energy – ICAE2015*, p. 6, 2015.
- [141] U.S DOE Energy Efficiency and Renewable Energy, 'Weather Data by Region', *EnergyPlus*, 2019. [Online]. Available: https://energyplus.net/weather-region/europe_wmo_region_6/GBR. [Accessed: 21-Jan-2016].
- [142] European Commission, 'JRC Photovoltaic Geographical Information System (PVGIS) - European Commission', *EU Science Hub*, 2019. [Online]. Available: https://re.jrc.ec.europa.eu/pvg_tools/en/tools.html. [Accessed: 08-Oct-2017].
- [143] BRE, 'The Government's Standard Assessment Procedure for Energy Rating of Dwellings', 2012.
- [144] J. Johnston, D. Miles-Shenton, D. Bell, M. Wingfield, 'Airtightness of Buildings — Towards higher Performance Final Report — Domestic Sector Airtightness', London, 2011.
- [145] I. Richardson, M. Thomson, D. Infield, and C. Clifford, 'Domestic Electricity Use: A high-Resolution Energy Demand Model', *Energy and Buildings*, vol. 42, no. 10, pp. 1878–1887, 2010.
- [146] Solimpeks, 'Powervolt – Solimpeks Solar Corp'. [Online]. Available: <http://www.solimpeks.com/product/volther-powervolt/>. [Accessed: 20-Jan-2019].
- [147] G. F. Hundy, A. R. Trott, T. C. Welch, G. F. Hundy, A. R. Trott, and T. C. Welch, 'The Refrigeration Cycle', in *Refrigeration, Air Conditioning and Heat Pumps*, Third., Butterworth-Heinemann, Ed. Oxford: Elsevier, 2016, pp. 19–39.
- [148] Health and Safety Executive, 'Legionella and Legionnaires' Disease', 2000. [Online]. Available: <http://www.hse.gov.uk/legionnaires/>.
- [149] Joule, 'Knowledge Centre - Unvented Cylinders', 2017. [Online]. Available: https://www.joule.ie/knowledge-centre/?_sft_wpdmcategory=cylinder&_sf_s=Cyclone Air Indirect. [Accessed: 20-Jan-2017].

- [150] HM Government, 'Department for Environment, Food & Rural Affairs', 2008. [Online]. Available: <https://www.gov.uk/government/organisations/department-for-environment-food-rural-affairs>. [Accessed: 30-Mar-2016].
- [151] Department for Environment Food & Rural Affairs, 'Future Water: The Government's Water Strategy for England', London, 2008.
- [152] Communities and Local Government, 'National Calculation Methodology (NCM) Modelling Guide For Buildings other than Dwellings in England and Wales', Building Research Establishment, 2008.
- [153] J. Armstrong, *CIBSE Concise Handbook*, 2008th ed. Norwich: CIBSE Publications Department Printed, 2008.
- [154] CIBSE, 'Degree-days: theory and application. TM41', 2006.
- [155] Uniq Solutions, 'Uniq Solutions Remote Monitoring Dashboard', *Energy Monitoring*, 2019. .
- [156] Ofgem, 'Feed-In Tariff Rates', 2012. [Online]. Available: <https://www.ofgem.gov.uk/environmental-programmes/fit/fit-tariff-rates>. [Accessed: 18-Mar-2018].
- [157] British Gas, 'Gas and Electricity', 2018. [Online]. Available: <https://www.britishgas.co.uk/energy/gas-and-electricity.html>. [Accessed: 18-Mar-2018].
- [158] N. J. Kelly and J. Cockroft, 'Analysis of Retrofit Air Source Heat Pump performance: Results from Detailed Simulations and Comparison to Field Trial Data', *Energy and Buildings*, vol. 43, no. 1, pp. 239–245, Jan. 2011.
- [159] F. L. Müller and B. Jansen, 'Large-Scale Demonstration of Precise Demand Response Provided by Residential Heat Pumps', *Applied Energy*, vol. 239, pp. 836–845, Apr. 2019.
- [160] L. Zhang, N. Good, and P. Mancarella, 'Building-to-Grid Flexibility: Modelling and Assessment Metrics for Residential Demand Response from Heat Pump Aggregations', *Applied Energy*, vol. 233–234, pp. 709–723, Jan. 2019.
- [161] S. Steinle, M. Zimmerlin, F. Mueller, L. Held, M. R. Suriyah, and T. Leibfried, 'Time-Dependent Flexibility Potential of Heat Pump Systems for Smart Energy System Operation', *Energies*, vol. 13, no. 4, p. 903, Feb. 2020.
- [162] R. Hirmiz, H. M. Teamah, M. F. Lightstone, and J. S. Cotton, 'Performance of Heat Pump Integrated Phase Change Material thermal Storage for Electric Load Shifting in Building demand Side Management', *Energy and Buildings*, vol. 190, pp. 103–118, May 2019.
- [163] M. Wetter, 'Co-simulation of building energy and control systems with the Building Controls Virtual Test Bed', *Journal of Building Performance Simulation*, vol. 4, no. 3, pp. 185–203, 2011.
- [164] U.S. Department of Energy National Laboratory Managed by the University of California, 'Berkeley Lab — Lawrence Berkeley National Laboratory'. [Online]. Available: <http://www.lbl.gov/>. [Accessed: 25-Nov-2015].
- [165] M. E. Baran and F. F. Wu, 'Network Reconfiguration in Distribution Systems for Loss Reduction and Load Balancing', *IEEE Transactions on Power Delivery*, vol. 4, no. 2, pp. 1401–1407, Apr. 1989.

- [166] P. Li *et al.*, ‘Coordinated Control Method of Voltage and Reactive Power for Active Distribution Networks Based on Soft Open Point’, *IEEE Transactions on Sustainable Energy*, vol. 8, no. 4, pp. 1430–1442, Oct. 2017.
- [167] A. Lyden and P. Tuohy, ‘Heat Pump and Thermal Storage Sizing with Time-of-Use Electricity Pricing’, in *13th International Renewable Energy Storage Conference*, 2019, pp. 29–40.
- [168] L. R. Gay, ‘CIBSE Knowledge Series, Comfort’, London, 2008.
- [169] N. J. Kelly, P. G. Tuohy, and A. D. Hawkes, ‘Performance Assessment of Tariff-based Air Source Heat Pump Load Shifting in a UK Detached Dwelling featuring Phase Change-Enhanced Buffering’, *Applied Thermal Engineering*, vol. 71, no. 2, pp. 809–820, 2014.
- [170] British Standards Institution, ‘BS EN 14511-3:2013 - Air Conditioners, Liquid Chilling Packages and Heat pumps with Electrically Driven Compressors for Space Heating and Cooling. Test Methods’, *BSI*, 2013. [Online]. Available: <https://shop.bsigroup.com/ProductDetail/?pid=000000000030271674>. [Accessed: 16-Aug-2017].
- [171] Mitsubishi, ‘Community Heating Schemes’, 2016. [Online]. Available: [https://heating.mitsubishielectric.co.uk/KnowledgeBase/Public/Community Heating Schemes Brochure.pdf](https://heating.mitsubishielectric.co.uk/KnowledgeBase/Public/Community%20Heating%20Schemes%20Brochure.pdf). [Accessed: 16-Aug-2017].
- [172] C. Brand, J. Anable, I. Ketsopoulou, and J. Watson, ‘Road to Zero or Road to nowhere? Disrupting Transport and Energy in a Zero Carbon World’, *Energy Policy*, vol. 139, no. 111334, pp. 2–4, 2020.
- [173] R. M. Oviedo, Z. Fan, and M. Sooriyabandara, ‘Ecoisland: A Hydrogen Refueler and Storage System with Renewable Energy Sources’, *2014 IEEE PES T&D Conference and Exposition*, pp. 1–5, 2014.
- [174] M. Balat, ‘Potential Importance of Hydrogen as a Future Solution to Environmental and Transportation Problems’, *International Journal of Hydrogen Energy*, vol. 33, no. 15, pp. 4013–4029, 2008.
- [175] D. B. Lata and A. Misra, ‘Theoretical and Experimental Investigations on the Performance of Dual Fuel Diesel Engine with Hydrogen and LPG as secondary fuels’, *International Journal of Hydrogen Energy*, vol. 35, no. 21, pp. 11918–11931, 2010.
- [176] S. Verhelst and T. Wallner, ‘Hydrogen-Fueled Internal Combustion Engines’, *Progress in Energy and Combustion Science*, vol. 35, no. 6, pp. 490–527, 2009.
- [177] D. Apostolou and G. Xydis, ‘A Literature Review on Hydrogen Refuelling Stations and Infrastructure. Current Status and Future Prospects’, *Renewable and Sustainable Energy Reviews*, vol. 113, p. 109292, 2019.
- [178] C. Brand, J. Anable, and M. Tran, ‘Accelerating the Transformation to a Low Carbon Passenger Transport System: The Role of Car Purchase Taxes, Feebates, Road taxes and Scrappage incentives in the UK’, *Transportation Research Part A: Policy and Practice*, vol. 49, pp. 132–148, 2013.
- [179] F. Rigas and S. Sklavounos, ‘Evaluation of Hazards Associated with Hydrogen Storage Facilities’, *International Journal of Hydrogen Energy*, vol. 30, no. 13–14, pp. 1501–1510, 2005.

- [180] Viridian Solar, 'PV-T with Matching Solar Thermal and Solar Photovoltaic Panels'. [Online]. Available: http://www.viridiansolar.co.uk/Products_Solar_PV-T.htm. [Accessed: 06-Apr-2016].
- [181] The Hydrogen Office, 'Levenmouth Community Energy Project - Bright Green Hydrogen', *Bright Green Hydrogen Website*, 2016. [Online]. Available: <http://www.brightgreenhydrogen.org.uk/bgh-services/levenmouth-community-energy-project/>. [Accessed: 16-Jun-2018].
- [182] Toshiba Corporation, 'Toshiba Corporation to Participate in Large-scale Hydrogen Research Project in Scotland', *Toshiba Leading Innovation Press Releases*, 2015. [Online]. Available: https://www.toshiba.co.jp/about/press/2015_03/pr1801.htm. [Accessed: 16-Jun-2018].
- [183] S. Nistor, S. Dave, Z. Fan, and M. Sooriyabandaraa, 'Technical and Economic Analysis of Hydrogen Refuelling', *Applied Energy*, vol. 167, pp. 211–220, 2016.
- [184] Toshiba's Telecommunications Research Laboratory, 'LCEP Learning Data Repository', *Levenmouth Community Energy Project*, 2013. [Online]. Available: <http://ldr.toshiba-trel.com/portal/>. [Accessed: 25-Jun-2018].
- [185] Wind Turbine Global Market Place, 'Global Wind Power GWP47-750', *Wind-Turbine*, 2018. [Online]. Available: <https://en.wind-turbine.com/wind-turbines/10920/global-wind-power-gwp47-750.html>. [Accessed: 12-May-2020].
- [186] J. A. Sánchez, C. Veganzones, S. Martínez, F. Blázquez, N. Herrero, and J. R. Wilhelmi, 'Dynamic Model of Wind Energy Conversion Systems with Variable Speed Synchronous Generator and Full-Size Power Converter for Large-Scale Power System Stability Studies', *Renewable Energy*, vol. 33, no. 6, pp. 1186–1198, Jun. 2008.
- [187] R. Parmar, A. K. Tripathi, S. Kumar, C. Banerjee, K. Yadav, and M. Kumar, 'Solar Photovoltaic Power Converters: Technologies and Their Testing Protocols for Indian Inevitabilities', in *International Conference on Power Electronics, Control and Automation (ICPECA)*, 2019, pp. 1–6.
- [188] Toshiba Research Europe Laboratories, 'Levenmouth Community Energy Project Learning Data Repository'. [Online]. Available: <http://ldr.toshiba-trel.com/portal/>. [Accessed: 01-Aug-2018].
- [189] S. K. Sahoo, A. Modi, M. Balamurugan, R. Sultana, and S. Chhawchharia, 'Reduction of Inrush Current Using Point On Wave Switching In Power Transformers', *International Conference on Innovations in Power and Advanced Computing Technologies*, pp. 1–6, 2017.
- [190] 'Hydrogenics Corporation', 1995. [Online]. Available: <http://www.hydrogenics.com/>. [Accessed: 25-Jun-2018].
- [191] F. Marangio, M. Santarelli, and M. Cali, 'Theoretical Model and Experimental Analysis of a High Pressure PEM Water Electrolyser for Hydrogen Production', *International Journal of Hydrogen Energy*, vol. 34, no. 3, pp. 1143–1158, 2009.
- [192] S. M. Riedl, 'Development of a Hydrogen Refueling Station Design Tool', *International Journal of Hydrogen Energy*, vol. 45, no. 1, pp. 1–9, Jan. 2020.
- [193] S. P. de Visser, 'Van der Waals Equation of State Revisited: Importance of the Dispersion Correction', *The Journal of Physical Chemistry B*, vol. 115, no. 16, pp. 4709–4717, Apr. 2011.

- [194] M. N. Berberan-Santos, E. N. Bodunov, and L. Pogliani, ‘The Van der Waals Equation: analytical and approximate solutions’, *Journal of Mathematical Chemistry*, vol. 43, no. 4, pp. 1437–1457, May 2008.
- [195] ITM Power, ‘Island Hydrogen’, 2013. [Online]. Available: <http://www.itm-power.com/project/island-hydrogen>. [Accessed: 25-Jun-2018].
- [196] T. Jeff, ‘Hydrogen vehicles: Fuel of the future’, *Nature*, vol. 464, pp. 1262–1264, 2010.
- [197] Department for Transport, ‘Statistics at DfT’, *GOV.UK*, 2017. [Online]. Available: <https://www.gov.uk/government/organisations/department-for-transport/about/statistics>. [Accessed: 25-Jun-2018].
- [198] A. S. Tijani, N. A. B. Yusup, and A. H. A. Rahim, ‘Mathematical Modelling and Simulation Analysis of Advanced Alkaline Electrolyzer System for Hydrogen Production’, *Procedia Technology*, vol. 15, no. 3, pp. 798–806, 2014.

APPENDIX A

A1 BUILDING FABRIC DATA

Table A1- 1 describes the building fabric data that refers to structural materials, cladding, insulation, and finishes, that enclose the interior of the residential buildings, separating the internal from the external.

Table A1- 1: Building fabric data

| Components | Material | Conductivity (W/m/°C) | Specific Heat (J/kg°C) | Mass Density (kg/m ³) |
|----------------------|------------------------------|--------------------------|------------------------------|---|
| Bricks | Facing brown | 0.96 | 2000 | 650 |
| | Concrete Milton Keynes block | 1.06 | 1950 | 1000 |
| | Flooring block | 0.17 | 600 | 1000 |
| Insulation | Full cavity | 0.03 | 25 | 1000 |
| | Mineral wool | 0.05 | 12 | 1000 |
| | Rockwool rollbatt | 0.04 | 25 | 1000 |
| | Insulation board | 0.02 | 12 | 1030 |
| Plaster/Board | Plasterboard | 0.21 | 900 | 1000 |
| | On dabs | 0.08 | 400 | 837 |
| | Weather boiled proof plywood | 0.15 | 700 | 1420 |
| | Flooring chipboard | 0.15 | 800 | 2093 |
| | Roof tile battens | 0.16 | 800 | 2093 |
| | Plywood deck | 0.13 | 500 | 1500 |
| Miscellaneous | External render | 0.57 | 1300 | 1000 |
| | Cement sand render | 1.40 | 2100 | 650 |
| | Steel for partitions | 50 | 7800 | 502 |
| | Ceiling (Plaster) | 0.38 | 112 | 840 |
| | Oak for doors | 0.19 | 700 | 2390 |
| | Plate glass for windows | 0.70 | 2710 | 837 |
| | Plain roof tiles | 1.10 | 2100 | 837 |

A2 HEAT LOSS CALCULATIONS

In this section, the results from manual heat loss calculations are compared to EnergyPlus software simulation results on a typical winter day (1st of January). In order to illustrate the manual heat loss calculation, a simple domestic dwelling (Figure A2- 1) was examined using the residential building construction materials and the ground floor dimensions of the modelled Electric Homes. Characteristics of attention of domestic dwellings include:

- Volume: 8.50m long x 5.48m wide x 3.50m high
- Windows sizes: 0.94m long x 0.94m high
- Door size: 0.84m long x 2.50m high
- Ventilation and infiltration rate: 0.5 *ACH*
- Ground (0-10 cm depth), outdoor and indoor temperatures: 6.5°C, 0.4°C, and 19°C

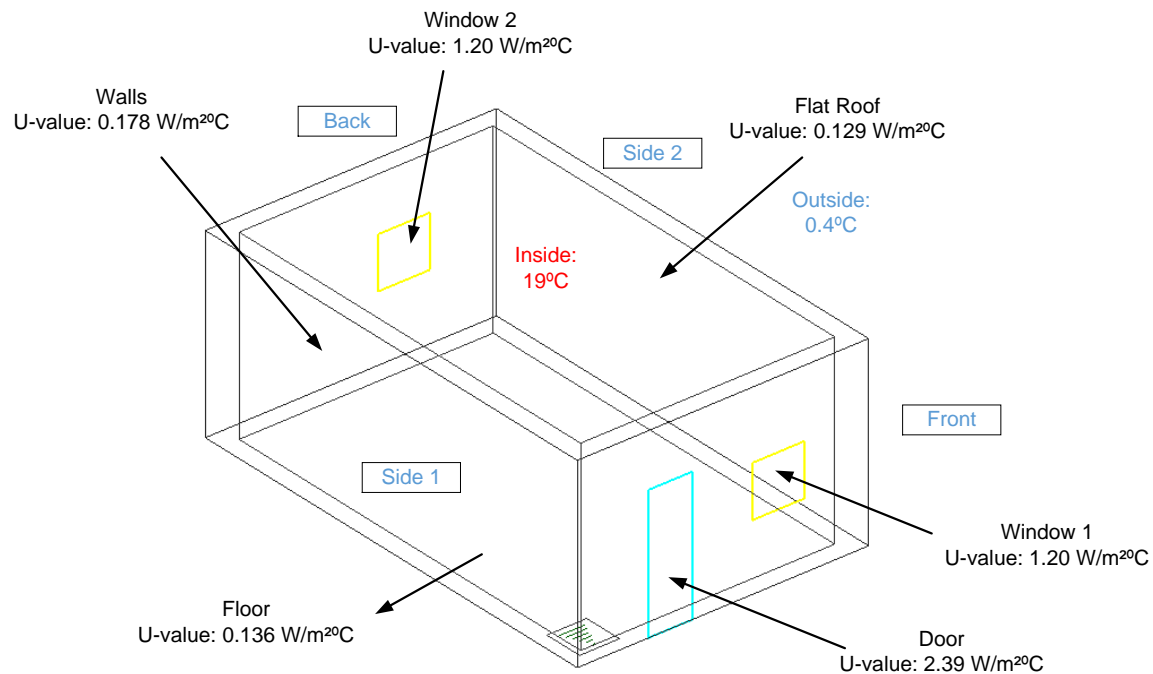


Figure A2- 1: Representation of a simple building model

The simple domestic dwelling was also modelled, and a simulation was performed using the GUI-DesignBuilder and EnergyPlus software. See Figure A2- 2.

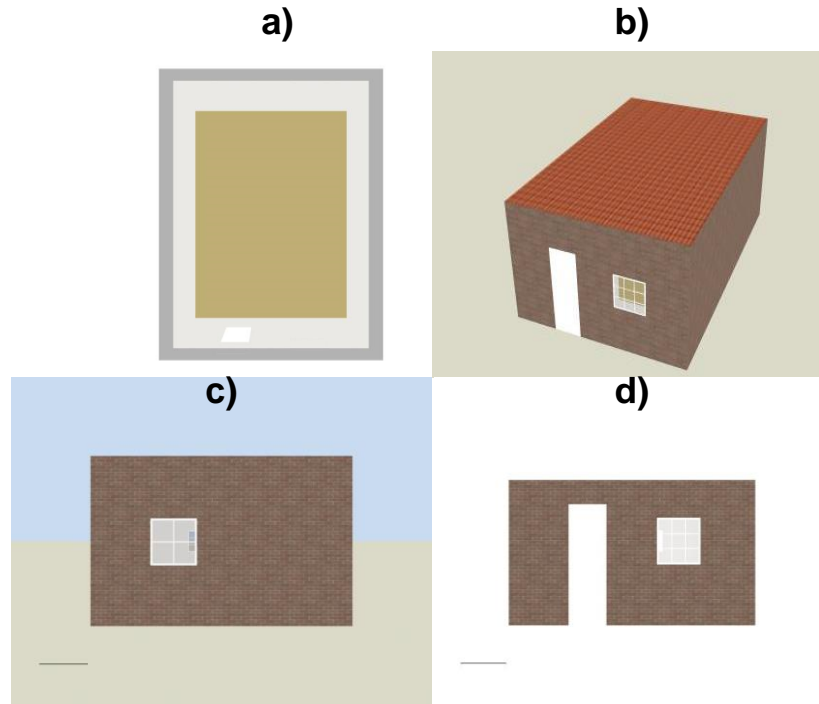


Figure A2- 2: 3D building model representation. a) plan view. b) axonometric. c) back view. d) front view

A2.1. Manual Calculation

The objective of the heat load calculation was to calculate the heat losses of a simple domestic dwelling and compare the results using the building modelling and simulation tool EnergyPlus. In order to perform the total heat losses calculation, the following steps were accomplished:

1st - Heat losses (Q_{trans}) through the building envelope:

Windows 1 and 2

$$Q_{trans,window1} = (U_i A_i)(t_{in} - t_{out}) = (1.20 ((0.94) (0.94)))(19 - 0.4) = 15.94W$$

$$Q_{trans,window2} = (U_i A_i)(t_{in} - t_{out}) = (1.20((0.94)(0.94)))(19 - 0.4) = 15.94W$$

Wall sides 1 and 2

$$Q_{trans,wallside1} = (U_i A_i)(t_{in} - t_{out}) = (0.178((8.50)(3.50)))(19 - 0.4) = 98.49W$$

$$Q_{trans,wallside2} = (U_i A_i)(t_{in} - t_{out}) = (0.178((8.50)(3.50)))(19 - 0.4) = 98.49W$$

Front wall

$$Q_{trans, frontwall} = (U_i A_i)(t_{in} - t_{out}) = \left[(0.178 ((5.48) (3.50))) - (0.88 + 2.2) \right] (19 - 0.4) = 53.30W$$

Where, 0.88 and 2.2 are, respectively, the window 1 and door areas in m²

Back wall

$$Q_{trans, backwall} = (U_i A_i)(t_{in} - t_{out}) = \left[(0.178 ((5.48)(3.50))) - (2.2) \right] (19 - 0.4) = 56.21W$$

Where, 2.2 is window 2 areas in m²

Door

$$Q_{trans, door} = (U_i A_i)(t_{in} - t_{out}) = (2.39((0.84)(2.50)))(19 - 0.4) = 93.35W$$

Floor

$$Q_{trans, floor} = (U_i A_i)(t_{in} - t_{out}) = (0.136((8.50)(3.50)))(19 - 6.5) = 50.57W$$

Roof

$$Q_{trans, roof} = (U_i A_i)(t_{in} - t_{out}) = (0.129(8.50)(3.50))(19 - 0.4) = 71.38W$$

2nd Heat Losses caused by ventilation and infiltration:

$$Q_{vent/inf} = \left[\left(\frac{V(ACH)}{3600} \right) \rho_{air} C_{p,air} (t_r - t_o) \right] =$$
$$\left[\left(\left(\frac{0.5((5.48)(3.5)(8.5))}{3600} \right) \right) \left((1.20)(1.01 \times 10^3) \right) \right] (19 - 0.4) = 510W$$

3rd Total heat power losses:

$$Q_{bl} = ((15.94) \times (2)) + ((98.48) \times (2)) + 93.35 + 53.30 + 56.21 + 50.57$$
$$+ 71.38 + 510 = 1063.57W$$

A2.2 Manual Calculation vs Simulation Results

The results of the hand calculations resulted 0.22% higher than the simulation results (Figure A1- 1). These results show the degree to which the simulation model and its associated data accurately represent the heat losses through the building envelope.

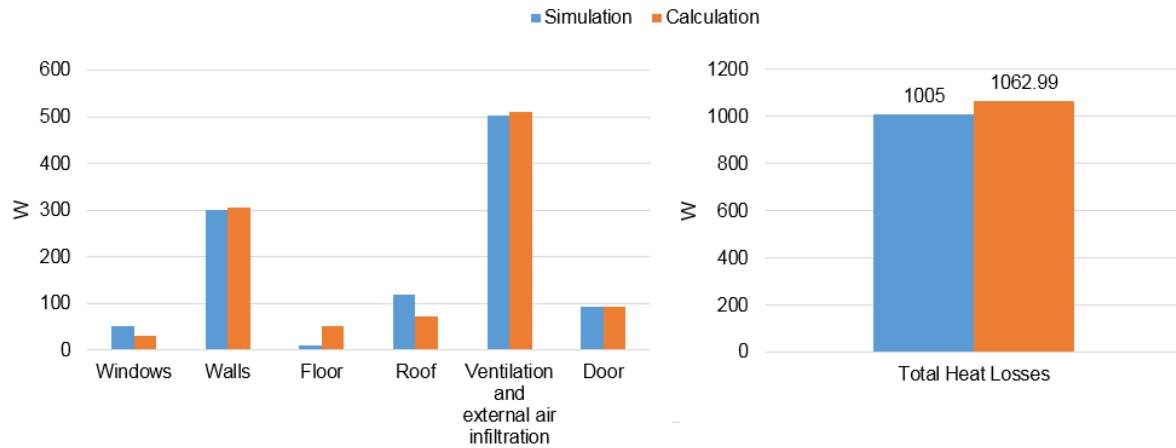


Figure A1- 1: Comparison of heat power losses from simulation and calculation results

A3 SOLAR PV/T PANELS MODELLING AND VERIFICATION

METHOD

A3.1 MATLAB Model

1st Step: To begin with, it was necessary to obtain the absorptance¹⁰ ($\alpha=0.70$) of the absorber plate, which depends on the angle of incidence (θ). In this case, the transmittance (τ) value was set as 0.91.

2nd Step: This step consisted on calculating the incident solar radiation ($I_{dir} \cos \theta + I_{diff}$) on the PV/T panel surface. The incident solar irradiance is determined by the direct solar irradiance (I_{dir}), diffuse solar irradiance (I_{diff}) and angle of incidence (θ).

3rd Step: Next, was to calculate the amount of solar radiation absorbed by the absorber plate ($(I_{dir} \cos \theta + I_{diff}) (\tau\alpha)$). This value is a function of the transmittance ($\tau=0.91$) and absorptance ($\alpha=0.70$) of the collector. Thus, the total solar radiation absorbed (Q_{solar}) each by the PV/T resulted as shown in below.

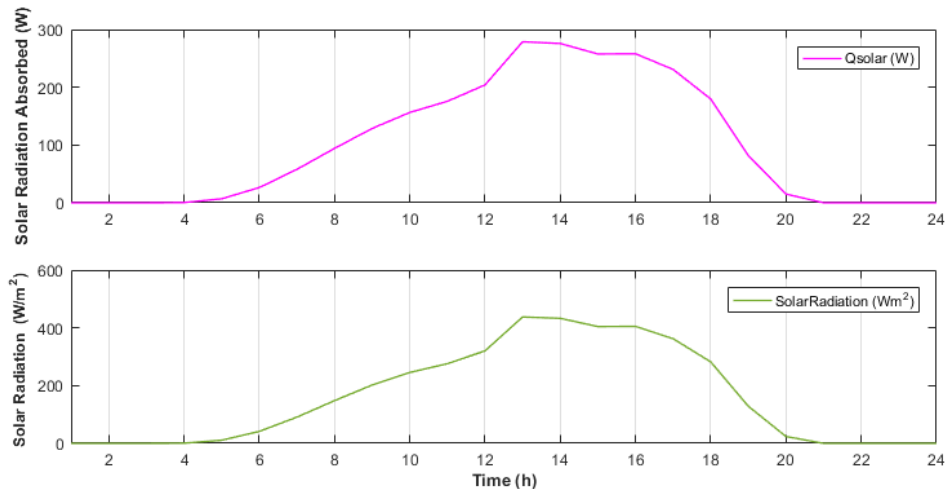


Figure A3- 1: Solar radiation absorbed by the absorber plate (top) and solar radiation (bottom)-1st June

4th Step: The calculation of the electrical energy produced by the PV/T collector is a function of the incident solar irradiance ($(I_{dir} \cos \theta + I_{diff})$) and temperature difference ($T-T_{air}$) of the PV/T panel at standard conditions (STC) and outdoor temperature. Hence, as the PV/T panel temperature increases in temperature it will lose a percentage of its power for every degree its temperature rises.

¹⁰ The ratio of the amount of radiation absorbed by a surface to the amount of radiation incident upon it

In this case the solar cells have a temperature coefficient (E_t) of 0.45% °C, an efficiency (E_o) of 17.5%; module temperature (T) of 25°C at STC, and total area (A_{surf}) of 1.37m². The cell packing factor, which is 0.86, was calculated as follows:

$$P.F = (A_{cell} \text{Number of Cells}) / (A_{surf}) = 0.86$$

where, A_{cell} is 0.0156m², the total *Number of Cells* are 72, and A_{surf} is 1.37m².

On the above premises and considering the transmittance value ($\tau = 0.91$), the total electrical energy produced (Q_{el}) from the collector on the 1st of June resulted as 0.48kWh.

5th Step: In order to obtain the useful heat generated by the PV/T panel, the heat losses (Q_{loss}) should also be also considered. For this reason, this step consisted on calculating the heat losses from the exposed surfaces of the collector. Taking the thermal loss coefficient (U_L) of 0.3W/m²°C, fluid inlet temperature (T_i) of 40°C, and the Birmingham outdoor temperature (T_{air}), the Q_{loss} resulted as shown by Figure A3- 2

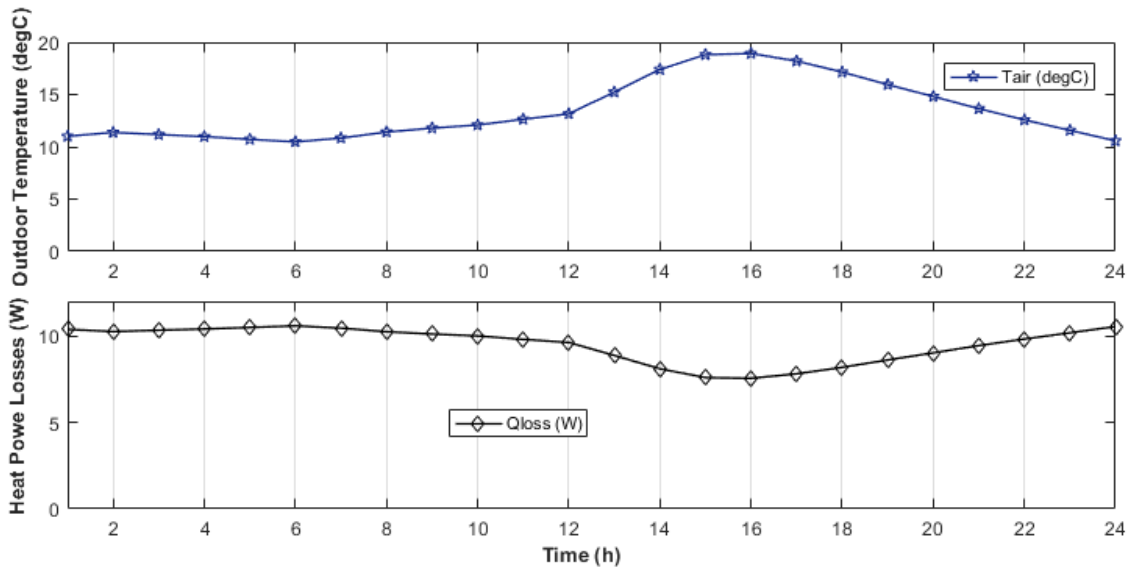


Figure A3- 2: Outdoor temperature (top) and heat power losses by the PV/T panel (bottom)

6th Step: As a final step, the useful heat generated (Q_{useful}) was calculated. Considering a heat removal factor (FR) of 0.86, and a total absorber area (A_{abs}) of 1.19m², the total Q_{useful} generated on the 1st of June resulted as 1.87kWh_e.

A3.2 EnergyPlus Simulation Method

1st Step: As a starting point, a simple building was modelled to attach the PV/T panel on the roof. The roof was considered to have an angle of inclination of 45°.

2nd Step: This step consisted of setting the PV/T panel input parameters. From the list of parameters, under “Solar Collector: FlatPlate: PhotovoltaicThermal” the surface was listed along with its performance characteristics which were defined under “Solar Collector: FlatPlate: PhotovoltaicThermal: Simple”. The PV cell was defined, as well as the working fluid type (water), and the corresponding inlet and outlet nodes. The parameters are summarised in Table A3- 1. An important note is that the model ignores the module heat loss coefficient (U_L).

Table A3- 1: PV/T parameters

| PV/T parameters | |
|---|------|
| A_{surf} -PV/T Panel Area (m ²) | 1.37 |
| η_{el} -Module Efficiency | 15.6 |
| P.F-Packing Factor | 0.82 |
| E_o - Cell Efficiency (%) | 17.5 |
| $P_{mpp-200}$ (W) | 200 |

3rd Step: Finally, the simulation was achieved, and the total electrical and thermal energy was collected. The PV modules determined the energy produced by the solar panels, and they are assumed to always function when the total incident solar ($I_{dir} \cos \theta + I_{diff}$) is greater than 0.3W/m². The usable electric power produced by each PV surface was calculated by:

$$Q_{el} = A_{surf} P.F (I_{dir} \cos(\theta) + I_{diff}) E_o$$

The PV/T model heats the circulating liquid through the pipes and when the working fluid is flowing the model calculates the collected heat as follows:

$$Q_{useful} = A_{surf} P.F (I_{dir} \cos(\theta) + I_{diff}) \eta_{thermal}$$

where $\eta_{thermal}$ is the PV/T thermal efficiency.

Table A3- 2: EnergyPlus PV/T panel simulation results-1st of June

| Q_{el} (kWh) | Q_{useful} (kWh) |
|----------------|--------------------|
| 0.63 | 1.95 |

A3.3 Verification of Solar PV/T Model

The performance of a solar PV/T collector depends on design parameters, weather, and operating conditions (e.g. irradiance, ambient temperature, absorber plate temperature, etc.). Therefore, the PV/T model's performance on a summer day (1st of June) is also evaluated. The solar PV/T collector is modelled using EnergyPlus software and it was verified with MATLAB software. In order to carry out the analysis with MATLAB, the parameters of the PV/T collector described in Chapter 3 (Table 3-5) are implemented, considering a fluid inlet temperature (T_i) of 40°C and a tilt angle of 45°.

In Figure A1- 2, it is observed that the electrical power production of PV/T collector modelled in MATLAB and using EnergyPlus has an important deviation from 13.00h to 17.00h. During these hours, the deviation is larger, and this could be explained by the fact that EnergyPlus considers fewer input values than the MATLAB model.

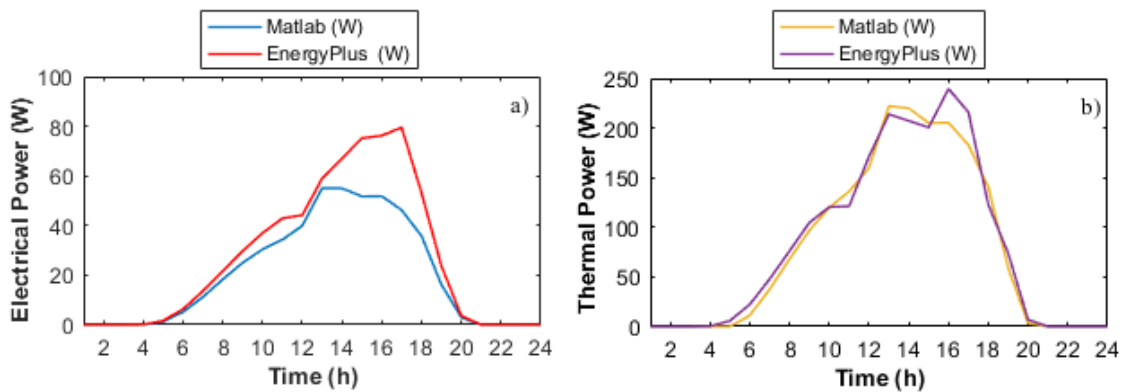


Figure A1- 2: PV/T MATLAB and EnergyPlus results. a) electrical power generated and b) thermal power generated - 1st of June.

As Table A3- 3 shows, the percentage error between EnergyPlus and MATLAB results is 4.5% for the thermal energy generated and 24% for the electrical energy generated. The electrical energy generation provides a high percentage error, and this could be due to the considered power losses during the PV/T MATLAB model. The higher the solar radiation, the higher the PV/T panel temperature, and therefore, the lower the electricity production. Conversely, the thermal energy production of the PV/T collector calculated by hand and using the simulation tool is approximately the same.

Table A3- 3: Solar PV/T simulation results difference between MATLAB and EnergyPlus

| Parameter | MATLAB | EnergyPlus | Difference |
|-------------------|-------------|-------------|------------|
| Thermal Energy | 0.48kWh/day | 0.63kWh/day | 24% |
| Electrical Energy | 1.87kWh/day | 1.95kWh/day | 4.5% |

APPENDIX B

B1 TRANSFORMER AND NETWORK PARAMETERS

Table B1- 1: Transformer and Network Parameters

| Capacity (kVA) | Primary(kV) | Secondary (kV) | R (p.u) | X (p.u) |
|----------------|-------------|----------------|---------|---------|
| 500 | 11 | 0.416 | 0.0190 | 0.0408 |

| From | To | R (p.u) | X (p.u) | From | To | R (p.u) | X (p.u) |
|------|----|---------|---------|------|----|---------|---------|
| 2 | 3 | 0.03076 | 0.01567 | 2 | 19 | 0.01023 | 0.00976 |
| 3 | 4 | 0.02284 | 0.01163 | 19 | 20 | 0.09385 | 0.08457 |
| 4 | 5 | 0.02378 | 0.01211 | 20 | 21 | 0.02555 | 0.02985 |
| 5 | 6 | 0.0511 | 0.04411 | 21 | 22 | 0.04423 | 0.05848 |
| 6 | 7 | 0.01168 | 0.03861 | 3 | 23 | 0.02815 | 0.01924 |
| 7 | 8 | 0.04439 | 0.01467 | 23 | 24 | 0.05603 | 0.04424 |
| 8 | 9 | 0.06426 | 0.04617 | 24 | 25 | 0.0559 | 0.04374 |
| 9 | 10 | 0.06514 | 0.04617 | 6 | 26 | 0.01267 | 0.00645 |
| 10 | 11 | 0.01227 | 0.00406 | 26 | 27 | 0.01773 | 0.00903 |
| 11 | 12 | 0.02336 | 0.00772 | 27 | 28 | 0.06607 | 0.05826 |
| 12 | 13 | 0.09159 | 0.07206 | 28 | 29 | 0.05018 | 0.04371 |
| 13 | 14 | 0.03379 | 0.04448 | 29 | 30 | 0.03166 | 0.01613 |
| 14 | 15 | 0.03687 | 0.03282 | 30 | 31 | 0.0608 | 0.06008 |
| 15 | 16 | 0.04656 | 0.034 | 31 | 32 | 0.01937 | 0.02258 |
| 16 | 17 | 0.08042 | 0.10738 | 32 | 33 | 0.02128 | 0.03319 |
| 17 | 18 | 0.04567 | 0.03581 | 1 | 2 | 0.00575 | 0.00293 |

B2 ELECTRICAL NETWORK POWER FLOW- NEWTON RAPHSON

A primary issue related to electric power flow is associated to determining the complex voltages at all nodes available within a network. In this study, the values of source voltage and loads were determined from the current lines so as to calculate both active and reactive power flows. Each electrical network node, hence, was solved after incorporating five variables, as listed in the following:

- Voltage magnitude, V (v)
- Phase angle, θ ($^{\circ}$)
- Current, I (A)

- Active or Real power, P (kW_e) and Reactive power, Q ($kVAr$)

In addition, these electrical nodes are classified as follows:

- *Slack node*: Reference node in which V and θ are specified, while P and Q injections are unknown
- *Load node* or *PQ node*: P and Q injections are known, therefore, V and θ need to be determined
- *Source node* or *PV node*: Buses attached to a generator, where P and V are given, but θ and Q need to be specified

Various methods can be used to solve power systems after translating them into non-linear equations. Nevertheless, the most popular method, which is also applied in MATPOWER, refers to the nodal method approach. This approach is based on the Kirchhoff's Current Law (*KCL*), which asserts that the sum of all current injections is equivalent to zero at each node. Therefore, in conducting the electrical load flow analysis, the following had been weighed in for the power system equations:

- A symmetry between the phases of the power system
- The network was assumed to be operating under balanced conditions and represented by its positive sequence network
- The load of each network was assumed to be a single-phase balanced load.

B2.1. Nodal Formulation and Admittance Matrix

In the nodal method, the sum of all net power injections within the system is equivalent to zero. The equations are also called power mismatches at node n for both active and reactive power, as expressed in the following:

$$\begin{aligned}\Delta P_n &= P_{Gn} - P_{Dn} - P_{Tn} = P_{Rn} - P_{Tn} = 0 \\ \Delta Q_n &= Q_{Gn} - Q_{Dn} - Q_{Tn} = Q_{Rn} - Q_{Tn} = 0\end{aligned}\tag{B1}$$

where,

- the terms P_{Gn} and Q_{Gn} represent, respectively, generator injections of real and reactive power at node n . These variables are assumed to have been determined prior to load flow analysis.
- P_{Dn} and Q_{Dn} are, respectively, the input data for real and reactive power load demands at node n . The generation and load can be measured, thus, the net values of P_{Dn} and Q_{Dn} are the required power in which supply meets demand.
- P_{Tn} and Q_{Tn} are the transmitted real and reactive power injections.

In order to solve issues related to electrical flow, all nodes of the networks were classified to build the nodal admittance matrix. The admittance matrix consisted of data concerning connectivity and line characteristics of each network.

Example

Figure B2- 1 illustrates the formation of admittance matrix using a three-node power system, for instance.

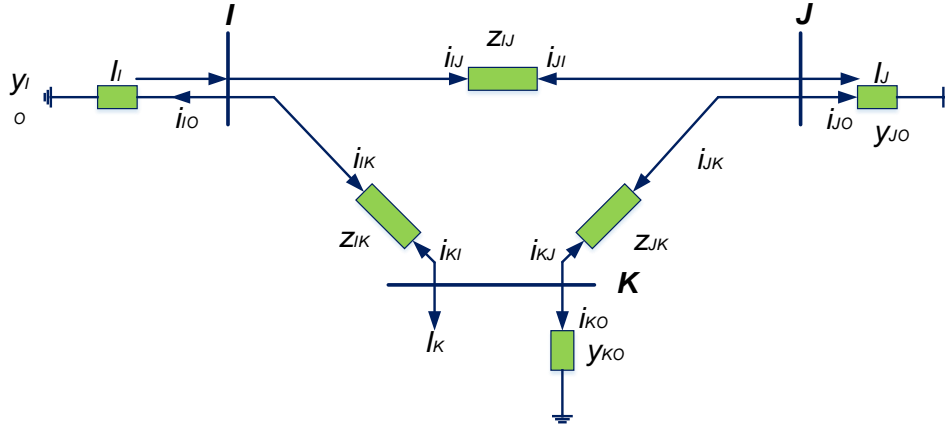


Figure B2- 1: Example of three-node electrical network

where,

- $I_I, I_J, \text{ and } I_K$ are the injected nodal currents, respectively, at nodes $I, J, \text{ and } K$,
- $z_{IJ}, z_{JK}, \text{ and } z_{IK}$ are the positive sequence impedances between the nodes (Ω), and
- $y_{I0}, y_{J0}, \text{ and } y_{K0}$ are the positive sequence shunt admittances.

All nodal voltages are bus-to-ground values, whilst node I reflects the slack busbar. Nonetheless, the flow of nodal current into the system from generators is not less intricate. The admittance value is inversed to the impedance, and the following equation is related to the application of KCL within the network portrayed in Figure B2- 1:

$$\begin{aligned}
 I_I &= i_{IJ} - i_{IK} - i_{I0} = Y_{IJ}(V_I - V_J) + Y_{IK}(V_I - V_K) + Y_{I0}(V_I) \\
 I_J &= i_{JI} - i_{JK} - i_{J0} = Y_{JI}(V_J - V_I) + Y_{JK}(V_J - V_K) + Y_{J0}(V_J) \\
 I_K &= i_{KI} - i_{KJ} - i_{K0} = Y_{KJ}(V_K - V_I) + Y_{KJ}(V_K - V_J) + Y_{K0}(V_K)
 \end{aligned}
 \tag{B2}$$

Rearranging the above equation:

$$\begin{aligned}
 I_I &= (Y_{IJ} + Y_{IK} + Y_{I0})V_I - (Y_{IJ})V_J - (Y_{IK})V_K \\
 I_J &= -(Y_{JI})V_I + (Y_{JI} + Y_{JK} + Y_{J0})V_J - (Y_{JK})V_K \\
 I_K &= -(Y_{KI})V_I + (Y_{KJ})V_J + (Y_{KI} + Y_{KJ} + Y_{K0})V_K
 \end{aligned}
 \tag{B3}$$

Therefore, defining the admittances for the matrix models as follows:

$$\begin{aligned}
Y_{II} &= Y_{IJ} + Y_{IK} + Y_{I0} \\
Y_{JJ} &= Y_{JI} + Y_{JK} + Y_{J0} \\
Y_{KK} &= Y_{KI} + Y_{KJ} + Y_{K0} \\
Y_{IJ} &= Y_{JI} = -Y_{JI} \\
Y_{JK} &= Y_{KJ} = -Y_{JK} \\
Y_{IK} &= Y_{KI} = -Y_{IK}
\end{aligned} \tag{B4}$$

The sum of admittances further simplifies the expressions for nodal currents, as follows:

$$\begin{aligned}
I_I &= Y_{II}V_I + Y_{IJ}V_J + Y_{IK}V_K \\
I_J &= Y_{JI}V_I + Y_{JK}V_J + Y_{JK}V_K \\
I_K &= Y_{KJ}V_I + Y_{KJ}V_J + Y_{KK}V_K
\end{aligned} \tag{B5}$$

In representing the above equation as a matrix:

$$\begin{bmatrix} I_I \\ I_J \\ I_K \end{bmatrix} = \begin{bmatrix} Y_{II} & Y_{IJ} & Y_{IK} \\ Y_{JI} & Y_{JJ} & Y_{JK} \\ Y_{KI} & Y_{KJ} & Y_{KK} \end{bmatrix} \begin{bmatrix} V_I \\ V_J \\ V_K \end{bmatrix} \tag{B6}$$

Consequently, it can be generalised into:

$$\begin{bmatrix} I_{node} \end{bmatrix} = \begin{bmatrix} Y_{node} \end{bmatrix} \begin{bmatrix} V_{node} \end{bmatrix} \tag{B7}$$

where,

- I_{node} is the vector injected nodal currents
- Y_{node} is the nodal admittance matrix, and
- V_{node} is the vector nodal magnitude voltages measured with respect to the slack node.

The current that flows through the electrical networks is initially unknown, thus determined from power equation. This forms a correlation between nodal currents and voltages. The net nodal power injection at node I can be determined as follows:

$$S_I = P_I \pm jQ_I = V_I(I_I)^* \tag{B8}$$

where,

- I_I^* is the complex conjugate number of the current injected at node I
- j is the imaginary number
- $V_I, P_I, Q_I,$ and S_I are the voltage, active, reactive, and apparent power at node I .

After determining the values of power and voltage from the above equation, the current injected through the line from busbar I , is calculated as follows:

$$I_I^* = \frac{P_I \pm jQ_I}{V_I} = V_I \sum_{n=1}^N (V_n Y_{In})^* \quad \text{B9}$$

where,

- Y is the admittance matrix ($1/Z$)
- Z is the impedance ($R + jX$)
- V is the voltage
- N is the total number of nodes in the electricity network
- n is the number of nodes $I, J,$ and K

The terms Y_{In} , V_I and V_n can be expressed in polar form as:

$$\begin{aligned} Y_{In} &= |Y_{In}| \angle \theta_{In} \\ V_I &= |V_I| \angle \delta_I \\ V_n &= |V_n| \angle \delta_n \end{aligned} \quad \text{B10}$$

where,

- θ is the admittance phase angle at the admittance magnitude $|Y_{In}|$
- δ is the voltage phase angle between the voltage magnitudes $|V_I|$ and $|V_n|$

Thus, P_I and Q_I can be developed in polar form by multiplying the above terms (Y_{In} , V_I , and V_n), hence deduced as follows:

$$\begin{aligned} P_I + jQ_I &= \sum_{n=1}^N |Y_{In}| |V_I| |V_n| \angle (\theta_{In} + \delta_I + \delta_n) \\ P_I - jQ_I &= \sum_{n=1}^N |Y_{In}| |V_I| |V_n| \angle (\theta_{In} + \delta_I - \delta_n) \end{aligned} \quad \text{B11}$$

Let,

$$Y_{In} = G_{In} + jB_{In} \quad \text{and} \quad V_I = a_I + jb_I \quad \text{B12}$$

where,

- G is the conductance (real component) in Ω^{-1}
- B the susceptance (imaginary component) in S
- a is the voltage in the real component (v)
- b is the voltage in the imaginary component (v)

Then,

$$\begin{aligned}
 P_I + jQ_I &= \sum_{n=1}^N |G_{I_n} + jB_{I_n}| |V_I| |a_I + jb_I| \angle(\theta_{I_n} + \delta_I + \delta_n) \\
 P_I - jQ_I &= \sum_{n=1}^N |G_{I_n} + jB_{I_n}| |V_I| |a_I + jb_I| \angle(\theta_{I_n} + \delta_I - \delta_n)
 \end{aligned}
 \tag{B13}$$

From which $P_I + jQ_I$:

$$\begin{aligned}
 P_I &= \sum_{n=1}^N |G_{I_n} + jB_{I_n}| |V_I| |a_I + jb_I| \cos(\theta_{I_n} + \delta_I + \delta_n) \\
 Q_I &= \sum_{n=1}^N |G_{I_n} + jB_{I_n}| |V_I| |a_I + jb_I| \sin(\theta_{I_n} + \delta_I - \delta_n)
 \end{aligned}
 \tag{B14}$$

and for $P_I - jQ_I$:

$$\begin{aligned}
 P_I &= \sum_{n=1}^N |G_{I_n} + jB_{I_n}| |V_I| |a_I + jb_I| \cos(\theta_{I_n} + \delta_I + \delta_n) \\
 Q_I &= -\sum_{n=1}^N |G_{I_n} + jB_{I_n}| |V_I| |a_I + jb_I| \sin(\theta_{I_n} + \delta_I - \delta_n)
 \end{aligned}
 \tag{B15}$$

B2.2. Solution of Electrical Power Flow by Newton-Raphson Method

A satisfactory answer in electrical load flow studies was found when an iterative solver reduced the power mismatch below the specified tolerance value (ε) $10e^{-4}$, which is defined for a node n as:

$$\begin{aligned}
 |\Delta P_n| &\leq \varepsilon_P \\
 |\Delta Q_n| &\leq \varepsilon_Q
 \end{aligned}
 \tag{B16}$$

There are various methods to solve the mismatch in which solvers should run until the above equation is solved. Amidst the varied available techniques, the literature highlights that methods that can efficiently reduce computation time has a huge advantage.

As such, the Newton Raphson approach was selected in this study against other methods (e.g.: Gauss-Seidl and Hardy Cross). The Newton Raphson method was expanded from Taylor's method by employing the sparsity of connectivity matrix in order to gain a straightforward formulation, as well as a solution independent of the network size for analysis. The technique is described as follows:

$$f(x_0 + \Delta x) = f(x_0) + f'(x_0)\Delta x + \frac{f''(x_0)\Delta x^2}{2!} + \dots + \sum_{k=0}^{\infty} \frac{f^{(k)}(x_0)\Delta x^k}{k!}
 \tag{B17}$$

where,

- x_0 represents the set of unknown state variables
- k is $0, 1, 2, 3 \dots \infty$
- $k!$ denotes the factorial of n
- $f^{(n)}(x_0)$ denotes the n^{th} derivative of f evaluated at the point x_0

Upon considering that the value given at each iteration is close to its prior value, the expressions beyond the first derivative can be disregarded, as follows:

$$f(x_0 + \Delta x) = f(x_0) + f'(x_0)\Delta x = 0 \quad \text{B18}$$

Hence, the variation Δx that should ensure the approach of $f(x_0 + \Delta x)$ is equivalent to zero is given below:

$$\Delta x = -[f'(x_0)]^{-1} = f(x_0) \quad \text{B19}$$

where,

- $[f(x_0)]^{-1}$ is the matrix of first partial derivatives referred as *Jacobian* (J)

After simplifying the expression for the i -th iteration, the above equation is expressed as follows:

$$\Delta x^{i+1} = -[J^i]^{-1} = f(x_0^i) \quad \text{B20}$$

When variation Δx is calculated, the iterative approximation of the state variables is updated as a function of its values of the prior iteration, along with the correction values, as follows:

$$x_0^{i+1} = x_0^i + \Delta x^{i+1} \quad \text{B21}$$

This calculation is repeated in MATPOWER during the flow of electrical power as many times until Δx is within the tolerance (ϵ) value of $10e^{-4}$. As for the electrical system load flow, the state variables of the system represented by x_0 in the above equation refer to the nodal voltage magnitudes and the phase angles. As such, the Newton Raphson algorithm is represented by the following equation:

$$\begin{bmatrix} \Delta \theta \\ \Delta V / V \end{bmatrix} = [J]^{-1} \begin{bmatrix} \Delta P \\ \Delta Q \end{bmatrix} = \begin{bmatrix} \frac{\partial P}{\partial \theta} & \frac{\partial P}{\partial V / V} \\ \frac{\partial Q}{\partial \theta} & \frac{\partial Q}{\partial V / V} \end{bmatrix}^{-1} \begin{bmatrix} \Delta P \\ \Delta Q \end{bmatrix} \quad \text{B22}$$

where,

- The terms ΔV are divided by V to correct the PQ nodes and
- $\Delta\theta$ is the correction to PV and PQ nodes

For convenience purpose, the Jacobian matrix can be formed by using entries $J_A, J_B, J_C,$ and J_D from the node connectivity data. Therefore, in taking the prior equation as the basis, the following is obtained:

$$\begin{bmatrix} \Delta P \\ \Delta Q \end{bmatrix} = \begin{bmatrix} J_A & J_B \\ J_C & J_D \end{bmatrix} \begin{bmatrix} \Delta\theta \\ \Delta V / V \end{bmatrix} \quad \text{B23}$$

Example

Figure B2- 2 illustrates the electrical network after weighing in the two nodes, I and J , which are connected as one element - IJ .

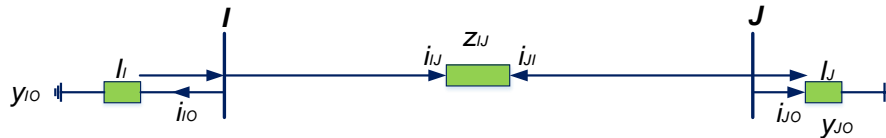


Figure B2- 2: Example of a two-node network

As for the diagonal elements, the matrix may be comprised of two or four terms, depending on the classification of node I , which could be either a PV or a PQ node:

- If node I is a PV node:
 - Reactive power becomes unknown and the term ΔQ is neglected
 - J_C and J_D are discarded, and similarly
 - J_B can be omitted since the voltage magnitude is fixed to be PV in node I
 - Only J_A is considered as a generator node
- If node I is a PQ node:
 - All four elements: $J_A, J_B, J_C,$ and $J_D,$ are considered

Overall, two cases may arise when building the first partial derivatives for buses I and J : diagonal and non-diagonal elements.

For **diagonal**:

$$\begin{aligned}
J_A &= \frac{\partial P_I}{\partial \theta_I} = -V_I^2 B_{II} - Q_{T_I} \\
J_B &= \frac{\partial P_I}{\partial V_I / V_I} = V_I^2 G_{II} - P_{T_{II}} \\
J_C &= \frac{\partial Q_I}{\partial \theta_I} = -V_I^2 G_{II} + P_{T_I} \\
J_D &= \frac{\partial Q_I}{\partial V_I / V_I} = -V_I^2 B_{II} + Q_{T_I}
\end{aligned}
\tag{B24}$$

For **non-diagonal**:

$$\begin{aligned}
J_A &= \frac{\partial P_I}{\partial \theta_J} = V_I V_J (G_{IJ} \sin \delta_{IJ} - B_{IJ} \cos \delta_{IJ}) \\
J_B &= V_J \frac{\partial P_I}{\partial V_J} = V_I V_J (G_{IJ} \sin \delta_{IJ} + B_{IJ} \cos \delta_{IJ}) \\
J_C &= \frac{\partial Q_I}{\partial \theta_J} = -V_I V_J (G_{IJ} \sin \delta_{IJ} + B_{IJ} \cos \delta_{IJ}) \\
J_D &= V_J \frac{\partial Q_I}{\partial V_J} = V_I V_J (G_{IJ} \sin \delta_{IJ} - B_{IJ} \cos \delta_{IJ})
\end{aligned}
\tag{B25}$$

Upon detecting a mismatch, the final result of the state variables for node I is updated. For instance, the voltage and the phase angle for i -th iteration are represented as follows:

$$V_I^{i+1} = V_I^i \left[1 + \left(\frac{\Delta V_I}{V_I} \right)^{i+1} \right]
\tag{B26}$$

$$\theta_I^{i+1} = \theta_I^i + \Delta \theta_I^{i+1}$$

Finally, once the flows and losses in the line are calculated, the net power injection by the slack node can be determined as well. Figure B2- 3 illustrates a flow diagram of the Newton Raphson flow algorithm for the electrical system developed using the MATLAB platform.

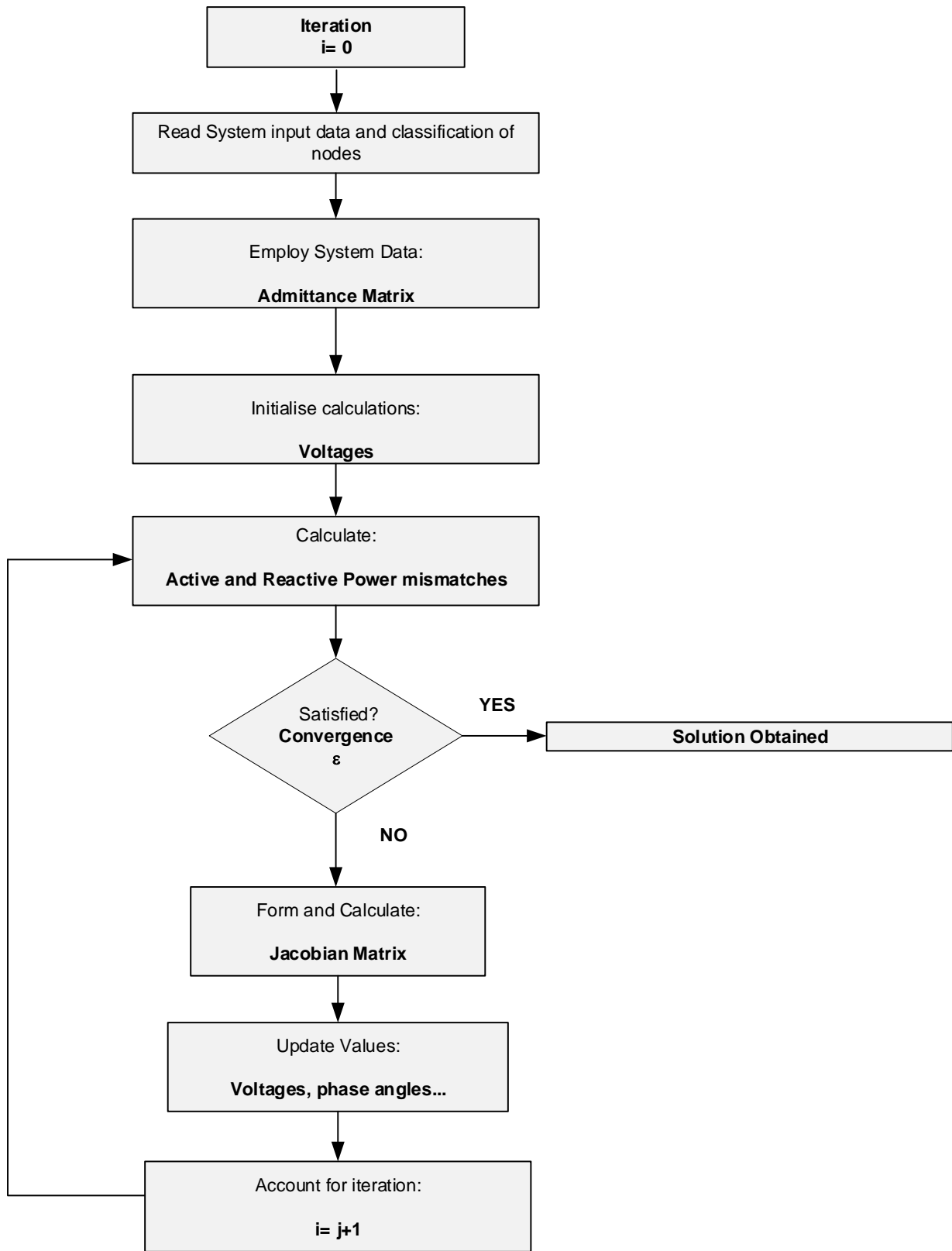


Figure B2- 3: Flow diagram of the electrical load flow algorithm using Newton Raphson

B3 VOLTAGE CALCULATION METHOD FOR A RADIAL NETWORK

Voltages on a distribution circuit can be obtained by knowing the active and reactive powers and the line impedance. A simple calculation of voltages from a two-busbar distribution circuit, illustrated in Figure B3- 1, is given as follows:

$$V_R = V_S - (R + jX) \frac{[P - jQ]}{V_S^*} \quad \text{B27}$$

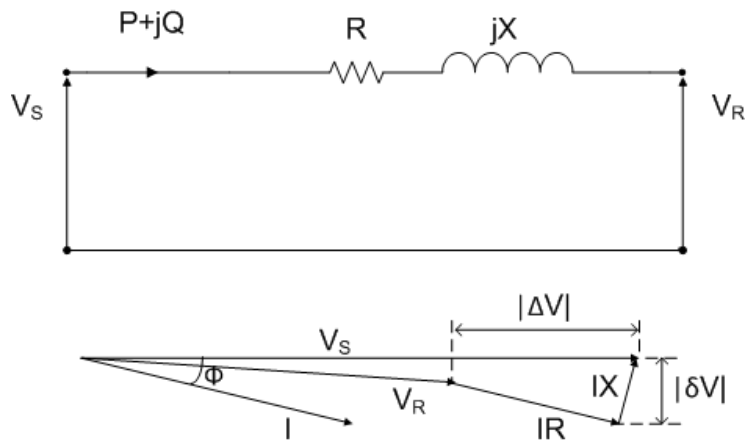


Figure B3- 1: Network equivalent circuit and phasor diagram

Considering V_S as reference, the above equation is written rewritten:

$$V_R = V_S - \frac{[RP + XQ]}{V_S} - j \frac{[XP + RQ]}{V_S} \quad \text{B28}$$

For a distribution circuit where $R \gg X$ the last term ($|\delta V|$) as shown in Figure B3- 1, can be neglected:

$$V_R = V_S - \frac{[RP + XQ]}{V_S} \quad \text{B29}$$

A simple radial feeder is illustrated in Figure B3- 2. To calculate the voltages at the end of the feeder without an iterative procedure an assumption is required. The powers at the sending end, P and Q, are known and can be approximated as follows:

$$P \simeq \sum_{i=1}^n P_i \quad Q \simeq \sum_{i=1}^n Q_i \quad \text{B30}$$

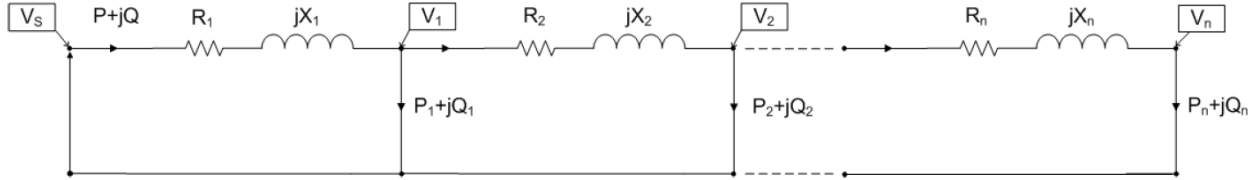


Figure B3- 2: Network equivalent of a radial feeder

The voltage at busbars 1 and 2 is given by:

$$V_1 = V_s - \frac{[R_1(P_1 + P_2 + \dots P_n) + X_1(Q_1 + Q_2 + \dots Q_n)]}{V_s} \quad \text{B31}$$

$$V_2 = V_1 - \frac{[R_2(P_2 + P_3 + \dots P_n) + X_2(Q_2 + Q_3 + \dots Q_n)]}{V_1}$$

Substituting Voltage at busbar 1 into busbar 2:

$$V_2 = V_s - \frac{[R_1(P_1 + P_2 + \dots P_n) + X_1(Q_1 + Q_2 + \dots Q_n)]}{V_s} - \frac{[R_2(P_2 + P_3 + \dots P_n) + X_2(Q_2 + Q_3 + \dots Q_n)]}{V_1}$$

$$\cong V_s - \frac{[R_1(P_1 + P_2 + \dots P_n) + R_2(P_2 + P_3 + \dots P_n) + \dots R_n P_n]}{V_s} - \dots$$

$$- \frac{[X_1(Q_1 + Q_2 + \dots Q_n) + X_2(Q_2 + Q_3 + \dots Q_n) + \dots X_n Q_n]}{V_s} = \quad \text{B32}$$

$$= V_s - \frac{\left[\sum_{i=1}^n \left(R_i \sum_{j=i}^n P_j \right) + \sum_{i=1}^n \left(X_i \sum_{j=i}^n Q_j \right) \right]}{V_s}$$

APPENDIX C

C1 ELECTRICITY GENERATION EQUIPMENT

Table C1- 1: Green electricity generation equipment parameters

| Wind Turbine | | PV Panels | | 8 x Inverters | |
|------------------|--------------------|------------------------------------|---------------------|----------------------|-------------------|
| Rated Power | 750kW _e | Rated Power | 255W _p | Maximum Output Power | 20kW _e |
| Rated Speed | 12m/s | PV Cell efficiency | 16.5% | | |
| Cut-in-Speed | 3m/s | Solar Cell Temperature Coefficient | 0.0039% | Efficiency | 94.8% |
| Cut-out-Speed | 25m/s | Temperature at Standard Conditions | 25°C | | |
| Rotor Swept Area | 1735m ² | Total number of Cells | 60 | | |
| Rotor Diameter | 47m | Area of PV cell | 0.026m ² | | |
| Tower/Hub Height | 65m | Area of PV panel | 1.611m ² | | |

C2 SOLAR PV PANEL SCHEMATICS

Fife Renewables and Innovation Centre

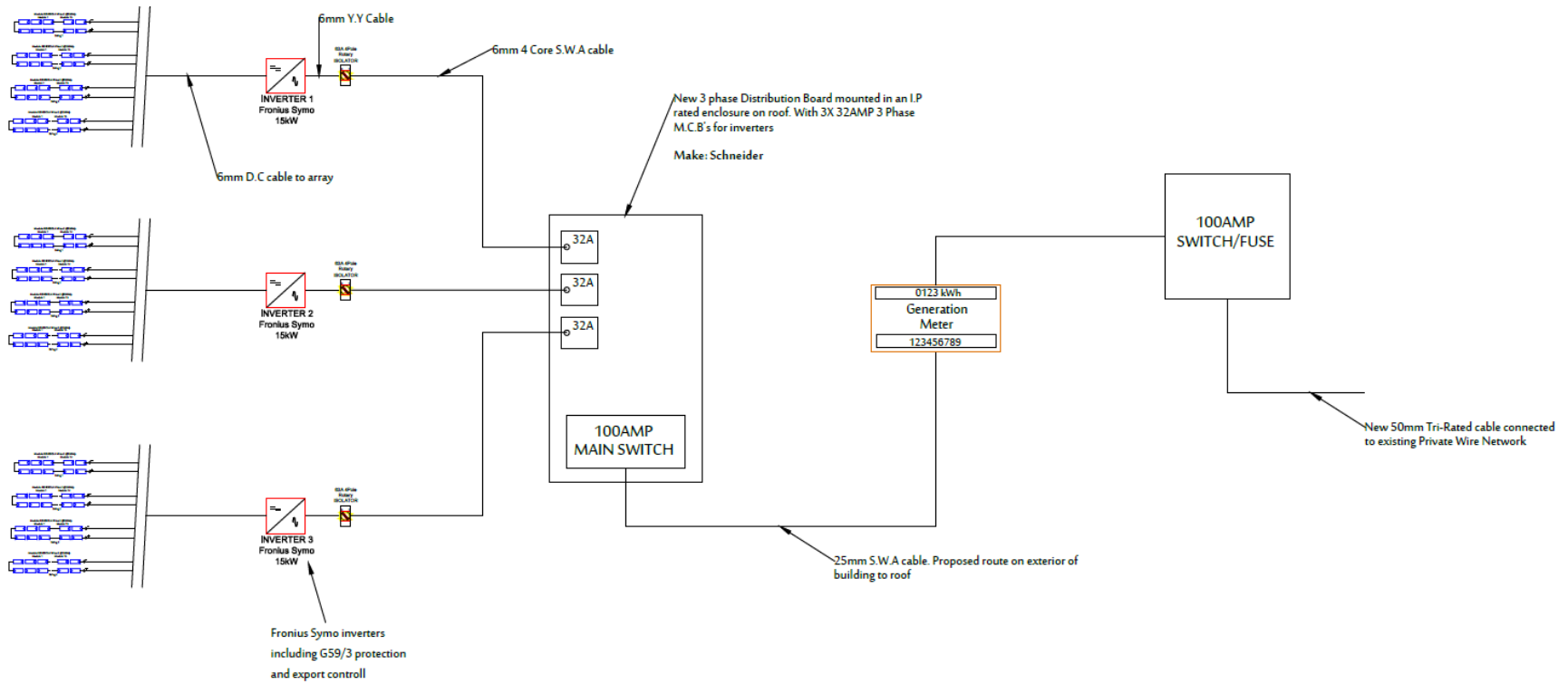


Figure C1- 1: Fife Renewables and Innovation Centre Solar PV Schematic. Courtesy of Bright Green Hydrogen

Bayview Ground Mount

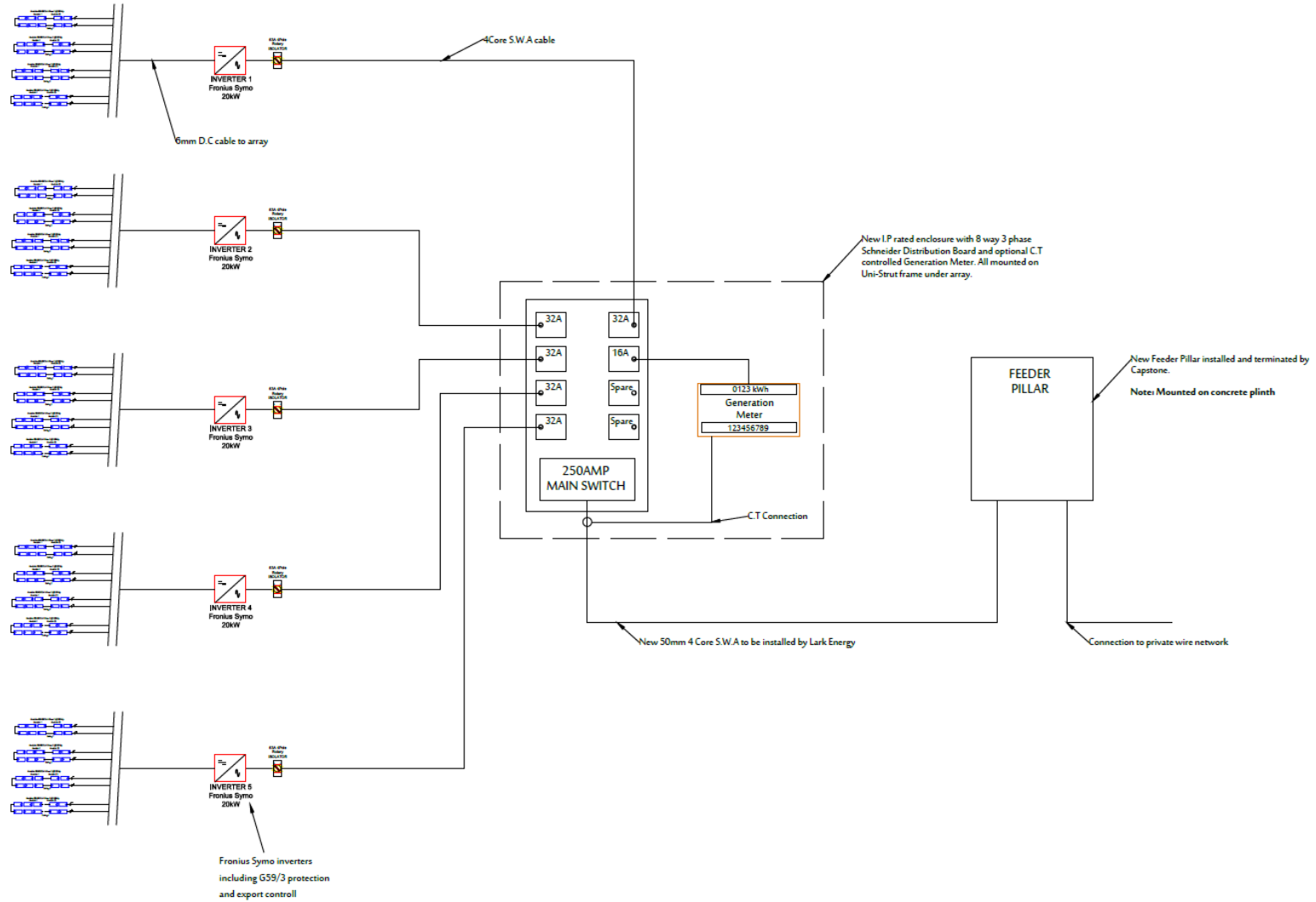


Figure C1- 2: Bayview Ground Mount Solar PV Schematics. Courtesy of Bright Green Hydrogen Bright Green Hydrogen

C3 HYDROGEN REFUELLING STATION PARAMETERS

Table C3- 1: H2 Refuelling Station Parameters. Courtesy of Bright Green Hydrogen

| Electrolyser | | Compressor | |
|---|--|-----------------------------------|---------------------------|
| Electrolyser Rated Power | 60kW _e | Rated Power | 10kW _e |
| Number of Cells per Stack | 20 | | |
| Stack Rated Power | 6.2kW _e | Mechanical Efficiency | 80% |
| Reversible Cell Voltage | 1.295A | | |
| Number of Stacks | 10 | Temperature | 300K |
| Faraday Constant | 26.8 Ah/mol or 96485.33 °C/mol | Polytropic Index | 1.609 |
| Empirical Parameters (a ₁ , a ₂ , a ₃ , a ₄ , a ₅ , a ₆ , and a ₇) | (0.995, -9.578m ² /A, -0.0555m ² /A°C, 0, 1502.70m ⁴ /A, -70.8005m ² /A°C, and 0). | Buffer Tank | |
| Area of Cell Electrode | 0.025m ² | Volume | 0.85m ³ |
| Temperature of the Cell | 353K | Pressure | 30bars |
| Anode Partial Pressure | 13.1 bars | Temperature | 300K |
| Cathode Partial Pressure | 2.063 bars | H₂ Storage Tank | |
| Water Pressure | 1bar | Volume | 1.013m ³ |
| Membrane Thickness and Cross-section | 0.0178cm and 250cm ² | Pressure | 30bars |
| Anode and Cathode Transfer Coefficient | 2 and 0.5 | Temperature | 300K |
| Anode and Cathode Transfer Resistances | 1 ohm | FCEV's | |
| Concentration and Diffusivity of H ₂ ions in the Membrane | 1200mol/m ³ and 4.5e ⁻¹⁰ m ² /s | Model | Hyundai ix35 |
| Exchange current density in Anode and Cathode | 1e ⁻⁶ A/cm ² and 0.287A/m ² | Tank Maximum Capacity | 144 Liters |
| | | Fuel Consumption | 9.7L/100Km (10.30Km/L) |
| | | Maximum Driving Range | 369miles (593Km) |